

UNCLASSIFIED

AD NUMBER
AD884790
NEW LIMITATION CHANGE
TO Approved for public release, distribution unlimited
FROM Distribution authorized to U.S. Gov't. agencies and their contractors; Critical Technology; MAR 1971. Other requests shall be referred to Air Force Flight Dynamics Laboratory, Attn: FBR, Wright-Patterson AFB, OH 45433.
AUTHORITY
AFFDL notice, 13 Aug 1971

THIS PAGE IS UNCLASSIFIED

AD884790

AFFDL-TR-70-149

INVESTIGATION AND ANALYSIS DEVELOPMENT
OF EARLY LIFE AIRCRAFT
STRUCTURAL FAILURES

ROBERT J. GRAN AND FRED D. ORAZIO, JR.
UNIVERSAL TECHNOLOGY CORPORATION
DAYTON, OHIO



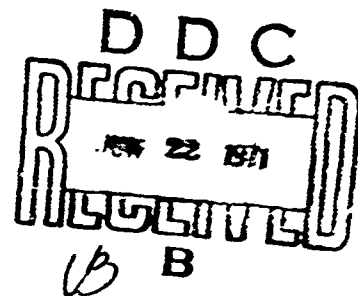
Handwritten initials 'JB'

AND

PAUL C. PARIS, GEORGE R. IRWIN AND RICHARD HERTZBERG
D&L RESEARCH CORPORATION
BETHLEHEM, PENNSYLVANIA

TECHNICAL REPORT AFFDL-TR-70-149

MARCH 1971



AD No. _____
DDC FILE COPY

This document is subject to special export controls and each transmittal to foreign governments or foreign nationals may be made only with prior approval of the Air Force Flight Dynamics Laboratory (FBR), Wright-Patterson Air Force Base, Ohio 45433.

AIR FORCE FLIGHT DYNAMICS LABORATORY
AIR FORCE SYSTEMS COMMAND
WRIGHT-PATTERSON AIR FORCE BASE, OHIO

269

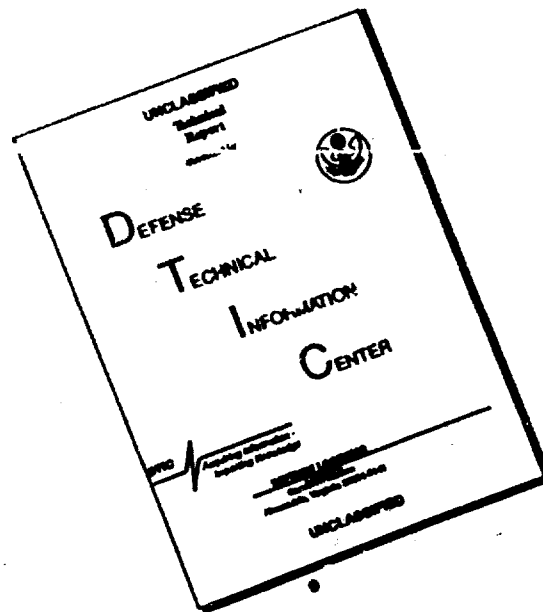
NOTICE

When Government drawings, specifications, or other data are used for any purpose other than in connection with a definitely related Government procurement operation, the United States Government thereby incurs no responsibility nor any obligation whatsoever; and the fact that the Government may have formulated, furnished, or in any way supplied the said drawings, specifications, or other data, is not to be regarded by implication or otherwise as in any manner licensing the holder or any other person or corporation, or conveying any rights or permission to manufacture, use, or sell any patented invention that may in any way be related thereto.

ACQUISITION NO.		
CPST	WRITE SECTION	<input type="checkbox"/>
DC	BREF SECTION	<input checked="" type="checkbox"/>
ACQUISITION		<input type="checkbox"/>
DISTRIBUTION/AVAILABILITY CODES		
DIST.	AVAIL.	SEC. OR SPECIAL
2		

Copies of this report should not be returned unless return is required by security considerations, contractual obligations, or notice on a specific document

DISCLAIMER NOTICE



THIS DOCUMENT IS BEST QUALITY AVAILABLE. THE COPY FURNISHED TO DTIC CONTAINED A SIGNIFICANT NUMBER OF PAGES WHICH DO NOT REPRODUCE LEGIBLY.

UNCLASSIFIED

Security Classification

DOCUMENT CONTROL DATA - R & D

(Security classification of title, body of abstract and indexing annotation must be entered when the overall report is classified.)

1. ORIGINATING ACTIVITY (Corporate author) Universal Technology Corporation, Dayton, Ohio and Del Research Corporation, Bethlehem, PA		2a. REPORT SECURITY CLASSIFICATION Unclassified	
		2b. GROUP S/A	
3. REPORT TITLE INVESTIGATION AND ANALYSIS DEVELOPMENT OF EARLY LIFE AIRCRAFT STRUCTURAL FAILURES			
4. DESCRIPTIVE NOTES (Type of report and inclusive dates) Final report of work conducted from 15 April 1968 to 15 October 1970			
5. AUTHOR(S) (First name, middle initial, last name) Gran, Robert J. Paris, Paul C. Hertzberg, Richard Oraxio, Fred D., Jr. Irwin, George R.			
6. REPORT DATE 15 OCT 1970		7a. TOTAL NO OF PAGES 264	7b. NO OF REFS 50
8a. CONTRACT OR GRANT NO F33615-68-C-1503 <i>NEW</i>		9a. ORIGINATOR'S REPORT NUMBER(S) UTC-TR-S316	
8b. PROJECT NO 1467		9b. OTHER REPORT NO(S) (Any other numbers that may be assigned this report) AFFDL-TR-70-149	
8c. TASK NO 146704			
10. DISTRIBUTION STATEMENT This document has been approved for public release and sale; its distribution is unlimited.			
11. SUPPLEMENTARY NOTES		12. SPONSORING MILITARY ACTIVITY Air Force Flight Dynamics Laboratory (FBR) Air Force Systems Command Wright-Patterson AFB, OH 45433	
13. ABSTRACT An investigation and analysis of aircraft structural failures was conducted to assess the condition surrounding early life failures and initiate improved methods for the structural analysis of such failure problems. The primary objective was to identify critical structural component areas and define an analysis approach which would consider the useful life of a flawed or damaged structure. Initial program efforts involved the survey of Government and Industry organizations concerned with engineering and maintenance of present operational aircraft. Failure data was gathered on airframe structures, landing gear components and highly stressed aircraft sub-components which experienced operational failures. The data gathered was tabulated under various categories related to component description, failure circumstances, stress history and environmental influences in an attempt to identify significant or contributing variables. Results of these failure correlations are presented in tabular form. The failure analysis methods utilized in the program were based on the fracture mechanics approach, which takes into consideration the existence of a flawed or damaged structure with localized stress concentrations in this region. The principles of fracture mechanics, its application criteria and structural failure behavior patterns are presented.			

DD FORM 1473

UNCLASSIFIED

Security Classification

BEST AVAILABLE COPY

UNCLASSIFIED

Security Classification

KEY WORDS	LINK A		LINK B		LINK C	
	ROLE	WT	ROLE	WT	ROLE	WT
Aircraft Structural Failures Fleet failure experience Failure analysis Fracture mechanics						

UNCLASSIFIED

Security Classification

**INVESTIGATION AND ANALYSIS DEVELOPMENT
OF EARLY LIFE AIRCRAFT
STRUCTURAL FAILURES**

ROBERT J. GRAN AND FRED D. ORAZIO, JR.

*UNIVERSAL TECHNOLOGY CORPORATION
DAYTON, OHIO*

AND

PAUL C. PARIS, GEORGE R. IRWIN AND RICHARD HERTZBERG

*DEL RESEARCH CORPORATION
BETHLEHEM, PENNSYLVANIA*

This document is subject to special export controls and each transmittal to foreign governments or foreign nationals may be made only with prior approval of the Air Force Flight Dynamics Laboratory (FDR), Wright-Patterson Air Force Base, Ohio 45433.

The distribution of this report is limited because unlimited distribution would significantly diminish the technological lead time of the United States and friendly foreign nations by revealing techniques having a potential strategic or economic value not generally known throughout the world.

FOREWORD

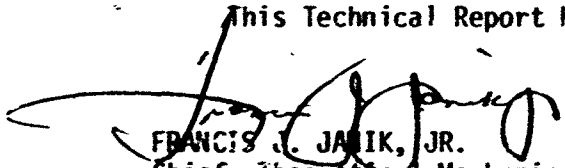
This report was prepared by Universal Technology Corporation, Dayton, Ohio, and Del Research Corporation, Bethlehem, Pennsylvania, under Contract F33615-68-C-1503, Project 1467. The work was administered under the direction of the Structures Division (FBR), Air Force Flight Dynamics Laboratory, with Mr. Howard A. Wood as the Air Force project engineer. This report covers the work conducted from 15 April 1968 through 15 August 1969.

The program efforts related to aircraft failure data gathering, review and correlation was accomplished by Universal Technology Corporation with Mr. Robert J. Gran as program manager. The program efforts related to failure analysis development and analysis of specific failures was accomplished by Del Research Corporation with Dr. Paul C. Paris as project leader.

Acknowledgment and appreciation is offered herein to those Air Force organizations, other Government agencies and Aircraft Industry members who provided component failure documentation for inclusion in this program. Such valuable information contributed directly to the conclusions and results of this program.

This report was submitted by the authors on 1 November 1970 for publication as an AFFDL Technical Report.

This Technical Report has been reviewed and is approved.



FRANCIS J. JANI~~K~~, JR.
Chief, Theoretical Mechanics Branch
Structures Division

ABSTRACT

An investigation and analysis of aircraft structural failures was conducted to assess the condition surrounding early life failures and initiate improved methods for the structural analysis of such failure problems. The primary objective was to identify critical structural component areas and define an analysis approach which would consider the useful life of a flawed or damaged structure.

Initial program efforts involved the survey of Government and Industry organizations concerned with engineering and maintenance of present operational aircraft. Failure data was gathered on airframe structures, landing gear components and highly stressed aircraft sub-components which experienced operational failures. The data gathered was tabulated under various categories related to component description, failure circumstances, stress history and environmental influences in an attempt to identify significant or contributing variables. Results of these failure correlations are presented in tabular form.

The failure analysis methods utilized in this program were based on the fracture mechanics approach, which takes into consideration the existence of a flawed or damaged structure with localized stress concentrations in this region. The principles of fracture mechanics, its application criteria and structural failure behavior patterns are presented. These analysis methods and procedures are intended to provide guidance and direction in the analysis of various types of structural components. The necessary data for adequate fracture mechanics analysis for failure investigation is presented, and analysis limitations or proper utilization are defined. As a means of demonstrating this analysis method, detailed failure analyses were performed on actual failed structural components in which information was obtained during the failure data gathering phase of the program. Conclusions and recommendations in the utilization of this analysis method are summarized.

TABLE OF CONTENTS

<u>SECTION</u>	<u>PAGE</u>
I INTRODUCTION.....	1
II FAILURE DATA REVIEW AND CORRELATION.....	5
A. Failure Information Survey.....	5
1. Systems Considered for Failure Data.....	5
2. Data Sources Solicited.....	8
3. Data Request Format and Procedures.....	12
B. Failure Data Compilation.....	24
1. AFM 66-1 Data.....	24
2. Mechanical Reliability Report (MRR).....	31
3. Unsatisfactory Report (EUR/UR) Data.....	32
4. Detailed Failure Data Documentation.....	33
5. Data Limitations and Problems.....	35
C. Failure Data Correlation.....	41
1. General Failure Data Categorizing and Correlation.....	41
2. Significant Failure Data Categorizing and Correlation.....	43
3. Data Correlation Assessment.....	57
III FAILURE ANALYSIS DEVELOPMENT.....	65
A. Fracture Mechanics Analysis Tools.....	66
1. Fundamentals of Fracture Mechanics Analysis.....	66
2. Formulas and Estimates for Applied Stress Intensity Factors.....	103
B. Fracture Examination and Identification.....	115
1. Macroscopic Aspects of Fracture.....	115
2. Microscopic Examination.....	132
3. Void Coalescence.....	138
4. Cleavage.....	141
5. Fatigue Process.....	144
6. Fracture Markings at Instability.....	151
C. Materials Behavior Patterns.....	153
1. Property Data Useful in Failure Analysis.....	153
2. Selected Mechanical Property Data.....	162
3. Sources for Alloy Behavior Data.....	164
D. Individual Component Failure Analysis.....	167
1. Suggested List of Raw Data Necessary for Complete Failure Analysis.....	167
2. Component Failure Analysis Examples.....	177
Example 1.....	179
Example 2.....	191
Example 3.....	205
Example 4.....	215
Example 5.....	221
Example 6.....	231

TABLE OF CONTENTS (Continued)

<u>SECTION</u>	<u>PAGE</u>
IV PROGRAM CONCLUSIONS.....	241
REFERENCES.....	245
APPENDIX A.....Computer Programs for AFM 66-1 Data Retrieval.....	249

LIST OF ILLUSTRATIONS

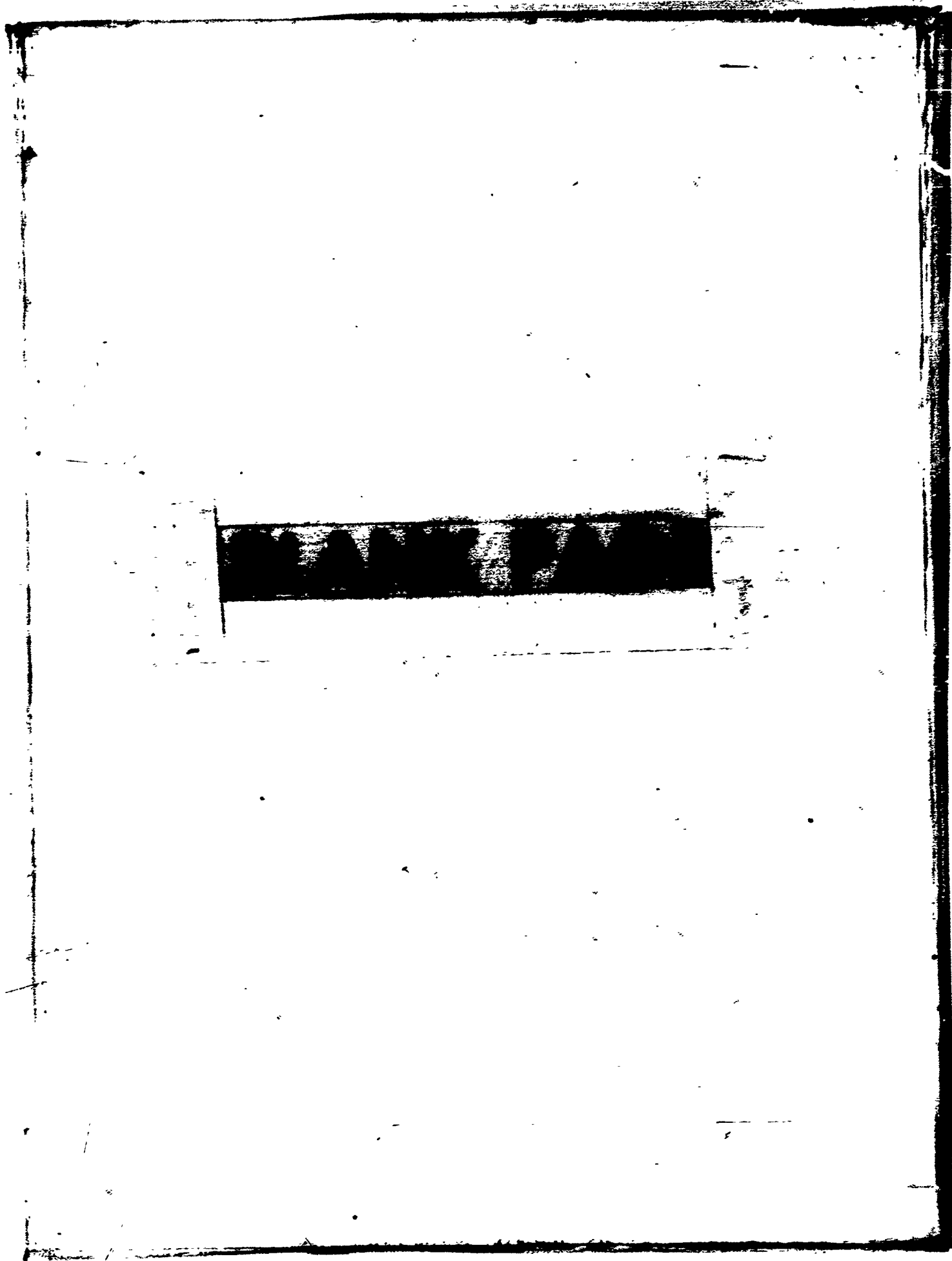
<u>FIGURE</u>		<u>PAGE</u>
1	Card for Identifying Survey and Processing Status.....	21
2	Aircraft Summary Sheet.....	22
3	Item Summary Worksheet.....	23
4	Sample Work Unit Code Manual Pages.....	28
5	Sample Work Unit Code Manual Pages.....	29
6	Detailed Failure Information Processing Sequence.....	34
7	Statistical Distribution of Failures on Air Force Cargo Aircraft.....	46
8	Statistical Distribution of Failures on Air Force Fighter/ Trainer Aircraft.....	47
9	Statistical Distribution of Failures on Air Force Bomber Aircraft.....	48
10	Statistical Distribution of Failures on Air Force Helicopters.....	49
11	Statistical Distribution of Failures on Selected Commercial Jet Aircraft.....	50
12	Statistical Distribution of Total Failures Recorded.....	51
13a, 13b	Statistical Distribution of Comprehensive Failure Data for Various Correlation Categories.....	59,60
14	Stress Field Coordinate System.....	68
15	Crack Displacement Modes.....	71
16	Plastic Zone Representation in Plates.....	79
17	Stress Distribution Ahead of Crack.....	81
18	Plot of K_c vs r_p/B for Various Thicknesses.....	86
19	Correlation of Crack Growth Rates in 7075-T6 Aluminum Alloy Under Sinusoidal Loading.....	91
20	Crack Growth Rate vs Stress Field Intensity.....	92
21	Bowie's Factor for Cracks Emanating from Holes.....	106
22	Quarter-Elliptical Flaw Geometry.....	109
23	Notation for Flaw Geometry.....	109
24	Crack Progression Irregularities.....	113
25	Crack Geometry for $a > c$	114
26	Partial Through-Crack Geometry.....	114
27	Schematic of the Leading Edge Region of a Crack.....	120
28	Schematic Representation of Crack Extension Behaviors.....	123
29	Asperities and Splits for "Steel Type" Edge of a Shear Fracture and Flow Markings for an "Al Type" Edge.....	128
30	Fractograph Revealing Void Coalescence in the Form of "Equiaxed Dimples".....	140
31	Fractograph Revealing Void Coalescence in the Form of "Elongated Dimples".....	140
32	Cleavage Facet with Associated Cleavage Steps.....	142
33	Fractograph Revealing "Quasi-Cleavage" Region Containing Localized Steps and "River Markings".....	144

LIST OF ILLUSTRATIONS (Continued)

<u>FIGURE</u>		<u>PAGE</u>
34	Fatigue Striations Resulting from Uniform Sinusoidal Loading.....	146
35	Plot of Stress Intensity Range versus Rate of Crack Propagation and Striation Spacings.....	148
36	Fatigue Striations Resulting from Random Loading.....	150
37	"Stretched Zone" and Dimpled Rupture Resulting from Overload During Fatigue Cycling.....	152
38	Actuator Cylinder Geometry and Fracture Description for Case I.....	194
39	Component Geometry and Fracture Description for Case II.....	198
40	Plate Flaw Geometry at Final Failure.....	206
41	Photographs of Fracture Surface after Final Failure.....	209
42	Data on High Strength Steels Showing Deviation from the Usual Curve.....	211
43	Spar Cap Cross Section Geometry and Fracture Description.....	216
44	Fracture Surface Appearance of Wing Carry-Through Forging....	222
45	Geometry for a Crack Emanating from a Circular Hole in a Plate.....	232
46	Plot of Critical Crack Length vs. Stress for a 7075-T6 Panel.....	235
47	Geometry of a Corner Crack Emanating from a Hole in the Plate.....	239
A-1	The Computer Program RCCT.....	250
A-2	RCCT Output.....	251
A-3a	The Computer Program	253
A-3b	The Computer Program (Continued).....	254
A-4	SELECT Output.....	255
A-5a	The Computer Program WUCCOL.....	258
A-5b	The Computer Program WUCCOL (Continued).....	259
A-5c	The Computer Program WUCCOL (Continued).....	260
A-6	WUCCOL Output.....	262
A-7	WUCCOL Output Continued.....	263

LIST OF TABLES

<u>TABLE</u>		<u>PAGE</u>
I	Aircraft Considered for Data Gathering.....	7
II	Aircraft Systems Investigated.....	7
III	Structural Components Included in This Program.....	14
IV	Air Force Manual 66-1 Information.....	16
V	Pertinent AFM 66-1 Data Entry Code Information.....	26
VI	Aircraft Suffix Codes of Interest for Data Retrieval.....	27
VII	Component Coding for General Failure Data.....	42
VIII	Numerical Tabulation of Failure Data from AFM 66-1 and MRR Records.....	44
IX	Statistical Tabulation of Failure Data from AFM 66-1 and MRR Records.....	45
X	Coding System for the Comprehensive Failure Data Form.....	52
XI	Comprehensive Failure Data List.....	55
XII	Comprehensive Failure Data Statistical Distribution in Each Category.....	58
XIII	Stress Intensity for a Crack Emanating from a Hole.....	106
XIV	Mechanical Properties of Selected Engineering Alloys.....	163
XV	Summary of Data Obtained from Failure Reports.....	173
A-I	Input Data for the Computer Program SELECT.....	256
A-II	Input Data for the Computer Program WUCCOL.....	264



SECTION I

INTRODUCTION

The progress in improved structural design has evolved around the development and improvement of stress analysis methods and further understanding of materials behavior. These attempts, however, have been hindered by the increased complexity of aircraft structures, greater demands for varied performance capabilities and requirements for longer operating life. On the other hand, progress has been made in defining the operating environment and actual loading conditions experienced by present aircraft. Also, extensive and varied failure analysis efforts have been conducted in order to better understand and more accurately predict aircraft structural life. Basically, the aim is to develop analytical techniques which will most accurately predict or define the useful service life of the aircraft airframe or structural component.

Various design or failure analysis techniques or theories have been developed and utilized, including static stress analysis, cumulative damage, fracture analysis and experimental evaluation. These analysis techniques or theories take into consideration various boundary conditions or model assumptions, depending on the intended application, known factors, or experience of the investigator. The approach taken in developing these analyses may also differ markedly, depending on the direction of view such as engineering, stress analysis, solid mechanics or metallurgical and whether a general or specific solution is desired. Although the interest is more oriented toward specific design and

failure analyses, these likewise require a more precise definition of inputs and analytical procedures. In the real aircraft operating situation this is a complex and many-variable problem, which defies a general or universal analytical solution.

Aircraft structural component failures have continued to be major flight worthy and safety problems, as well as maintenance and economic burdens. Efforts to eliminate or minimize such failures have been directed toward improved prediction methods, more thorough maintenance, more comprehensive design efforts, improved manufacturing procedures and utilization of better materials. The successful analysis and utilization of a flaw-free material under ideal stress conditions is not possible, therefore, the consideration of such imperfections in failure analysis or life prediction is necessary. Likewise, the subsequent initiation of a flaw or crack in a structural component does not warrant immediate replacement, but rather a determination of its criticality and estimation of remaining component life. In aircraft structural applications, failure analysis attempts are further complicated when considering random loading conditions, variations in environmental influences, and the uncertainty in materials characterization. The availability of additional or improved analysis methods and life prediction techniques could offer a valuable tool for the stress analyst.

Because of these above needs, this program was directed toward the identification of in-service, early life failures and the development of an improved failure analysis method based on such failure

circumstances. The survey and analysis objectives were to establish criteria, guidelines and approaches to analyze component failure problems rather than a comprehensive solution for each service failure investigated. Existing or available component failure information and material property data were used in developing the analysis method.

A survey of actual service failures was conducted for the purpose of identifying significant failure areas and reviewing circumstances surrounding such failures. The failure data was analyzed and correlated to define critical problem areas and identify key variables which would be important in the development of an improved analysis. This portion of the program is presented in Section II and was accomplished by Universal Technology Corporation.

The development of an improved failure analysis method, under this program, is based on the fracture mechanics approach. This method takes into consideration the existence of a flaw or defect and localized stress concentrations in this region. This analysis method has received considerable attention in materials testing and component evaluation in recent years. Further development, however, is required in order to apply it to analysis of complex structures and operational conditions. This failure analysis discussion and the application of this method to individual in-service failures is presented in Section III and was accomplished by Del Research Corporation.

Program conclusions and recommendations are presented in Section IV. Supporting survey data and computer programs are contained in the Appendix.

SECTION II
FAILURE DATA REVIEW AND CORRELATION

A. Failure Information Survey

A survey was conducted of Government and the aircraft Industries for the purpose of identifying and reviewing structural failure documentation related to Air Force aircraft and similar commercial aircraft. Specific component in-service failure records were examined to determine component description and failure circumstance which would contribute to the failure data tabulation and analysis development efforts. The objective of the survey was to obtain a broad cross-section of past and present component failure experience on a wide variety of aircraft types and structural components. This general survey identified numerous types of service failures and enabled a comprehensive overview of the failure investigation and correction problem. From this general survey, specific component failures were selected for further review and data gathering. These selected components provided service failure data for the development of the failure analysis method presented in Section III of this report.

A discussion of the aircraft systems investigated, sources solicited, type data requested and data limitations are contained in the following paragraphs.

1. Systems Considered for Failure Data

The aircraft initially considered as candidates for service failure data included as many of the systems as possible which the Air Force has in its present inventory or has maintenance responsibility. The objective

of such a broad preliminary survey was to permit the maximum insight into the historical nature of structural failures in Air Force aircraft and select those systems and component failures which offered the best potential for investigation and analysis. This aircraft system selection represented a complete cross-section of aircraft type, mission and accumulated flight time. Although the primary survey interest was in the Air Force fixed wing fleet, other systems such as commercial aircraft and military helicopters were briefly investigated.

A list of those aircraft initially considered for the survey and failure data gathering is summarized in Table I. The aircraft are grouped into general mission categories to permit classifying failure data and comparing similar service operation even though specific mission profiles may vary within each group, or aircraft system itself. Thus, specific component failures and statistical tabulations can be presented without identifying specific aircraft.

The extent of failure data necessary for analysis development and the program limitations required that the number of aircraft systems be reduced to a representative group which would be sufficient and of greatest value for failure data gathering and analysis. Those aircraft which were selected for investigation of structural failures to various degrees throughout this program are listed in Table II. The fighter and trainer categories are combined because of similar structural components and flight operation. These aircraft were selected because they represented the major Air Force systems in the present fleet, the complete range of material/structural

TABLE I. AIRCRAFT CONSIDERED FOR DATA GATHERING

TRAINERS	FIGHTERS	BOMBERS	CARGO	COMMERCIAL JET	HELICOPTERS
T-33 T-37 T-38 T-39	A-37 F-4 F-5 F-86 F-100 F-101 F-102 F-104 F-105 F-106 F-111	B-52 B-57 B-58 B-66	C-5 C-7 C-9 C-119 C-123 C-124 C-130 C-133 KC/C-135 C-140 C-141	B-707 B-720 B-737 DC-8 DC-9 880	UH-1 CH-3 H-21 HH-43

TABLE II. AIRCRAFT SYSTEMS INVESTIGATED

FIGHTERS & TRAINERS	BOMBERS	CARGO	COMMERCIAL JET	HELICOPTERS
F-4 F-100 F-101 F-105 T-37/A-37 T-38/F-5	B-52 B-58	C-130 C-133 KC/C-135 C-141	B-707 B-720 DC-9	UH-1 CH-3 HH-43

concepts and current interests for investigation of structural failure problems. Also, these aircraft offered the complete spectrum for purposes of statistical evaluation and the best possibility of detailed and specific failure documentation for purposes of analysis development. The commercial jet aircraft were selected on the basis that they represented similar or identical structural components to the Air Force cargo versions, which would permit comparison of different operational and maintenance characteristics. The complete range of accumulated flight hours from "low-time" to "high-time" are of interest to assess the historical nature of early life structural failures, however, new inventory aircraft with little operational experience were not considered. It was concluded that the aircraft systems in Table II would give the best overall insight into the failure characteristics of the total Air Force fleet and comparison with similar aircraft. These aircraft appeared to offer the greatest potential for obtaining the maximum amount of early life structural data for statistical tabulation and analysis development.

2. Data Sources Solicited

The failure information gathered for analysis and statistical development was obtained from various Government and industry organizations which were directly concerned with aircraft structural failure problems. Much of the failure information was gained from direct contact with these organizations and from correspondence, documentation requests and telephone communications during the program. These sources of information are outlined as follows and represent all of the organizations contacted for failure data during the conduct of this program.

Sources Solicited for Failure Data Information

- (a) Air Force Logistics Command Hdq.
 - (1) DCS/Maintenance Engineering
Service Engineering Division (SMC)
Analysis & Utilization Systems (AUS)
Flight Safety Office (FSO)

- (b) Air Force Air Material Areas
 - (1) Warner-Robins AMA (WRAMA)
Structures Branch (WRNEA)
Systems Management (WRNH)
 - (2) Oklahoma City AMA (OCAMA)
Aeronautical Branch (OCNEA)
 - (3) Ogden AMA (OOAMA)
Structures Branch (OOEWS)
Landing Gear (OONED)
Mechanical Systems (OONEP)
Systems Management (OONET)
Metallurgical and NDT Section (OONED)
 - (4) Sacramento AMA (SMAMA)
Structures Branch (SMNEAS)
Systems Management (SM-DA)
 - (5) San Antonio AMA (SAAMA)
Aeronautical Branch (SA-NEA)

- (c) Aeronautical Systems Division Hdq.
 - (1) Airframe Subsystems Eng. (ASSE)
 - (2) C-141 SPO (ASZL)
 - (3) F-111 SPO (ASL)
 - (4) F-4C SPO (ASZ4)
 - (5) C-130 SPO (ASZL)
 - (6) T-37/A-37 SPO (ASZC)
 - (7) F-5/T-38 SPO (ASZCE)

- (d) Air Force Materials Laboratory Hdq.
 - (1) Materials Engineering (ME)

- (e) Naval Air Systems Command Hdq.
 - (1) Air Force F-4 Liaison (AF-4L)
 - (2) Fighter Aircraft Structures (FAS)

* The organization name on Survey Form 101 is the organization name used in the survey

(f) Airframe Manufacturers

- (1) Lockheed Georgia Co., Marietta, Georgia
Structural Integrity Division
Research Laboratory
- (2) The Boeing Company,
Vertol Division, Morton, Pennsylvania
Commercial Airplane Division, Seattle, Washington
Wichita Division, Wichita, Kansas
Technology Laboratory, Seattle, Washington
- (3) McDonnell-Douglas Corp., St. Louis, Missouri
Structures Engineering
Engineering Reliability
- (4) Cessna Aircraft Co., Wichita, Kansas
Military Division
- (5) Northrop-Horair, Hawthorne, California
Structures and Mechanical Systems
Structural Analysis
Landing Gear Systems
- (6) North American-Rockwell, Los Angeles, California
Structures Division
Structural Fatigue
Materials and Processes

(g) Aerospace Industry Association (AIA)

- (1) Civil Aviation Division, Washington, DC

(h) Air Transport Association (ATA)

- (1) Engineering Division, Washington, DC

(i) Federal Aviation Administration (FAA)

- (1) Washington, DC
Flight Standards Service (FS-123)
Maintenance Division (FS-310)
- (2) Oklahoma City, Aeronautical Center
Maintenance Branch
Maintenance Analysis Center

(j) Commercial Airlines, Maintenance & Engineering Division

- (1) Air West, San Francisco, California
- (2) American Airlines, Tulsa, Oklahoma
- (3) Braniff Airways, Dallas, Texas
- (4) Continental Airlines, Los Angeles, California
- (5) Pan American World Airways, New York, New York
- (6) Southern Airways, Atlanta, Georgia
- (7) Trans-Texas Airways, Houston, Texas
- (8) Trans World Airlines, Kansas City, Missouri
- (9) Delta Airlines, Atlanta, Georgia
- (10) Eastern Airlines, Miami, Florida
- (11) Northwest Airlines, St. Paul, Minnesota
- (12) Ozark Airlines, St. Louis, Missouri
- (13) United Airlines, San Francisco, California
- (14) Western Airlines, Los Angeles, California

Although these organizations were the primary sources for failure data, it was found that detailed information on any one particular failure was very difficult to obtain, even from those organizations that directly handled the investigation and solution of the specific failure problem. Numerous contacts were made with many individuals in these organizations in order to gather the information contained in this report.

The initial sources solicited were Air Force maintenance and engineering organizations with subsequent contacts made with the manufacturers of the various military aircraft. For commercial aircraft, initial contact was made with the FAA, AIA and ATA with subsequent contacts made with the air carriers and aircraft manufacturers. Only the B-707, B-720 and DC-9 were considered in data gathering because of their similarity to Air Force aircraft. The more substantial and detailed data for failure analysis development was obtained from Air Force maintenance and engineering sources and several aircraft manufacturers. The other failure information obtained was sufficient only for statistical evaluation purposes.

3. Data Request Format and Procedures

The data gathering efforts on the program were directed toward two areas. (1) general fleet failure information for statistical evaluation and (2) detailed failure documentation on individual structural components for analysis development. Although both areas were concerned with the same aircraft component areas and types of failure the depth of data requested was significantly different. For the aircraft identified in Table II failure information was limited to the specific aircraft component areas defined in Table III which were of a primary or secondary structural nature. This program investigation did not include: engine components, mechanical fasteners, non-metallic materials, adhesive bonded joints, wheels, brakes, control linkages or fuselage accessories. Further, the failure information of interest was concerned with cracking or fracture of metal components as the result of aircraft operation or environmental exposure.

The general failure data gathering for the statistical evaluation phase of the program was concerned with identification of individual structural failures for all aircraft systems considered and over a maximum operating time period. The type of data for this phase is summarized in the following checklist.

1. AIRCRAFT DESCRIPTION:
 - a. Aircraft System (F-100, B-52, C-130, etc)
 - b. Model (A, B, C, RC, etc)
 - c. Aircraft Number
 - d. Flight Hours
 - e. Number of Landings

II. COMPONENT IDENTIFICATION

- a. Part Name and Location
- b. Part Number
- c. Structural Use
- d. Material Designation (7075, 4340, etc.)
- e. Part Form (forging, casting, etc.)
- f. Processing/Treatments Performed

III. FAILURE DESCRIPTION

- a. Origin of Failure (the crack initiation point, a bolt hole, internal flaw, etc.)
- b. Failure Mode (fatigue, stress corrosion, etc.)
- c. Contributing Influences (corrosion, poor surface condition, etc.)
- d. Environmental Factors (humid, cold, salt water, etc.)

The data for the statistical analysis was obtained from AFM-66-1 data bank, Emergency Unsatisfactory Reports/Unsatisfactory Reports, Incidence Reports, Mechanical Reliability Reports (FAA) and individual failure documentation. These sources of failure data were used to identify the more significant and interesting component failures for subsequent data gathering in providing information for the detailed failure analysis development.

The AFM 66-1 data system which is maintained by the Air Force Logistics Command (AFLC) contains fleet maintenance historical data on all aircraft in the Air Force inventory. This maintenance data is submitted by the operating Commands to AFLC Headquarters for magnetic tape data storage. Various data retrieval programs are conducted to extract desired data from these random access tapes. In general, the only component failure information this data contains is the indication that a failure occurred in a specific location on a given aircraft, with the failed part

**TABLE III. STRUCTURAL COMPONENTS INCLUDED
IN THIS PROGRAM**

LOCATION ON AIRCRAFT	COMPONENT
Fuselage	Skins and Plates Stringers Bulkheads Frames
Empennage	Vertical Stabilizers Horizontal Stabilizers Skins and Plates Frames Attachment Fittings Control Surface Structures
Wings	Skins and Plates Spars and Longerons Main Frame Control Surface Structures
Landing Gear	Axles and Struts Mechanical Linkages Actuator Cylinders Attachment Fittings Doors
Other	Actuator Cylinders Engine Mounts Nacelles Pylon Attachments

number sometimes identified. This data is selective enough, however, to sort out the type of data which is of particular interest in the statistical phase of this program. The specific information requested from the AFM 66-1 data system is identified in Table IV.

Another form of failure information reviewed was the Emergency Unsatisfactory Report (EUR) or Unsatisfactory Report (UR). These reports are prepared by operating commands when significant component failures occur and contain the same information as the AFM 66-1 report plus additional data in the form of failure comments. These comments give information on airframe hours, number of landings, and particulars about the component failure. The EUR/UR files were examined at AFLC Headquarters and included all Air Force systems identified in Table II. These reports were considered to be more valuable in identifying significant structural component failures than the AFM 66-1 data, and provided an identification of failures to examine in greater detail.

The Mechanical Reliability Reports (MRR) of the Federal Aviation Administration were reviewed for the purpose of obtaining statistical data on several commercial aircraft systems.

This MRR data was stored chronologically on microfilm and required manual searching. There was considerably less data than that of the 66-1 information however it was sufficient for statistical purposes. The data contained in these reports included: aircraft type and model, airline operator, date of failure, failed component location, part number, type of failure, airframe hours and some failure description or comments.

TABLE IV. AIR FORCE MANUAL 66-1 INFORMATION

NAME	SAMPLE ENTRY	EXPLANATION
Aircraft System	RF-4C	Aircraft type and model designation
Aircraft Serial No.	64-0653	Tail number of the particular aircraft
Part Number	3P22542-139	Number designation of the failed part
Work Unit Code	1308A	Identifies the system category (13), subsystem (D) and component (8A) which required maintenance
Suffix Code	C6	Identifies aircraft system and/or user
How-Malfunction Code	190	Identifies cause of failure
Date	28019	Date of report to AFLC in Day (28), Month (01), Year (9)
Type Maintenance	P	Identifies the type of maintenance performed on the component
Command Code	Q	Command under which aircraft is operated
Work Center Code	Q3345	Where work was accomplished
Action Taken Code	F	What was done to failed component
When Discovered Code	H	When the failure was discovered
Time to Repair	0035	Number of tenths of hours to repair failure or conduct maintenance

The comments were usually very brief with many reports only giving the general location of the failure and crack length.

The detailed failure data gathering for the development of an improved analysis, which is presented in Section III, was directed toward collection of documentation on specific components. This data was obtained from various files and records of fleet engineering and maintenance organizations, and aircraft manufacturers. Selection of these individual failures was based on the identification of repeated failures during the statistical data gathering phase and identification of the more completely documented component failures. Of particular interest were comprehensive failure reports; including metallurgical reports, failure investigation documents, micro/macro-photographs and descriptions of the circumstances surrounding the failure. The following outline is a comprehensive checklist of the information required for a thorough fracture mechanics failure analysis and determination of environmental influence. Those headings marked with an asterisk are of primary importance in the analysis development, while the others can be deleted without impairing the strength of the analysis although they could be useful in checking or correcting inconsistencies in the primary results and identifying environmental effects.

CHECKLIST FOR DETAILED COMPONENT FAILURE

DATA GATHERING

*I. COMPONENT DESCRIPTION

A. Size, shape, dimensions

B. Part photographs and/or drawings

II. COMPONENT MANUFACTURING PROCESSES

- * A. Forged, cast, machined, spun, rolled, combination fabrication
- * B. Joining method (welded, brazed, bolted, bonded, etc)
- * C. Surface treatment
 - *1. Shot peening and other deliberate compressive surface stresses to component
 - *2. Manufacture induced residual stresses
 - a. In a large section (thermal or transformation)
 - b. Due to welds
 - 3. Pickling or other cleaning treatments
 - 4. Cadmium plating and/or other hydrogen charging process

III. COMPONENT METALLURGY

- *A. Component material
 - 1. Alloy compositional variations within specifications
 - a. Interstitial content (titanium alloys)
 - b. Carbon, phosphorus and sulfur content (steels)
 - c. Other tramp elements in alloys
- B. Melting practice and ingot breakdown
 - 1. Techniques to improve purity (vacuum degassing, electric melting, etc)
 - 2. Cross rolling or unidirectional rolling
- C. Heat Treatment
 - 1. With hardness, mechanical property tests and metallographic sections attempt to answer the following:
 - a. Was tempering temperature correct (steels)
 - b. Was aging temperature correct (Al and Ti alloys)
 - c. Was 500 and 850°F embrittlement present (steels)
- D. Microstructure
 - 1. Mechanical fibering and banding from chemical segregation
 - 2. Grain size and shape

- a. Elongated with respect to stress axis
- b. Grain run-out in machined forgings and mill stock

E. Anisotropy

1. If possible, with available material determine K_{IC} , K , yield strength and elongation with respect to critical flaw orientation

*IV. STRESS STATE FOR COMPONENT

A. Type of stresses

1. Magnitude of stress levels (design stress)
2. Type of stress (e.g., Mode I, II, III or combinations)
3. Presence of stress gradients
4. Magnitude or possibility of fit-up stresses

*B. State of stress - plane strain vs plane stress

1. From fracture surface appearance (shear lip percent)
2. From calculations of estimated plastic zone/thickness ratio

*C. Effect of load variation (time and loading frequency)

1. Hours of flying time
2. Flight profiles
3. Cyclic loads
4. Single or multiple overloads (wind gusts and landings)
5. Random loading

V. MACRO AND MICROSCOPIC EXAMINATION OF FRACTURE SURFACE

A. Critical flaw leading to fracture

- *1. Location of critical flaw by macroscopic examination
- *2. Critical flaw size, shape and orientation before instability
- *3. Macro- or micro- evidence of fatigue and/or corrosive attack (e.g., rust, beach marks, etc)
4. Surface or imbedded flaw (evidence of fretting)
5. Direction of crack propagation (chevron markings, beach marks)

*B. Manufacturing flaws

1. Scratches
2. Undercuts

3. Weld defects (geometrical, hot or cold cracks)
4. Misfit components

***C. Metallurgical flaws**

1. Inclusions
2. Large second phase particles
3. Entrapped slag
4. Voids
5. Weak internal interfaces

***D. Fractographic observations**

1. Mechanism(s) of failure (dimpled rupture, cleavage, quasi-cleavage, intercrystalline fracture, fatigue striations)

VI. SERVICE INFORMATION

A. Aircraft location and conditions

1. Weather experience (home base or enroute)
2. Cold weather de-icing chemicals
3. Water or salt water environment
4. Oils and fuel

B. Overhaul information

1. Cleaning fluids
2. Refurbishing procedures

This failure data gathering format was used during survey and selection phases of the program. In order that the data might be arranged for easier handling and sorting, data sheet formats were used as a means of compiling information. Formats for these data sheets are presented in Figures 1, 2 and 3.

DATA SOURCE/STATUS CARD

<p>Aircraft Type _____</p> <p>Serial Nr. _____</p> <p>Agency _____</p> <p>Manufacturer _____</p> <p>Data Source _____</p> <p>Location _____</p> <p>Department _____</p> <p>Contact _____</p> <p>File Ref. _____</p>	<p>Part Nr. _____</p> <p>Name _____</p> <p>Data Worksheet Nr. _____</p> <p>Review Priority (1 to 10) _____</p> <p>Total Reported Failures _____</p> <p>Nr. Failures Analyzed _____</p> <p>Data Acquisition Date _____</p> <p>Reviewed by _____</p>
<p>Remarks: _____</p>	
<p><input type="checkbox"/> Reference Data on File <input type="checkbox"/> Worksheet Completed <input type="checkbox"/> Reviewed by Del</p>	

Figure 1. Card for Identifying Survey and Processing Status

A/C Type _____		Agency _____		A/C Code _____	
Manufacturer _____					
PART I - AIRCRAFT IDENTIFICATION AND INFORMATION					
Model Designations:					
<u>Model Nr.</u>	<u>A/C Nr. (Inclusive)</u>	<u>Qty. Prod.</u>	<u>Present Inv.</u>	<u>Flight Hr. Range</u>	
Mission Description (General):					
Flight Profile - <input type="checkbox"/> On File <input checked="" type="checkbox"/> Available <input type="checkbox"/> Unknown					
Operational Failure Item List:					
Static & Fatigue Test Programs:					
Tests Performed:					
References:					
Information Sources:					
Airframe -					
Landing Gear -					
Subsystems -					

Figure 2. Aircraft Summary Sheet

Preparation Date _____	Prepared by _____	Priority _____		
PART II - COMPONENT DESCRIPTION				
Part Nr _____	Part Code _____			
Part Name _____				
Location on A/C _____				
Material _____	Heat Treat _____	Specification _____		
Part Form _____	Part Manufacturer _____			
Metallurgical/Processing Conditions _____				
Surface Treatment _____				
PART III - COMPONENT DESIGN FACTORS				
Structure Function:	<input type="checkbox"/> Primary	<input checked="" type="checkbox"/> Secondary	<input type="checkbox"/> Subsystem	<input type="checkbox"/> Unknown
Design Stress:				
Magnitude _____	Type _____			
Loading Mode _____	<input type="checkbox"/> Static	<input checked="" type="checkbox"/> Cyclic	<input type="checkbox"/> Combination	<input type="checkbox"/> Unknown
Design Life _____	Load Factor _____	Safety Factor _____		
Proof Tests Conducted _____				
Other Considerations _____				
Component Modification:				
<input type="checkbox"/> Design Changes				
<input type="checkbox"/> Material Change				
<input type="checkbox"/> Fabrication Change				
<input type="checkbox"/> Other				
PART IV - COMPONENT FAILURE HISTORY				
Total Reported Failures _____	Nr Parts per A/C _____			
Nr Failures Reviewed _____	Date of Last Failure _____			
Failure Classification	<input type="checkbox"/> Isolated Instance	<input type="checkbox"/> Recent Failure		
	<input type="checkbox"/> Frequent Occurrence	<input type="checkbox"/> Unknown		
Failure Summary _____				
PART V - SUPPORTING INFORMATION				
On Hand:	<input type="checkbox"/> Failure Report	<input type="checkbox"/> Metallurgical Report	<input type="checkbox"/> Failed Part	
General Documentation or References:				
On File -				
Available -				

Figure 3. Item Summary Worksheet

B. Failure Data Compilation

The failure data survey, screening and compilation phases of the program involved processing data in various formats and from numerous sources. Also the number of aircraft systems considered for data gathering required certain categorizing and grouping to be established for tabulation and statistical purposes. For the most part, the different types of data (i.e., AFM 66-1, MRR, EUR/UR and individual Failure Documentation) required different processing procedures and compilation methods. The individual data description and processing procedures for these various types of data are described in the following paragraphs.

1. AFM 66-1 Data

The primary purpose for reviewing and compiling Air Force 66-1 data was to obtain a general identification of the total fleet structural component failures for statistical evaluation. The 66-1 data storage system offered a centralized source which permitted rapid extraction and sorting of selected component failures for specific aircraft systems and failure reporting periods. The failures reported in this system were not of sufficient detail to enable consideration for the failure analysis development phase of this program.

The 66-1 data, being in a different form than other data, was handled separately. The magnetic tape data was obtained from the Air Force maintenance data bank and contained data records on the Air Force aircraft identified in Table II for the reporting period August 1968 to January

1969. Only selected structural component categories and certain failure causes were extracted from the master file and entered on the master tape. Although the initial request was for failure data records for the complete operating lifetime of the aircraft, only the above six-month period was obtained since the master tape search time and number of entries was extensive. The resulting tape for the 15 systems selected contained approximately 234,660 data records, although not all were failures in the specific categories of interest.

The Air Force Manual 66-1 data is maintained primarily for fleet maintenance and reliability records and corrective action. By using certain portions of this data record, aircraft component failures can be identified and tabulated. A listing of those 66-1 data entries which were of interest in this program are summarized in Table II, which describes more fully the information of Table IV. Further breakout of the selected aircraft systems by Suffix Code are presented in Table III and Table IV, various models and utilization which are coded separately for 66-1 data storage. A complete Work Unit Code (WUC) description for each aircraft system is contained in a "Work Unit Code Manual" which contains several sample pages are shown in Figure 4 and Figure 5. The category identifier (the first two digits) are identical for all systems in a category. The last three digits may represent different components for different aircraft. These 66-1 entries and codes were, therefore, used to identify and categorize component failure data for statistical analysis.

During the processing of the 66-1 data, three programs were used. These three programs were:

TABLE V. PERTINENT AFM 66-1 DATA ENTRY CODE INFORMATION

DATA ENTRY	DESCRIPTION OR CATEGORY
Aircraft System	Suffix codes listed in Table VI
Work Unit Code	Per Work Unit Code Manual (Figures 4 & 5): 11000 - Airframe 13000 - Landing Gear 14000 - Flight Control (Structure) 23000 - Engines (Supports & Mounts)
Part Number	Technical Order Part Designation
How Malfunction Code	Type of discrepancy or failure: 070 - Broken 190 - Cracked
Type Maintenance Code	Maintenance performed on part: A - Service B - Unscheduled Maintenance C - Postflight & Thruflight Inspection D - Preflight or Scheduled Inspection P - Periodic, Phased or Major Inspection R - Depot Maintenance
Action Taken Code	Type of maintenance action: D - Bench Checked G - Repair and/or Replace P - Removed Only R - Removed and Replace with New Part
When Discovered Code	When failure was found: A - Before Flight (Abort) B - Before Flight (No Abort) C - In-flight (Abort) D - In-flight (No Abort) E - After Flight F - Between Flights (Ground Crew) H - Post Flight Inspection J - Preflight Inspection M - Periodic/Phased/Major Inspection Q - Special Inspection S - Depot Level Maintenance U - Non-Destructive Inspection

TABLE VI. AIRCRAFT SUFFIX CODES OF INTEREST FOR DATA RETRIEVAL

AIRCRAFT SYSTEM	SUFFIX CODE	AIRCRAFT SYSTEM	SUFFIX CODE
C-141A	CH	C-133	CU
C-141A LTF*	C8	C-133A 60th MAW	03
C-141A 60th MAW	01	C-133B 60th MAW	04
C-141A 62nd MAW	12	C-133A 436th MAW	32
C-141A 437th MAW	27	C-133B 436th MAW	33
C-141A 436th MAW	30		
C-141A LTF* 60th MAW	50	RC-135 C&H	CA
C-141A LTF* 436th MAW	51	C-135A & RC-135A	CV
C-141A LTF* 437th MAW	52	KC-135A	CX
C-141A 58th MAS	53	KC-135A LTF*	CI
C-141A 63rd MAW	54	WC-135B	C5
C-141A 438th MAW	55	EC-135N	EA
		KC-135Q	EB
C-130A & D, RC-130	CF	EC-135A,G,H,K,P	ED
C-130E	CH	RC-135D & S,	
C-130B	CR	KC-135R	
AC-130A	C6	EC-135C & J,	EE
HC-130H & P	C7	RC-135E	
WC-130A,B,E	C9	C-135B	EF
C-130E 60th MAW	06	EC-135L	EH
C-130E UR-8 MATW	10	C-135B 60th MAW	05
C-130E 438th MAW	21	C-135A 61st MAW	09
C-130E 477th MAW	30	C-135A 438th MAW	23
		C-135B 438th MAW	24
B-52C	BC	C-135B 89th MSMW	40
B-52E	BE		
B-52F	BF	F-105D	FK
B-52G	BG	F-105B	FM
B-52A, B	BL	F-105F	FR
B-52D	BN		
B-52H	BP	F-5	FX
B-58	BQ	T-38	TF
B-58 LTF* POD	BS	T-38 LTF*	TT
B-58 LTF*	BY		
B-58 POD	BZ	CH-3C, CH-3E, HH-3E	HH
		CH-3B	HU
F-4C	FP	HH-43	HG
F-4D	FS		
F-4E	FT	F-100	FE
RF-4C	FW		
F-4C LTF*	FY	F-101B,F	FF
F-4D LTF*	F9	F-101A,C	FG
		RF-101A,C	FH
		RF-101G,H	FQ

*Lead-The-Force

10-1951434-04

1354A
1354B
1354C

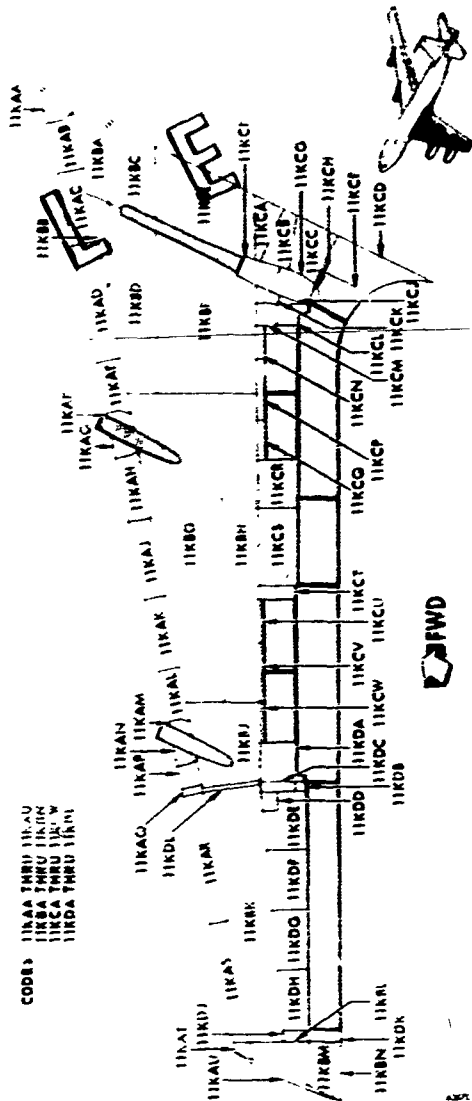
1354D SIDE STRUT
1354E STABILIZER
1354F SEAR ACTUATOR
1354G SEAR ACTUATOR
1354H PISTON ASSEMBLY
1354I LPGA ACTUATOR
1354J LPGA ACTUATOR
1354K PISTON ASSEMBLY

AIRCRAFT BASIC AIRFRAME

T.O. 1C 13XK1A 96

LEFT WING TOP SIDE SKIN PANELS

CODES
11AAA THRU 11KAD
11KBA THRU 11KBN
11KCA THRU 11KCV
11KDA THRU 11KNI



FORWARD

WORK UNIT CODE	
23000	TURBO JET ENGINE
23000	nacelle structure
23000	cone, aft nose
23000	centerbody, aft
23000	nose cone
23000	adapter,
23000	centerbody
23000	hood, access, c/s
23000	clamp
23000	assy. fwd
23000	rib seal
23000	seal assy. air
23000	blanky, heat
23000	shields, heat,
23000	upper nacelle
23000	hood, air inlet
23000	structure assy.
23000	upper nacelle
23000	lowerhood, upper
23000	nac
23000	cover plate, upper
23000	nac
23000	structure assy.
23000	lower nacelle
23000	lowerhood, lower
23000	nac
23000	splice plate,
23000	lower nacelle
23000	frame, lower nac
23000	hinge pin, lower
23000	nac
23000	nac
23000	mounts
23000	mount assy. top
23000	fwd
23000	fitting, top fwd
23000	mount
23000	clamp assy. top
23000	fwd fitting
23000	link assy. top fwd
23000	mount
23000	mount assy. lh fwd
23000	fitting, nac.
23000	fwd
23000	link assy. lh
23000	mount
23000	mount assy. e/c
23000	aft lh
23000	bracket assy. aft
23000	lh
23000	fitting, aft lh
23000	mount
23000	link assy. aft lh
23000	mount
23000	bracket assy. aft
23000	oh
23000	fitting, aft oh
23000	mount
23000	link assy. aft oh
23000	mount

SECTION 1	
14000	FLIGHT CONTROL
14000	ELEVON ASSEMBLY
14000	INSTALLATION
14000	(CONTINUED)
14000	FITTING, EXPANSION
14000	INTERMEDIATE
14000	ELEVON
14000	FITTING, EXPANSION
14000	INTERMEDIATE
14000	ELEVON
14000	FITTING, JOINT, IN
14000	ELEVON
14000	BUSHING, JOINT FIT
14000	PIN, HINGE
14000	BUSHING, PIN, ACTU
14000	ATTACH. BUSHING, ATTACH P
14000	FITTING, SPAR SPL
14000	ELEVON
14000	FITTING, SPAR SPL
14000	INTERMEDIATE
14000	ELEVON
14000	FITTING, SPAR SPL
14000	INTERMEDIATE
14000	ELEVON
14000	SPAR, FWD
14000	SPAR, FWD
14000	SPAR, REAR
14000	RIB, US
14000	RIB, US
14000	RIB, US
14000	RIB, US
14000	RIB, LEA
14000	STRUT, LE
14000	EDGE
14000	FITTING, ELEVON H
14000	ACTUATOR
14000	FITTING, ELEVON H
14000	OUTBO
14000	WEBBE
14000	DOUBLER
14000	NOC
14000	ELEVON S
14000	LH INTER

SECTION 1	T.O. 18-50A-06		WORK UNIT CODE	
11000	AIRFRAME	11000	FLOOR ASSEMBLY	
11000	LOCKING MECHANISM	11000	FLOOR ASSEMBLY	
11000	(CONTINUED)	11000	FLOOR ASSEMBLY	
11000	LATCH	11000	FLOOR ASSEMBLY	
11000	LONG DRAW SPRING	11000	FLOOR ASSEMBLY	
11000	STOPPING	11000	FLOOR ASSEMBLY	
11000	STOPPING	11000	FLOOR ASSEMBLY	
11000	TOPPLE WIRE	11000	FLOOR ASSEMBLY	
11000	NOC	11000	FLOOR ASSEMBLY	
11000	CANOPY EJECTION MECHANISM	11000	FLOOR ASSEMBLY	
11000	HANDLE	11000	FLOOR ASSEMBLY	
11000	ARM	11000	FLOOR ASSEMBLY	
11000	STOP PLATE	11000	FLOOR ASSEMBLY	
11000	ROCKERS BEARING	11000	FLOOR ASSEMBLY	
11000	LATCH HINGE DISCONNECT	11000	FLOOR ASSEMBLY	
11000	DAMPER	11000	FLOOR ASSEMBLY	
11000	BRACKET	11000	FLOOR ASSEMBLY	
11000	NOC	11000	FLOOR ASSEMBLY	
11000	CANOPY EJECTION MECHANISM (EXTERNAL)	11000	FLOOR ASSEMBLY	
11000	HANDLE	11000	FLOOR ASSEMBLY	
11000	CABLE	11000	FLOOR ASSEMBLY	
11000	CLIPS (2 - 1/2)	11000	FLOOR ASSEMBLY	
11000	NOC	11000	FLOOR ASSEMBLY	
11000	BUSHING GEAR	11000	FLOOR ASSEMBLY	
11000	STOP	11000	FLOOR ASSEMBLY	
11000	RIDE GEAR	11000	FLOOR ASSEMBLY	
11000	STRUT BAR (ATTACHED)	11000	FLOOR ASSEMBLY	
11000	PIP PIN	11000	FLOOR ASSEMBLY	
11000	SWIV	11000	FLOOR ASSEMBLY	
11000	STOP ASSEMBLY	11000	FLOOR ASSEMBLY	
11000	HINGE	11000	FLOOR ASSEMBLY	
11000	STRUCTURE	11000	FLOOR ASSEMBLY	
11000	LINK	11000	FLOOR ASSEMBLY	
11000	BRACKET	11000	FLOOR ASSEMBLY	
11000	LOCKING MECHANISM	11000	FLOOR ASSEMBLY	
11000	CABLE	11000	FLOOR ASSEMBLY	
11000	NOC	11000	FLOOR ASSEMBLY	
11000	PIA GEAR (GROUP 11)	11000	FLOOR ASSEMBLY	
11000	SWIV	11000	FLOOR ASSEMBLY	
11000	STOP ASSEMBLY	11000	FLOOR ASSEMBLY	
11000	(INTERNAL)	11000	FLOOR ASSEMBLY	
11000	HINGE	11000	FLOOR ASSEMBLY	
11000	STRUCTURE	11000	FLOOR ASSEMBLY	
11000	HINGE PIN	11000	FLOOR ASSEMBLY	
11000	LOCKING MECHANISM	11000	FLOOR ASSEMBLY	
11000	ONE	11000	FLOOR ASSEMBLY	
11000	LINK	11000	FLOOR ASSEMBLY	
11000	BRACKET	11000	FLOOR ASSEMBLY	
11000	NOC	11000	FLOOR ASSEMBLY	
11000	PIA GEAR (GROUP 11)	11000	FLOOR ASSEMBLY	
11000	STOP ASSEMBLY	11000	FLOOR ASSEMBLY	
11000	(ATTACHED)	11000	FLOOR ASSEMBLY	
11000		11000	FLOOR ASSEMBLY	

Figure 5. Sample Work Unit Code Manual Pages

- a. RCCT (Identify data format and content)
- b. SELECT (Retrieval of all data records for a given aircraft)
- c. MUCCOL (Similar to SELECT plus the feature of tabulating each structural component category)

These will be described in the order in which they were used in the data processing.

Since the 66-1 data system utilizes about ten different data record formats, it was necessary to identify these formats and decode the magnetic tape. The program RCCT, which was previously written, was used to determine these formats. RCCT is a very simple program which reads the data on the tapes and prints it out in block form no matter what the format. The output of this program revealed that only three of the ten formats were used in the data records of interest to this retrieval effort. Additional detail on RCCT description, program and sample printout is presented in Appendix A-I. The RCCT program output permitted a more selective and precise computer retrieval program to be prepared and employed which minimized manual screening of data printout.

Program SELECT was written to provide a highly selective retrieval of all data records for a single aircraft system, or any number of systems. This program was written to get a better idea of the quantity and kind of data available on each aircraft system. This program also provided an insight for preparing and evaluating techniques for retrieving the 66-1 data in its most useful form and eliminate extraneous or unnecessary data records. Additional detail on program SELECT description

and sample printout is presented in Appendix A-II. The information from this program was used to prepare the final computer program.

Program MUCCOL is similar to SELECT, however, it is much more specific in identifying and grouping of structural component categories. In MUCCOL the computer searches the data records not only for a specific aircraft system but for specific Work Unit Codes which indicate the location of the failed part on a given aircraft. Once this search is completed the output of the program is twofold. First, every data record for that particular aircraft system with the selected Work Unit Code is printed out individually. Secondly, after this printout, a tabulation of the Work Unit Codes encountered with the number of occurrences for each is printed out. This final tabulation provides the basis for the statistical analysis. Further detail on program MUCCOL description and sample printouts are contained in Appendix A-III.

2. Mechanical Reliability Report (MRR)

The MRR data system is maintained by the FAA at Oklahoma City for the purpose of identifying failure or maintenance problem areas on the commercial aircraft. For this program, certain structural component areas of the B-707, B-720 and DC-9 were screened for failure data. The data was limited to these systems as they represented similar or identical structural components to those of the Air Force KC/C-135 and C-9 aircraft. Failure data was categorized similar to the AFM 66-1 system, however, not as detailed. The general categories in which failure data was gathered were: (1) Landing Gear (Code 32),

(2) Fuselage (Code 53) and (3) Wings (Code 57). Components identified as fractured, cracked or broken were manually screened and tabulated. Due to program survey limitations, only MRR records submitted to FAA during the January 1967 to October 1968 time period were reviewed. For each such failure the following information was recorded:

- (a) Microfilm entry frame number
- (b) Aircraft type and model
- (c) Airline operator
- (d) Failed part category and description
- (e) Airframe flight hours.

Information on material identification, cause of failure or failure mode were not available.

3. Unsatisfactory Report (EUR/UR) Data

The Air Force EUR/UR system offered a central source for identification of specific structural component failures on the selected aircraft. Individual reports are submitted by the fleet operating organizations on significant failures which are not described in maintenance manuals or T.O.'s. The same aircraft and component categories and codes as the AFM.66-1 system are used in the EUR/UR reporting, however, manual searching was required. The screened and tabulated data on each system contained the following information:

- a. EUR/UR Number
- b. Aircraft model, type and serial number

- c. Part Number
- d. Airframe flight hours
- e. Fracture description (crack length, location, etc.)

The EUR/UR files were reviewed for the reporting period January 1967 thru September 1968. This corresponds to the similar reporting period for the MRR data.

4. Detailed Failure Data Documentation

The various component failure reports and information were obtained from a wide variety of sources. This detailed failure documentation gathered included:

- a. Component failure reports
- b. Failure investigation reports
- c. Metallurgical reports
- d. Component test reports (static or fatigue)
- e. Stress analysis reports
- f. Flight loads reports
- g. Component drawings/photographs.

This detailed failure data was gathered only on military aircraft and on structural components which contained significant documentation in these above areas. A schematic of the data handling sequence is presented in Figure 6. The Checklist previously described on pages 17 thru 20 and Data Forms in Figures 1, 2 and 3 were utilized in screening, compiling and cataloging the various failure information. Aircraft and failed

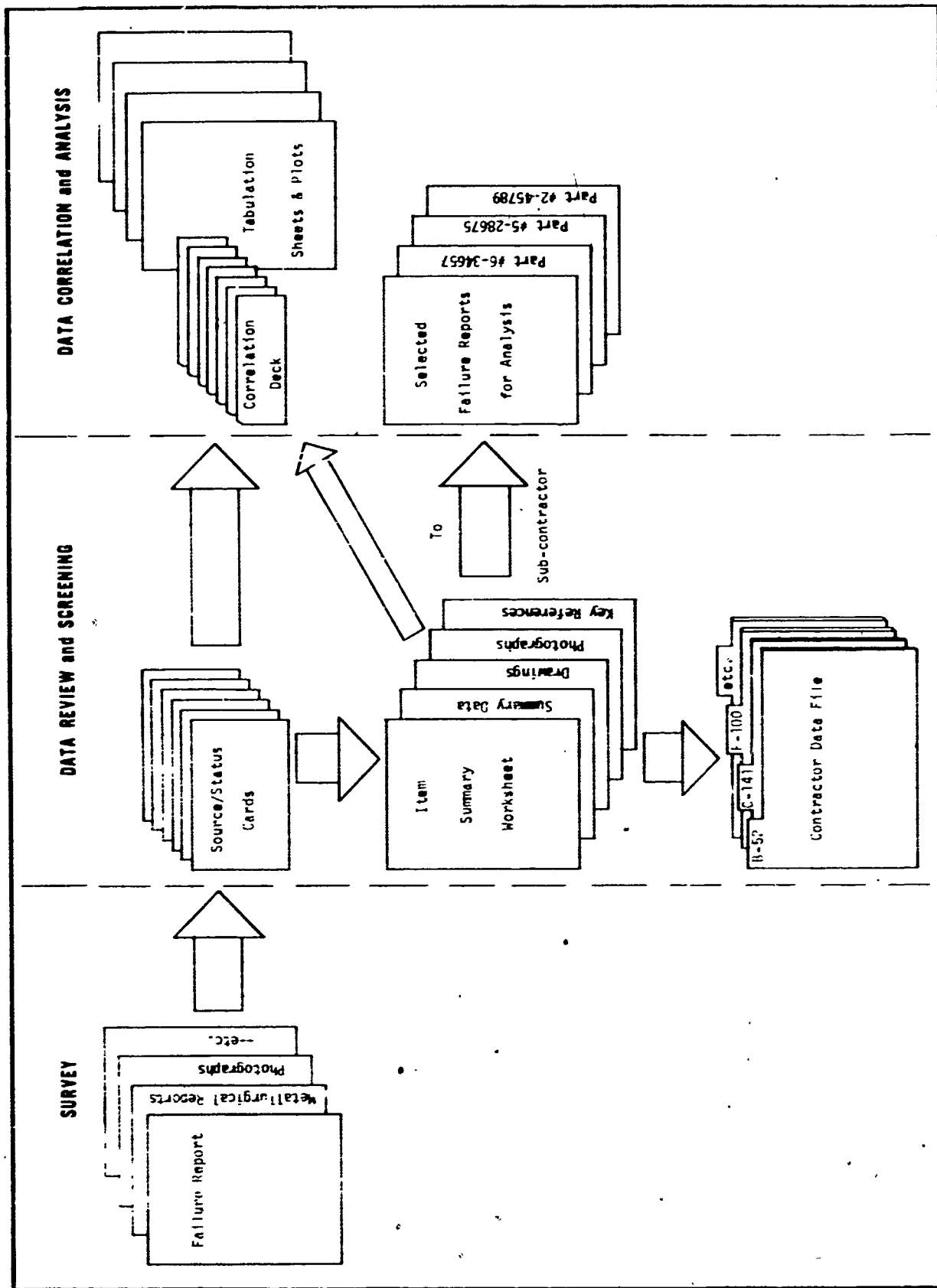


Figure 6. Detailed Failure Information Processing Sequence

component identification were coded for the purpose of simplifying the component datalogging and correlating procedures. Also, failure information on each component was categorized and coded for punch card format with manual or machine sorting. This permitted rapid identification and tabulation of specific failure data in any desired category.

Individual component data packages were prepared and forwarded to the sub-contractor for analysis on those failures where more complete documentation was obtained. In all such data packages metallurgical and failure investigation reports were required. Also, actual failed parts were obtained, whenever possible, to aid in the analysis effort.

During the detailed failure data gathering and screening efforts, about 100 different types of components representing approximately 1500 individual failures were identified and categorized as containing sufficient information for correlation. In many cases, however, important or key information was not available or had not been documented in sufficient detail to permit failure categorizing or an analysis attempt. A number of the more significant or better documented component failures are contained in Section III.D. No attempt was made to include failure summary reports on all components cataloged as the content would be voluminous and much significant data, such as part photographs and photomicrographs, being non-reproducible.

5. Data Limitations and Problems

During the failure data survey, screening and classifying efforts for the statistical correlation and failure analysis development

phases of the program, a number of limitations and problems were encountered which compromised the validity and accuracy of the results. Several of these limitations or problems are worthy of mention as they reflect the content and interpretation of the program results and conclusions.

The statistical failure data obtained from the AFM 66-1, MRR and EUR/UR systems represent reported failure occurrences for specific periods of time during the operational life of the aircraft. For most aircraft systems the gathered data represented only a small segment of the total fleet structural failure history. For example, in the AFM 66-1 data searched for the six month period, if a rash of a particular type of failure occurred during this period for certain aircraft, it would bias the statistics. Also the possibility exists that fleet-wide inspection directives or technical orders might require certain parts to be inspected and replaced, and reported in the 66-1 information system during that period. There is also the possibility that a given part failure resulted in more than one entry to the 66-1 data; such as one each for inspection, removal, repair, and part replacement. The reliability of the data entry may also be questioned since it is possible to make a coding entry error or to enter an incorrect Work Unit Code if a suitable one is not immediately known.

Also, over-reporting, under-reporting or inconsistent reporting procedures may contribute to the inaccuracy or validity of the statistical results. This is also true for the MRR and EUR/UR data, although

a much longer data reporting period was utilized. Program limitations did not permit gathering extensive data for the complete operational life of the aircraft examined.

The survey and review of individual failures for detailed data correlation and analysis encountered several limitations and problems. Probably the greatest limitation was the lack of pertinent and complete data, from a fracture mechanics analysis standpoint. The type of data necessary for this analysis is not normally detailed in a failure investigation since the primary importance is the fix rather than the systematic investigation of the failure mechanism. Another related problem is that for the majority of failure histories, all data surrounding the failure was not obtainable from a single location. To obtain the complete failure history on a given part, several individuals and organizations were contacted with much of the needed information not documented but obtained through personal discussions. The investigation of a typical failure required contacts with Air Force and industry design test and maintenance engineers as well as metallurgists and management personnel. The primary data source for the various failures differed considerably, and depended on the status of production, years in inventory, organization assigned maintenance responsibility and contractor system obligations. Another problem involved the identification of the failure history and number of occurrences for a given component during the airframe operational lifetime. Transferring engineering and maintenance responsibility and changes in the aircraft base of operation made the fleet failure statistical evaluation extremely

difficult. One central source for such historical failure data was the AFM 66-1 and EUR/UR data files, however, this would require extensive data search and screening efforts.

The recording of precise and valid information on the data sheets (Figures 1, 2 and 3) presented several problems. Any one source of information generally resulted in partial or sketchy information in a number of data categories. An attempt to obtain missing data via other sources or documentation raised the problem of identifying the correct failure, part or aircraft. Thus, it was very possible that different failures, failure locations, operational histories, failure causes or environmental influences could be entered as a single, complete failure data occurrence. Also, failure data inaccuracies are possible as the result of part replacement or changes during the airframe lifetime and could involve a number of different configurations, materials, part numbers, heat treats or processing steps which appear in the documentation to represent a single component operational lifetime. Although the extent of comprehensive failure data varied widely for different component failures, generally some problems were encountered in identifying data on the following specific items:

a. Component description - Availability of part drawings or photographs.

b. Material description - Some failures contained no alloy identification, only the identification as steel, aluminum, etc. A number of failures contained no heat treatment identification and most contained no information on heat treat-fabrication steps.

c. Type of failure - Generally limited to a single cause such as fatigue, stress-corrosion, over-stress and brief identification of failure origin. Usually no description of progression through various stages of failure were described during the crack initiation and growth. Initial flaw size or dimensions were not identified in many cases. For most component failures involving a number of occurrences only the first ones were examined and documented in detail with subsequent failures resulting in little or no failure documentation, as it was assumed the same failure mode and cause applied and a like fix was sufficient.

d. Failure location - The general location on the part was identified, however, critical dimensional information was lacking.

e. Environmental conditions - With the exception of identifying atmospheric corrosion, little was noted on other possible environmental conditions prior to failure or at final failure.

f. Influencing factors - Only in a few failure occurrences were contributing factors such as: abnormal flight, landing or taxi conditions, gross weight estimates, component inspection history or maintenance history identified.

g. Aircraft history - Generally aircraft flight hours, and sometimes number of landings, were recorded for individual failures. Also, general flight loads and flight profiles were available, specific stress level estimates at the failure location were not stated or were difficult to determine.

h. Structural design - Stress analysis documentation was difficult to obtain for the older aircraft systems where the files had been retired or discarded. The identification of component redesign, engineering change or modification data and documentation was very difficult to determine.

These above problems, to varying degrees, were encountered throughout the detailed failure data gathering and screening, and generally limited the completeness and usefulness of the failure information for subsequent development of failure analysis methods utilizing fracture mechanics.

C. Failure Data Correlation

The classifying and statistical correlation of the various failure data gathered was grouped under two main headings: (1) general failure reporting and (2) significant failure occurrences. The first category consists of the AFM 66-1 and MRR data while the second category includes the tabulation of the more critical failure documentation and EUR/UR data. Because of the different form and nature of these two types of data, separate statistical correlation and tabulation efforts were conducted.

1. General Failure Data Categorizing and Correlation

a. Data Classifying and Coding

The AFM 66-1 magnetic tape data, as described in Section II.B.1, represents the military aircraft failure data from which statistical data was generated. In the categorizing and coding of structural components each Work Unit Code was examined to see what components were described and if they were pertinent to the failure data of interest. Each work unit code of interest, for each aircraft system, was listed and the number of times it appeared was tabulated. The component areas were then grouped into the categories and codes listed in Table VII. All the WUCs associated with these codes were summed under each heading to indicate the number of failures in each category. Also, incorporated into this data tabulation under the commercial jet heading was the FAA MRR data. From this tabulation a statistical analysis was conducted to indicate the areas of the aircraft which were sensitive to failure.

TABLE VII. Component Coding for General Failure Data

CODE	COMPONENT CATEGORY
1.	LANDING GEAR
1.1	Nose Gear
1.1.1	Gear Doors
1.1.2	Mechanical and Hydraulic Components
1.1.3	Gear Supports and Attachments
1.2	Main Gear
1.2.1	Gear Doors
1.2.2	Mechanical and Hydraulic Components
1.2.3	Gear Supports and Attachments
2.	FUSELAGE
2.1	Main Frame
2.1.1	Forward Fuselage
2.1.2	Center Fuselage
2.1.3	Aft Fuselage
2.2	Plates and Skins
2.2.1	Forward Fuselage
2.2.2	Center Fuselage
2.2.3	Aft Fuselage
3.	WINGS
3.1	Main Frame
3.1.1	Inboard Section
3.1.2	Outboard Section
3.1.3	Center Section
3.2	Plates and Skins
3.2.1	Inboard Section
3.2.2	Outboard Section
3.2.3	Center Section
4.	NACELLES AND PYLONS
4.1	Main Frame
4.1.1	Inboard Section
4.1.2	Outboard Section
4.2	Plates and Skins
4.2.1	Inboard Section
4.2.2	Outboard Section
4.3	Engine Attachment
4.3.1	Mounts and Fittings
5.	STABILIZERS
5.1	Horizontal
5.1.1	Frames
5.1.2	Plates and Skins
5.2	Vertical
5.2.1	Frames
5.2.2	Plates and Skins

b. Statistical Data Tabulation

The tabulation and correlation results for the AFM 66-1 and MRR data are presented in Tables VIII and IX, and Figures 7 through 12. Table VIII contains the numerical tabulation of the AFM 66-1 and the MRR data in accordance with the categories in Table VII. The five different aircraft categories consist of the systems identified earlier in Table II and includes the number of failures recorded during the particular reporting period. The statistical tabulation of the data in Table VIII is presented in Table IX for the same component categories. A graphical representation of the Table IX statistical data for each aircraft category is contained in Figures 7 through 12.

2. Significant Failure Data Categorizing and Correlation

a. Data Classifying and Coding

In the case of the comprehensive failure data, each documented failure was listed in code form to enable manual or mechanical sorting. Each failure was coded for the different aspects describing the failure, with each entry numbered to identify the component. Table X contains a list of these different codes and identifies the data categories and entry items. All failures reviewed were categorized based on parameter selection from the coding system. This allows one to identify the more significant items or areas where failures occur. The coding system format was established for use in data processing with computer card entry position identified in the last column of Table X. The complete tabulation and coding of all individual failure data reviewed and recorded during the survey effort are presented in Table XI. This

TABLE VIII. Numerical Tabulation of Failure Data from AFM 66-1 and MRR Records

CATEGORY	CARGO	FIGHTER	BOMBER	HELICOPTER	COMMERCIAL JET	TOTAL
1.1.1	296	58	0	*	7	361
1.1.2	19	234	0	*	5	258
1.1.3	0	0	0	*	4	4
1.2.1	667	520	270	*	0	1457
1.2.2	69	125	0	*	12	206
1.2.3	0	18	0	*	6	24
2.1.1	584	586	88	*	34	1292
2.1.2	1325	330	104	416	25	2200
2.1.3	2149	2650	0	0	10	4809
2.2.1	203	1881	0	94	24	2202
2.2.2	621	903	236	97	11	1868
2.2.3	112	2115	0	89	1	2317
3.1.1	970	791	1364	*	74	3199
3.1.2	486	983	68	*	45	1582
3.1.3	107	375	0	*	14	496
3.2.1	1154	714	1173	*	156	3197
3.2.2	1921	1765	412	*	96	4194
3.2.3	25	53	355	*	53	486
4.1.1	206	81	0	0	-	287
4.1.2	68	0	0	0	-	68
4.2.1	761	0	69	0	-	830
4.2.2	326	0	45	16	-	387
4.3.1	262	20	0	0	-	282
5.1.1	33	128	0	*	-	161
5.1.2	120	0	0	*	-	120
5.2.1	0	115	153	55	-	323
5.2.2	0	163	0	0	No Data Gathered	163
TOTAL	12484	14608	4337	767	577	32773

*NO CATEGORY

Table 17. Statistical Tabulation of Failure Data from AFM 66-1 and MRR Records

CATEGORY	CARGO (%)	FIG-TER (%)	BOMBER (%)	HELICOPTER (%)	COMMERCIAL JET (%)	TOTAL (%)
1.1.1	2.37	.39	.00	*	1.21	1.10
1.1.2	.15	1.50	.00	*	.86	.78
1.1.3	.00	.00	.00	*	.69	.01
1.2.1	5.34	3.55	6.98	*	.00	4.44
1.2.2	.55	.85	.00	*	2.07	.62
1.2.3	.00	.12	.00	*	1.03	.07
2.1.1	4.67	4.01	2.27	*	5.89	3.94
2.1.2	10.61	2.25	2.68	54.23	4.33	6.71
2.1.3	17.21	18.14	.00	.00	1.73	14.67
2.2.1	1.62	12.87	.00	12.25	4.15	6.71
2.2.2	4.97	6.18	6.10	12.64	1.90	5.69
2.2.3	.89	14.47	.00	11.60	.17	7.06
3.1.1	7.76	5.41	35.27	*	12.82	9.76
3.1.2	3.89	6.72	1.75	*	7.79	4.82
3.1.3	.85	2.56	.00	*	2.42	1.51
3.2.1	9.24	4.88	22.73	*	27.03	9.75
3.2.2	15.38	12.08	6.10	*	16.63	12.79
3.2.3	.20	.36	9.18	*	9.18	1.48
4.1.1	1.65	.55	.00	.00	-	.87
4.1.2	.54	.00	.00	.00	-	.20
4.2.1	6.09	.00	1.78	.00	-	2.53
4.2.2	2.61	.00	1.16	2.08	-	1.18
4.3.1	2.09	.13	.00	.00	-	.86
5.1.1	.26	.87	.00	*	-	.49
5.1.2	.96	.00	.00	*	-	.36
5.2.1	.00	.78	3.95	7.17	No Data Gathered	.98
5.2.2	.00	1.11	.00	.00	-	.49

*NO CATEGOR.

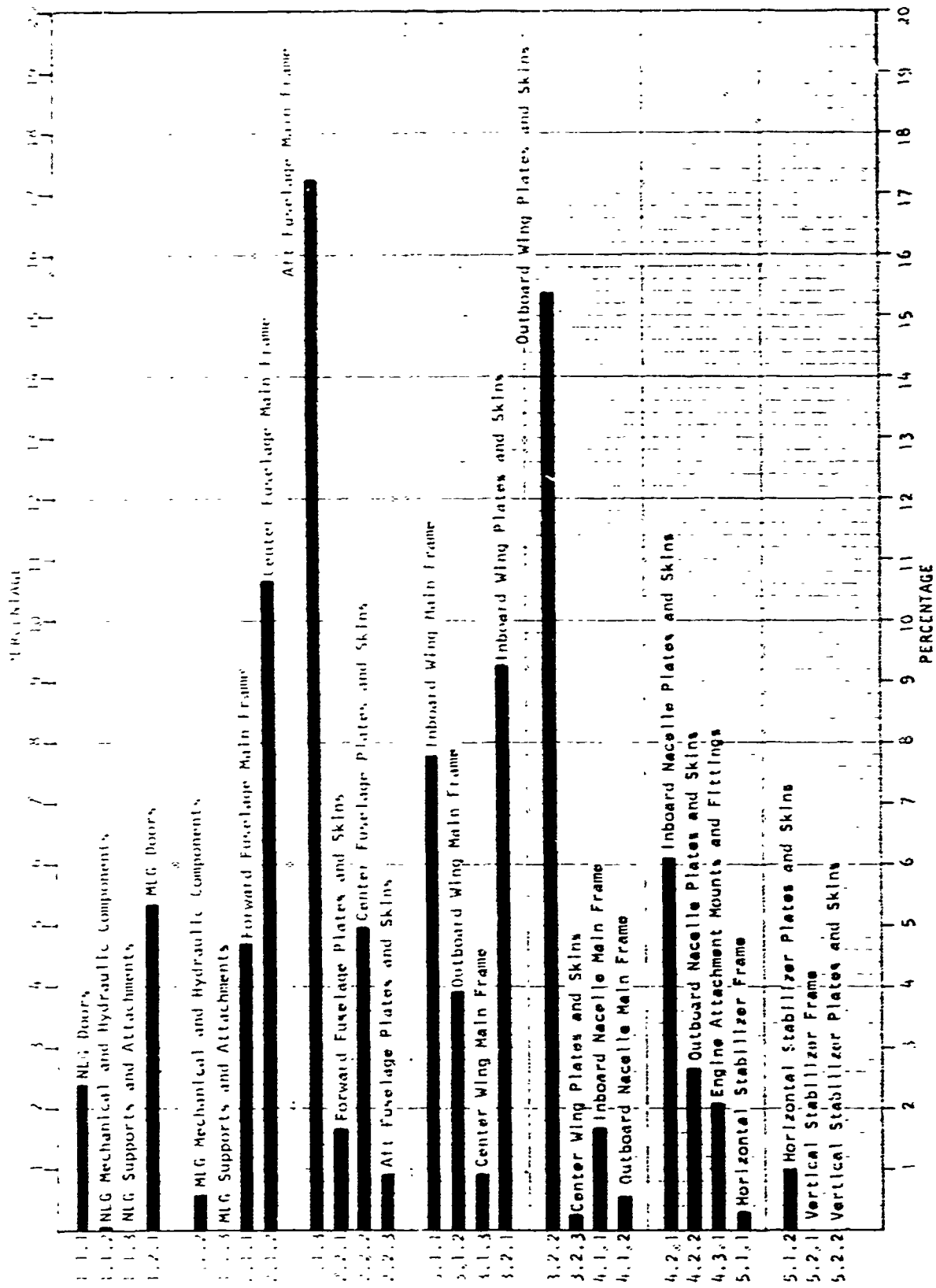


Figure 7. Statistical Distribution of Failures on Air Force Cargo Aircraft

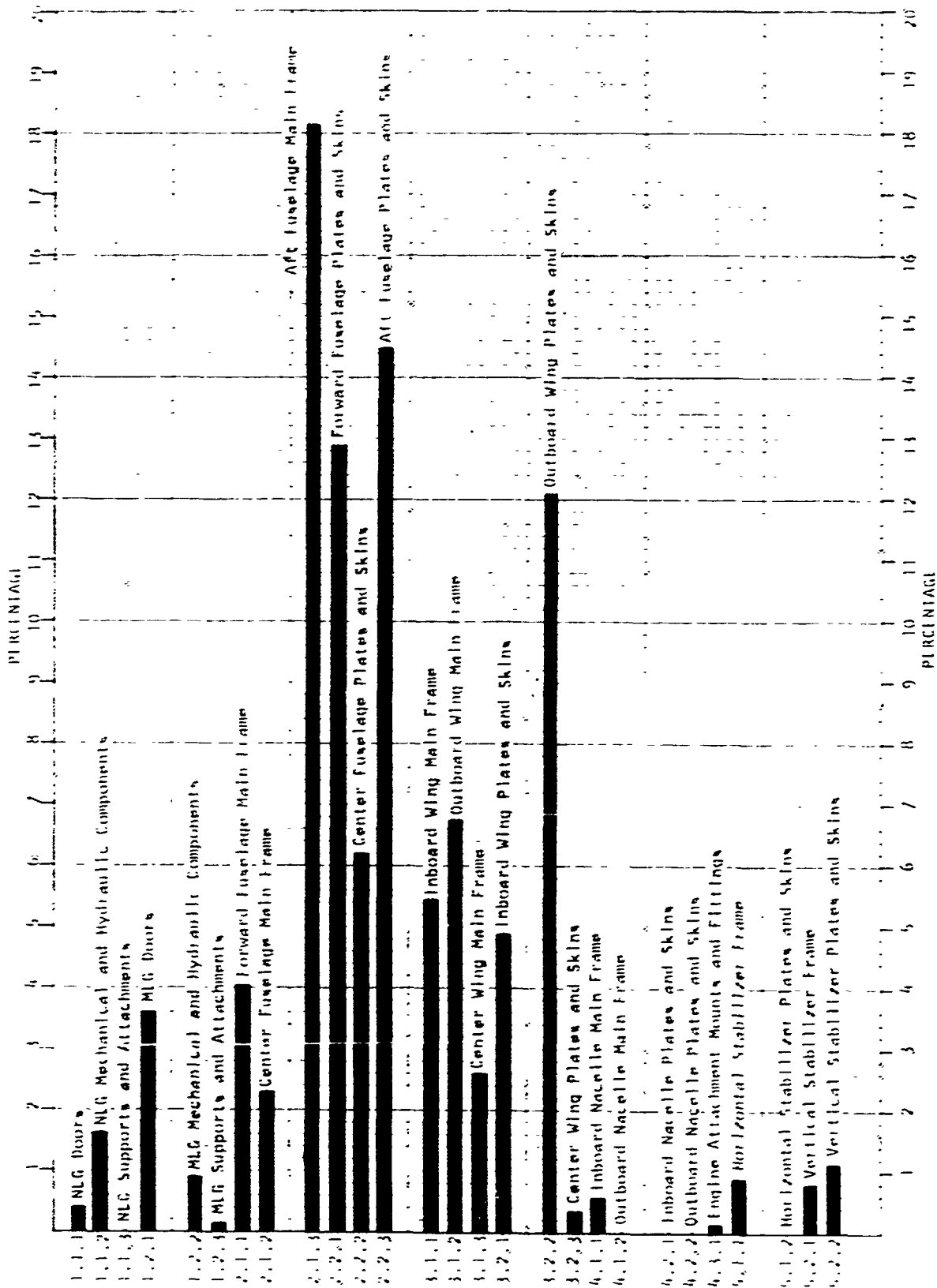


Figure 8. Statistical Distribution of Failures on Air Force Fighter/Trainer Aircraft

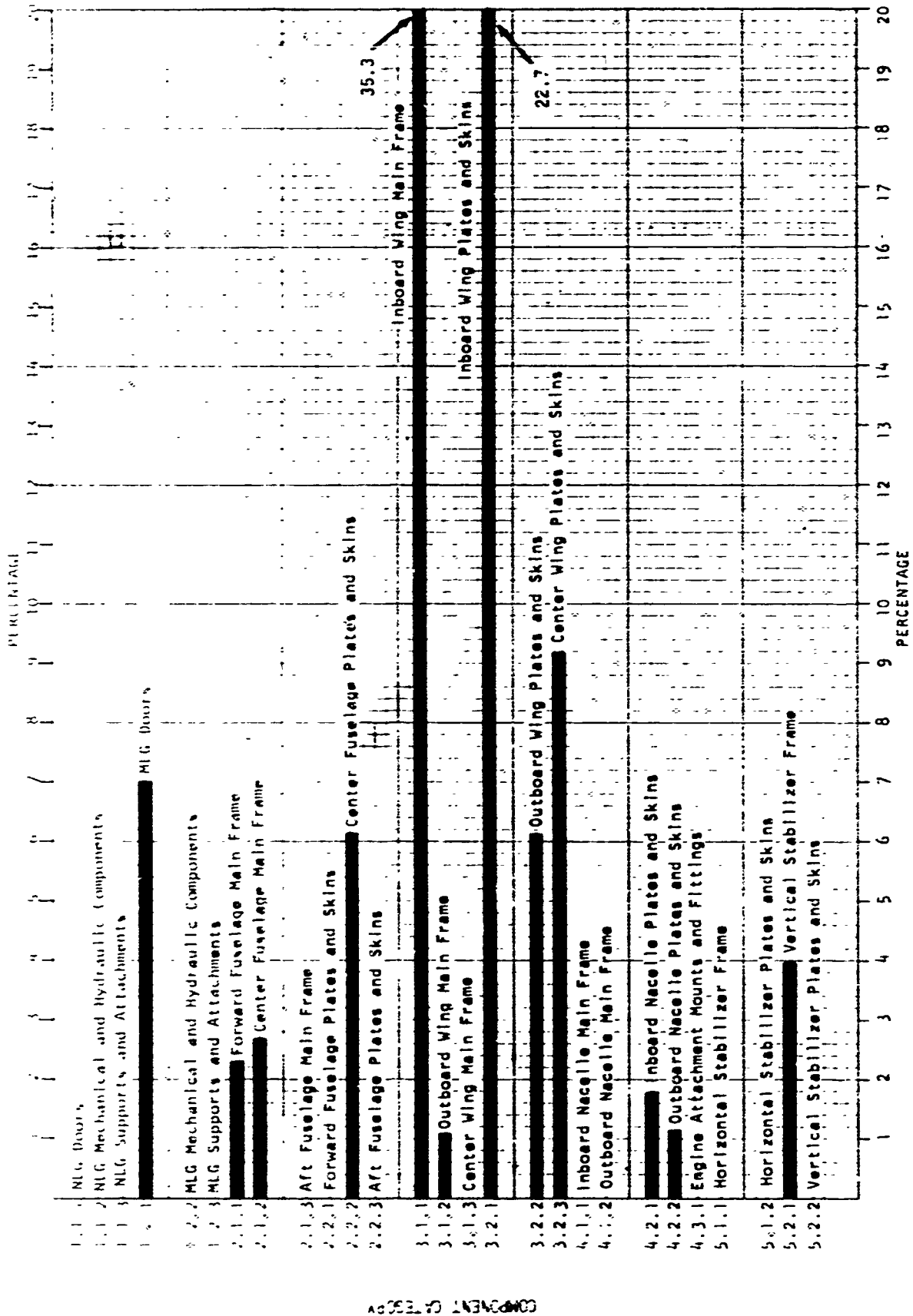


Figure 9. Statistical Distribution of Failures on Air Force Bomber Aircraft

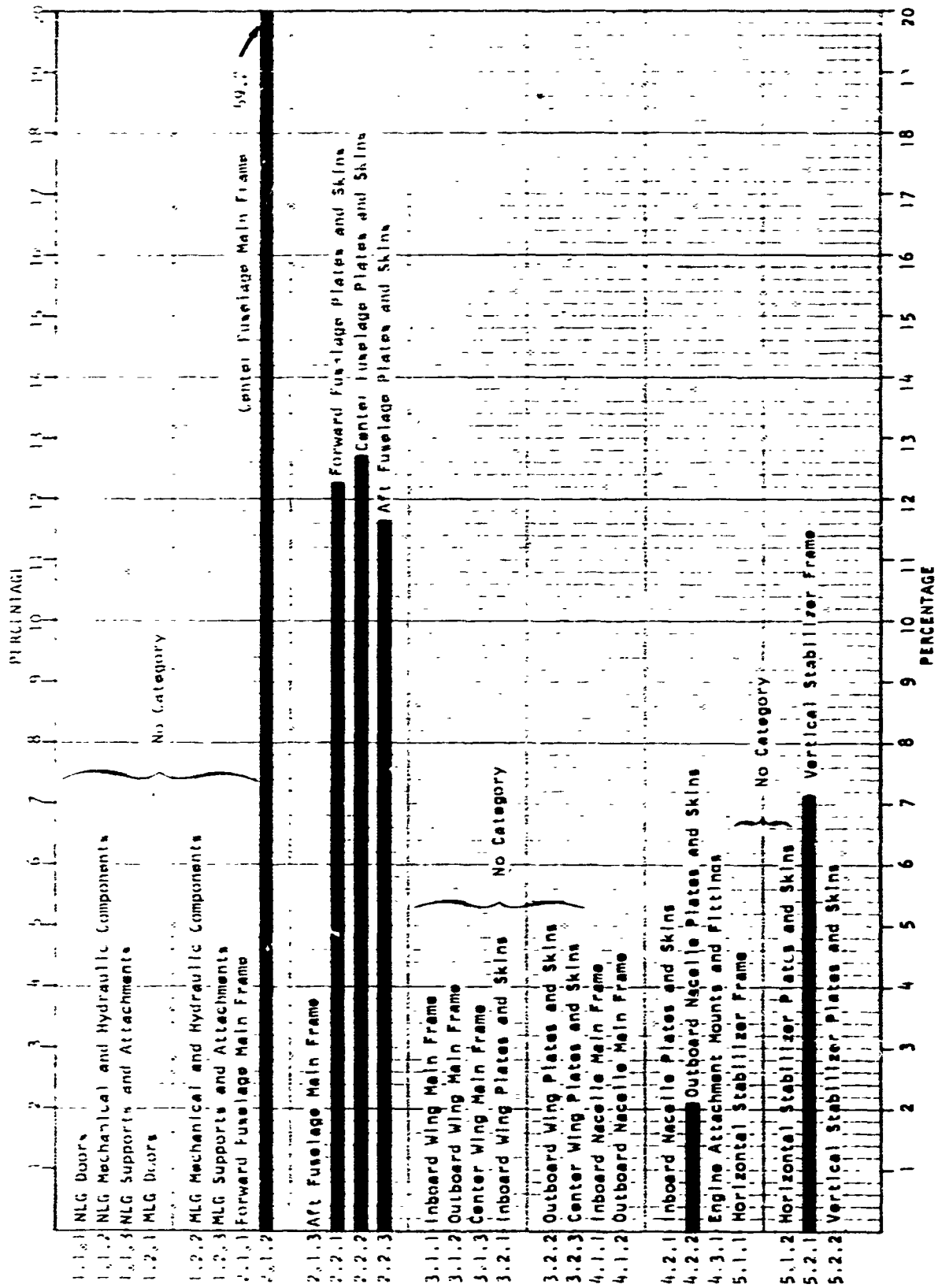


Figure 10. Statistical Distribution of Failures on Air Force Helicopters

COPIED FROM

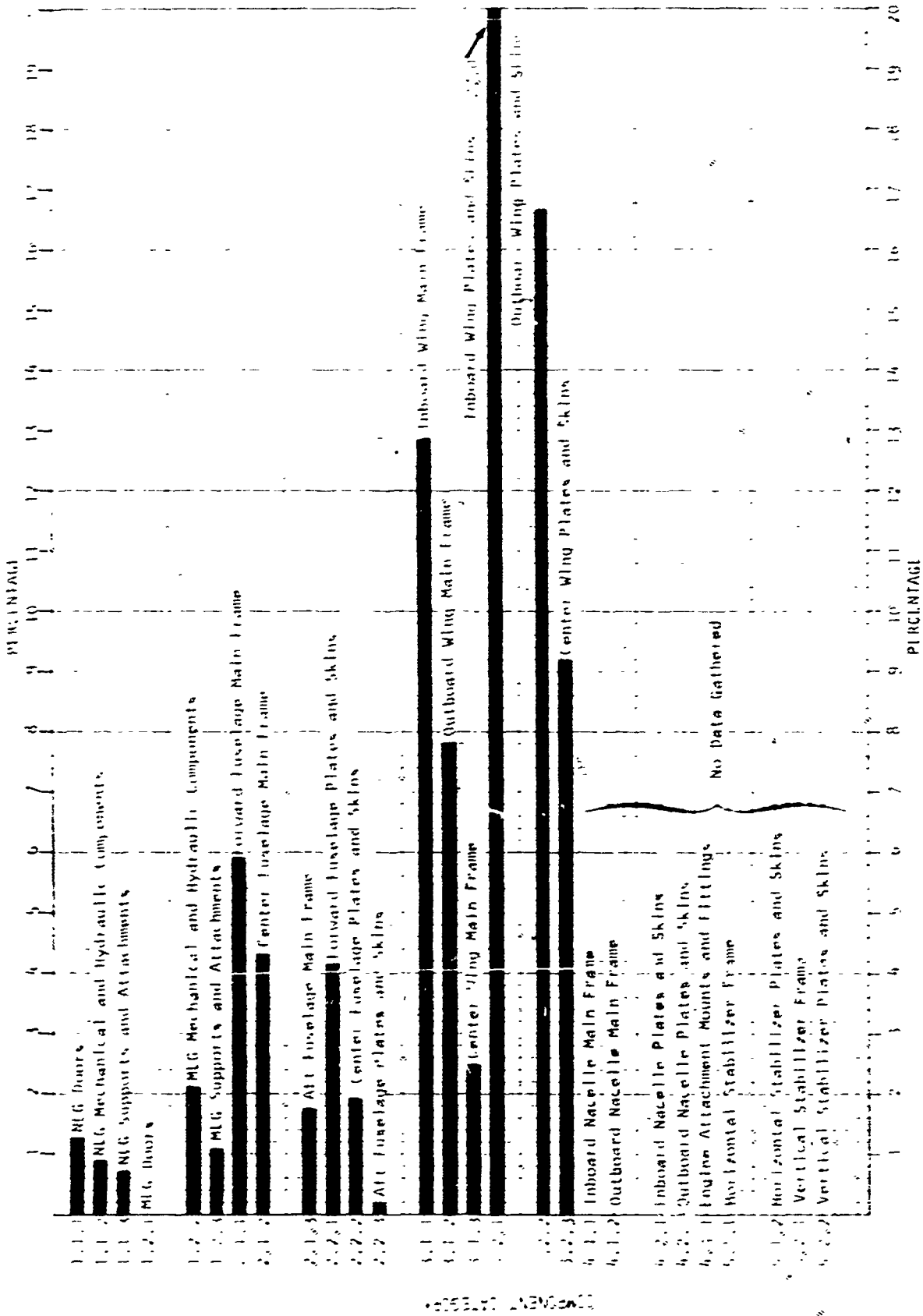


Figure 11. Statistical Distribution of Failures on Selected Commercial Jet Aircraft

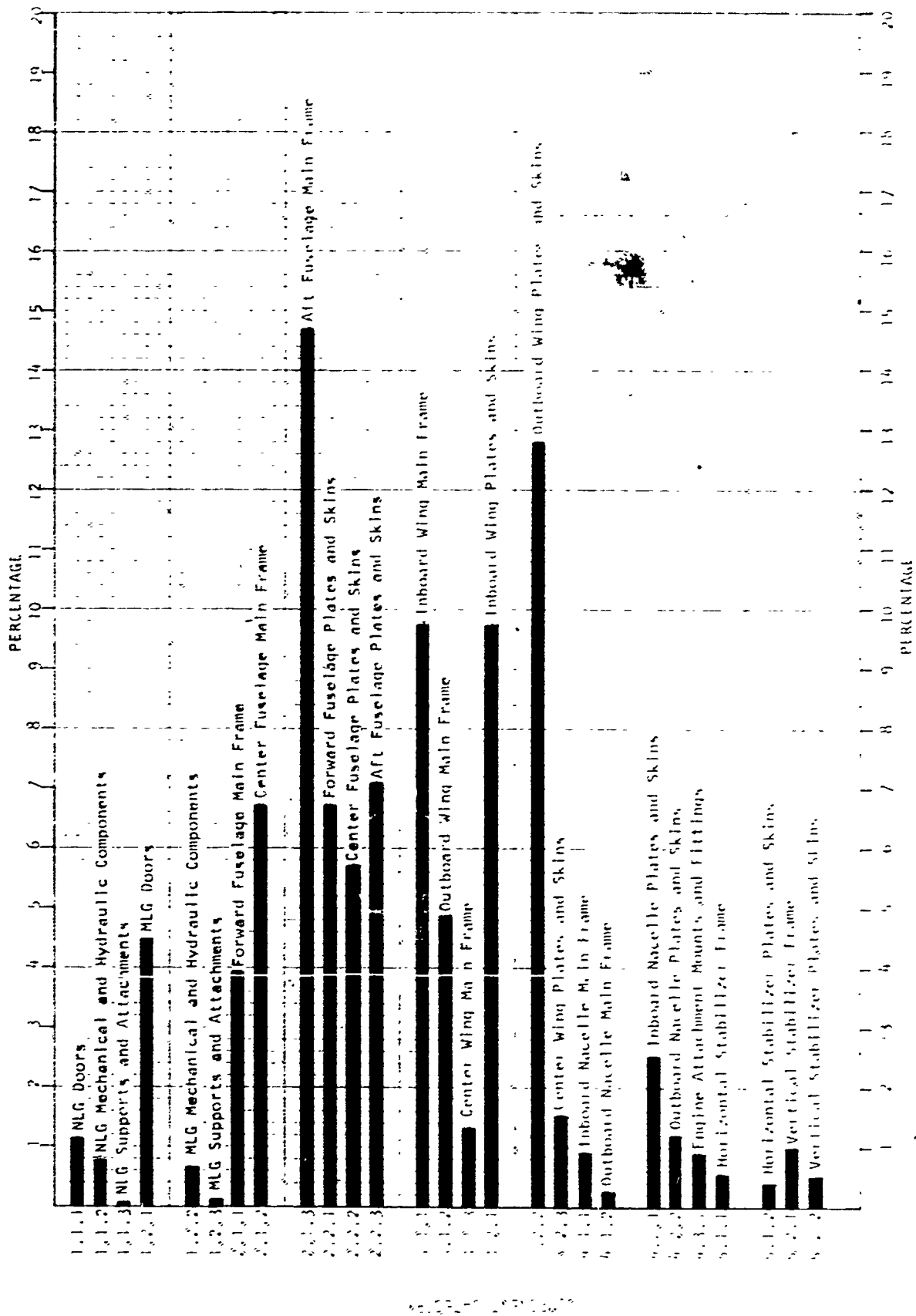


Figure 12. Statistical Distribution of Total Failures Recorded

TABLE X. CODING SYSTEM FOR THE COMPREHENSIVE FAILURE DATA FORM

DIVISION	SUB-DIVISION NAME OR DESCRIPTION	CODE	COL. LOCATION ON IBM CARD	CATEGORY CODE (TABLE XII & FIG. 13a,b)
1. Type of Structure	Airframe	1	3	1.1
	Landing Gear	2		1.2
	Flight Controls	3		1.3
	Other	4		1.4
2. Structural Importance	Primary Structure	1	5	2.1
	Secondary Structure	2		2.2
	Other	3		2.3
3. Part Form	Forging	1	7	3.1
	Casting	2		3.2
	Sheet	3		3.3
	Plate	4		3.4
	Rod	5		3.5
	Bolts and Fasteners	6		3.6
	Extrusions	7		3.7
	Other	8		3.8
4. Part Material	7075-T6	01	9-10	4.01
	7079-T6	02		4.02
	7079-T73	03		4.03
	2014-T6	04		4.04
	2024-T6	05		4.05
	4130	06		4.06
	4340	07		4.07
	4330	08		4.08
	356-T6	09		4.09
	7079-T0	10		4.10
	7178-T6	11		4.11
	17-4PH	12		4.12
	4335 M	13		4.13
	7075-T73	14		4.14
	7079-T651	15		4.15
	988V40	16		4.16

TABLE X (Continued)

DIVISION	SUB-DIVISION NAME OR DESCRIPTION	CODE	COL. LOCATION ON IBM CARD	CATEGORY CODE (TABLE VII & FIG. 12a,b)
5. Surface Treatment	None/Unknown	01	12-13	5.01
	Anodized	02		5.02
	Shot Peened	03		5.03
	Alodined	04		5.04
	Zinc Chromate	05		5.05
	Shot Peened & Anodized	06		5.06
	Chem-Milled	07		5.07
	Chrome Plated	08		5.08
	Chromic Acid Anodize	09		5.09
6. Type of Failure	Fatigue	1	15	6.1
	Stress-Corrosion	2		6.2
	High Static Stress	3		6.3
	High Impact Load	4		6.4
	Unknown	5		6.5
7. Failure Origin	Unknown	01	17-18	7.01
	Surface Flaw	02		7.02
	Bolt or Rivet Hole	03		7.03
	Lightening Hole	04		7.04
	Tool Scratch	05		7.05
	Corrosion Pit	06		7.06
	Sharp Corner	07		7.07
	Internal Flaw	08		7.08
	Forging Flaw	09		7.09
	Weld Flaw	10		7.10
	Inservice Wear Scratches	11		7.11
	Forging Parting Plane	12		7.12
8. Influencing Factors	None/Unknown	01	20-21	8.01
	Fit-Up Stress	02		8.02
	Residual Stress	03		8.03
	Corrosion	04		8.04
	Stress Riser	05		8.05
	Surface Imperfections	06		8.06
	Layer of Untempered Martensite	07		8.07
	Excessive Vibration	08		8.08

TABLE X (Concluded)

DIVISION	SUB-DIVISION NAME OR DESCRIPTION	CODE	COL. LOCATION ON IBM CARD	CATEGORY CODE (TABLE XII & FIG. 13a,b)
9. Number of Known Failures	Actual Number of Failures Recorded	(None)	23-26	(None)
10. Written Description of Failure	The Alloy, Part Form, and Type of Failure	(None)	30-70	(None)
11. Aircraft Code Number	Every Aircraft Has Its Own Two-Digit Code Number	Not Listed in This Report	73-74	(None)
12. Failure Sequence Number	Component Failures for Each Aircraft are Coded in Sequence According to Part and Failure Description	001 and up	76-78	(None)

TABLE XI. COMPREHENSIVE FAILURE DATA TABULATION

PART DESCRIPTION									WRITTEN DATA	FAILURE NO.	
*1	2	3	4	5	6	7	8	9	10	11	12
*1	1	4	01	01	1	01	01	0003	7075-T6, Plate, Fatigue	35	001
	1	1	01	01	2	08	03	0003	7075-T6, Forging, Stress Corrosion	35	002
	1	1	01	01	2	03	02	0060	7075-T6, Forging, Stress Corrosion	35	003
	4	3	2	09	01	3	01	010	356-T6, Casting, High Static Stress	35	004
	1	1	1	10	04	2	09	010	7079, Forging, Stress Corrosion	35	005
	1	1	4	01	01	1	03	010008	7075-T6, Plate, Fatigue	31	001
	1	1	1	04	05	2	03	030014	2014-T6, Forging, Stress Corrosion	31	002
	2	1	1	07	01	1	03	040006	4340, Forging, Fatigue	31	003
	3	2	1	04	06	1	02	010180	2014-T6, Forging, Fatigue	38	001
	4	2	6	08	01	1	01	010002	4330, Forging, Fatigue	38	002
	2	1	1	01	03	1	05	050004	7075-T6, Forging, Fatigue	38	003
	2	1	1	16	01	1	11	040050	988V40, Forging, Fatigue	38	004
	1	1	4	01	07	1	03	010001	7075-T6, Plate, Fatigue	14	001
	2	1	1	01	01	2	03	030007	7075-T6, Forging, Stress Corrosion	14	002
	1	1	1	02	02	2	03	030030	7079-T6, Forging, Stress Corrosion	14	004
	1	1	1	07	03	2	03	010002	4340, Forging, Stress Corrosion	14	005
	2	1	1	07	08	2	06	030004	4340, Forging, Stress Corrosion	14	006
	2	1	1	07	08	3	07	040002	4340, Forging, Overstress	14	007
	2	1	1	04	09	1	07	040001	2014-T6, Forging, Fatigue	14	008
	2	1	1	01	05	2	12	040001	7075-T6, Forging, Stress Corrosion	14	009
	2	1	1	07	08	2	02	030004	4340, Forging, Stress Corrosion	14	010
	1	1	7	11	01	1	03	010405	7178-T6, Extrusion, Fatigue	11	001
	1	2	7	11	01	1	06	040010	7178-T6, Extrusion, Fatigue	11	002
	1	1	1	01	03	2	07	050016	7075-T6, Forging, Stress Corrosion	11	004
	2	1	1	07	01	1	02	040002	4340, Forging, Fatigue	11	005
	2	1	1	07	01	2	02	060003	4340, Forging, Stress Corrosion	11	006
	2	1	1	07	08	1	02	050002	4340, Forging, Fatigue	11	007
	2	1	1	07	01	1	06	050001	4340, Forging, Fatigue	11	008
	2	1	1	07	01	2	05	010002	4340, Forging, Stress Corrosion	11	009
	2	1	1	07	01	2	01	040001	4340, Forging, Stress Corrosion	11	010
	2	2	1	07	03	1	07	040002	4340, Forging, Fatigue	11	011
	1	2	3	05	01	1	03	080001	2024-T6, Sheet, Fatigue	11	012
	1	2	3	01	01	2	07	030001	7075-T6, Sheet, Stress Corrosion	11	013
	1	1	7	01	01	2	07	030002	7075-T6, Extrusion, Stress Corrosion	11	014

*Codes Identified in Table X

TABLE XI (Continued)

PART DESCRIPTION									WRITTEN DATA	FAILURE NO.	
1	2	3	4	5	6	7	8	9	10	11	12
1	1	1	01	01	2	03	03	0001	7075-T6, Forging, Stress Corrosion	11	015
1	1	7	01	01	1	03	02	0001	7075-T6, Extrusion, Fatigue	11	016
2	1	1	07	03	4	07	04	0016	4340, Forging, Impact Load	11	017
2	1	1	07	01	1	06	04	0001	4340, Forging, Fatigue	11	018
1	2	1	01	01	2	03	02	0001	7075-T6, Forging, Stress Corrosion	11	019
2	1	1	07	01	5	01	06	0001	4340, Forging, Unknown	11	020
2	1	1	07	08	1	09	01	0001	4340, Forging, Fatigue	11	021
4	2	6	12	01	2	01	01	0007	17-4PH, Machined, Stress Corrosion	13	001
2	1	1	01	02	2	01	03	0027	7075-T6, Forging, Stress Corrosion	13	002
1	1	1	08	01	2	03	02	0130	4330, Forging, Stress Corrosion	13	003
2	1	1	07	01	2	03	07	0002	4340, Forging, Stress Corrosion	13	004
2	1	1	01	02	2	03	02	0005	7075-T6, Forging, Stress Corrosion	13	005
2	1	1	07	01	2	03	02	0002	4340, Forging, Stress Corrosion	13	006
1	1	1	04	07	3	01	02	0023	2014-T6, Forging, High Static Stress	20	001
1	1	1	02	01	2	03	02	0003	7079-T6, Forging, Stress Corrosion	20	002
1	1	1	13	01	1	10	05	0004	4335H, Forging, Fatigue	20	004
2	1	1	14	01	2	01	04	0001	7075-T73, Forging, Stress Corrosion	20	005
1	1	1	01	01	3	01	01	0001	7075-T6, Forging, High Static Stress	33	001
1	1	3	01	01	1	07	04	0050	7075-T6, Sheet, Fatigue	22	001
1	2	1	15	01	2	07	02	0001	7079-T651, Forging, Stress Corrosion	22	002
2	1	7	01	01	2	07	02	0001	7075-T6, Extrusion, Stress Corrosion	22	003
1	1	3	01	01	1	07	06	0078	7075-T6, Sheet, Fatigue	22	004
1	1	1	07	01	2	03	07	0001	4340, Forging, Stress Corrosion	22	005
4	1	1	15	01	2	07	01	0002	7079-T651, Forging, Stress Corrosion	22	006
2	1	1	02	01	1	11	05	0039	7079-T6, Forging, Fatigue	52	001
2	1	1	02	01	2	12	02	0003	7079-T6, Forging, Stress Corrosion	52	002
2	1	1	02	03	2	12	01	0015	7079-T6, Forging, Stress Corrosion	52	003
2	1	1	02	01	2	03	04	0001	7079-T6, Forging, Stress Corrosion	52	004
1	1	1	01	01	1	09	04	0002	7075-T6, Forging, Fatigue	51	001
1	1	7	01	01	1	03	04	0001	7075-T6, Extrusion, Fatigue	51	002

list consists of only those significant or major failures which were identified and cataloged under this program. No attempt was made to assure that all failures were recorded for the total fleet and complete operating lifetime.

b. Data Correlation

The coded comprehensive failure data presented in Table XI is tabulated in Table XII for the various individual categories of interest in the statistical analysis. The number of failures in each category and the distribution within the major categories are presented in this tabulation. This statistical distribution in the various data categories is graphically presented in Figures 13a and 13b.

3. Data Correlation Assessment

The conclusions that can be drawn from the information in the previous sections are limited in several ways. The statistical data from the AFM 66-1, MRR reports, EUR/UR files and the comprehensive data from documented failures all have limitations which must be understood before any valid conclusions can be drawn from the data presented.

In the case of the AFM 66-1 and MRR data, their limitations were discussed more fully in Section II.B.5. These limitations involve the limited operational time span of the reported data, the reliability of the data, data interpretation and other influencing factors. With an understanding of these limitations the statistical data shown in Figures 7 through 12 should represent the general trends with respect to component failures. Thus, if the total fleet history of failures for

TABLE XII. COMPREHENSIVE FAILURE DATA STATISTICAL
DISTRIBUTION IN EACH CATEGORY

CATEGORY (TABLE X)	NUMBER OF FAILURES	PERCENT	CATEGORY (TABLE X)	NUMBER OF FAILURES	PERCENT
1.1	29	45.31	5.01	43	67.18
1.2	30	46.87	5.02	3	4.68
1.3	1	1.56	5.03	6	9.37
1.4	4	6.25	5.04	1	1.56
2.1	54	84.37	5.05	2	3.12
2.2	9	14.06	5.06	1	1.56
2.3	1	1.56	5.07	2	3.12
3.1	48	75.00	5.08	5	7.81
3.2	1	1.56	5.09	1	1.56
3.3	4	6.25	6.1	25	39.06
3.4	3	4.68	6.2	33	51.56
3.5	0	0.00	6.3	4	6.25
3.6	2	3.12	6.4	1	1.56
3.7	6	9.37	6.5	1	1.56
3.8	0	0.00	7.01	10	15.62
4.01	22	34.37	7.02	5	7.81
4.02	6	9.37	7.03	21	32.81
4.03	0	0.00	7.04	0	0.00
4.04	4	6.25	7.05	2	3.12
4.05	1	1.56	7.06	4	6.25
4.06	0	0.00	7.07	12	18.75
4.07	19	29.68	7.08	1	1.56
4.08	2	3.12	7.09	3	4.68
4.09	1	1.56	7.10	1	1.56
4.10	1	1.56	7.11	2	3.12
4.11	2	3.12	7.12	3	4.68
4.12	1	1.56	8.01	15	23.43
4.13	1	1.56	8.02	11	17.18
4.14	1	1.56	8.03	10	15.62
4.15	2	3.12	8.04	16	25.00
4.16	1	1.56	8.05	6	9.37
			8.06	3	4.68
			8.07	2	3.12
			8.08	1	1.56

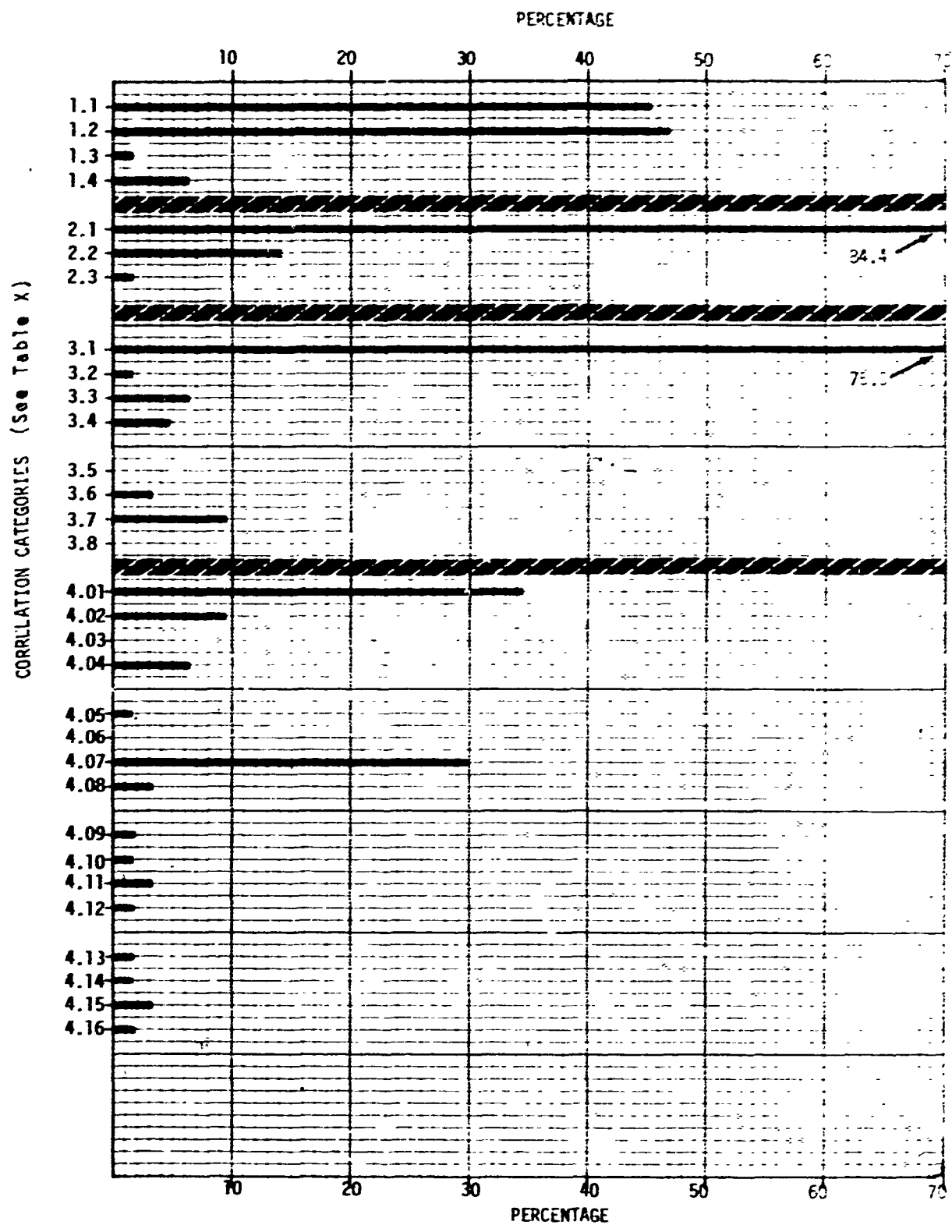


Figure 13a. Statistical Distribution of Comprehensive Failure Data for Various Correlation Categories

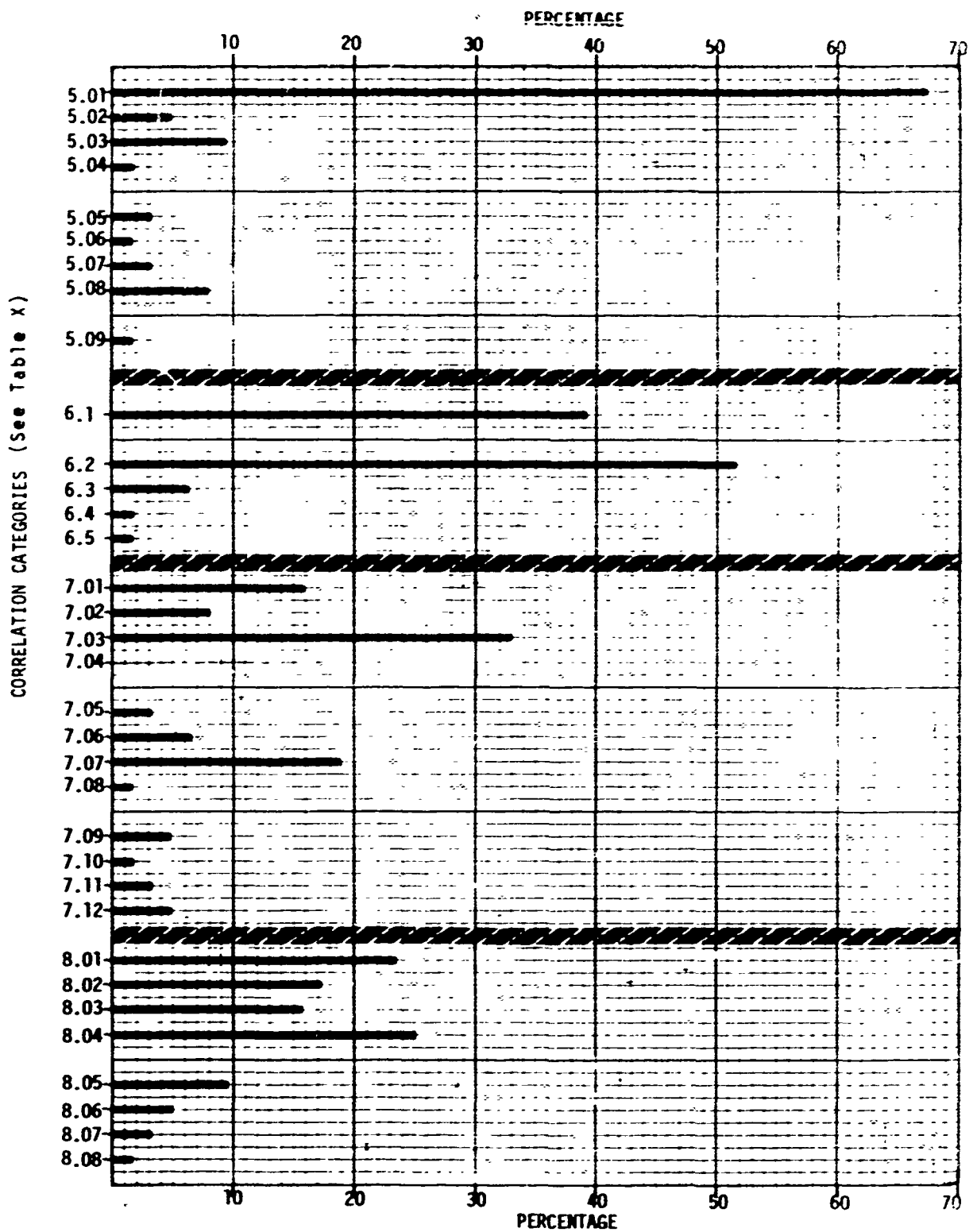


Figure 13b. Statistical Distribution of Comprehensive Failure Data For Various Correlation Categories

the type of interest to this program were obtained, it would reflect the trends indicated in the restricted view of these reported failures that was shown in this correlation section. Figure 12 summarizes these results in a gross sense, with the primary failure areas easily identified. In order of numerical occurrences the four primary failure areas are: Aft Fuselage Main Frame (2.1.3); Outboard Wings, Plates and Skins (3.2.2); Inboard Wings, Main Frame (3.1.1); and Inboard Wings, Plates and Skins (3.2.1). It may seem odd that the frame, plate or skin areas should have the greatest number of reported failures in comparison to the landing gear, however, the sheer number of components and possible crack initiation locations far exceed the other airframe areas. It should also be realized that a majority of these reported failures are insignificant or of minor concern in the operation or maintenance of the aircraft. The critical or significant failures may represent only a small portion of these reported failures.

The comprehensive failure data, although not statistically accurate, does give an indication of those types of failures which are most significant and pose the greatest problem in fleet operation and failure investigation efforts. As can be determined from Table XII and Figure 13, the greatest number of significant failures in the major categories can be attributed to the following: landing gear (1.2), forgings (3.1), 7075-T6 aluminum (4.01), no surface treatment (5.01), stress corrosion (6.2), bolt or rivet hole origin (7.03), and corrosion influence (8.04). This does not contradict the statistical data from the 66-1 and MRR systems, but rather, it further identifies the more significant failures

and circumstances involved. Although more failures occur in the wings and fuselage than in the landing gear, these latter failures are much more significant with respect to aircraft operation and safety. The landing gear of any aircraft, being one of the most highly stressed parts of the structure, a small crack could become a catastrophic failure in a very short period of time even in the presence of only small flaws or defects. The wing structure, on the other hand, is also highly loaded in some areas, however, redundancy and multiple load paths make this part of the structure more forgiving. Long cracks in the skin, and sometimes in spars, can be tolerated for short periods of time without the risk of catastrophic failure. The fabricated nature of the wing and fuselage with its thinner materials and many rivet holes provides the basis for large numbers of cracks. Hence, these correlation results are not significantly different from previous views or historical estimates.

Further, study of the correlation data does not reveal many more significant trends of statistical value, however many observations or postulations may be possible. It can be seen that certain high strength materials, which are prone to fatigue and stress corrosion, make up the bulk of the comprehensive failures, and likewise the airframe. These are such materials as 7075-T6, 4340, and 7079-T6. Also the failure origins, most identified in this investigation are: bolt and rivet holes, sharp corners, and surface flaws. Other influencing factors of major importance were corrosion, fit up stresses, and residual stresses. All of these trends, however, are confined to the data which was specifically selected for investigation and represent the most difficult problems for failure solution. These more significant failure areas and

causes should, therefore, receive the primary attention in the development of improved failure analysis methods. Using these individual component failures as a base, the following Section III of the report investigates the application of fracture mechanics analysis methods and procedures to the structural failure problem.

SECTION III

FAILURE ANALYSIS DEVELOPMENT

Attempts to develop improved methods of structural life analysis have involved various approaches, two of which are: (1) the direct life comparison and (2) the examination of fracture initiation, growth and final failure. The primary effort in this program is the second approach, that of investigating the fracture surface and surrounding circumstance, with the employment of Fracture Mechanics in structural failure analysis development. The Fracture Mechanics approach is simply the application of a definitive and proper stress analysis of flaws, defects and cracks in order to clearly separate and identify the role of stress in the progression of a fracture. Much has been accomplished in the development of this analysis method; however, these efforts have involved simplified or idealized conditions and are based almost exclusively on laboratory test data. The goal of this effort is to project this analysis method into the investigation and solution of actual structural failure problems.

The first part of this analysis development section is devoted to summarizing the available analysis tools for Fracture Mechanics, including a review of fundamentals, identification of applicable formulae, and especially application of the stress intensity concept. These subjects are intended to provide the reader with some background on Fracture Mechanics methods to enable a better understanding of its application in analyzing specific failures.

The second part of this section discusses the macroscopic and microscopic features of the fracture surface which are important in the Fracture Mechanics approach. The critical examination of the fracture and identification of specific characteristics or evidence is very important to the successful application of this analysis method.

The third part of this section provides a brief summary of information related to general materials behavior for initiation or progression of a crack. References or sources of existing failure data on a wide variety of materials and under various test conditions are provided as further supporting information for the development of a failure analysis method.

The last part of this section contains the failure analysis of actual service failures for which data have been gathered. Analysis procedures and results are discussed for each failure examined, and missing or inadequate data is identified in the attempt to conduct and illustrate detailed and valid analysis methods.

A. Fracture Mechanics Analysis Tools

1. Fundamentals of Fracture Mechanics Analysis

So called "linear-elastic fracture mechanics" forms the basis of all currently widely accepted methods of fracture analysis. Thus, it is relevant in discussing improved failure analysis methods to first review the fundamentals of fracture mechanics. Most important is that it provides a "language" for which accurate descriptions of failures can

be accomplished. Moreover, it provides a quantitative means of assessing design improvements, the effectiveness of improving inspection, etc., which is most important to following up a failure analysis with suggestion of improvement or alternately anticipating the propensity for fracture failure of a design.

a. The Crack Tip Stress Field Concept

Linear-elastic fracture mechanics is based on certain results of analysis by theory of elasticity applied to crack problems. The single perhaps most significant result comes from an analysis of the adjacent elastic stress field (surrounding the non-linear core or plastic zone) at the tip of a loaded crack. For any crack where the crack surfaces are directly opened due to loading the body (Mode I), the elastic stress field is (see reference [1] for full derivation):

$$\begin{aligned}\sigma_y &= \frac{K}{\sqrt{2\pi r}} \cos \frac{\theta}{2} \left[1 + \sin \frac{\theta}{2} \sin \frac{3\theta}{2} \right] \\ \sigma_x &= \frac{K}{\sqrt{2\pi r}} \cos \frac{\theta}{2} \left[1 - \sin \frac{\theta}{2} \sin \frac{3\theta}{2} \right] \\ \tau_{xy} &= \frac{K}{\sqrt{2\pi r}} \sin \frac{\theta}{2} \cos \frac{\theta}{2} \cos \frac{3\theta}{2}\end{aligned}\tag{1}$$

where the coordinates, r and θ and stress components, are as shown in Figure 14. The surrounding crack tip stress field contains the factor, K , which is formally called the crack tip stress field intensity factor (or "stress intensity factor"), and which reflects the intensity or

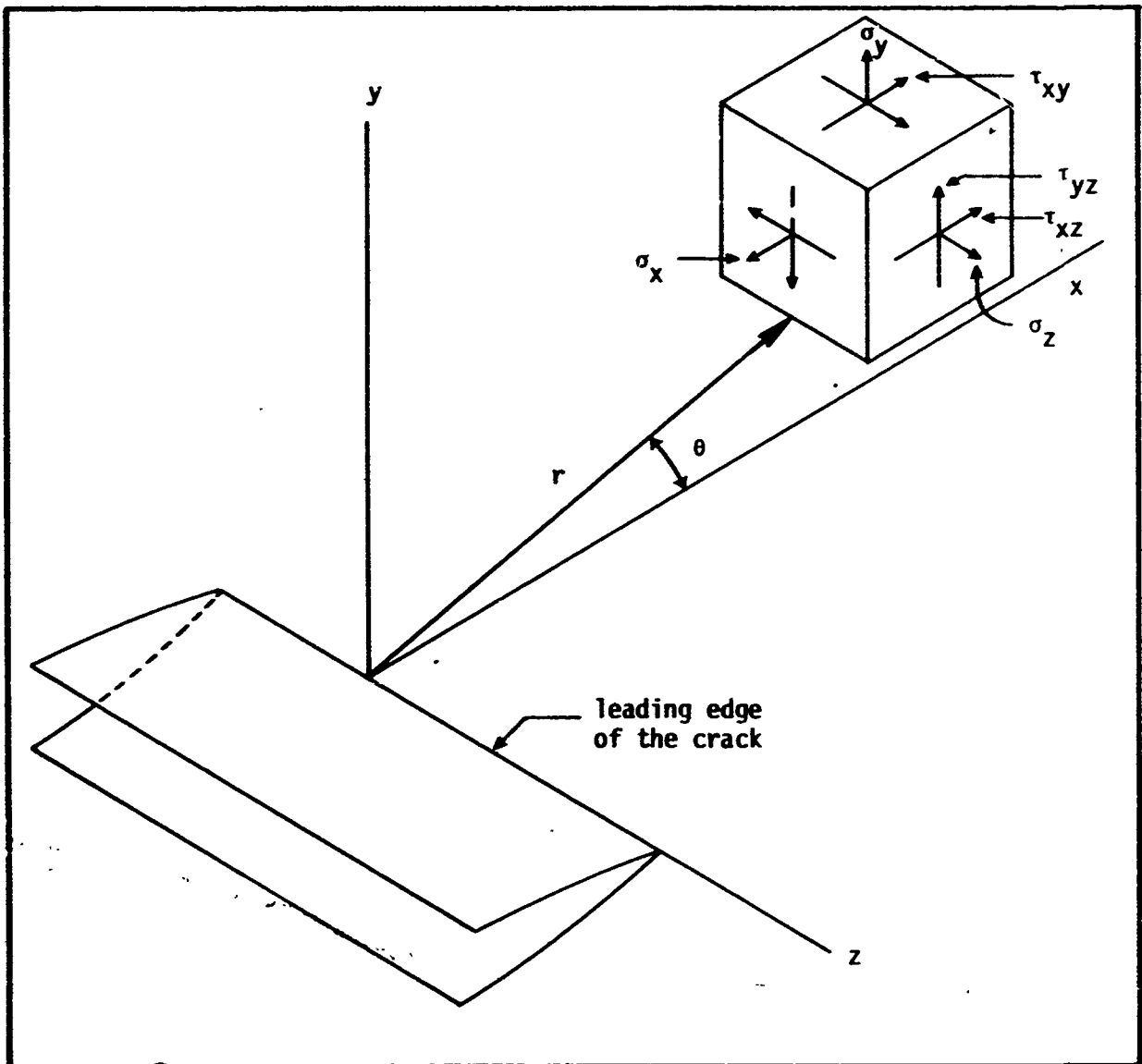


Figure 14. Stress Field Coordinate System

magnitude of the crack tip stress field caused by the applied loads and geometrical shape of the body.

All cracks which are pulled open, regardless of the geometrical shape of the body or the location or method of load application, have this same distribution of stress, equations (1), surrounding the crack tip. Thus, K is a one parameter description, (similar to the Burgers vector value of a dislocation), of the whole surrounding crack tip stress field. The non-linear core, embedded within this field, includes plasticity and other phenomena as well as the fracture process itself.

Now it follows, in assessing the fracture processes or crack growth possibilities in a body, that it is sensible to view cracking as a two step cause-effect process:

(1) The applied loads and geometrical shape of a body determine how much local load shall pass nearby a crack tip which is reflected by the intensity of the surrounding crack tip stress field, K .

(2) The stress field as described by its intensity, K , is the cause of that which occurs within it as its non-linear core including the fracture process.

Thus, it is clear that the first cause-effect step, (1), is simply an assessment of the redistribution of load paths in a body around a crack and, in particular, how much load is transmitted through the crack tip region as reflected by K . If, as in this document, analysis is

normally centered on fracture well below the yield point of structural members, it is completely appropriate to assess, K , by methods of elastic analysis of redistribution of forces in bodies, i.e., theory of elasticity. Therefore, one part of fracture analysis is resolved to determining in terms of elastic stress analysis formulas (or their equivalent) the applied crack tip stress field intensity, K .

The second cause-effect step, (2), is a matter of the material's non-linear response at the crack tip as caused by a surrounding stress field of intensity, K . If, for example, the surrounding stress field, K , is raised to a level which causes self-perpetuating separation of material, fracture ensues. This level is called the critical value of crack tip stress-intensity, K_c , which is a property of the material's crack tip processes response.

Moreover, if an aggressive environment is present whose reaction rate is influential, then separation and fracturing may ensue which is controlled by K but also time dependent due to an environmental influence. Or if the applied K for a crack is cycled due to cycling loads on a body, the response in simple terms is fatigue crack growth. These are perhaps oversimplified views of the material's response characteristics (which are very complicated and non-linear, etc.). But making use of the crack tip stress field concept, using K as the local load or stress intensity variable which can be derived as and computed from elastic stress analysis formulas, lends a great simplification to problems of categorizing and measuring in a controlled manner a material's response

characteristics.

b. The Generality and Limitations of the Crack Tip Stress Field Concepts

Equations (1) present the elastic crack tip stress field equations for a crack which is opened (Mode I) in a material whose elastic properties (constants) are isotropic and homogeneous (on a macro scale). Figure 15 depicts the three possible modes of crack displacement with:

- Mode I - Directly Opening Mode
- Mode II - Planar Shear Mode
- Mode III - Anti-plane Shear Mode

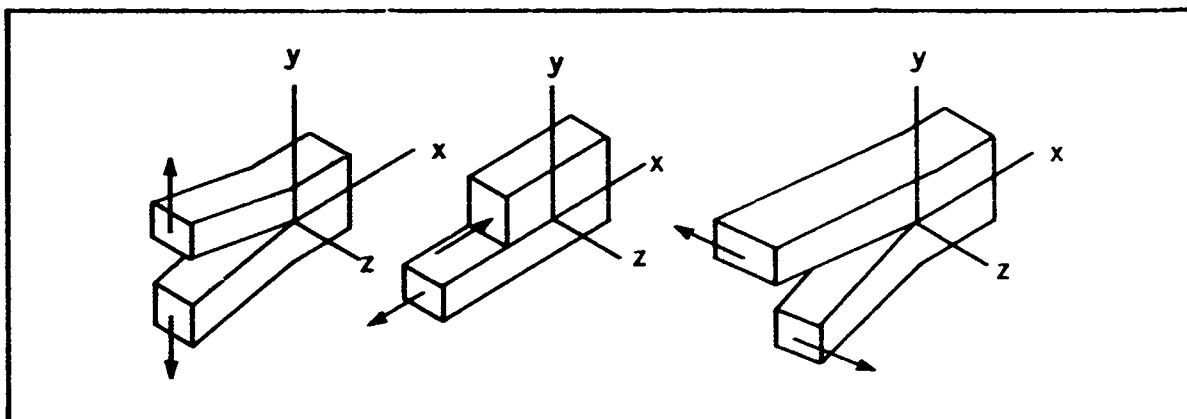


Figure 15. Crack Displacement Modes

The crack tip stress field equations for Mode II and Mode III are similar to Mode I in that they contain the $1/\sqrt{r}$ singularity but have different functions of θ associated with each (i.e., different distributions of stress). Thus for full generality, there are three types of crack tip stress fields (like the types of dislocations in crystals) each having its own intensity factor, K_I , K_{II} , and K_{III} . Moreover, the most general loading (or displacement) of a crack can be described by the superposition of these three modes. Thus the most general leading edge stress field requires a three parameter description, K_I , K_{II} and K_{III} . For a more complete analysis of all three modes, see Reference [1]. However, in applications to failure analysis, Mode II and Mode III are very seldom influential. This is because cracks tend to almost always form on planes perpendicular to principal tension directions which cause the cracks to open; the material's resistance to cracking seems to favor crack formation and propagation on such planes. Therefore, it is quite appropriate normally to refer to "the crack tip stress intensity factor, K " when it is meant to imply Mode I or K_I only.

In this report, Mode II and Mode III are only occasionally mentioned in passing and will not be further discussed here. The reader is referred to [1] for a fuller exposition of the stress analysis of Modes II and III.

Cases where the elastic properties (constants) of a material vary with direction, i.e., elastic-anisotropic media are also discussed in References [1] and [2]. Though the analysis of elastic problems in

such a media is very complicated (beyond the objectives of the current discussion), a summary of the results is relevant. In the most general elastic anisotropic case, crack tip stress field equations (like equations (1)) can be derived for each mode. The essential form of the crack tip field is preserved in that the $1/\sqrt{r}$ (singularity) still appears in the distribution. Moreover, stress intensity factors for the three modes appear K_I , K_{II} , and K_{III} whose dimensional character is preserved and whose formulas for a configuration and load are usually identical to the isotropic case. Therefore, in conclusion, elastic anisotropy does not limit the application of fracture mechanics stress analysis.

Of course, in the second step of the cause-effect view of crack extension, i.e., the material's response, anisotropy of the material's cracking resistance is often rather strong, so that, K_c , and like material properties are most appropriately quoted with the cracking direction specified.

In a similar fashion fine scale (compared to crack size, etc.) inhomogeneity of material can effect a material's response characteristic. This is reflected by, for example, the effect of material "cleanliness" on, K_c , etc. Moreover, in recent analysis of large scale elastic inhomogeneity such as cracks forming on or near the boundary between two phases or bond lines between media some results relevant to large scale inhomogeneity are available [3]. Thus neither anisotropy or inhomogeneity represent an essential limitation to fracture mechanics

but, though they do not make it inappropriate for applications, they do make applications just a bit more complicated.

Thus, the application of the stress analysis of linear-elastic fracture mechanics is not limited by mode differences, anisotropy or inhomogeneity. It is very general indeed, but it does have limitations.

The basis of fracture mechanics, i.e., appropriate linear-elastic stress analysis for determination of the intensity of the field of stress surrounding the non-linear core at a crack tip within which processes occur promoting crack extension, is really limited in two ways implied by this description. First, progressive extension of a crack as a result of processes within the non-linear core (or plastic zone) must be the mode of failure. This is almost always the case; however, it is relevant to note the materials such as composites, etc., are often designed to defeat progressive crack extension (at least on a gross scale though not necessarily on a fine multiple crack scale). Second, and perhaps most important, linear-elastic fracture mechanics is most appropriate only where an elastic crack tip field fully surrounds the non-linear core or "plastic zone" at the crack tip. Thus, fully justified application without reservations can be made only in cases where the crack tip plastic zone is small compared to crack size, net section dimensions, etc., (in general, all dimensions in directions normal to the line which is the leading edge of a crack). The compromising effect of too large a plastic zone is two-fold. First, it creates a situation where the stress field surrounding the non-linear zone is not that given by

equations (1) (or like equivalents), thus the cause of the material's response, e.g., K_c , is not a representative cause of a single type of stress field of identical distribution to others. Second, with large amounts of plasticity, the redistribution of forces transmitted through a member with a crack will not follow the elastic redistribution pattern sufficiently to fully justify using elastic analysis to compute formulas or values for the applied K .

The extent to which the size of crack tip plasticity represents a limitation of fracture mechanics is not fully clear; moreover, it depends on the required degree of accuracy in applications. For example, to assure both that the crack tip plasticity will not affect the surrounding stress field and that the redistribution of forces will make elastically computed formulas for K applied very accurate, the ASTM E-24 [4] fracture committee suggests test specimen dimensions which are approximately 20 times the nominal size of the crack tip plastic zone. That seems sufficient for the rather absolute precision required of rigidly standardizing test procedures. On the other extreme, the ~~redistribution of loads~~ transmitted through a body containing a crack is not so vastly changed with yielding across the whole net section that the trends suggested by K -formulas based on elastic analysis are much changed. Moreover, it is not evident for practical purposes that the crack tip be surrounded by exactly the correct elastic stress field to evoke much of the same material response for a given elastically computed applied K . Thus, it is not surprising to find that linear-elastic fracture mechanics and its modifications are often used with good success

right up to net section yielding where the plastic zone size is of the order of other specimen dimensions. It is simply a matter of degree of applicability and judgment of required accuracy which sets this limitation. And it should be pointed out that the clarity of concepts in fracture mechanics which make it possible to clearly understand possible sources and degree of error, should not lead to electing alternate fracture analysis methods with vague concepts where qualitative or empirical nature lacks the clarity of understanding limitations. On the contrary, it is an advantageous feature of linear-elastic fracture mechanics that limitations can be clearly understood, and with experience, the methods can be sensibly and artfully extrapolated well beyond normal limitations.

c. Crack Tip Plastic Zone Size Estimates; Plane Stress and Plane Strain

The plastic zone associated with a crack tip has been analyzed in considerable detail in recent years using various theories of plasticity [5, 6]. These detailed analyses have led to a much better understanding of the physical state inside the plastic zone but also leave much unclarified to date. At least no single method of elastic-plastic fracture mechanics has a dominating position to date and currently the methods simply augment linear-elastic fracture mechanics methodology. Therefore, here the discussion will center on the first order plastic zone size estimate and a discussion of its usefulness and implications in extending the applicability of fracture mechanics in

failure analysis.

Nearby the leading edge of a crack, the magnitude of stresses and strains is very high compared to values at some relatively greater distances away. In the wholly elastic situation, the stresses and strains vary with the inverse square root of the distance away ($1/\sqrt{r}$) as noted in equations (1). Within the non-linear or plastic zone similar high gradients of deformation occur. Thus, due to this high degree of tensile deformation, the material near the leading edge tends to shrink due to a Poisson's ratio effect in a direction parallel to the leading edge. However, the shrinkage is constrained by any surrounding material which is less deformed. The amount of constraint experienced by the plastic zone (i.e., a cylinder of material lying along the leading edge of the crack) depends on the gradients of the tendency for deformation normal to the leading edge and especially the length of the plastic zone cylinder compared to its other dimensions.

As a consequence, if the plastic zone accompanying the leading edge of a crack is constraining by elastic material surrounding it, and if the leading edge length is long compared to other dimensions of the plastic zone, then it is fully constrained against shrinkage parallel to the leading edge or in a state of "plane strain". Or, if the plastic zone dimensions are small compared to the leading edge length of the crack, then viewing the plastic zone as a short cylinder with free ends, it is relatively unconstrained or in a state of "plane stress". These considerations are equally relevant for three dimensional cracks

with curved crack fronts.

However, these concepts are most simply viewed and described in the case of through-the-thickness cracks in plates. As in Figure 16, the plasticity ahead of a crack may be viewed as a cylinder running through the thickness dimension of the plate. If (as in Figure 16), the plastic zone size is large compared to the plate thickness, locally within and adjacent to the plastic zone, the material is free to contract in thickness or plane stress exists:

$$\sigma_z = \tau_{xz} = \tau_{xy} = 0 \quad (2)$$

On the other hand, if the plate is thick compared to the plastic zone size, as in Figure 16, the elastic material constrains the plastic zone against thickness contraction in the interior, where (relatively) plane strain will exist:

$$\epsilon_z = \gamma_{xz} = \gamma_{yz} = 0 \quad (3)$$

Of course, plane stress would still exist at the free surfaces of a thick plate.

Since constraint will promote "triaxiality of stresses" and inhibit yielding, the plane strain plastic zone size is smaller than that for plane stress. Thus, for the thick plates, the plastic zone will be a cylinder with flared ends due to plane stress near the plate surfaces.

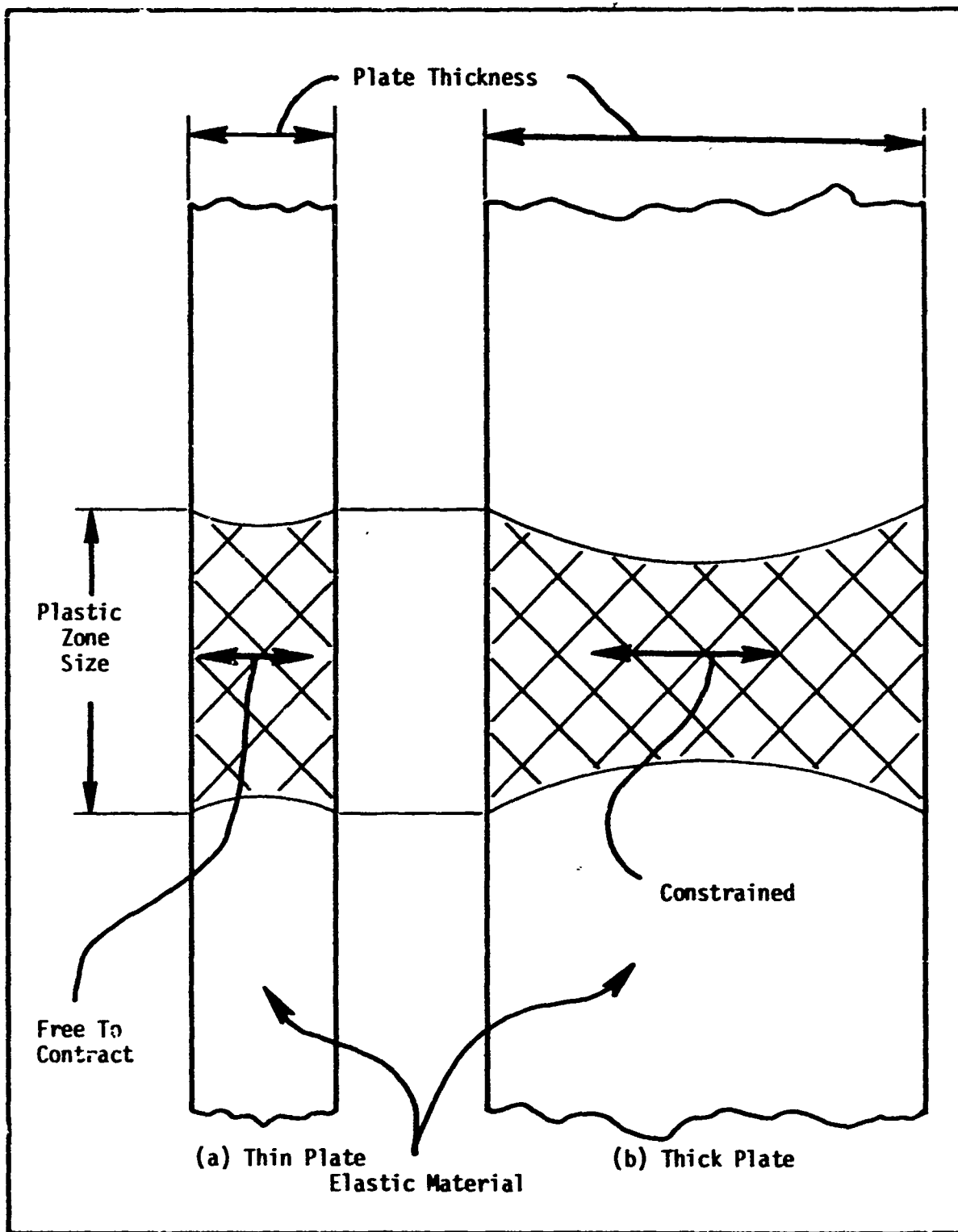


Figure 16. Plastic Zone Representation in Plates

With these views in mind, it is appropriate to develop a size estimate of plane stress and plane strain plastic zones. From equations (1), the normal stress in the elastic field on the crack plane just ahead of the crack is (see Figure 17)

$$\sigma_y = \frac{K}{\sqrt{2\pi r}} \quad (4)$$

If the situation were purely linear-elastic, the resulting stress distribution ahead of the crack would be as in Figure 17(a). But the plasticity at the crack tip relaxes the stresses as in Figure 17(b) in such a manner that from the elastic stresses, the crack appears to be longer, a_{eff} , than the actual crack size, a , by an amount proportional to the plastic zone size [7]. From the apparent or effective crack tip, a_{eff} , the distance to the edge of the plastic zone, r_y , can be estimated from equation (4). The result is [7]:

$$r_y = \frac{K^2}{2\pi\sigma_{yp}^2} \quad (\text{plane stress}) \quad (5)$$

where this result is relevant to plane stress using either the maximum shear stress or distortion energy yield theories. Making use of equations (3) instead of (2) to note the three dimensional character of stress, and adjusting for effects of shape in predicting the nominal plastic zone size, it is noted that the plane strain plastic zone is about three times smaller [5, 6, 7] than that for plane stress:

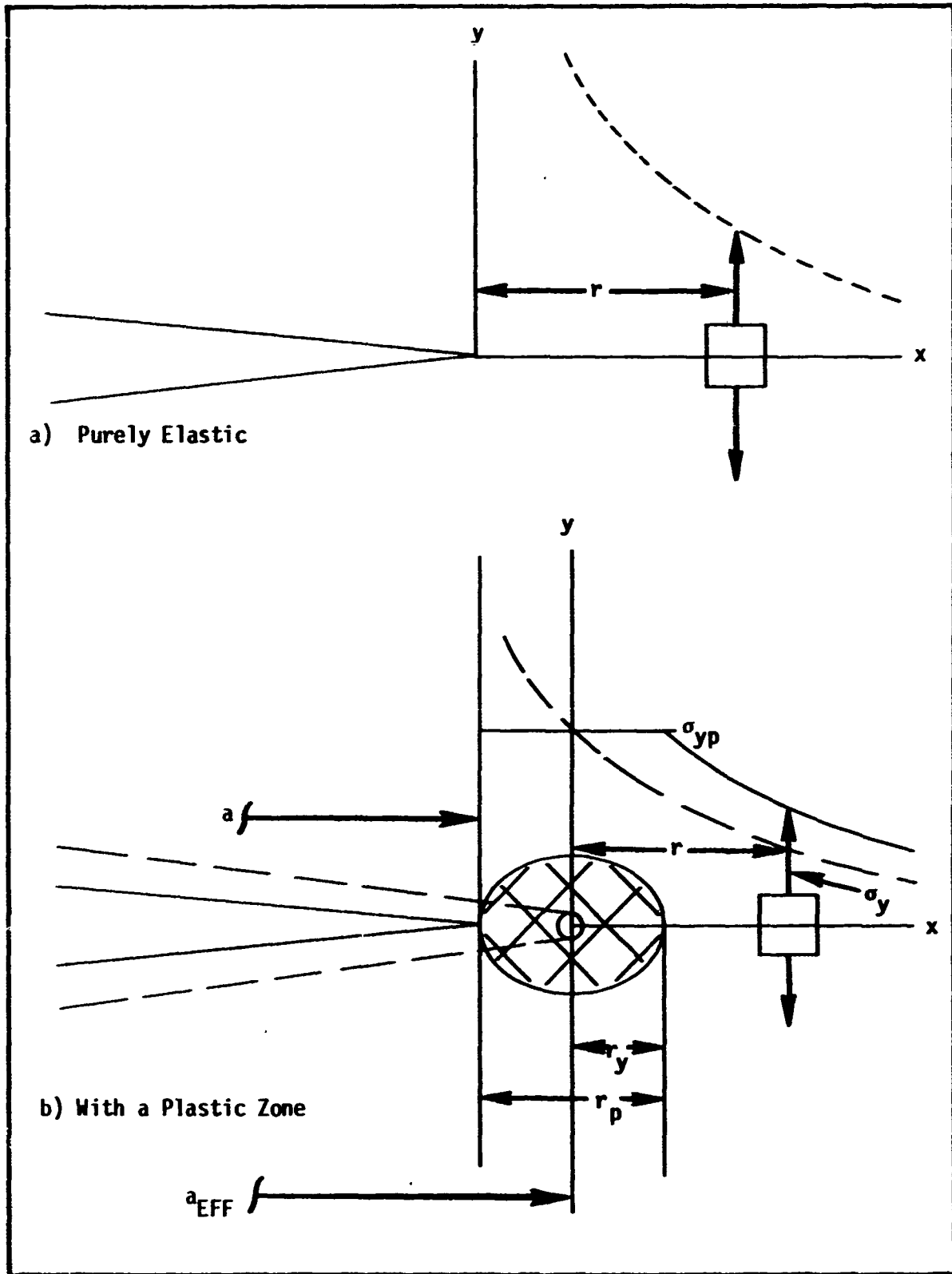


Figure 17. Stress Distribution Ahead of Crack

$$r_y = \frac{K^2}{6\pi\sigma_{yp}^2} \quad (\text{plane strain}) \quad (6)$$

The center of the elastic coordinates at a_{eff} is ahead of the actual crack tip by an amount which should be proportional to the plastic zone size. Considering the redistribution of stresses due to plasticity in Figure 17, equilibrium demands that the net area (positive vs. negative) between the dashed (elastic) and solid (elastic-plastic) stress distribution curves. Simple calculation based on this concept of equilibrium leads to an effective extension of the crack tip or center of elastic stress distribution coordinates by an amount equal to r_y , i.e.,

$$a_{\text{eff}} - a = r_y \quad (7)$$

This result has been verified by more refined plasticity considerations [5, 6]. It leads to a total plastic zone width of

$$r_p = 2r_y = \frac{K^2}{\pi\sigma_{yp}^2} \quad (\text{plane stress})$$

or (8)

$$r_p = 2r_y = \frac{K^2}{3\pi\sigma_{yp}^2} \quad (\text{plane strain})$$

Moreover, a more detailed plasticity analysis of the principal slip directions in the plastic zones shows 45° through the sheet slips in plane stress and up and down angular slips ahead of the crack in plane strain. This, in part, explains the 45° slant fracture surfaces in thin

sheets (plane stress) and flat fractures in thick sheets or heavy sections (plane strain). Moreover, the partial shear lips for intermediate (mixed) thickness of sheets or on heavy sections is the plane stress surface effects accompanying constraint and plane strain on the interior leading edge of cracks. Thus, it is also evident that normally the partial shear lips formed will be of a width proportional to the plane stress plastic zone size (normally about the plane stress $r_y/2$ to r_y in size). The balance of discussion of fracture appearance is left for later sections.

d. Fracture Energy Rates vs Stress Field Concepts

The original Griffith theory and its Irwin-Orowan modification base analysis of fracture on an energy balance approach. The basic idea was a similar two step cause-effect concept, as also discussed earlier, which is as follows: the effect of remote loads on crack extension in a principally elastic body can be represented by the plastic energy made available, G , at the crack tip per unit of new crack surface area created. On the other hand, the material's resistance to crack extension is viewed as the characteristic or critical energy dissipated, G_c , crack tip per unit of new crack surface area created required for continuous separation (or steady state self-perpetuating crack growth). Thus, the fracture criteria was:

$$G = G_c \quad (9)$$

rather than the stress field concept criterion:

$$K = K_c \quad (10)$$

In both cases, the left-hand sides of equations (9) and (10) are elastically analyzed causes of the local crack tip conditions promoting fracture and, in fact, they are equivalent concepts. Their inter-relationship is derived in detail in [1] and [8] and is:

$$G = \frac{K^2}{E} \quad (\text{plane stress})$$
$$G = \frac{(1-\nu^2)K^2}{E} \quad (\text{plane strain})$$
(11)

where E is the Young's modulus of elasticity and ν is Poisson's ratio. Thus, (9) and (10) are identical fracture criteria.

Moreover, this equivalence of the analysis methods can be generalized [1, 2] to include all three modes of crack displacement, and arbitrarily anisotropic elastic media, as well as other considerations.

e. Direct Elementary Applications to Material Properties Characterizing Fracture Behavior

The preceding concepts and discussion of the crack tip stress field (elastic surrounding field) and its intensity factor, K , have built a fairly extensive view of using K as a one parameter description of the local load variable or stress intensity "cause" of crack extension phenomena. It is, therefore, relevant at this point to discuss the material's response characteristics or direct "effects" in terms of this "cause".

The concept that the crack tip stress intensity, K , can be raised in a given material to a certain critical level, K_C , at which self-perpetuating or unstable fast running fracture occurs has already been introduced. But a given material's fast fracture resistance or K_C depends on several additional conditions (or variables) such as thickness effects (plane stress, plane strain or mixed conditions), temperature, metallurgical and manufacturing processing (such as heat treatment, etc.) and cracking directions (especially with a material whose plasticity properties are highly anisotropic or materials containing planes of fairly large scale inclusions or weaknesses, etc.) and other conditions. Most important to discuss are the thickness effects.

For through-the-thickness cracks, the preceding section on crack tip plastic zones discussed the effects of the plastic zone size to sheet thickness on constraint. The additional constraint of plane strain has the effect of diminishing the size of the crack tip plastic zone. Under these highly constrained conditions, unstable fast fracturing is more easily promoted. For that reason, a material's fast fracture resistance, K_C , is a function of the relative constraint for which ratio of the plane strain plastic zone size, r_p , to sheet thickness, B is a relevant index. It is, therefore, common to plot K_C data vs. r_p/B to show the thickness effect as shown in Figure 18 [9]. The data on Figure 18, is evidence that using the plastic zone size to sheet thickness, r_p/B , normalizes the data with respect to thickness effects. The minimum fracture resistance ($r_p/B \rightarrow$ small) relates to fully plane strain conditions and the K_C values in this region are especially labeled, K_{IC} , (or G_{IC}) in the literature

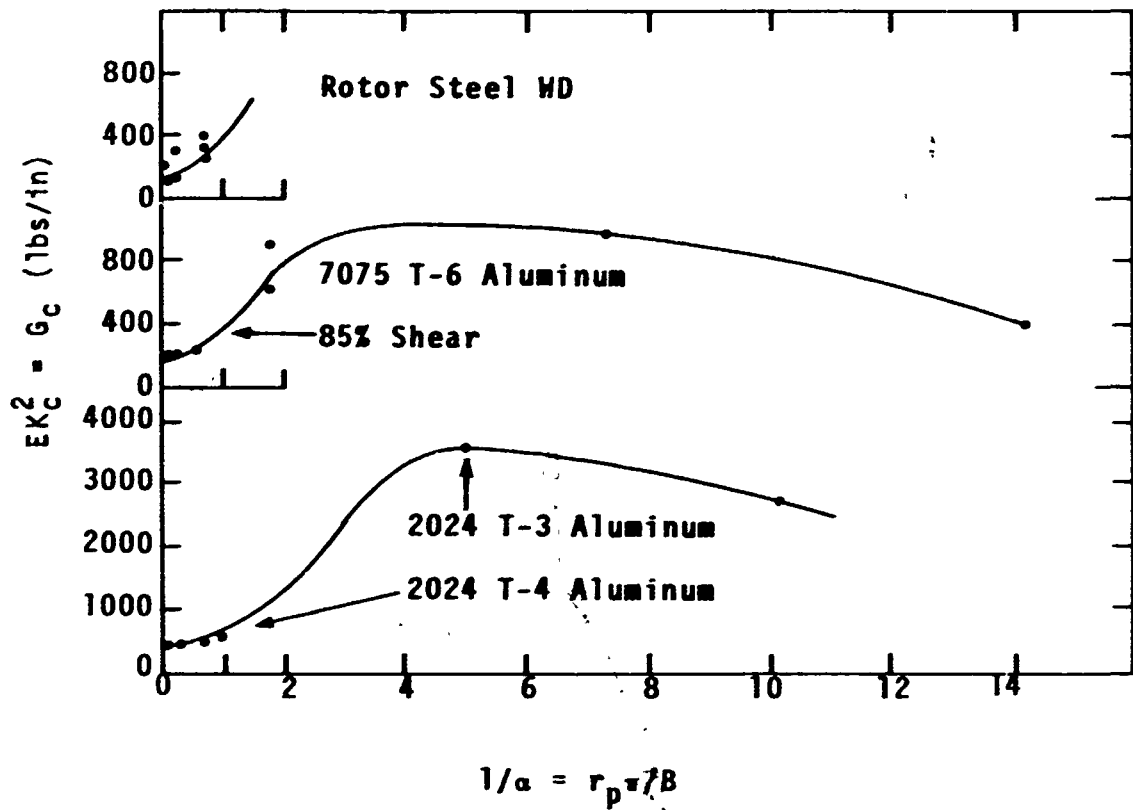


Figure 18. Plot of K_C vs r_p/B for Various Thicknesses

and called the "plane strain fracture toughness."

A useful empirical equation obtained [9] from the data on Figure 18 and other similar data is:

$$K_C = K_{Ic} \left[1 + 1.4 \frac{K_{Ic}^2}{B\sigma_{yp}^2} \right]^{1/2} \quad (12)$$

for use where:

$$r_p/B = \frac{K^2}{B\sigma_{yp}^2} \leq 1 \quad (13)$$

It is emphasized that this equation is a fit of the data only at the lower end of the curves shown in Figure 18 and is thus limited to nearly plane strain conditions. Nevertheless, it is useful in analysis of failure conditions which are only "nearly plane strain" and in relating them to plane strain values of fracture toughness, K_{Ic} , from laboratory tests. In using equation (12) and similar relationships, caution should be exercised in cases where materials delaminate in fracturing (i.e., separations of weak planes perpendicular to the fracture plane occurring during fracturing) which causes loss of plane strain constraint from that expected from simply calculated r_p/B considerations [10].

It is also clear at this point why the ASTM Committee E-24 recommended practice for plane strain fracture toughness test has a minimum size requirement, including specimen thickness, which is

$$\text{SIZE (MINIMUM)} \geq 2.5 \frac{K_{IC}^2}{\sigma_{yp}^2} \quad (14)$$

This guarantees a very low value of r_p/B to obtain plane strain as well as guaranteeing a small plastic zone compared to other planar specimen dimensions assuring that elastic analysis methods are appropriate.

Good accurate plane strain values of fracture toughness, K_{IC} , appear in the literature where these requirements and others have been met (this is usually only in recent data, i.e., since about 1966, so that older data should be checked carefully)(see later section for representative data). Moreover, quoted K_C values in the literature for thinner specimens are not determined by a standardized procedure. Therefore, quoted K_{IC} values from "ASTM-valid tests" may be normally regarded as at least $\pm 10\%$ determinations, whereas K_C values should be viewed as $\pm 25\%$ determinations at best. By careful interpretation of such values from multiple tests and sources, better precision can often be obtained.

The crack tip stress field concept can also be used to characterize a material's subcritical crack growth properties [4], i.e., crack growth due to fatigue (cyclic loads), environment, etc. In early life failures of structural components, subcritical flaw growth often plays a crucial role. This is because in subcritical growth of flaws the growth rate most often accelerates strongly with the crack size as it grows and as a consequence, most of the flaw growth life is spent in the early stages

of growth. This also implies that in analyzing the "causes" of failures, it is usually important to give most attention to the early stages of flaw growth.

Considering the characterization of fatigue crack growth rate properties in terms of the crack tip stress field intensity, K , is quite direct [11] since, K , as in equations (1), is a linear factor in the elastic stress field equations which reflects the influence of applied load, it must, as a consequence, be linearly proportional to the load. Thus as the load pulsates, K pulsates in proportion to the load but with an amplitude which changes with crack size. The rate of crack growth at any time as it grows may be regarded as "caused" by the pulsations of K experienced during that time. For cyclic (sinusoidal) loads with a superimposed mean load, the pulsating character of K may be regarded as described by the range of variation of crack tip stress intensity, ΔK , and its relative mean value, $\gamma = K_{\text{mean}}/\Delta K$. (Alternate descriptions* of the pulsating character of K are possible, but since ΔK is a very strongly influential variable compared to γ in fatigue crack growth rate properties, this choice of parameters is very convenient). Thus, a material's fatigue crack growth properties [11] may be considered to be a plot of ΔK vs. the crack growth per cycle, da/dn , averaged over small but finite increments of growth. Such a

*Frequently, load ratio, $R = K_{\text{MIN}}/K_{\text{MAX}}$, is used along with ΔK as an alternate description of the pulsating character of K in recent publications.

plot is shown in Figure 19 for 7075-T6 aluminum alloy in atmospheric environment (laboratory air).

In fatigue crack growth, although ΔK is the major variable effecting rates, the relative mean load, q , frequency, f , and environment (from vacuum or inert gas to water or hydrogen), are significant variables also influencing rates. Alloying, heat treatment, stress condition (plane stress vs. plane strain), etc., also effect rates of growth in moderate ways. In applying these ideas to failure analysis, the growth of cracks in structural members can be estimated quite well from data plots such as Figure 19 adjusted for the less major or minor variables. Some sources of such data are tabulated later in this report.

As a means of assessing flaw growth life of structural components, judicious numerical integration of crack growth rate data is suggested as the best method developed to date. Attempts to make use of integration of empirical curves fitting the data are less precise, since as mentioned earlier, the initial amount of growth of the crack is of dominating influence because of normally rapid acceleration of cracks. Thus, it is often only a small portion of the crack growth data which is of greatest influence in the life of any one crack. Consequently, empirical fitting of data is only useful in this context only insofar as it fits each small segment of data well. To date, curve fitting methods have not been developed in detail to fit each segment of data. Moreover, with all the variables involved and especially environmental effects, no curve fitting method has been devised to accommodate these effects [12, 13].

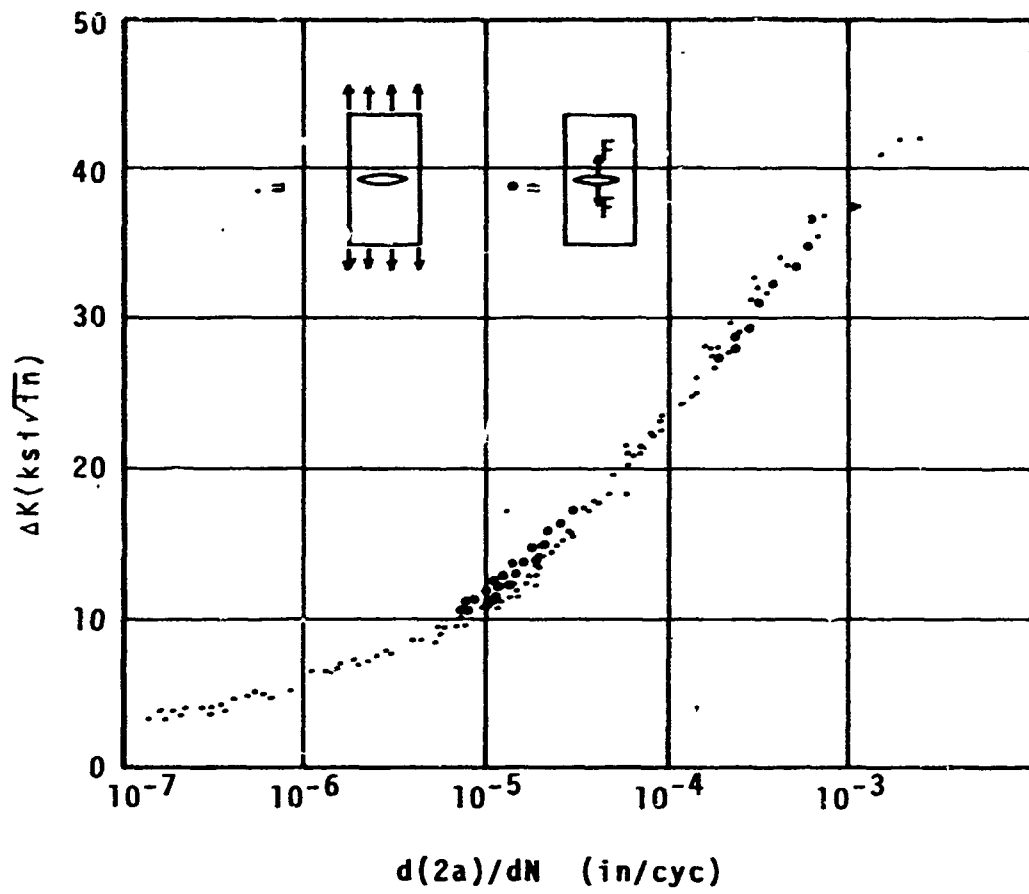


Figure 19. Correlation of Crack Growth Rates in 7076-T6 Aluminum Alloy Under Sinusoidal Loading[41]

In a similar manner, the stress corrosion or static environmental cracking properties of a material can be characterized using the crack tip stress intensity factor, K , as the local load parameter influencing (or controlling) the rate [11]. Figure 20 shows a data plot indicating this concept.

On Figure 20, it can be noted that there is a threshold for environmental cracking under static load, often labeled K_{ISCC} in the

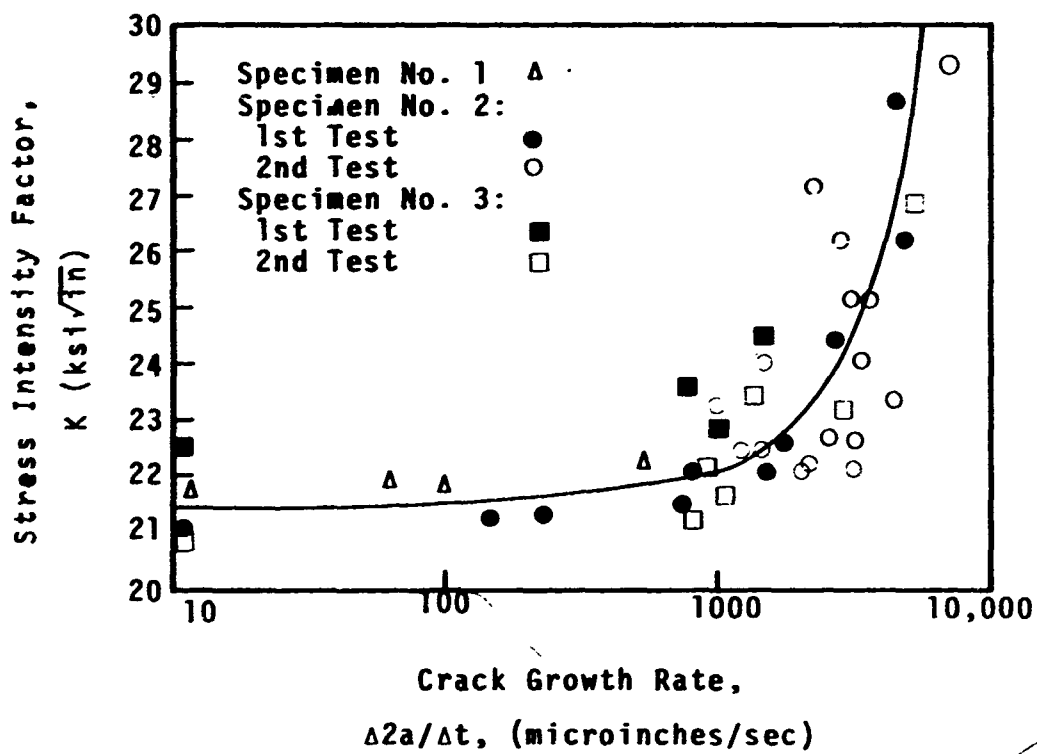


Figure 20. Crack Growth Rate vs Stress Field Intensity, Ti-8Al-1Mo-1V in 3-1/2% Aqueous NaCl Solution [50]

literature below which crack growth is very slow indeed (negligible in the practical application sense). Above this threshold, crack growth rates are normally quite fast or often so fast as to be intolerable in a structural component. Thus, in many failures, though the fracture markings are often most distinct for the onset of final running fracture, somewhat earlier in the crack growth process rather rapid growth due to environmental effects ensues with sometimes relatively little evidence on the fracture surface viewed with the naked eye. Therefore, careful microscopic examinations of fracture surfaces approaching onset of final failure markings often disclose rapid environmental cracking.

The significance of this threshold for fast environmental cracking is being currently further explored especially as influenced by fluctuating loading [e.g., 12] in the nature of mixed effects of environmental cracking simultaneous with and interacting with fatigue crack growth. It suffices to add that these effects should be carefully considered in any assessment of a failure or a design to prevent failure.

f. More Advanced Considerations and Applications to Fracture Behavior in Analysis of Early Life Aircraft Structural Failures.

In the preceding subsection methods of using fracture mechanics to synthesize material properties for the onset of final failure, fatigue crack growth, and environmental cracking were described in an elementary way. In the vast majority of actual failures, all three of these cracking phenomena are involved in events leading to failure. Moreover, they are involved and interacting in a complex manner which

requires either experience and judgment in their application to a failure analysis (or design), or test data which directly simulates conditions from initial flaws to the final failure event.

Moreover, successful analysis of failures frequently involves being able to dismiss certain details or unknown conditions as not strongly relevant and to proceed with a simple analysis which gives reasonable estimates of the events leading to failure. Therefore, it is appropriate to discuss here some features of cracking behavior interrelated with the complex loads and environments common to many aircraft components for which special considerations are necessary. They are as follows:

(1) Initiation of Cracking - early life failures almost always emanate from pre-existing flaws (or accidental damage to a structural component). Usually, inspection tends to minimize these flaws but does not eliminate them. All inspection methods have limitations of sensitivity and dependability.

Upon loading such flaws, they are normally dormant for some period prior to beginning growth. If they are in a part subjected to primarily static loads, and if the applied K level for each is below K_{ISCC} , they will not grow (a significant distance) at all. Moreover, if they are subject to fatigue loads but where the K level is below a characteristic threshold for fatigue crack growth again they will not grow. Thus, for small enough flaws and low enough stress levels initiation of cracking will not take place. However, due to high performance structures required in aircraft, it is unlikely that all of the structural components of any aircraft can meet such

conditions. Nevertheless, it is normal that only the largest of flaws in the most highly loaded components can meet conditions for the initiating and sustaining of cracking and often under only the most severe load-environment conditions.

Hence, it is relevant in failure analysis to examine the initial conditions for growth of the pre-existing flaw to quantitatively establish conditions which promoted first growth.

In initiating cracking from a flaw there is also frequently a delay in initiation (a time or number of cycles to initiation) for either fatigue or environmental cracking. It is conservative and usually sufficiently accurate to assume immediate initiation of growth from flaws in failure analyses. That is to say that initiation is usually only a small part of the life to failure. However, occasionally the initiation period is significant to required estimates of flaw growth life. The methods of determining initiation times are not now well developed. Simulation testing is, perhaps, the only currently reliable way to estimate initiation times and even so the test techniques themselves are not well developed.

(2) The Initial Growth Period in Cracking - immediately following the initiation period, cracking proceeds at rates which may be considered normal for crack tip stress intensity and environmental conditions imposed. However, these rates are usually the slowest rates of growth during the crack growth life since, as mentioned earlier, cracks tend to accelerate strongly as they lengthen due to the increase in crack tip stress intensity with crack size (with rare exceptions for odd shaped flaws

or unusual loadings). Hence, most of the crack growth life is usually spent where the crack has not grown far from the initial flaw. Therefore, in assessing life utmost attention (e.g., examination by electron fractography, etc.) should be given to the cracking just following initiation. Of course, attention should be given to the remainder of progression of the crack insofar as it also influences the life of a structural part. Moreover, the success of periodic inspections may depend on catching flaws following their growth to a substantial size in which case the latter stages of growth may be of paramount interest.

In summary, consideration should be given in the relative importance of the various portions of crack growth with the initial portions usually of dominating influence in life consideration.

(3) Load Profile Effects (First Approximations) - many structural components in aircraft sustain complex load time histories. Frequently, the loads sustained by a component are of a wide variety of levels, irregularly applied and are applied for a variety of times (equivalent frequencies). Moreover, the same components in two aircraft of identical types may experience quite different load profiles due to differences in usage of the aircraft, etc. In order to analyze the effects of such irregular loadings, some simplifications are in order.

A first approximation to the load profile effects on crack growth rates is to assume no interaction between load excursions, i.e., no history effects. In such a case, it is assumed that during a load excursion the current crack growth rate is not effected by past load excursions, nor by

how long loads may have been sustained in the past. The crack growth rate could then be computed for fatigue, as described in Figure 19, the range of crack tip stress intensity, ΔK , or for environmental cracking, as in Figure 20, from the applied K value. Moreover, it is relevant in cases of combined effect of fatigue and environment to simply add the effects of simultaneous action and neglect interaction as a first approximation [11, 12, 14, 15]. That is to say that if a load excursion causes the stress intensity, K, at the tip of a crack to exceed the threshold for environmental cracking, then the fatigue crack extension due to the ΔK from the load excursion and the environmental crack extension from the times K is above the threshold can be computed from data such as on Figures 19 and 20 and simply added to form an estimated rate of growth under combined effects. These first approximations, neglecting interaction effects and past history effects, always give the correct order of magnitude of crack growth rates. Usually, they are within a factor of three or better on estimating growth rates. And even in cases where better precision is desired, they can be used to first estimate if there is a real problem. For example, if the estimated growth rates lead to a prediction of a life more than ten times that required in some component (which is sometimes the case), then an immediate conclusion can be reached that there is no problem (or on the other hand if ten times less than required, the problem is exceedingly bad).

One simplification in addition to those mentioned above, which also applies to more refined estimates, is associated with components subjected to load spectra of very many levels. In such spectra, there are normally very high loads with very few occurrences to very low loads with extremely

large numbers of occurrences per unit aircraft life (frequently based on per 100 flight hours, etc.). In assessing the relative effects of high, medium and low loads and the respective number of occurrences on fatigue crack growth, frequently one of these load level bands is of overriding importance to the others. That some levels can be ignored within the precision of the estimate being made of crack growth rates is an often overlooked simplification. Moreover, the time rate of application (or equivalent frequency) of loads in each load level band is often different and relevant if environment enhanced fatigue crack growth is present. Therefore, finding that certain load level bands may be reasonably ignored in crack growth estimates leads to also concluding that less laboratory data, on effects of frequency on environment enhanced fatigue crack growth, is needed to make such estimates.

These above types of simplifications have been used, and appropriately so, in the analyses of actual failures which follow later in this report.

(4) Advanced Load Profile Considerations - the preceding first approximations on load profile effects ignore past history effects on both fatigue and environmental cracking rates. This may lead occasionally to slight overestimates of crack growth life (by factors as large as say 2), but, fortunately, normally leads to underestimates of life (by factors frequently as large as 3 or more). Therefore, the above first approximation estimating procedures are normally conservative approximations, which is a desirable tendency in a first estimate. However, in critical applications where more accurate life predictions are required even such conservative underestimates may be of a highly undesirable lack of precision.

Therefore, where greater precision is desired, past history, i.e., load excursion ordering and time effects, must be taken into account. This can be taken into account directly by performing crack growth tests where the actual load profile expected in service is used, and the data is compiled in an equivalent manner to Figures 19 and 20 (where time or cycle numbers may be replaced by flight hours, etc.). However, since an aircraft acts as a mechanical (dynamic) filter of the applied loads, actually each component and frequently portions of components experience quite different load profiles. Therefore, many tests with many different load profiles (as well as environments, frequencies, load ratios, etc.) would have to be accomplished in order to fully analyze a single aircraft. It is usually simply not economically feasible to take such an approach.

A much more reasonable approach is to make first approximation estimates of crack growth lives, as discussed above, for the multitude of components in an aircraft. This enables sorting out the few crucial components or areas of certain components where early life failures might be imminent. Consequently, the high precision calculations and/or tests can be concentrated on critical components. This limits the task but does not always eliminate the possibility that it is still quite enormous if undertaken as a test program utilizing actual load profiles for each critical component and area selected. More precise estimates of crack growth life including past history (load ordering and time) effects are desirable to resolve such situations economically and expediently.

For such estimates of the effect of past history on crack growth rates,

it is necessary to understand more about the physical nature of these effects. Observations to date note "delays" in crack growth due to fatigue and/or environment following a previous excursion to a higher load. The higher the previous excursion, the longer the "delay". The "delay" is by some or in some instances regarded as a stopping and reinitiation of crack growth where others or other instances observe slowing to below normal rates and later regaining normal rates of growth. Blunting of cracks, crack division, residual stress due to the plasticity caused by the high load excursion and crack surface interference have all been cited as possible causes of this effect. Moreover, large negative excursions in loads have been also observed to cause some temporary crack acceleration but the effects on overall life are noted to be much smaller than the "delay" or "overload" effects. Though some very limited quantitative data does exist on these phenomena, it is too specific and incomplete to warrant an exposition here. Moreover, the "mathematical models" of these effects are neither tested nor complete enough to warrant specific mention. It suffices to say that "delay effects" exist and that if in practice they are to be taken into account to eliminate a large testing program, then what is to be recommended as an interim measure is a small testing program to evaluate the delay effects for the individual aircraft components of special interest by testing their materials in the load ranges (especially ΔK ranges), environments, frequencies, load ratios, etc., of interest to develop special experimental-empirical models useful for relevant predictions.

With even a crude model or limited data on delays, the first

approximate estimates mentioned above may be improved. Similarly, having environmental control (simulating actual aircraft conditions) of fatigue crack growth test results at relevant frequencies and load ratios also enhances such estimates. These enhancements are real but even with the best estimate calculating, the crack growth life of a known specific flaw can seldom be done within a factor of 2. Nevertheless, such calculations are relevant and useful in failure analysis and design.

(5) Flaw Detection - flaw detection may be regarded as the weakest link in analysis of crack growth lives of actual structural components. In postmortem failure analyses, one can trace back to the flaw and accurately measure its size as a usually simple part of the procedure (see later sections); thus, it presents no special difficulties in that case.

The reason flaw detection and measurement are especially crucial in life estimates returns to the fact emphasized earlier that flaws accelerate rapidly with size. Hence, life is strongly dependent on initial flaw size.

Nondestructive flaw detection systems such as ultrasonics, radiography, etc., all have detection limits which depend on flaw type, location, orientation and equipment details and operator. Thus, specifying a detection limit is highly variable and at best statistical in nature. A factor of 2 variability in detection limit is probably an underestimate of the normal factor. Moreover, usually a factor of 2 on flaw size means a factor of 2 to 4 (or more) error in prediction of flaw growth life.

Therefore, if life must be guaranteed to exceed a certain value, it seems reasonable (and experience bears this out) that flaw detection systems must be an order of magnitude more sensitive, based on flaw size, than the flaw sizes which must be eliminated. Even then the statistical nature of these systems leaves a small probability that a critical flaw may be missed.

The alternative procedures of using proof testing (or in addition with acoustic emission crack detection equipment) are very promising and practical for all types of simple structures with simple (quiet) loading. However, they have the strong limitation that they only detect flaws which are nearly as large as in-service failure sizes. Moreover, proof testing alone is a destructive method of finding flaws larger than detectable size. Again, there are also circumstances in which flaws larger than normally detectable might be missed (e.g., blunt flaws which might pass a proof test prior to sharpening and failing, or flaws which have been somehow yielded in material processing limiting their ability to emit acoustic signals, etc.).

Flaw detection is similarly a problem in in-service periodic inspection, as a least reliable link in guaranteeing no failures by setting appropriate inspection intervals using the flaw growth life calculation methods described herein.

In summary, the methods described herein permit very simple order of magnitude estimates of flaw growth lives, thereby identifying problem components in aircraft structure susceptible to early life failures.

Successive refinements in these methods leading to better precision rely successively more heavily on elaboration of calculations and more refined data as required to identify critical components where full simulation testing or equally accurate elaborate tests and calculations are required.

In all of these calculations as well as in tests, the methodology and descriptive material parameters are based on utilization of the crack tip stress intensity factor concept. Therefore, it is of importance to be able to calculate or estimate with some reasonable accuracy ($\pm 5\%$ desired if possible) the applied K-formulas for complex components with a wide variety of flaws and subject to a variety of loadings. This is a separate task based on deriving formulas using the boundary value problem techniques of theory of elasticity for linear-elastic fracture mechanics applications. The sections to follow will be devoted to a discussion of K-formulas and estimates.

2. Formulas and Estimates for Applied Stress Intensity Factors

A compilation of formulas for stress intensity factors and an exposition on common methods of deriving such formulas is to be found in Reference [1]. Moreover, some methods of formulating estimates of K, i.e., estimating formulas, are also found in Reference [1]. Though this reference was published some years ago, no more extensive compilation is now available which includes the many significant formulas and estimates derived since that time.

In typical aircraft structural components, cracks tend to grow most frequently in areas of high stress, i.e., at stress raisers, and have

complicated often irregular shapes initially and during growth. This complicates the problem of developing estimates of applied K with reasonable precision; however, with experience and careful study, such estimates are normally possible. Occasionally, in extremely complex redundant structures with residual and/or fit-up stresses present, even local stresses (with cracks present) are difficult to estimate with desirable precision. In such cases, it is hardly the fault of this analysis method that local stresses or loads are not well known. And since these local stresses will have a strong influence on flaw growth life, it is assured in such cases that no high precision method will be really successful short of determining those unknown stresses or their equivalent. However, in such cases bounds on stress, such as the yield point, may be used to find bounds on applied K so that extreme lower limits of life may be calculated for areas where actual stresses and, therefore, actual lives are uncertain. These lower limits usually will give life bounds so short as to frequently be a not very useful exercise, however, they are sometimes sufficient to guarantee enough life between inspection intervals to be a sufficient design estimating technique.

Therefore, in any event, it is relevant to illustrate herein methods of estimating K -formulas for flaws near typical stress raisers in aircraft structure. The most common stress raiser is a round hole from which a crack emanates, so it will be used as the basic example. Moreover, the solutions and estimating techniques contained in Reference [1] will not be repeated here, but are recommended as preliminary material for study.

Other typical recent advanced estimates for particular flaw configurations will also not be repeated, but for example for surface flaw K-formulas the many works of Tiffany and Kobayashi (The Boeing Company and University of Washington) are recommended to the reader as an illustration of the elaboration and precision which may be incorporated into K-formula estimates. The remainder of this sub-section will be devoted to a discussion of the stress intensity analysis for cracks adjacent to circular holes in a uniformly stressed plate since it is one of the more frequently encountered conditions.

The two dimensional stress analysis of a through thickness crack emanating from a round hole in a plate subjected to uniform uniaxial tension has been treated by Bowie[40], and his solution is tabulated in Table XIII. One of the cases he treated is depicted in Figure 21. For this configuration, he found that the crack tip stress intensity was

$$K = \sigma(\pi L)^{1/2} F\left(\frac{L}{R}\right) \quad (15)$$

where $F(L/R)$ is plotted in Figure 21. These results are correct within about $\pm 5\%$ when taking into account uncertainties due to three dimensional effects (provided that the hole is of the order of the plate thickness or larger).

As an example of estimating procedures, the results can also be approximated from other solutions as follows. The stress concentration factor at the edge of the hole is 3. Therefore, for shallow cracks, ($L \ll R$) one

TABLE XIII. STRESS INTENSITY FOR A CRACK EMANATING FROM A HOLE

L/R	F(L/R) [Eq. (15)]	(3.39) [Eq. (16)]	$(\frac{1}{2} + \frac{R}{L})^{1/2}$ [Eq. (17)] (lower bound)	Best Estimate
0	3.39	3.39		
0.1	2.73			
0.2	2.30			
0.4	1.86		(1.73)	(1.90)
0.8	1.47		(1.32)	(1.45)
1.5	1.18		1.03	1.13
3.0	0.94		0.91	1.0
5.0	0.85		0.84	0.84
-	0.707		0.707	0.707

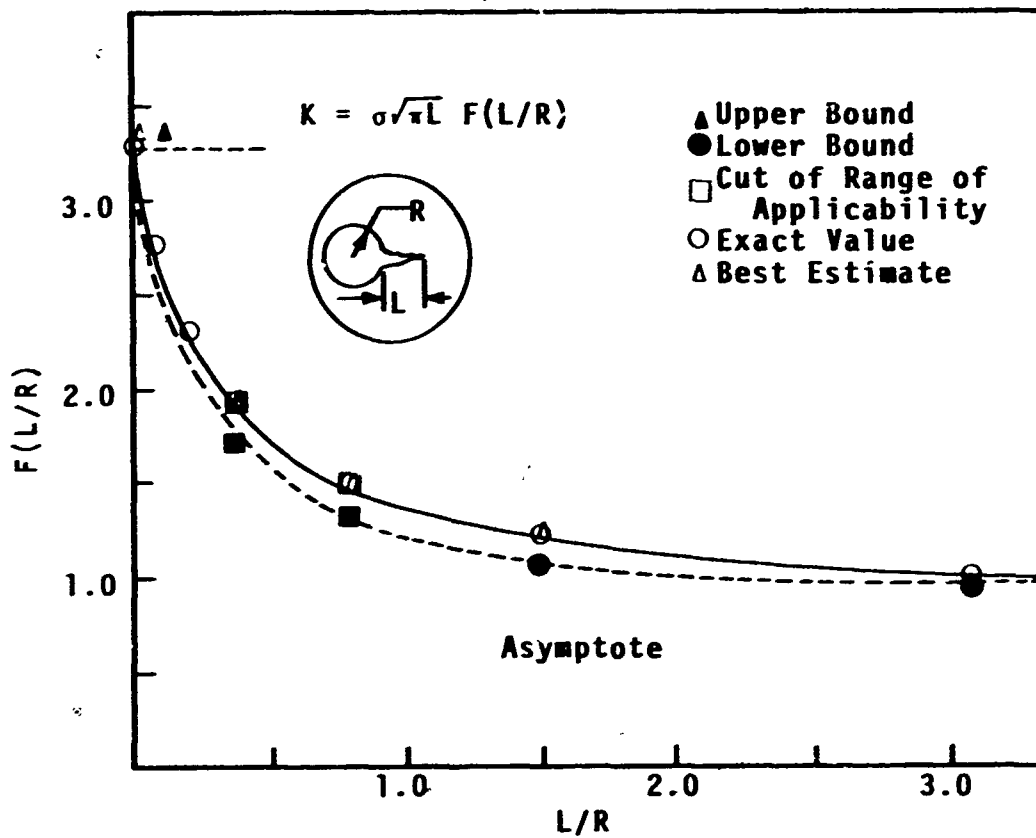


Figure 21. Bowie's Factor for Cracks Emanating from Holes

can view the problem as an edge crack in a semi-infinite plate for which,

$$K = 1.12(3\sigma)(\pi L)^{1/2} \quad (L \ll R) \quad (16)$$

It should be noted that as the crack deepens, it quickly runs out of the 3σ concentration of stress and the hole is more constraining than an infinitely long free surface. Consequently, Equation (16) rapidly overestimates K as the crack becomes larger relative to the size of the hole, (it is an upper bound).

On the other hand, if the crack is fairly large compared to the size of the hole ($L > R$), it can be viewed as equivalent to a crack of total length $L + 2R$. Using the solution for a crack alone in an infinite plate,

$$K = \sigma \left[\frac{\pi}{2} (L+2R) \right]^{1/2} \quad (L > R) \quad (17)$$

For the crack length to hole radius ratios of interest ($L/R > 1$), Equation (17) would underestimate the stress intensity K since the hole would remove some constraint for deformation. But this effect would be small, probably about 10%, and would decrease for higher L/R values.

From the approximate Equations (16) and (17), one may form a best estimate solution for the correction factor $F(L/R)$ in Equation (15). These are listed in Table XIII in columns 3, 4, and 5. The final column is the best estimate solution formed in the following way; for $L/R=0$, Equation (16) is used and $F=3.36$. For $L/R=0.4$ to 3.0 , the values were obtained from

Equation (17) with 10% added as indicated previously. At $L/R > 3$, the 10% has been dropped since the error in Equation (17) should diminish for higher L/R values.

These estimated values are then plotted on Figure 21 and a smooth curve drawn between the listed values. The values from Bowie's analytical solution, Equation (15), are also shown on Figure 21, so that the accuracy of the best-estimate curve can be compared to them. The results show the confidence that can be placed in estimating procedures.

Now, one should proceed to estimate for the quarter-elliptical flaw adjacent to a circular hole. Quantitative estimates will be stated in order to describe expected growth characteristics. For the quarter-elliptical flaw, the stress intensity, K , varies (continuously and smoothly) along the crack front. Therefore, it is appropriate to estimate the stress intensity at three locations, A, B, and C on Figure 22.

In order to make the estimates, some basic solutions are required. For an embedded elliptical flaw in a uniform stress field, Irwin's results are

$$K = \frac{\sigma(\pi a)^{1/2}}{\phi_0} \left(\sin^2 \beta + \frac{a^2}{c^2} \cos^2 \beta \right)^{1/4} \quad (18)$$

where ϕ_0 is the complete elliptic integral of the second kind.

$$\phi_0 = \int_0^{\pi/2} \left[1 - \frac{c^2 - a^2}{c^2} \sin^2 \theta \right]^{1/2} d\theta \quad (19)$$

The notation is further defined in the sketch of Figure 23.

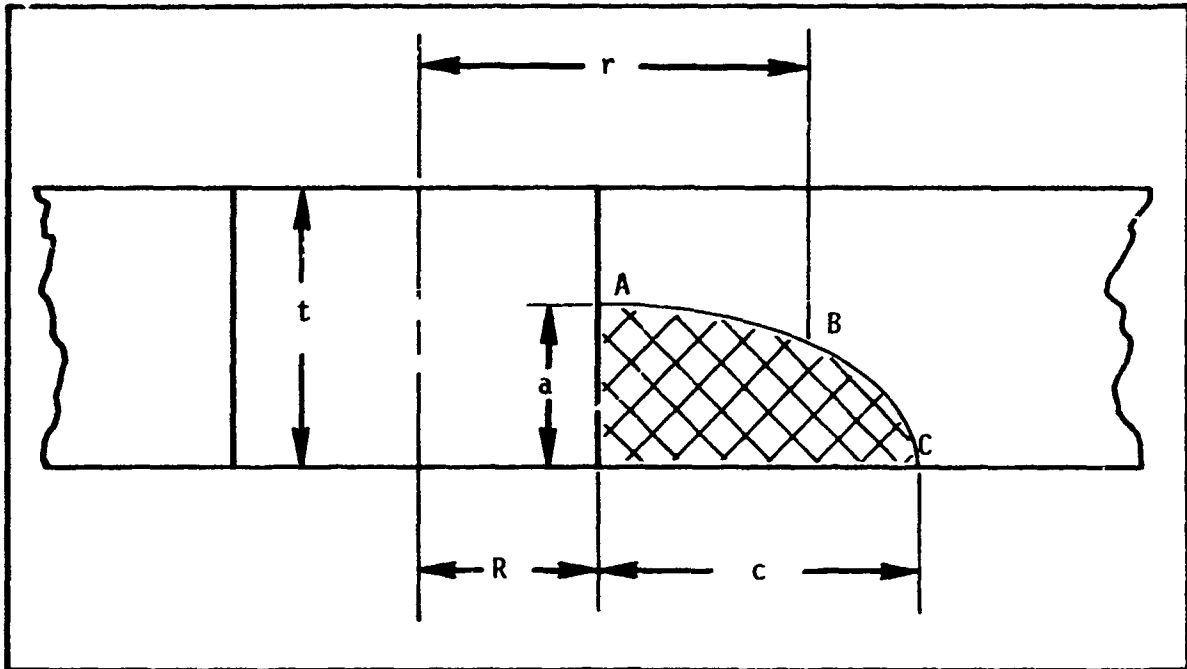


Figure 22. Quarter-Elliptical Flaw Geometry

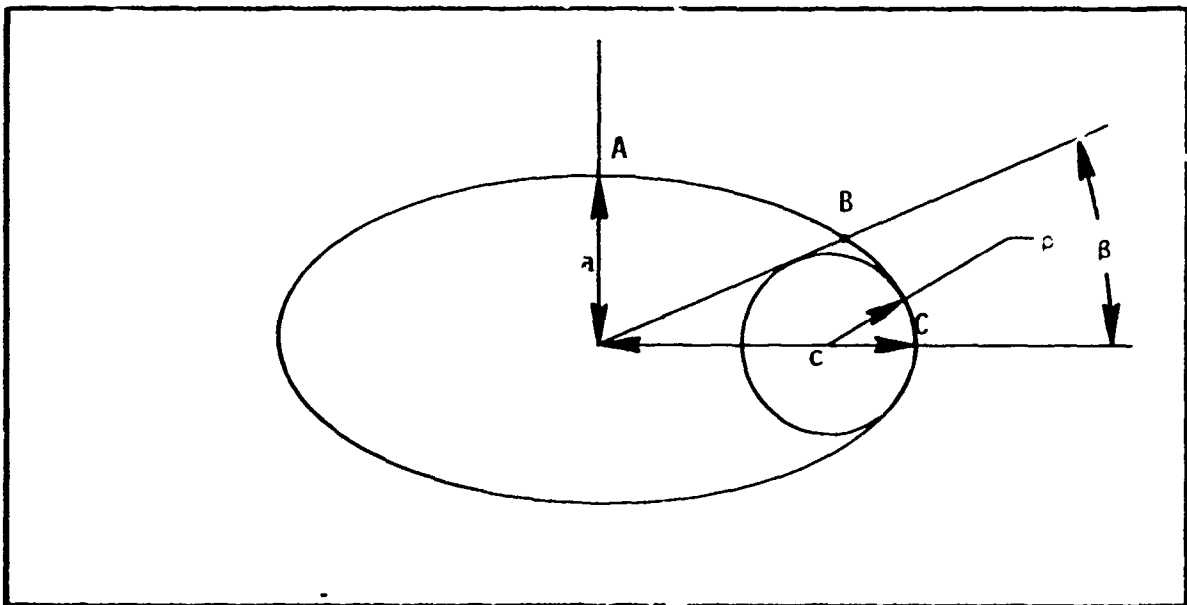


Figure 23. Notation for Flaw Geometry

For A, B ($\beta = 45^\circ$) and C on the ellipse with no corrections for the hole or plate surfaces:

$$\begin{aligned}
 K_A &= \frac{\sigma(\pi a)^{1/2}}{\phi_0} \\
 K_B &= \frac{\sigma(\pi)^{1/2}}{\phi_0} \left[\frac{a^2 + \rho^2}{2} \right]^{1/4} \\
 K_C &= \frac{\sigma(\pi \rho)^{1/2}}{\phi_0}
 \end{aligned}
 \tag{20}$$

where $\rho = a^2/c$ is the end radius of the ellipse. However, if the shape is an oval, which is not exactly an ellipse, it is evident that the actual end radius ρ should be used in the formulas rather than a^2/c , to get a best estimate.

In applying Equations (20) for a quarter ellipse near the hole and free surfaces of the plate in Figure 22, corrections should be made. For the various effects they are:

a. Near a round hole in a plate the stress at the actual location of the point of interest (A, B, or C) should be used or (see Figure 22.)

$$\sigma_{\text{ACTUAL}} = \sigma \left[1 + \frac{1}{2} \left(\frac{R}{r} \right)^2 + \frac{3}{2} \left(\frac{R}{r} \right)^4 \right]
 \tag{21}$$

b. The approximate corrections for a crack emanating from a free surface is a factor 1.12.

c. The effect of a crack front approaching a nearly parallel free surface is a strip (which has no bending rotation far away from the crack) is

$$\left[\frac{2t}{\pi a_{\text{eff}}} \tan \frac{\pi a_{\text{eff}}}{2t} \right]^{1/2} \quad (22)$$

which should be applied directly to A, with the effective crack depth

$$a_{\text{eff}} = \sqrt{\frac{a^2 + \rho^2}{2}} \text{ for B, and not at all at C.}$$

d. For out of shape ellipses, for B and C, a best approach to estimating ρ is not to use a^2/c , but to use the actual end radius, ρ , but with the value taken limited by $a^2/c \leq \rho \leq a$ (or c whichever is smallest). This rule of thumb accounts for any out of shape errors approximately and reasonably in this analysis.

Applying the corrections, Equations (20) become:

$$K_A = \frac{1.12(3\sigma)\sqrt{\pi a}}{\phi_0} \sqrt{\frac{2t}{\pi a} \tan \frac{\pi a}{2t}}$$

$$K_B = \frac{1.12\sigma \left[1 + \frac{1}{2} \left(\frac{R}{R+a} \right)^2 + \frac{3}{2} \left(\frac{R}{R+a} \right)^4 \right]}{\phi_0} \sqrt{\pi \sqrt{\frac{a^2 + \rho^2}{2}}} \times$$

$$\sqrt{\frac{2t}{\pi} \sqrt{\frac{2}{a^2 + c^2}} \tan \left(\frac{\pi}{2t} \sqrt{\frac{a^2 + \rho^2}{2}} \right)} \quad (23)$$

(r=R+a)

$$K_C = \frac{1.12\sigma \left[1 + \frac{1}{2} \left(\frac{R}{R+c} \right)^2 + \frac{3}{2} \left(\frac{R}{R+c} \right)^4 \right]}{\phi_0} \sqrt{\pi \rho}$$

(r=R+c)

These formulas, Equation (23), are rough estimates ($\pm 10\%$ to 15% for $a/t \leq 1/2$, and 20% to 30% for larger a/t values) and subject to some improvement. However, for their immediate purpose of analyzing the growth patterns of flaws adjacent to holes, they are sufficient to fully show all trends in behavior. Moreover, by estimating errors by alternate analysis, further improvements can be made in values for particular cracks ($\pm 10\%$).

Some further irregularities in the progression of typical crack front shapes from a hole are shown in Figure 24. In the typical progression of shapes shown, some new cases of shapes, for which K might be estimated, emerge.

For the shape shown in Figure 25, the ellipse with a greater than c , at A one may estimate

$$K = \frac{1.12(3\sigma)\sqrt{\pi\rho}}{\phi_0} \quad (24)$$

where the roles of a and c are interchanged in computing ρ and ϕ_0 from those in the previous examples ($\pm 20\%$ accuracy). For the case shown in Figure 26; where the crack has grown through the plate at A but not elsewhere leaving a long S-shaped front for which one might estimate that at A:

$$K = \sigma\sqrt{\pi d} \cdot F\left(\frac{d}{R}\right) \cdot \left(\frac{t}{t-a}\right)^{1/2} \quad (25)$$

where the factor $(t/t-a)^{1/2}$ is that usually used for side grooved specimens, and $F(d/R)$ is as in Table XIII ($\pm 20\%$ accuracy).

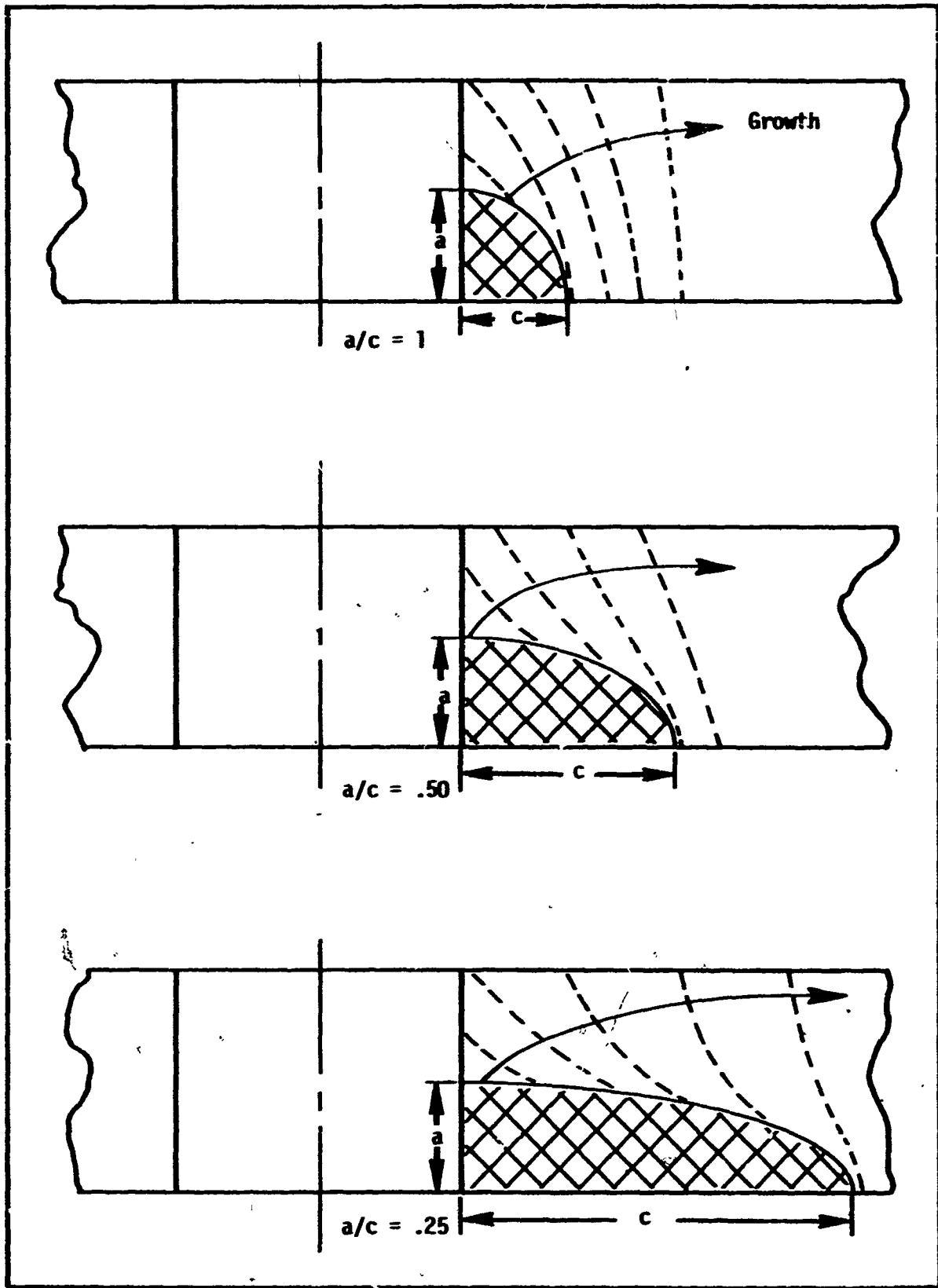


Figure 24. Crack Progression Irregularities

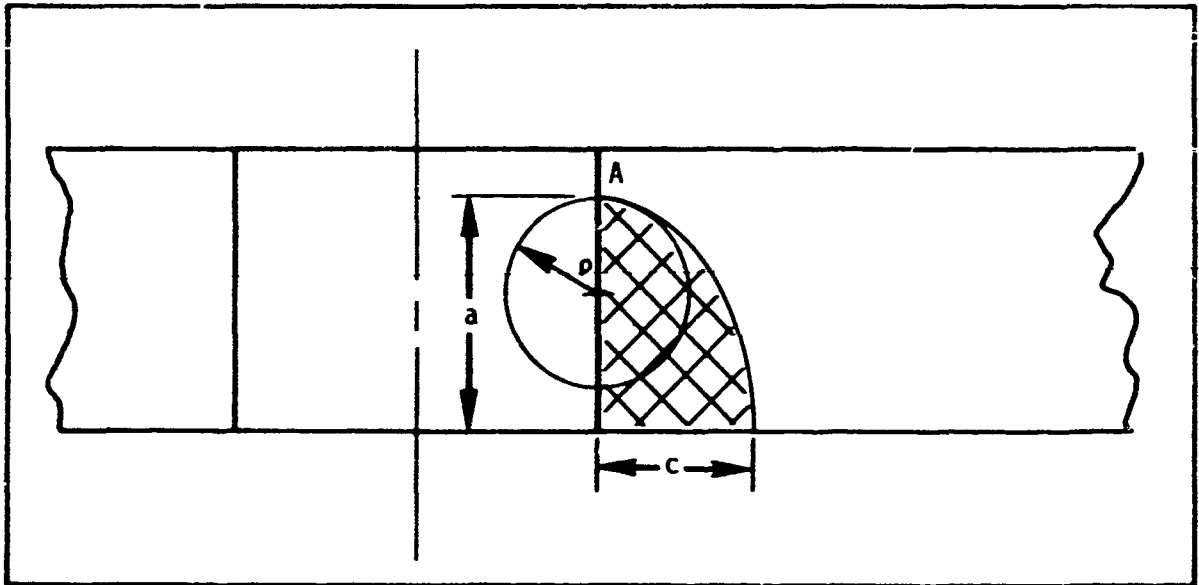


Figure 25. Crack Geometry for $a > c$

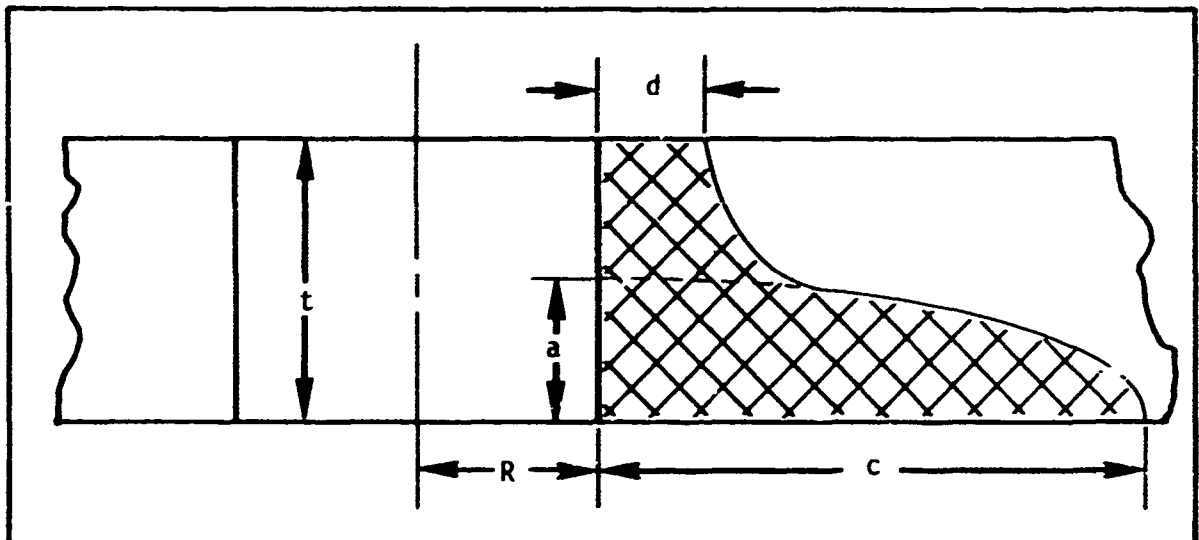


Figure 26. Partial Through-Crack Geometry

Other estimates and refinements of formulas could follow, but these examples, Equations (24) and (25) are sufficient to illustrate that calculations can be performed on the growth pattern of cracks to estimate, for example, rates of growth or arrest positions, for regular and odd shapes of cracks appearing near holes.

B. Fracture Examination and Identification

1. Macroscopic Aspects of Fracture

a. Introduction

Macroscopic fracture markings are used to establish direction of fracturing, the region of fracture initiation, and (when possible) the nature (size and geometry) of the defect which assisted development of fracture instability. Depending on circumstances and the skill of the observer, it may also be possible to establish approximate values for the fracture toughness and for the stress levels across various regions traversed by the fracture path(s).

A binocular microscope with 10x to 100x magnification is desirable for good macroscopic viewing of fracture surfaces. However, during initial examinations, use of such equipment is rarely feasible. Thus, the primary equipment with which one approaches the initial examination task consists of various hand lenses, a strong flashlight, a tape measure, and some cleaning equipment. For cleaning purposes, an inert solvent such as acetone and occasionally a soft bristle brush are useful. Compressed air and various other mild cleaning liquids are also helpful. Judgment is necessary with regard to removing surface material which was deposited after the fracture failure while, at the same time avoiding removal of fracture surface stains which occurred prior to final fracture failure. In the case of fractures of special importance, a considerable amount of additional examination of samples from the failure using laboratory

working conditions and equipment will be needed. Customarily, the planning of this laboratory work is done during or immediately after initial examinations. The efficiency of this work is greatly assisted if the examinations are guided and carried through with a good understanding of macroscopic fracture behaviors based upon fracture mechanics.

A brief review of macroscopic crack extension behavior patterns in association with fracture mechanics is given in reference [14]. A more extensive review of similar kind is given in reference [15]. Reference [16] discusses techniques of macroscopic fracture examination in considerable detail. The selection of topics to be discussed here is as follows: progressive fracturing, fracture failure examinations, running crack behaviors, estimates of K based upon plastic strain near the fracture, flat tensile and oblique shear separations, direction of fracturing, and typical starting crack defects.

b. Comments on Progressive Fracturing and Fracture Failure Examinations

Progressive fracturing occurs by the growth and joining of small advance separations near the leading edge of a crack. When the load on a metallic component is increased at a moderate rate until fracture occurs, examination of the fracture rarely shows more than one starting region for the entire separation. Thus, the expected fracture pattern is one which spreads out by progressive crack extension from a single primary-origin region. The consistency of this behavior depends upon the improbability of crack propagation developing simultaneously

from more than one "worst defect", and upon the quickness of fracture propagation. Only the competitive "worst defects", located near the fracture path are expected to be revealed by the fracture. With increased speed of loading into a time range smaller than the lowest vibration periods of the component, the probability of more than one primary fracture origin is greatly increased.

Methods of recognizing the direction of fracturing will be explained at a later point. A low stress structural fracture always has a single primary origin and use of fracture direction markings usually permits unambiguous identification of the region containing this origin. However, in the case of structural fracture failure of an airborne airplane, malfunctions related to the first fracture event may cause aerodynamic loads which result in additional fracture patterns while ground impact, combustion, and explosions may be expected to cause much additional fracturing.

After as many failed parts as can be found have been assembled, the failure analysis task should center attention upon establishing the time sequence of the various separational events. To do this, one looks for fracture origin regions, that is, positions from which the separation spreads out in opposite directions. Each individual crack segment terminates at a point of crack division, an intersection with a free edge (or surface), or a low stress fracture arrest region. Thus, families of crack segments, each related to a single origin are mapped out. Families of this nature which correspond to a single stress pattern and which have

close structural connections must have developed nearly simultaneously. A very close spacing of origins and short segments prior to crack division (along with other evidence) would correspond to explosive type loading speed.

The free edges (or surfaces) introduced by any one family of crack segments usually provide end-points for crack segments pertaining to other families. The time sequence of the various families of crack segments, thus established should indicate a single crack pattern (or a single group of closely spaced cracks in the case of a sudden impulse or explosion) which clearly happened prior to other cracking. Attention can then be centered upon the origin region (or regions) pertaining to the initial cracking as a means for deciding whether this fracture occurred at a stress level below the loads contemplated in design or whether the primary origin occurred from a high stress overload.

Unfortunately the assembled parts may be incomplete. Furthermore, it is possible for aerodynamic and other factors to "disconnect" the primary fracture origin from the balance of the fracturing. For example, in the case of a Navy developed aircraft, two flight trial planes were lost before these accidents were traced to fracture of the elevator control rod. Fracture of this rod caused the tail of the airplane to rise rapidly thereby generating critical stress conditions in the wings; it was initially concluded that wing fracture surface markings were associated with breaking of the wings from normal force on their upper surfaces.

When a service fracture failure of substantial complexity happens,

missing information and odd circumstances are normal to the situation. Indeed, it is not always possible to find a clear explanation. In such situations, it is necessary to obtain the maximum information possible from knowledge of the most probable load patterns and from such fracture patterns as are available for study.

c. Running Crack Behaviors

Figure 27 shows a schematic view of a region of plastic strain (slant shading) at the leading edge of a crack. The coordinates, r , θ , and x , y are also shown. x is the direction of expected crack extension. For the tensile fractures with which we are mainly concerned, y is the direction of largest average tension across the region ahead of the crack. From linear stress analysis, the y -direction extensional stress, σ_y , is given by

$$\sigma_y = \frac{k}{\sqrt{2-r}} \cos \frac{\theta}{2} \left[1 + \sin \frac{\theta}{2} \sin \frac{3\theta}{2} \right] \quad (26)$$

This is an approximate expression valid when r is substantially larger than r_{YS} while remaining very much smaller than distances from the leading edge to free surfaces or points of load application. k is the stress intensity factor, a function of the applied load, of crack size, and of other dimensional factors.

When the equations for σ_x and τ_{xy} are considered along with equation (26), one finds that the largest principle tension for a given value of γ is maximum along $\theta = -\pi/3$, and at this θ value, agrees in direction

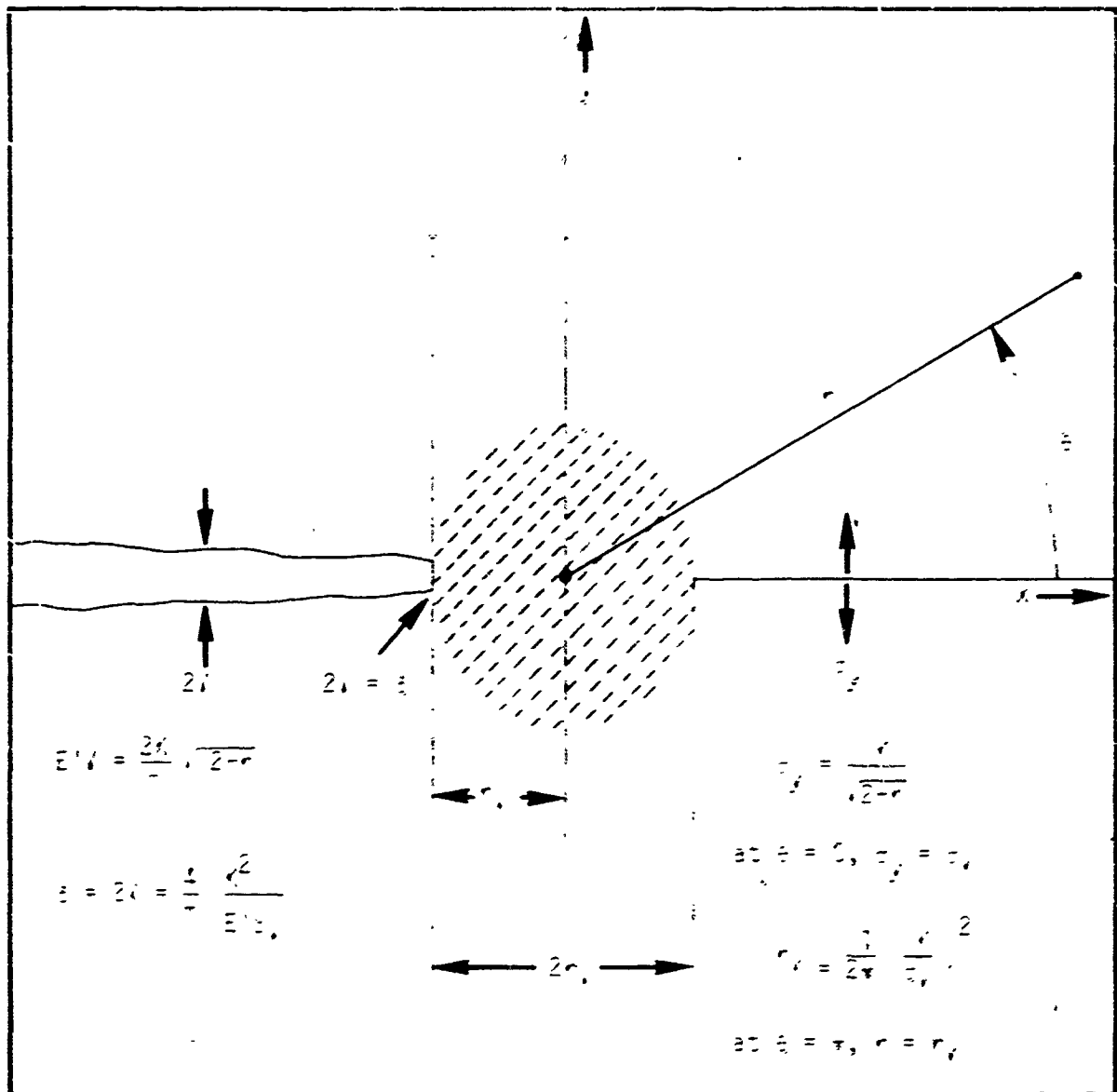


Figure 27. Schematic of the Leading Edge Region of a Crack

- r_p = Plastic Zone
- x, y = Rectangular Coordinates
- r, θ = Polar Coordinates
- σ_y = Normal Stress
- $2a$ = Crack Opening
- r_n = Crack Size Plasticity Adjustment
- $2r_n$ = Nominal Plastic Zone Size

with σ_y . From equation (26), the angle function portion of the expression has the magnitude 1.3 for $\theta = \pi/3$ and is equal to unity for $\theta = 0$. At this point, one should recall that progressive crack extension in structural metals occurs by growth and joining small advance separations. From this one can readily understand why fracture surfaces tend to be rough. In addition to the random location of points of weakness, the opening of small advance separations at locations above and below the x-axis line is obviously favored by the nature of the leading edge stress pattern. On the other hand the average direction of crack extension (in nearly isotropic material) remains normal to the direction of greatest tension. Exceptions to this occur only after the development of net section yielding.

When a moving crack approaches a free boundary (the edge of a plate or a prior crack), the crack can be expected to approach the free boundary along a line which is perpendicular to the boundary. This is necessary because, near the boundary, the direction parallel to the boundary is the direction of largest tension. As plastic yielding develops across the net ligament prior to final separation, weak paths for separation tend to develop along lines of largest shear deformation, and the final joining of the crack to the free boundary usually follows an oblique shear path. The normal orientation tendency of the crack approaching a free boundary and the oblique shear during the final separation supplement direction of fracturing judgments in the establishment of crack segment families and in deciding on the time sequence of fracture events.

The average speed of a running crack is balanced against the tensile driving force, K . For a given K there is a fixed average speed of crack

extension. The crack speed increases and decreases in phase with changes of the K value. However, the increase of crack speed with increase of K tends toward zero as the speed approaches a limiting value such that attempts to drive the crack at a speed higher than the limiting crack speed result in crack division. (See Figure 28.)

The initiation of rapid fracturing by increase of the K value at the leading edge of a stationary crack and the arrest of rapid fracturing with a sufficient lowering of K tend to occur in an abrupt manner. The special K values for crack division and crack arrest are material characteristics for a given material, plate thickness, and temperature. The K value for onset of rapid fracturing may also be regarded as a material property. (See Section C for representative fracture toughness material property data.) However, this K value depends also on speed of loading (for rate sensitive materials) and on the "bluntness" condition at the leading edge of the initial crack. The main emphasis in crack toughness evaluations has been upon determinations of the K value for onset of rapid fracturing. For such determinations, the practices currently favored require "sharpening" of the leading edge of the initial crack by a segment of low amplitude fatigue prior to application of the testing load.

Figure 27 shows the size of the leading edge plastic zone as $2r_y$. This is based upon use of r_y as a crack size plasticity adjustment factor where

$$r_y = \frac{1}{2\pi} \left(\frac{K}{\sigma_y} \right)^2 \quad (27)$$

The positioning of the linear analysis model leading edge at a distance

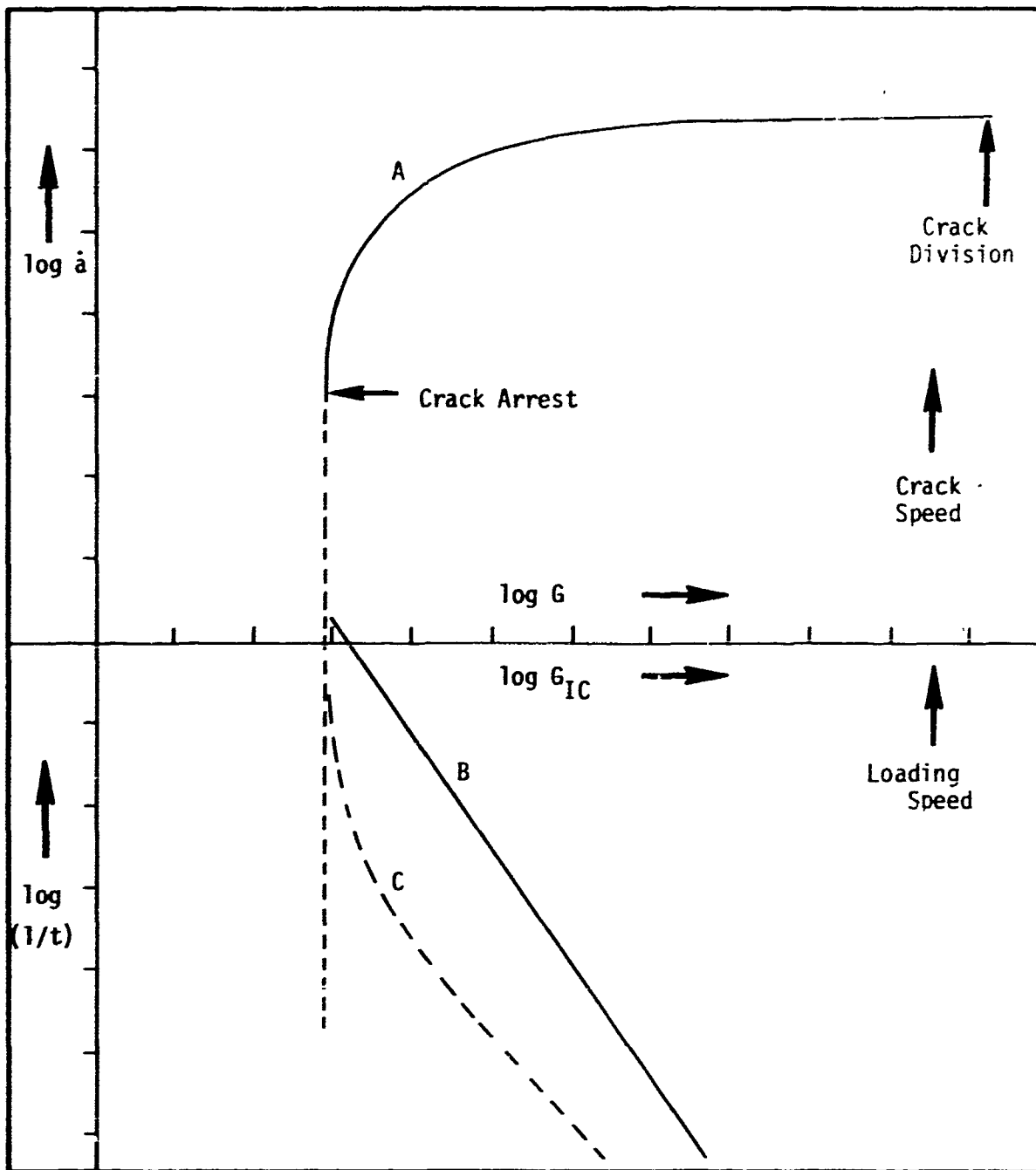


Figure 28. Schematic Representation of Crack Extension Behaviors[14, 15]

Curve A: Fast-Stable Regime

Curve B: G_{IC} Trend for a Rate Sensitive Steel

Curve C: Possible Effect of Large Increase of Crack Size

r_y ahead of the apparent leading edge of the crack improves the fit of the linear analysis stress field to the actual stress field and permits practical use of the corrected linear analysis up to stress levels nearly large enough for general yielding. The nominal size of the plastic zone, $2r_y$, is given by

$$2r_y = \frac{1}{\pi} \left(\frac{K}{\sigma_y} \right)^2 \quad (28)$$

Where we are concerned with through-cracks extending in a sheet or plate, σ_y is the uniaxial tensile yield point.

When the plate thickness is large enough in relation to the plastic zone size, the fracture will (normally) show a flat tensile appearance in central regions bordered by shear lips. In such cases, a rough estimate of K can be attempted based upon the empirical assumption that the width of each shear lip is roughly equal to r_y . Such estimates are of limited value unless they can be substantiated in other ways. In some materials the plastic deformation which would normally precede oblique shear fracturing can develop and, either from rapid strain aging or some other reason, the final separation will occur in the flat tensile matter. Certain heavy section steels ($\sigma_{YS} = 95\text{KSI}$) at 200°F and 2024-T3 aluminum alloy in 0.5 inch or greater thickness at room temperature provided examples of this behavior. Formation of shear lips can also be suppressed by a brittle surface layer as from nitriding of a steel. In general, when the plastic zone size is comparable to or larger than the plate thickness, the appearance aspect which serves best for making a judgment of crack

toughness or K value is the thickness reduction.

Trials of plate thickness reduction measurements have been made during crack toughness testing with the measurement points centered in the opposing plate surface dimples adjacent to the apparent leading edge of the crack.

$$T_R = \frac{K^2}{E\sigma_y} \quad (29)$$

From trials at several laboratories [19], the results could be approximately represented by equation (29), where T_R is the thickness reduction. The correlation with equation (29) tended to become poor when the nominal plastic zone size, $2r_y$, was less than the plate thickness. When $2r_y$ was comparable to or larger than plate thickness, the measured values tended to lie in the range of 85 percent to 100 percent of the value predicted by equation (29). When the measurements were made after the plate had been unloaded by fracturing, it was noted that addition of the yield point strain to the measured value of thickness reduction assisted correlation of the measurement result with equation (29). The theoretical basis for estimates of K from the above equation, while plausible, is incomplete and is not discussed in this report.

d. Direction Indications for Flat Tensile and Oblique Shear Separations.

As noted earlier, locations of points of weakness ahead of a moving crack tend to be random and the stress field favors advance separational developments above and below the line of expected crack extension.

Consider next the natural shape of the leading edge of a relatively brittle crack traversing a plate. For the plate region surrounding the leading edge, the crack opening constitutes in-plane bending and a tendency toward anti-elastic curvature [47] would be expected at the fracture surface. Correspondingly, the leading edge of the crack should have an arc shape. If there is no out-of-plane bending, the crack should lead slightly in the center plane region of the plate. Secondly, the natural crack speed for a given K tends to decrease with increase of the fracture work rate. Thus, an increase of the lag of the crack at the free surfaces of the plate is expected because the fracture work rate is larger there. The lag of the crack permits larger effective K values near the free surfaces. This assists the free surface fracturing to "keep up" with the speed of crack extension at the plate center.

In central regions of the plate, the advance separations which are furthest from the line of crack extension introduce fracture surface level differences. The joining of the region of separation associated with each such out-of-plane advance origin to the main fracture surface tends to occur along a "tear separation" line. Such lines are best seen with the unaided eye or low magnification. They tend to spread out from central regions of the plate toward the lagging regions of the fracture at the free surfaces. The common term for these lines is "chevron markings". Where a central advance separation produces "tear" lines with a chevron appearance, the chevron opens in the direction of crack propagation.

When reduction of magnification fails to reveal marking of the above chevron type as indication of fracture direction, one can only conclude

that these markings were obscured by the overriding size of inherent planes of weakness in the material. These are of two kinds:

(1) The planes of weakness may be solidification boundaries or grain boundaries as in the case of certain cast magnesium alloys. In such cases the extent of the fracture path on individual facets may be large enough so that study of these facets at high magnification shows the direction of fracturing.

(2) The planes of weakness may be "splits" or "delaminations" normal to the fracture surface due to through-the-thickness weakness of the plate material. In this case there will be a considerable amount of oblique shear separation and comments given in the next paragraphs would apply to determinations of direction of fracturing.

When there is no significant flat tensile region and the separation occurs mainly or entirely by oblique shear, it has been found that determination of the direction of fracturing can be assisted by the following examination procedure. Using either half of the fracture, examine the region of the plate surface indicated by Figure 29. In other words, look at the plate surface which has an oblique shear separation behind it. In the case of steels, one can see small splits at the top edge as shown in Figure 29a. The "thumb test" (not recommended) consists in stroking this edge in each direction to see which direction reveals the sharp asperities. In the case of aluminum alloys, generally the splits noted do not develop. However, the localized plastic flow which must precede such developments occurs and results in flow markings as shown in Figure 29b.

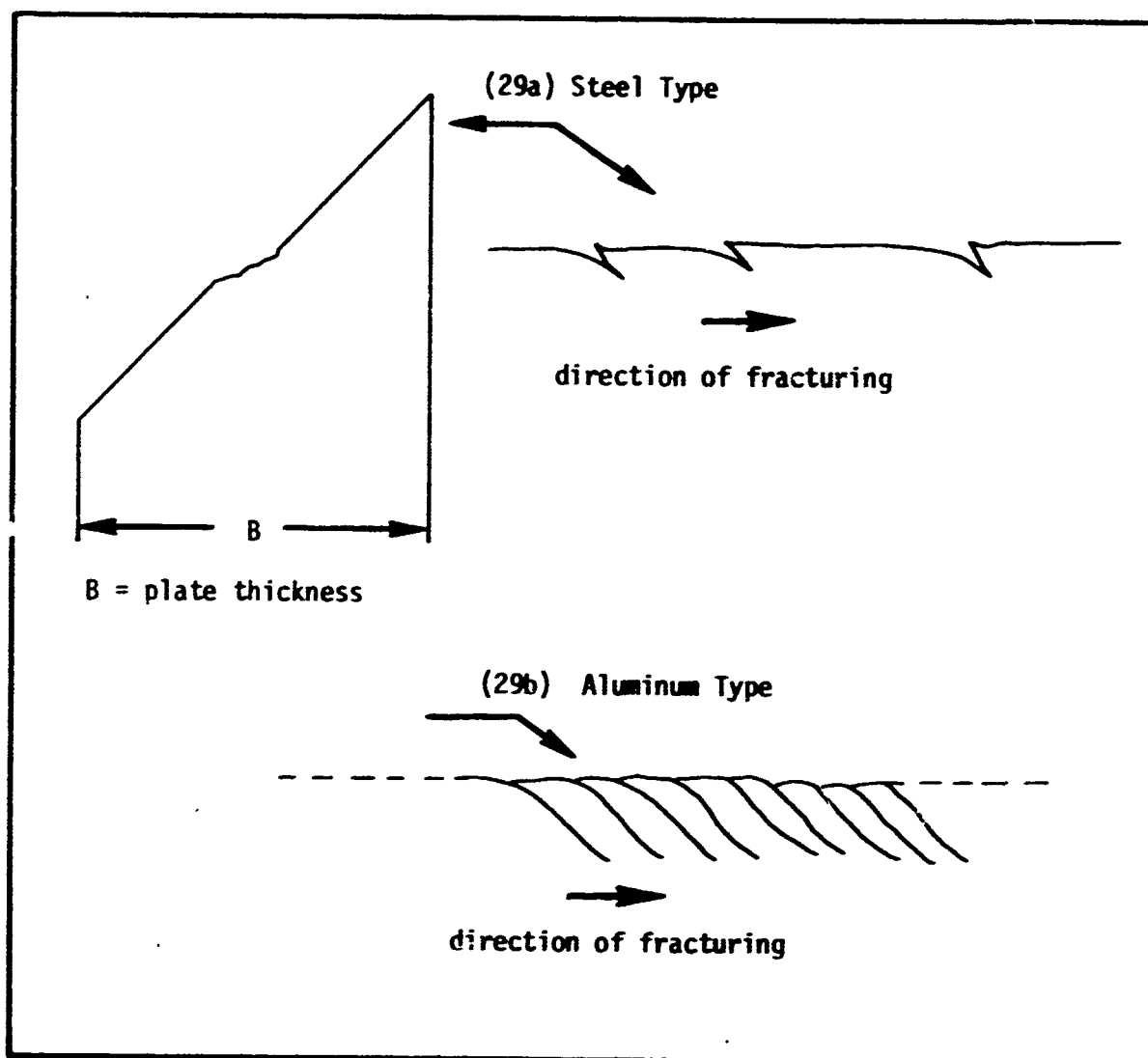


Figure 29. Asperities and Splits for "Steel Type" Edge of a Shear Fracture and Flow Markings for an "Al Type" Edge

The precise mechanism basic to the above indications of direction of oblique shear fracturing is not known. However, the behavior is as if the leading elements determining the separation path consisted in localized plastic flow at the plate surface (in contrast to advance separations near the center of the plate). In the case of superimposed tension and out-of-plane bending, the direction of fracturing may be clearly indicated only by the oblique shear edge at the high tension surface of the plate. In the case of about 90 percent oblique shear with symmetrical oblique shear fractures, one can look into the "trough" and find level difference lines curving toward the flat tensile strip at the bottom of the trough rather like inverted chevrons pointing toward the vague direction of fracturing.

e. Typical Starting Crack Defects

In aircraft structures the stress history tends to be dominated by load fluctuations. Thus, the development of fracture failures is generally assisted by fatigue. However, stress concentrations, prior cracks, and stress corrosion cracking may assist the achievement of a critical size for rapid fracturing prior to the expected life of the component. When the primary origin region of a fracture has been established, it is desirable to use estimates of the tensile stress across that region together with estimates of the material toughness to compute an approximate plausible size for the crack at onset of rapid fracturing. The last increments of fatigue crack extension prior to rapid fracturing tend to be relatively large and also indistinct. For this and other

reasons, the exact crack size at onset of rapid fracturing may not be clearly indicated. However, an estimate of crack size corresponding to the outer boundary of closely spaced fatigue "beach marks" is of value. In the case of a part-through crack of this nature in a thick section, one can assume the region of faint, widely spread beach marks pertain to K values very near to or above the K_{IC} for the material. Thus, the size estimate for the region of closely spaced striations should nearly match with the stress level and K_{IC} value. In this practice, the last few cycles of fatigue are treated as details of the final separation. The stress level at final separation might be regarded as average or possibly below average for normal operations. This treatment can be justified on a probability basis. However, reservations should be made for the possibility that the increase of fatigue beach mark spacing occurred because of increase of the size of the load fluctuations rather than due to a close approach of the crack size to instability.

In the case of welds of high strength metals, a common type of crack defect is a weld border crack starting at the weld metal-base metal boundary and extending into the heat affected zone. Such cracks tend to have a large surface length in comparison to depth at initial formation. Extension of such cracks by fatigue tends to increase the depth to surface length ratio. Estimates of K for such cracks may be made as illustrated by Tiffany and Masters in ASTM STP 381, Reference [17]. Segregation type weakness can also develop in central regions of a weld when the solidification structure tends to be unusually coarse. Vestiges of dendritic solidification patterns on the fracture surfaces can often be found in such

cases.

The assistance of stress corrosion in the development of a starting crack defect is more often suspected than proved. In the past, reliance has been placed largely on fracture appearances at micro-scale to decide whether a substantial amount of stress corrosion influence is present. Recent experimental work by Wei [18] substantiates the plausible idea that load-time dependent stress corrosion cracking and fatigue cracking are additive. When the stress corrosion influence is combined with fatigue, the typical markings associated with either kind of fracturing tend to be less clear. In many instances, the available measurements of fatigue crack growth rate (as a function of ΔK) will have been collected using the expected operating environment. An unusual effect of stress corrosion would not, then, be expected unless the load durations during service tended to be much longer than those used for fatigue testing.

In the case of rupture of pressure vessels under a fixed steady load, it is natural to look for a prior fabrication crack large enough so that the K value in service was above the threshold K_{ISCC} value for stress corrosion cracking. (See Section C for representative K_{ISCC} data). The caution to be borne in mind here pertains to the possible influence of crack depth, when small, upon the degree of aggressiveness of the environment. In the future, K_{ISCC} testing practices need to be supplemented by very long time exposure tests of stressed material containing small surface cracks of various depth.

In general, stress concentrations continue to represent the factor

primarily responsible for a substantial number of fracture failures. Cut-outs, holes, and redundantly connected plates often provide overstressed regions in which the development and growth of a crack may occur with unforeseen speed. The design should be adjusted so that all such cracks remain stable long enough to be found by inspection. However, oversights may occur. Regions subjected to dynamic overloads during hard landings or by an abrupt "pitch-up" deserve special attention because these regions may not be tested for such events during initial fatigue testing of the airplane and the number of such events which can be tolerated must be found by special testing of those parts.

2. Microscopic Examination

The most important preparatory step to be taken in a microscopic failure analysis is a thorough macroscopic examination since this leads the investigator to the critical area of the crack origin. In many cases the unknown of major importance relates to the micro-mechanisms of early crack formation and extension. For example, a particular service failure may appear to be predominantly fatigue in nature leading the engineer to consider a "fix" based only upon moderation of the cyclic loading conditions. However, the critical nucleation event may well have been due to some other factor such as a corrosive environment or inclusion-ridden defective material. Therefore, it is most important to record the approximate origin of the critical defect, its overall size, the texture of the fracture surface and any gross markings suggestive of a particular fracture mechanism. All of the above factors can be determined as a result of a

properly conducted macroscopic fracture surface examination.

When describing the manner of crack extension, one may cite the macroscopic fracture path (flat or slant type failure usually associated with conditions of plane strain and plane stress), the microscopic path (transcrystalline or intercrystalline) and the precise microscopic mechanism by which rupture occurs (related to electron microscopic observations). To make the latter two observations requires the use of high magnification, high resolution microscopes.

As recently as ten years ago, the major tool used in the microscopic examination of the fracture process was the light microscope. Due to the very shallow depth of focus, examination of the fracture surface is not possible except at very low magnifications. Consequently, the fracture surface analysis procedure entails the examination of a metallographic section containing a profile of the fracture surface. Using this technique, it is possible to obtain important information about the fracture path. For example, by comparing the path of the fracture with the metallographic grain structure, it is possible to determine whether the failure is of transcrystalline or intercrystalline nature. Clarification of this point is often more easily accomplished when secondary cracks are present in the sectioned component, thereby revealing profiles of mating fracture surfaces. Since the condition of the profile edge is critical for proper failure analysis, precautions are often taken to preserve the sharpness of the fracture profile. To this end, fracture surfaces are plated with nickel to protect the specimen edge from rounding due to the metallographic

polishing procedure. The most widely used procedures for metallographic specimen preparation are described in a standard metallurgical text [20].

In addition, to identifying the microscopic fracture path, metallographic sections are also useful in establishing the metallurgical condition of the material. Grain size and shape offer important clues to the thermo-mechanical history of the component. For example, a coarse grained structure is indicative of a very high temperature annealing process while an elongated grain structure indicates not only the application of a deformation process such as rolling, forging and drawing in the history of the material but also the direction in which this mechanical process was applied. Such mechanical processes often lead to the development of anisotropic mechanical properties. Consequently, it is important to know the relative orientation of the grain structure with respect to the predominant stress direction.

Identification of the microstructural constituents enables the examiner to determine whether the component has been heat treated properly. Identification of a possible grain boundary phase, for example, can explain the occurrence of an intercrystalline fracture. Finally, with the aid of an inclusion count, the relative cleanliness of the metallurgical structure can be determined. While it is not possible to express the fracture toughness of a material in terms of some measure of inclusion content, it is known that fracture toughness decreases with increasing inclusion content. Hence, a trained metallographer may ascertain from metallographic examination whether the material in question is representative of

good or bad stock.

The understanding of fracture mechanisms in metals improved by a quantum jump with the development of the electron microscope. With its superior depth of field and increased resolution, many topographical fracture surface features were observed for the first time. Many of these markings have since been interpreted in terms of current theories of fracture. Much of the fractographic work, to date, has been conducted on transmission electron microscopes*. Since the penetrating power of electrons is quite limited, it is necessary to make fracture surface observations with a replica of the fracture surface that allows transmission of the high energy electron beam. Consequently, before one can proceed with an interpretation of fracture surface markings, it is necessary to briefly describe replication techniques.

A considerable volume of literature has been developed during the past ten years dealing with techniques and interpretation of electron fractographic observations. To meet the objectives of this report it should not be necessary to describe in detail all the information that is now available in the open literature and in Government reports. Rather,

*During the past few years, encouraging progress has been made in the utilization of scanning electron microscopy in failure analysis. A major advantage of the scanning microscope for some cases is that the actual fractured sample may be viewed directly in the instrument, thereby obviating the need for replica preparation. When legal or other considerations do not permit the fractured component to be cut down in size to fit into the viewing chamber, the instrument cannot be used. At present, the resolution capability of scanning electron microscopes is less than that of the transmission electron microscopes. It is anticipated that later models of the SEM will be more competitive with respect to this specification, thereby leading one to foresee the need for both instruments in a laboratory committed to failure analysis.

it is desirable to highlight those major factors that have direct bearing on the subject of failure analysis. For a more complete description, the reader is referred to the text Electron Fractography, STP 436 [21], published by ASTM. This book contains articles dealing with routine and special fractographic techniques, application of fractography to failure analysis, environmental effects, and detailed descriptions of specific fracture mechanisms such as cleavage, void coalescence and fatigue. In addition, the reader is referred to the Electron Fractography Handbook [22] prepared under the auspices of the Air Force Materials Laboratory. A large collection of documented fractographs is contained in this report along with a discussion of replication procedures and interpretation of fractographic observations.

As described in the section dealing with macroscopic interpretation of fracture surface topography, care should be exercised in the cleaning of fracture surfaces. Foreign dirt particles, grease and oil, and loosely clinging rust should be removed cautiously with an inert solvent such as acetone. The use of chemically active alkaline or acid solutions should not be used since they will etch the fracture surface and obliterate important fracture markings. Similarly, debris should not be removed from the fracture surface with an abrasive instrument since this, too, will mar the fracture surface. A plastic type softened acetone, may be pressed onto the fracture surface and then removed, thereby stripping away loosely clinging dirt. After the cleaning process, the specimen fracture surface should be preserved in a dry environment or by the application of an acetone soluble lacquer spray.

Several replication procedures have been developed in the metallurgical laboratory for the optimization of certain conditions. For example, a one-step process, the direct carbon replication technique, generates a replica possessing the highest resolution. Though the highest possible resolution is always desirable, this procedure is not employed often since the specimen is destroyed in the replication process. The most commonly used technique is a nondestructive two stage process resulting in reasonably good resolution. A presoftened strip of cellulose acetate is pressed onto the fracture surface and allowed to dry. The tape is then stripped from the specimen carrying an impression of the fracture surface topography. Since this tape is opaque to the electron beam, further steps in the replication procedure are necessary. A layer of heavy metal is deposited onto the side of the tape bearing the fracture impression. This is done to improve the eventual contrast of the replica. Finally, a thin layer of carbon is vapor deposited onto the tape. The plastic tape-heavy metal-carbon composite is then placed in a bath of acetone where the plastic is dissolved. In the final step, the heavy metal-carbon replica is removed from the acetone bath and placed on mesh screens for viewing in the electron microscope. Since the viewing screens are only 1/8 inch in diameter, the importance of selecting the critical region for examination is most important. This factor, again, emphasizes the need for a carefully conducted macroscopic examination which should direct the examiner to the primary fracture site. By adhering to the recommended procedures for the preparation of replicas, little difficulty should be encountered.

The critical phase in electron fractography is the interpretation of the fracture markings in terms of actual fracture mechanisms. In addition to References [21] and [22], the reader is referred to the article by Beachem entitled, "The Interpretation of Electron Microscope Fractographs" [23]. Of particular importance in this article is a discussion of the interpretation of contrast effects which permit the viewer to gain a more accurate three dimensional picture of the fracture surface. In the following sections, the appearance of predominant fracture mechanisms is described briefly. The reader should, again, refer to the many articles in the open literature for a more detailed discussion of these points.

3. Void Coalescence

A major fracture mechanism common to most materials regardless of fundamental differences in crystal structure and alloy composition is that of void coalescence. It is believed that stress induced fracture of brittle particles, particle-matrix interface failure and, perhaps, complex dislocation interactions lead to the formation of microcracks or pores within the stressed component. These mechanically induced micropores should not be confused with preexistent microporosity sometimes present as a result of casting procedures. At increasing stress levels, the voids grow larger and finally coalesce into a broad crack front. At some point, this growing flaw reaches critical dimensions resulting in total failure of the component. Even after the point of instability, the unstable crack often grows by a repetitive process of void formation and subsequent

coalescence with the main crack front.

Three distinct processes for void formation and coalescence can be envisioned depending upon the state of stress. Under simple uniaxial loading conditions, the microvoids will tend to form in association with fractured particles and/or interfaces and grow out in a plane generally normal to the stress axis. The resulting micron sized "equiaxed dimples" are generally spherical in shape, as shown in Figure 30. Since the growth and coalescence of these voids involves a plastic deformation process, it is to be expected that total fracture energy should be related in some fashion with the size of these dimples. It has been shown in laboratory experiments that fracture energy does increase with increasing depth and width of the observed dimples. At best, dimple size and general degree of roughness of the fracture surface can be used as a first order approximation of energy consumed in the fracture process.

When failure is influenced by shear stresses, the voids which nucleate in the same manner as cited above, grow and subsequently coalesce along the planes of maximum shear stress which are often inclined to the surface of the component. Consequently, these voids tend to be elongated and result in the formation of parabolically shaped depressions on the fracture surface, as shown in Figure 31. If one were to compare the orientation of these "elongated dimples" from matching fracture faces, one would find that the voids are elongated in the direction of the shear stresses and point in opposite directions on the two surfaces.

Finally, when the stress state is one of combined tension and bending,



Figure 30. Fractograph Revealing Void Coalescence in the Form of "Equiaxed Dimples." Plain Carbon Steel. 7000 x.



Figure 31. Fractograph Revealing Void Coalescence in the Form of "Elongated Dimples." Al-Al₃Ni Eutectic Alloy. 6600x.

the resulting tearing process produces "elongated dimples" which can appear on gross planes normal to the direction of loading. The basic difference between these "elongated dimples" and the ones produced by shear is that the tear dimples point in the same direction on both halves of the fracture surface. It is important to note that these dimples point back toward the crack origin. Consequently, when viewing a replica which contains impressions of tear dimples, they may be used to direct the viewer to the crack origin. This technique is described at greater length by Whiteson, et.al.[24]. This procedure should be used to compare results with crack direction determinations as described in the previous section on macrofractography.

It may be desirable to determine the chemical composition of the particle responsible for the initiation of the voids. By selected area diffraction techniques employed in the electron microscope, it often is possible to identify the composition of particles extracted from the base of dimples. With this information, it may be possible to select a different heat treating procedure and/or select a similar alloy of higher purity so as to retard the void formation initiation processes.

4. Cleavage

The process of cleavage involves transcrystalline fracture along specific crystallographic planes and is usually associated with low energy fracture. The cleavage facet is flat and frequently contains sets of gradually diverging lines associated with cleavage fracture occurring on parallel sets of planes, as shown in Figure 32. The origin of fracture



Figure 32. Cleavage Facet with Associated Cleavage Steps. Cleaved Secondary Particle. 21,600x.

for such facets is the focal point for the cleavage lines. On other cleavage facets a network of cleavage steps in the shape of a "river pattern" may be observed where fine steps continually merge into larger ones. These markings again reflect the propagation of cleavage cracks on parallel planes. In this case, the origin of failure is in the direction of finer and more numerous steps in the pattern.

There is not much quantitative information to be obtained from cleavage facets that can be used in failure analysis. It is possible to estimate the critical flaw size by measuring the size of the cleavage facet. However, facets often assume the size of individual grains, the

size of which can be readily obtained by ordinary metallographic procedures. Some useful information can be obtained about the phase responsible for failure by noting the shape of the facet and comparing it to the morphology of different phases in the alloy.

In the case of materials that undergo a fracture mechanism transition (e.g., void coalescence to cleavage failure), it is possible to relate the presence of the cleavage mechanism to a general set of external conditions. In the case of mild steel which undergoes the above fracture mechanism transition, the observation of cleavage indicates that the component was subjected to some combinations of low temperature, high strain rate and/or high tensile triaxial stress conditions.

In many engineering materials, fracture facets that resemble cleavage facets are also observed. They are relatively flat and often contain localized "river patterns" as do cleavage facets but they cannot be considered as having been produced by a cleavage process since the surface of the facet does not correspond to any rational low index crystallographic plane. An example of this feature is shown in Figure 33. These "quasi-cleavage" facets also differ from true cleavage facets in at least one other aspect. Whereas, the cleavage facet fracture origin is at the edge of the facet, it is in the middle of the "quasi-cleavage" facet. The observance of these markings, like that of cleavage, generally reflects a low energy fracture process.

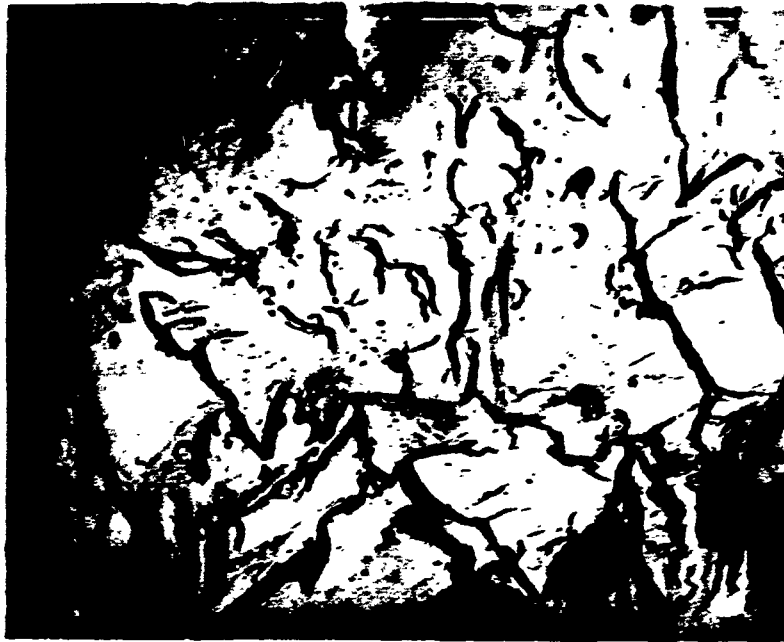


**Figure 33. Fractograph Revealing "Quasi-Cleavage" Region Containing Localized Steps and "River Markings."
T-1 Steel. 8600x.**

5. Fatigue Process

When a given component fails in service by a fatigue process the fracture surface often contains concentric arcs or rings emanating from the origin. These "clam shell" or "beach" markings are interpreted as having been produced during different periods of growth. Alternate crack growth and rest periods cause regions of the fracture surface to be oxidized and/or corroded by differing amounts, thereby, accounting for the nonuniformity in color of the "clam shell" markings. These markings represent periods of growth (perhaps the result of crack growth during one flight of an aircraft) and are not representative of individual load excursions. Individual load excursions are responsible for the formation

of one fatigue striation. This point will be discussed in greater detail below.

On occasion, fatigue crack propagation will be temporarily interrupted by a sudden overload causing local unstable crack extension by void coalescence. Subsequent to this localized "pop-in", fatigue induced extension of the crack is resumed. The shape of these "pop-ins" can be used to determine the direction of crack propagation. Such information has been used in the examination of two aircraft failures that are described in Section III.D on actual case histories as Examples 4 and 5.

As described previously, the relative orientation of the fracture surface is related to the extent of plane strain conditions depending upon the relative size of the plastic zone with respect to sheet thickness. This fact is clearly demonstrated for the case of fatigue crack propagation. Assuming a simple sinusoidal loading pattern, stress intensity conditions are low for small crack lengths resulting in the formation of a small plastic zone. When the sheet thickness is large compared to this zone size, plane strain conditions prevail and flat fracture usually results. With subsequent fatigue crack extension, the stress intensity factor and the plastic zone size increase. When the zone is large compared to specimen thickness, plane stress conditions and slant fracture are dominant. Depending upon the stress level and crack length, the fractured component will possess varying amounts of flat and slant fracture. By relating sheet thickness to the plastic zone size at the point of fracture mode transition, it is possible to estimate the stress level. This procedure is



Figure 34. Fatigue Striations Resulting from Uniform Sinusoidal Loading. 2024-T3 Aluminum Alloy. 12,600x

employed in several case histories reported in a following section.

As mentioned above, the fatigue fracture surface often reveals the presence of fatigue striations which represent the successive position of the crack front after a given loading cycle. An example of this is shown in Figure 34 for uniform sinusoidal loading. In addition to these striations are other regions on the fracture surface that contain mixtures of dimples, quasi-cleavage and other fracture mechanisms. The relative ease in observation of striations seems to vary with stress state and alloy content. Striations are most clearly observed on flat surfaces associated with plane strain conditions. Elongated dimples and evidence of

abrasion are the dominant fractographic features found on plane stress slant fracture surfaces. It is a much easier task to find striations on fatigue surfaces in aluminum alloys than in high strength steels. In some cases, it is virtually impossible to identify clearly defined areas of striations in the latter material, thereby making the fractographic examination most difficult.

The spacing between striations is a measure of crack growth during a given load cycle. Several investigators have shown that the striation spacing is strongly related to the macroscopic growth rate measured as a crack traverses a test panel. Both measurements are found to be strongly dependent upon the stress intensity conditions at the tip of the moving crack. Most commonly, the growth rate data is presented in the form of log-log plots of growth rate versus stress intensity factor range as shown in Figure 35. Such data is of great use in failure analysis. Knowing the specimen geometry, striation spacing, and crack length where the striations were measured, it is possible to obtain an estimate of the stress level in the component at the time of failure. The crack length and geometry information identify all the factors in the computation of the stress intensity level with the exception of the stress level which then becomes the only unknown once the striation measurement is made. This procedure is used in several case histories reported in the following section.

While this procedure is extremely useful, its implementation should be exercised with deliberate caution. First, it is critically important to accurately identify the crack length position where the striation spacing

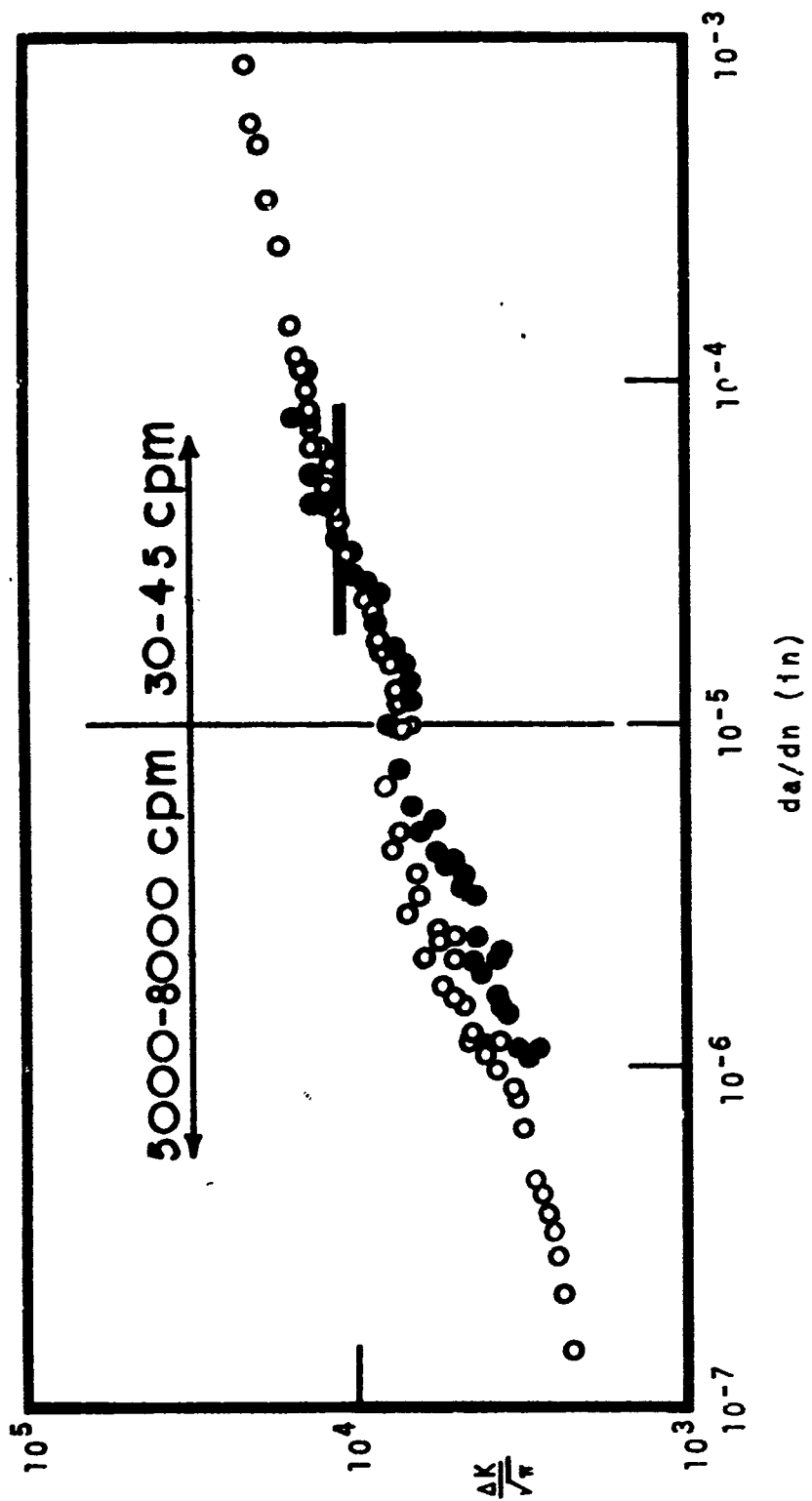


Figure 35. Plot of Stress Intensity Range Versus Rate of Crack Propagation and Striation Spacings for .064 Gage 2024-T3 Aluminum Alloy (○ Optical Growth Rate, ● Striation Spacings).

measurements were made. The stress level cannot be computed if the crack length is not known. In several of the reports examined, striation photographs were presented without a statement concerning the precise location of the region of the fracture surface. Without such information, the photograph serves only to identify the mechanism of failure but does not enable the examiner to perform any meaningful calculations.

Since striation formation is a highly localized event, it is dependent upon both stress intensity and metallurgical factors. It has been repeatedly shown in laboratory experiments that for constant stress intensity conditions, striation spacings in a local region may vary by a factor of two to four. To arrive at a meaningful estimate of crack growth rate at a particular crack length, many measurements of striation spacing should be made. In addition, measurements should be made at different crack length positions to serve as a comparative check on the computation.

The need for multiple readings of striation spacings is of paramount importance when the cause of component failure is related to random loading. Since the striation spacing is a function of the stress intensity factor range during each cycle, random load fracture surfaces should contain striation spacings with varying size. An example of this is shown in Figure 36. It would be a relatively simple matter to define the random load spectrum by measuring the resultant striation spacing were it not for the fact that striation spacing is affected by loading history. For example, when a simple sinusoidal loading pattern is interrupted by one peak overload cycle, the striations that form after the overload are

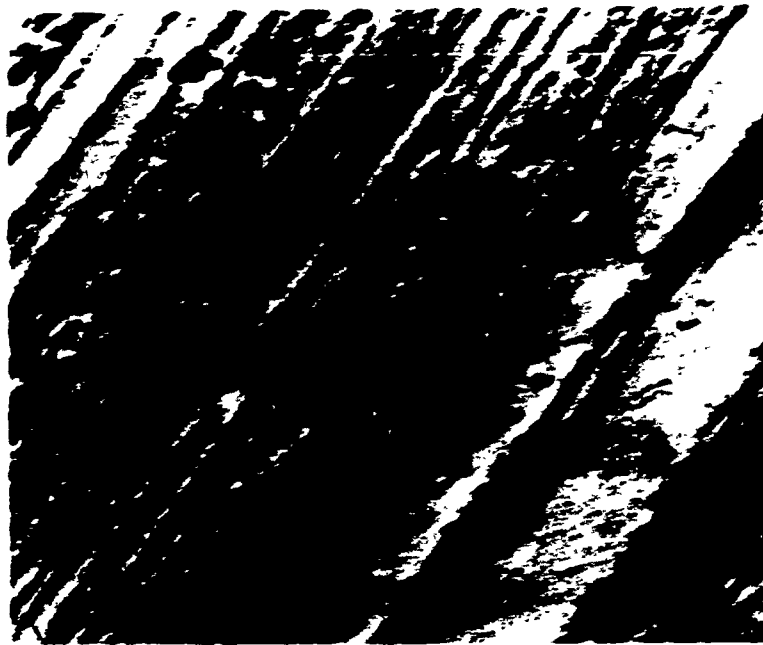


Figure 36. Fatigue Striations Resulting from Random Loading. 7075-T6 Aluminum Alloy. 18,000x (See case history Example 5.)

smaller than expected for some distance ahead of the position where the overload was applied. This effect is related to the existence of a compressive residual stress pattern resulting from the tensile overload. Since random load spectrum contain both low loads followed by high loads and vice versa, it is to be expected that some averaging effect would occur. Consequently, many readings of striation spacing should be made under random loading conditions.

Finally, it may be possible to make a crude estimate of the load level in the random spectrum that was responsible for final failure. At small crack lengths and associated low stress intensity levels, the highest components in the load spectrum could occur but would not cause total failure. In this way, the overall range including the peak values of the spectrum may be estimated by measurement of striation spacing at small

crack lengths. These peak levels may be assumed to reoccur at a later time when the crack length is longer and, thereby, constitute the critical event in the fracture process.

In none of the above discussion concerning the relationship between striation spacing and the stress intensity factor range was there mention of the effect of other variables. Little information is currently available to clearly define the role of such variables as mean stress, cyclic frequency and environment upon the size of fatigue striations. Consequently, the relation of striation size to ΔK should be considered as a first approximation of the dependence of stress intensity levels on crack extension rate.

6. Fracture Markings at Instability

Much interest has recently been focused on the fracture surface morphology at the onset of unstable crack extension in plane strain specimens. In this region a relatively smooth region, similar in appearance to a large fatigue striation, is observed. It is believed that this "stretched zone" reflects the extent of crack tip blunting prior to the point of crack instability. An example of this "stretched zone" is shown in Figure 37. Presuming this thought, it should be possible to relate the extent of crack tip blunting (i.e., measure the width of the stretched zone) to the crack tip opening displacement and material fracture toughness. The most complete study to date has been performed by a task group of Subcommittee II of ASTM E-24 [25]. Stretched zone measurements were recorded from the plane strain fracture surfaces of several grades of maraging steel, two

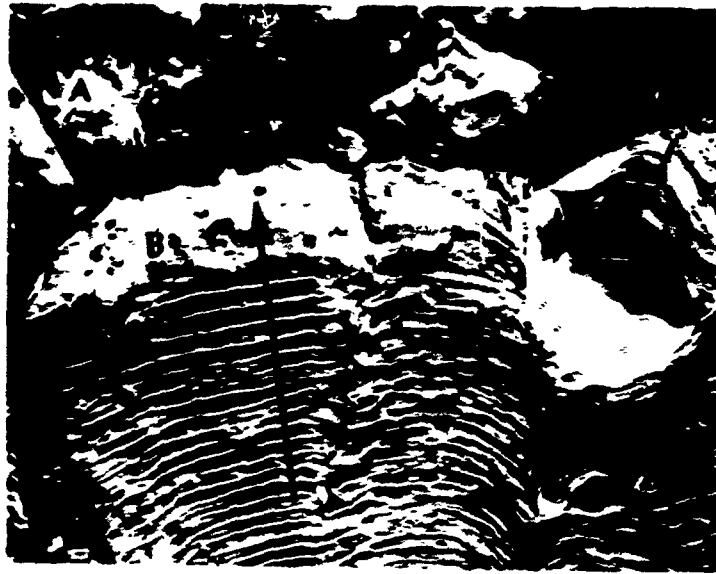


Figure 37. "Stretched Zone" (B) and Dimpled Rupture (A) Resulting from Overload During Fatigue Cycling [26]. 2024-T3 Aluminum Alloy. 8000x

aluminum alloys and a titanium alloy. The size of the stretched zones increased with increasing K_{IC} levels and were in general agreement with computed values of the crack opening displacement, $2V_c$. It is too early to know whether such measurements will be of use in failure analysis. The reader is advised to remain aware of new developments concerning this matter. A note of caution is raised, however, based upon the recent work of Von Elm [26]. Interjecting 50% and 75% overloads into a simple sinusoidal loading pattern, he found that the peak load produced both a large striation or stretched zone and a region of void formation depending upon the local stress intensity level. At low stress intensity levels only the stretched region was produced while at larger stress intensity levels, both stretching and dimple formation was observed. These observations illustrate that fracture mechanisms associated with the crack opening

displacement are not solely related to the stretching process.

C. Material Behavior Patterns

1. Property Data Useful in Failure Analysis

The theory and experimental verification of fracture mechanics as an effective tool in failure analysis have been described in the previous section. The concept of the stress intensity factor, its mathematical and physical significance, and its dominant influence upon fracture modes and mechanisms have been clearly outlined. At this point, the magnitude of stress amplification at crack tips will be compared with the limiting capacity of engineering materials to resist fracture. In a fundamental sense, fracture occurs when the stress exceeds the tensile strength of the material. By analogy, conditions for fracture are met when the applied stress intensity factor level exceeds the material's resistance to fracture, the fracture toughness.

The likelihood of performing a successful failure analysis is considerably enhanced if the mechanical properties of the component material are thoroughly characterized. In the past, it was standard procedure to define yield and tensile strength, percent elongation and reduction in area, fatigue endurance, and occasionally some additional data such as elevated temperature tensile behavior. More recently, it has been shown that further information is desirable and necessary for a complete analysis. As will be shown in several service failure case histories, the additional knowledge of the material plane strain fracture toughness value and

characterization of fatigue crack propagation rates in terms of stress intensity factors proved to be the key to the solution of the problem.

In terms of the current state of knowledge in the area of failure analysis, yield and tensile strengths, degree of ductility, plane strain and plane stress fracture toughness values, fatigue data relating crack growth rates to stress intensity conditions and effects of environment upon both static and dynamic loading conditions are considered to be the most critical mechanical properties affecting the onset of fracture. It should be added that variation in these properties with specimen orientation is also of prime concern. A brief tabulation of these properties for selected engineering alloys is included at the end of this Section C. The table is not intended to be complete with respect to any one alloy or group of alloys since this would constitute a major effort in itself and would not add significantly to the purpose of this report. The data are presented to acquaint the reader with the range of properties exhibited within several alloy groups and to enable the reader to establish a relative figure of merit of one alloy with respect to another.

To more fully understand the utility and interrelation of these data, further discussion is contained in the following paragraphs.

a. Yield and Tensile Strength. Metal alloys can be strengthened by one or more of several strengthening mechanisms such as: precipitation hardening, dispersion hardening, solid solution strengthening, strain hardening, martensitic strengthening and other mechanisms.

Many low alloy steels are strengthened by a martensite transformation and subsequent tempering treatment while most aluminum and titanium alloys, and maraging steels are strengthened by a precipitation hardening process. In both cases, the desired mechanical properties are critically dependent upon the proper heat treatment. Consequently, it is important to verify whether the failed component was heat treated properly to attain the desired strength levels. Aside from the preparation of tensile specimens from the component material, it is often possible to estimate the actual strength level of an alloy with hardness measurements and metallographic examination of the microstructure.

b. Fracture Toughness. As a result of differences in alloy content, processing sequence, heat treatment and other factors, the fracture toughness level may assume a large range of possible values. Here again, it is critically important to verify whether the failed component under investigation had been prepared in the proper manner. In the overwhelming majority of engineering alloys, it has been found that as the yield and tensile strength are increased, ductility and fracture toughness levels are correspondingly reduced. This critical fact is of overwhelming importance when consideration is given to material and material property selection. Since the weight of individual components is of major importance in aircraft design, one is always tempted to reduce weight by choosing a stronger material since any increase in component strength will be matched by a corresponding reduction in weight. Unfortunately, the material is rendered more susceptible to brittle fracture as a result of the reduction in fracture toughness associated with the higher strength

level. The following simple example is presented to demonstrate this effect.

Assume that a component in the shape of a large sheet is to be fabricated from 0.45C-Ni-Cr-Mo steel. It is required that the critical flaw size be greater than 1/8 inch, the resolution limit of flaw detection procedures. A design stress level of one half the tensile strength is indicated. To save weight an increase in the tensile strength from 220,000 to 300,000 psi is suggested. Is such a strength increment allowable?

The answer to this question bears heavily upon the changes in fracture toughness of the material resulting from the increase in tensile strength. At the 220,000 psi strength level, it is found that the K_{IC} value is 60,000 psi $\sqrt{\text{in}}$ while at 300,000 psi, K_{IC} drops sharply to 30,000 psi $\sqrt{\text{in}}$ [27]. For a large sheet the stress intensity factor may be estimated by the following relationship

$$K = \sigma\sqrt{\pi a} \quad (30)$$

where σ = design stress

a = half crack length

For the alloy heat treated to the 220,000 psi strength level

$$60,000 \text{ psi } \sqrt{\text{in}} = 110,000 \text{ psi } \sqrt{\pi a} \quad (31)$$

$$2a = 0.19 \text{ inch}$$

which exceeds the minimum flaw size requirements. At the 300,000 psi strength level

$$30,000 \text{ psi } \sqrt{in} = 150,000 \text{ psi } \sqrt{a} \quad (32)$$

$$2a = .025 \text{ inch}$$

which is five times smaller than the minimum flaw size requirement and approximately eight times smaller than the maximum flaw to be tolerated at the 220,000 psi strength level. Therefore, it is not possible to raise the strength of the alloy to 300,000 psi. Furthermore, using the same flaw size found in the 220,000 psi material for the 300,000 psi alloy would necessitate a decrease in design stress from 150,000 psi to 55,000 psi

$$\sigma = \frac{30,000 \text{ psi } \sqrt{in}}{\sqrt{\pi}(.095 \text{ in})} = 55,000 \text{ psi} \quad (33)$$

Therefore, under similar flaw size conditions, the allowable stress level in the stronger alloy could be only half that in the weaker alloy resulting in a two fold increase in the weight of the component.

The recommended procedures for valid K_{IC} testing were outlined in ASTM STP 410 by Brown and Srawley in 1966 [28]. When making use of K_{IC} data from the literature, it is important to verify whether the data is valid as per the recommended procedures. This is especially true for data generated prior to 1966 since K_{IC} values were often overestimated due to the prevailing experimental procedures and definitions for "valid" plane strain fracture testing.

When an engineering component experiences stress intensity conditions below the K_{IC} level, fracture may still occur. It has been shown for the case of many materials that sub-critical flaw growth will occur under

static loading conditions in the presence of an aggressive environment. This stress corrosion cracking will extend the crack to its critical length whereupon plane strain fracture will occur. Detailed investigations have shown that environmental stress corrosion cracking will not occur until the stress intensity level is above some minimum value, the K_{ISCC} threshold level [29]. For purposes of comparison, selected K_{ISCC} values are included in the data compilation. It is to be noted that while some alloys possess K_{ISCC} levels close to the K_{IC} value, other alloys show the K_{ISCC}/K_{IC} ratio to be only about 0.2, thereby, rendering the material extremely sensitive to stress corrosion cracking. As was the case with the K_{IC} property, it has been found that the K_{ISCC} level decreases with increasing yield strength [30]. In fact, the relative drop in K_{ISCC} level is greater than the corresponding change in K_{IC} resulting in a lower K_{ISCC}/K_{IC} ratio.

c. Fatigue Properties. Considerable progress has been made in the application of fracture mechanics methods to the fatigue process in engineering materials. Beginning with the work of Paris [31], a considerable body of experimental data has been generated revealing a strong relationship between fatigue crack propagation rate and the prevailing stress intensity conditions at the tip of the moving crack. Often these data are described in the form

$$\frac{da}{dn} = C\Delta\sigma^m f(a)^n \quad (34)$$

where da/dn = fatigue crack growth rate

C, m, n = material constants

a = crack length

n = number of load cycles

While this formulation may represent many data in a convenient manner, the relationship is by no means unique. Different methods of data correlation have been suggested by others [32, 33]. It must be emphasized that goodness of data fit with any relationships is more important than the convenient form of the relation.

Equation (34) can provide a reasonable estimate of crack growth rate for a given set of stress intensity conditions once the material constant values have been determined. It has been observed that the material constants are dependent to a varying degree upon other factors such as the mean stress intensity level, test environment, cyclic frequency, modulus of elasticity, alloy content and other metallurgical factors. Consequently, when analyzing a service failure using Equation (34), it is desirable to have some laboratory data obtained under simulated service conditions.

As mentioned above, the material constants are sensitive to environmental conditions existing during the fatigue process. Consequently, when the service conditions are severe and/or when the material is heat treated to an environmentally sensitive condition, the material constants C , m , and n should increase. It is important to note that even when the cyclic stress intensity level is below K_{ISCC} , corrosion enhanced fatigue crack growth will occur [34, 35]. The mechanism(s) for this event remains

an area of intensive study.

As a result of post failure fractographic analysis, an estimate of crack growth rate at a given crack length position can be obtained by measuring the width of fatigue striations. Using such data along with the appropriate material constants*, it is possible to compute an approximate stress range from Equation (34). This procedure was used in several service failure case histories to be described in a later section.

As part of a failure analysis, it is often most important to compute an estimate of component life which can then be compared with the actual service life. Thus computation can be performed by rearranging Equation (34) in the following form

$$\int_0^{N_f} dn = \frac{1}{C\Delta\sigma^m} \int_{a_0}^{a_f} \frac{da}{f(a)^m} \quad (35)$$

where N_f = number of cycles to failure

a_0 = initial crack size

a_f = final crack size

In the general case where $\frac{da}{dn} = Cf(\Delta K)$, $\int_0^{N_f} dn = \int_{a_0}^{a_f} \frac{da}{Cf(\Delta K)}$ (36)

When the functional form of ΔK is not known, the fatigue life can be

*Based upon available experimental data, some concern exists as to whether there are two sets of material constants for macroscopic and microscopic crack growth rate, respectively. Further study is indicated in this area.

computed by numerical integration. In most cases $a_0 \ll a_f$, consequently the computed fatigue life is not sensitive to the final crack length, a_f , but is strongly dependent upon the estimate of the starting crack length, a_0 . When the actual component life, the material constants, crack lengths and functional relationship of crack length are known with reasonable accuracy, then Equation (35) can be used to compute the prevailing stress state for comparison with the original design stress level.

To illustrate the use of Equation (35) in the computation of fatigue life, a second example problem is presented. Reconsider the material selection problem described in the previous section. 0.45C-Ni-Cr-Mo steel is available in both the 300,000 psi and 220,000 psi tensile strength levels. A design stress level of one half tensile strength is required. It is necessary to estimate the fatigue life of a component manufactured from the material in the two strength conditions. Using the design stress levels, a stress range of 150,000 psi and 110,000 psi will be experienced by the 300,000 psi and 220,000 psi material, respectively. It is immediately obvious from Equation (35) that all things being equal, the total fatigue life will decrease with increasing stress range. Using a value of $m = 2.25$ as found by Barsom [35] for nineteen steels, the fatigue life in the stronger material would be reduced by almost a factor of two. This should be considered as a minimum estimate of reduction in fatigue life since there is evidence to indicate that the exponent m increases with decreasing fracture toughness [36]. Furthermore, recalling that the critical flaw size in the 300,000 psi level material is only 1/5 that found in the 220,000 psi alloy, the computed service life in the stronger alloy will

be significantly reduced. This is especially true when the initial crack size is large compared to the critical flaw size. Therefore, it is concluded that the stronger material is inferior in terms of potential fatigue life as well as critical flaw size and associated fracture toughness.

In view of recent findings, it may be possible to conclude this discussion of fatigue on a cautiously optimistic note. It has been shown by Paris and Schmidt [37] and Johnson, et.al. [33], that some limiting value of ΔK exists below which fatigue crack growth is essentially non-existent. By defining this level for a given material, a component may be designed to minimize the problem of fatigue. Unfortunately, large factors of safety will be necessary since the observed threshold levels are quite low. Further developments are expected in this research activity.

2. Selected Mechanical Property Data

In the following Table XIV an abbreviated list of mechanical properties for several grades of aluminum, titanium and steel engineering alloys currently being used in the aircraft industry is provided. The list is by no means complete: (1) properties of many other alloys are not included, (2) little information is given concerning property variation as a function of heat treatment, specimen orientation, minor compositional variations and other variables. Those data which have been tabulated should be used with an appropriate degree of caution. Since fracture toughness and other important fracture properties are often strongly dependent upon one or more of the above mentioned variables, it is not possible to know a priori whether the data in the table do apply to

TABLE XIV. MECHANICAL PROPERTIES OF SELECTED ENGINEERING ALLOYS

MATERIAL	HEAT TREATMENT	ORIENTATION	σ_{YS} (ksi)	σ_{TS} (ksi)	K _{IC} (ksi \sqrt{in})	K _{ISCC} (ksi \sqrt{in})	REF.
T1-6Al-0.5Sn-1V	As Received	RW	127.3	128.9	77-92		1
T1-8Al-1Mo-1V	Duplex Anneal	0.5" plate			100	30(3.5% NaCl Solution)	8
T1-6Al-4V	Mill Anneal	0.5" plate			90	35(3.5% NaCl Solution)	8
T1-6Al-4V	1700 F/1 hr/WQ/900 F/2 hr/AC	RW	132.5	150.5	101-112		1
T1-6Al-4V	1700 F/1 hr/WQ/900 F/2 hr/AC	WR	140.1	155.9	104-114		1
T1-6Al-4V	1700 F/AQ/1000 F/4 hr		150	175	50		2
T1-6Al-4Zr-2Mo	1800 F/1 hr/WQ/1000 F/2 hr/AC	WR	132.0	147.1	92-102		1
T1-6Al-4Zr-2Sn-0.5Mo-0.5V	1825 F/1 hr/WQ/900 F/4 hr/AC	RW	121.3	129.1	124-131		1
4340	1550 F Salt/00/1 hr + 1 hr @ 500F		220	260	55		2
4340		WR	200		60	8 (see water)	7
4340		WR	125		90	70 (see water)	7
17-7PH	1750 F/10 min/cool to -110F for 8 hr/age 950 F/1 hr		208	222	70		2
15-7Mo	1400 F/90 min/cool to 55/age 1130 F/90 min		191	194	75		2
15-7Mo	Same as above except age 1050/90 min		205	233	45		2
2020-T651		Long.	76	82	21-24		3
2020-T651		Trans.	77	82	17.5-20.8		3
2024-T851		Long.	66	72	22.5-25.5		3
2024-T851		Trans.	65	71	18.8-22.6		3
7075-T651		Long.	75-80	84-89	24.5-28		3
7075-T651		Trans.	73-77	82-86	20.6-24.6		3
7079-T651		Long.	75-77	82-84	28.7-31		3
7079-T651		Trans.	72-74	82-83	25		3

the material under investigation in any failure analysis. In fact, Davis, et. al.[38], have shown that K_{IC} values will vary with the specimen configuration, reflecting crack orientation and material anisotropy effects. The large variation in K_{IC} values for the Ti-6Al-4V alloy listed in Table XIV (with fairly similar heat treatment) focuses attention on this point.

As a further guide to material properties, the associated bibliography contains the alloy designations under study in each reference.

3. Sources for Alloy Behavior Data

Additional information on alloy mechanical properties may be obtained from the following technical papers and reports. The alloy designations for which data was obtained is listed with each reference.

1. C. N. Freed, "Fracture Toughness Parameters for Titanium Alloys", Engineering Fracture Mechanics, Vol. 1, No. 1, June 1968, p. 175.

Ti-6Al-4Sn-1V	Ti-6.5Al-5Zr-1V
Ti-6Al-6V-2.5Sn	Ti-6Al-4Zr-2Mo
Ti-8Al-2Cb-1Ta	Ti-6Al-4V-2Sn
Ti-6Al-4V	Ti-5Al-4Zr-2Sn-0.5Mo-0.5V

2. E. A. Steigensald, "Plane Strain Fracture Toughness of High Strength Materials", Engineering Fracture Mechanics, Vol. 1, No. 3, April 1969, p. 473.

4340 steel	PH 15-7Mo stainless steel
4140 steel	PH 17-4PH stainless steel
5Cr-Mo-V steels	AM 355 stainless steel
17-7PH stainless steel	Ti-6Al-4V titanium

3. J. G. Kaufman, F. G. Nelson, Jr., and M. Holt, "Fracture Toughness of Aluminum Alloy Plate Determined with Center-Notch Tension, Single-Edge-Notch Tension and Notch-Bend Tests", Engineering Fracture Mechanics, Vol. 1, No. 2, August 1968, p. 259.

2020-T651
2024-T351
2024-T851
2219-T851
7001-T75

7005-T6351
7075-T651
7075-T7351
7079-T651
7178-T7651

4. W. G. Clark, Jr., "Subcritical Crack Growth and its Effect Upon the Fatigue Characteristics of Structural Alloys", Engineering Fracture Mechanics, Vol. 1, No. 2, August 1968, p. 385.

7079-T6 aluminum
5456-H321 aluminum

HP 9-4-25 steel
Ni-Mo-V steel

5. C. M. Hudson and J. T. Scardina, "Effect of Stress Ratio on Fatigue Crack Growth in 7075-T6 Aluminum Alloy Sheet", Engineering Fracture Mechanics, Vol. 1, No. 3, April 1969, p. 429.

7075-T6

6. H. H. Johnson and P. C. Paris, "Subcritical Flaw Growth", Engineering Fracture Mechanics, Vol. 1, No. 1, June 1968, p. 3.

Various steel, aluminum, titanium alloys

7. M. H. Peterson, B. F. Brown, R. L. Newbegin and R. E. Groover, "Stress Corrosion Cracking of High Strength Steels and Titanium Alloys in Chloride Solutions at Ambient Temperature", Corrosion, 23, p. 142, 1967.

4340 steel
Titanium alloys:
5Al-2.5Sn

6Al-2.5Sn
6Al-2Mo
7Al-1Ta

6Al-4V
6Al-1Sn

7Al-3Mo
8Al-1Mo-1V

8. D. E. Piper, S. H. Smith and R. V. Carter, "Corrosion Fatigue and Stress-Corrosion Cracking in Aqueous Environments", ASM National Metal Congress, October 31, 1966.

Ti-8Al-1Mo-1V
Ti-6Al-4V

9. J. M. Barsom, "Investigation of Subcritical Crack Propagation", Ph.D. Dissertation, University of Pittsburgh, 1969.

10Ni-Cr-Mo-Co steel
12Ni-5Cr-3Mo steel

10. J. M. Barsom, E. J. Imhof, Jr., and S. T. Rolfe, "Fatigue-Crack Propagation in High-Strength Steels", AD 846 1276, December 1968 (Available from Defense Documentation Center).

12Ni steel
10Ni steel
Hy-130
Hy-80

11. C. M. Carman and J. M. Katlin, "Low Cyclic Fatigue Crack Propagation Characteristics of High-Strength Steels", ASME Paper No. 66-Met-3, 1966.

Steel alloys: 300m, D6AC, H-11, 250 maraging, 17-7PH

12. "Fracture Toughness and Tear Tests", Technical Documentary Report No. ML TDR 64-238, AFML, 1964.

Ti-8Al-1Mo-1V titanium alloy
AM 350 stainless steel
Inconel 718 nickel alloy

Ti-6Al-4V titanium alloy
PH 14-8Mo stainless steel

Editorial note: Report also contains extensive fatigue crack propagation data.

D. Individual Component Failure Analysis

1. Suggested List of Raw Data Necessary for Complete Failure Analysis

Having been introduced to the fundamentals of fracture mechanics analysis, stress intensity analysis of cracks, macroscopic and microscopic features of the fracture surface, and an indication of what pertinent mechanical property data is necessary to adequately characterize the performance of a given material, the reader should be in a position to synthesize this information and thereby solve a current service failure problem. To assist the investigator in his task, the following outline entered below is proposed. The outline, making reference to the component geometry, stress state, flaw characterization, fractographic observations, metallurgical information including component manufacture, and other service information, summarizes the raw data necessary for a complete failure analysis of a fractured component. Table XV is provided to summarize the data obtained for four of the example case histories to be described in the following section. Note that in some cases, it was possible to make a reasonably complete failure analysis without benefit of all the suggested raw data information. Certainly, a successful failure analysis will depend upon both the quality and quantity of information obtained concerning the component fracture.

I. Component, size, shape, use (specify areas of stress concentration)

II. Stress State for Component

A. Type of Stresses

1. Magnitude of stress levels (design stress)
2. Type of stress (e.g., Mode I, II, III or combinations)
3. Presence of stress gradients

B. State of Stress - Plane Strain vs Plane Stress

1. From fracture surface appearance
 - a. Percent shear lip on fracture surface
2. From calculations of estimated $\frac{\text{plastic zone}}{\text{thickness}}$ ratio

C. Effect of Load Variation (time and loading frequency)

1. Hours of flying time
2. Estimate of number of loading cycles per unit time
3. Type of flight patterns
 - a. Random loading
 - b. Overloads (wind gusts and landings)
 - (1) Single or multiple

III. Macroscopic and Microscopic Examination

A. Nature of Critical Flaw Leading to Fracture (make use of clearly labeled, i.e., accurate magnifications, etc., and accurate macrophoto-micrographs).

1. Location of critical flaw by macroscopic examination
2. Critical flaw size shape and orientation before instability

3. Macro- or micro-evidence of fatigue and/or corrosive attack (e.g., rust, beach marks, etc.)

4. Surface or imbedded flaw

a. Evidence of fretting

5. Direction of crack propagation

a. Chevron markings, beach marks, pop-in indications

B. Manufacturing Flaws

1. Scratches, undercuts, weld defects (geometrical and hot and cold cracks), misfit components

C. Metallurgical Flaws

1. Inclusions, large second phase particles, entrapped slag, voids, weak internal interfaces

D. Fractographic Observations

1. Qualitative observations

a. Dimpled rupture, cleavage, quasi-cleavage, intercrystalline fracture, fatigue striations

2. Quantitative observations

a. Striation spacings at known crack length positions

b. Striation spacing evidence of uniform or random loading

c. Stretch zone width at onset of unstable crack extension

IV. Component Metallurgy

A. Alloy Designation

B. Mechanical Properties

1. σ_{ys}
2. σ_{TS}
3. % elongation or % reduction of area
4. K_{IC} and/or K_c data
5. K_{ISCC} value
6. Fatigue data relating crack growth rate to stress intensity

conditions with environment specified

C. Melting Practice, Ingot Breakdown and Alloy Composition

1. Techniques to improve purity
 - a. Vacuum degassing, electric melting, etc.
2. Cross rolling or unidirectional rolling
3. Compositional variations within specifications for alloy
 - a. Interstitial content in titanium alloys
 - b. Carbon content in steels (also P and S)
 - c. Other tramp elements in alloys

D. Heat Treatment

1. With hardness, mechanical property tests and metallographic sections attempt to answer the following:
 - a. Was tempering temperature correct (low alloy steels)
 - b. Was aging temperature correct (Al and Ti alloys, maraging steels)
 - c. Was 500 and 850°F embrittlement present (steels)

E. Microstructure

1. Mechanical fibering and banding from chemical segregation
2. Grain size and shape
 - a. Elongated with respect to stress axis
 - b. Grain run-out in forgings

F. Anisotropy

1. If possible, with available material determine K_{IC} , K , yield strength and elongation with respect to critical flaw orientation.

V. Component Manufacture

- A. Forged, cast, machined, spun, etc.
- B. Joined: Welded, brazed, bolted, etc.
- C. Surface Treatment

1. Shot peening and other deliberate compressive surface stresses to component
2. Manufacturing induced residual stresses
 - a. In a large section (thermal or transformation)
 - b. Due to welds
3. Pickling and other cleaning treatments
4. Cadmium plating and/or other hydrogen charging process

VI. Service Information

- A. Home Base for Aircraft
 1. Weather experience

- a. Related to home base and route history
2. Cold weather de-icing chemicals
3. Water or salt water environment
4. Oils and fuel

B. Overhaul Information and Schedule

1. Cleaning fluids

TABLE XV. SUMMARY OF DATA OBTAINED FROM SELECTED FAILURE REPORTS

FAILURE DATA	SPAR FAILURE (Example 1)	AILERON POWER CYLINDER (Example 2)	WING CARRYTHROUGH (Example 5)	WING SPAR (Example 4)
I.	D-shaped rotor spar 5" width x .045" thick	Cylinder contains four bores pressurized by two pumps. Cracks grew from bore-bore and bore-outer wall. Bore diameter = 2 3/16". Wall thickness = .033"	Wing spar with 2.6" long x 0.26" thick web section with 0.8" wide x 0.4" high flange	Lower front wing spar consisting of a spar cap 0.5" thick with two 0.168" flanges containing fastener holes
II. A. 1.	Mean estimated to be 35 ksi; alternating estimated to be in range of 16-14 ksi	Mean normal pressure ~ 1800 psi varies from 750-2250 psi due to aerodynamic loading fluctuations. Due to aileron maneuvers, pressure rises to 3000 psi with transient pulses to 4500 psi	$\sigma_{max} = 35$ ksi (estimated)	259 loads equivalent to 20,000 psi stress in critical area
2.	Mode I	Mode I	Mode I	Mode I
3.	Not great due to thin sections	No great influence	possible	
B. 1.	Fracture mode transition @ 2.3" from origin	Plane strain	Instable crack in flange area had shear lip -0.025"	Small shear lip indicates strong plane strain influence
C. 1.	56.7 hours	300-400 hours	5269 hours	6012 hours
2.	56.7 hours x 230 rpm = 780,000 cycles	?	?	
3.	a.b.v. possible	See II.A.1., above	a.b.v., probable	Probable random loading
III. A. 1.	1" from heel of spar	Surface flaws	Crack initiated at forging delamination which extended through flange into web section	Crack grew from fastener hole in both directions. Eventually entire flange was cracked and crack extended into corner of spar cap section. The corner crack was -0.25" deep at its greatest penetration along a 45° line in from the corner

TABLE XV. (Continued)

FAILURE DATA	SPAR FAILURE	AILERON POWER CYLINDER	WING CARRYTHROUGH	WING SPAR
11. A. B.	Initial semi-elliptical flaw with $2c = .100"$ & $a = .020"$ @ 35° to surface grew through thickness and along width of spar, crack grew 1 to stress axis	Case I: $a = 0.25"$, $2c = 0.56$ through thickness crack length = $1.1716"$ Case II: $a =$ through thickness = $0.38"$, $2c = 15/16$ & $3/16"$ through thickness crack length = $1.2"$ Case III: $a = 0.29"$, $2c = 0.69"$	Crack extended $0.4"$ from surface of flange and $\pm 0.2"$ from delamination line	See III.A.1., above
3.	Evidence of fatigue	Evidence of fatigue & fracture mechanism change before instability	Evidence of fatigue	Evidence of fatigue
4.	Surface flaw (lap)	Surface flaw	Surface flaw growing from delamination	Evidence of fretting at fastener hole
5.		Pop-in occurrence	Pop-in occurrence shows crack $0.4"$ long & growing out from delamination line	Pop-in markings indicate direction of cracking into spar cap section
B. 1.	Surface lap			
C.		Inclusion believed to be initiation site	Weak internal interface delaminated under stress. Related to forging lines	
D. 1.	Dimpled rupture fatigue striations	Fatigue striations	Fatigue striations & dimples in pop-in regions	Fatigue striations
2. A.	9×10^{-7} " at base of origin, $2 \times 10^{-6}"$ @ $\pm 0.4"$ from origin after becoming through thickness crack		(Fractographic data by Del Research personnel) $0.05"$ from delamination striation size varied from 3.1×10^{-6} to $4.5 \times 10^{-6}"$ @ $1.5"$; 4.1×10^{-6} to $6.8 \times 10^{-6}"$ @ $1.23"$; 9.4×10^{-6} to $2 \times 10^{-4}"$	

TABLE XV. (Continued)

FAILURE DATA	SPAR FAILURE	AILERON POWER CYLINDER	WING CARRYTHROUGH	WING SPAR
III D. 2. b. c.	Fairly uniform loading pattern		Random loading 2 x 10 ⁻⁴ "	
IV. A.	4340	2014-T6	7075-T6	7075-T6
B.		Not specified, handbook values used	Not specified, handbook values used	Not specified, handbook values used
B. 1.	140,000 psi			
2.	150,000 psi			
6.	Some fatigue data relating da/dn to ΔK			
C. 2.	Cold drawn	Forging	Forging	
3.	O.D.			
E. 1.	Fibering			
2.		Hoop stress in bore are normal to short transverse direction	Pronounced forging grain alignment. Grain runout normal to flange surface where delamination was nucleated	Elongated due to extrusion process
2. a.	Yes			
b.	Laps caused by drawing separation			
V. A.	Drawn	Forged	Forged	Extruded
C.		Shot peened and anodized		

TABLE XV. (Concluded)

FAILURE DATA	SPAR FAILURE	AILERON POWER CYLINDER	WING CARRYTHROUGH	WING SPAR
V. C. 1.	Grit blasted			
2.	Shallow surface residual stresses < 60,000 psi			
VI. A.	?			Failure during routine training mission at Reese AFB, Texas
1. a.	Failed in California			

2. Component Failure Analysis Examples

The previous sections summarized the analysis method, significant fracture features and material behavior which are important in failure analysis development and its application to the investigation of actual in-service failure problems. The following pages contain the detailed analysis of individual failures in which at least some minimum level of failure data was obtained. The examples are intended to demonstrate the implementation of Fracture Mechanics as an analysis tool and identify areas where more complete failure data and improved analysis techniques are required.

Below is a list of those case histories on in-service failures which are examined in detail on the following pages:

	<u>Page</u>
Example 1 - Analysis of Fatigue Failure of Helicopter Rotor Blade.....	179
Example 2 - Analysis of Aileron Power Control Cylinder Service Failures.....	191
Example 3 - Analysis of Crack Development During a Center Wing Section Structural Fatigue Test.....	205
Example 4 - Failure Analysis of Lower Front Wing Spar Cap.....	215
Example 5 - Failure Analysis of Wing Carry-Through Forging.....	221

Example 6 - Summary of Center Wing Section
Analytical Investigation..... 231

Other structural failures were investigated and examined as a part of this program effort, however, much important component failure data was missing, or lacking in clarity. In these cases only partial failure analysis could be accomplished, which resulted in various missing links in the logical application of Fracture Mechanics procedures. Since these rather incomplete examples did not offer a comprehensive and meaningful failure analysis approach, they are not included in this report.

EXAMPLE 1

ANALYSIS OF FATIGUE FAILURE OF HELICOPTER ROTOR BLADE

From corporate reports, information concerning this failure was obtained and entered into the suggested list of raw data as described in the previous section necessary for complete failure analysis of the component. In summary, a 0.020 inch deep lap in a 0.045 inch thick section of 4340 steel was found to grow under cyclic loading conditions, first through the component thickness and then as a through thickness crack until total failure occurred.

In this failure analysis, two major factors were evaluated: (1) the determination of the stress level and (2) calculation of component fatigue life. The analysis procedures for each factor are outlined below:

I. Determination of stress level

- A. Use information pertaining to fracture mode transition.
- B. Use information pertaining to striation spacings at different crack length locations.

II. Calculation of fatigue life

- A. Determine cyclic life to develop through thickness crack.
- B. Determine cyclic life from through thickness crack to failure.

I. Determination of the Stress Level

- A. Use of information pertaining to fracture mode transition.

For all calculations in this analysis, it is considered that $\Delta K = K_{MAX}$ for simplicity of calculations (Subsequent to these calculations, more detailed estimates of stress level were obtained from the manufacturer.)

From the data sheets, the following information is available:

1. Fracture mode transition was complete at 2.3 inches from crack origin.
2. Section thickness = 0.045 inches.
3. Yield strength = 140,000 psi.

The geometry of the cracked component at the fracture mode transition could be considered similar to a centrally notched panel where "a" = 2.3 inches. The finite panel width correction factor was not considered to be very significant.

$$\Delta K = \alpha \Delta \sigma \sqrt{\pi a} \quad (37)$$

where α = finite width correction factor and is in range of

1.0 to 1.2

a = 2.3 inches (crack length at the fracture mode transition)

so that

$$\Delta K = 2.7 \Delta \sigma \text{ to } 3.25 \Delta \sigma.$$

For 100% shear failure

$$B = \frac{1}{B_c} \frac{\Delta K^2}{\sigma_{ys}^2} \quad (38)$$

where B = thickness (0.045 inches)

$$\sigma_{ys} = 140,000 \text{ psi}$$

$$B_c = 2\pi$$

$$.045 = \frac{1}{2\pi} \frac{(2.7\Delta\sigma \text{ or } 3.25\Delta\sigma)^2}{(140,000)^2}$$

$$\Delta\sigma = 27,600 \text{ psi for } \alpha = 1.0$$

$$= 19,200 \text{ psi for } \alpha = 1.2$$

B. Use of information pertaining to striation spacings at different crack length locations.

$$\text{Assume } da/dn = C\Delta K^n \text{ where } n = 4$$

To evaluate "C", data were extracted from a Carman and Katlin report[43] on fatigue crack propagation of steels. Where $da/dn = 10^{-4}$ and $\Delta K = 80,000$ (similar data by Carman and Katlin are shown in Example 3, Figure 41).

$$10^{-4} = C(80,000)^4$$

$$C = 2.4 \times 10^{-24}$$

In some preliminary studies, the manufacturers evaluated the exponent "n" to be 3.7. The resulting computed value of "C" was within 10% of the value based on $n = 4$. Therefore, the value of $C = 2.4 \times 10^{-24}$ was used in further computations for simplicity where "n" = 4.

Striation spacings of 2×10^{-6} inches were found on the fracture surface at ± 0.4 inches from the crack origin.

$$2 \times 10^{-6} = 2.4 \times 10^{-24} (\Delta K)^4$$

$$\Delta K = 30,000$$

$$\text{with } \Delta K = \alpha \Delta \sigma \sqrt{\pi a}$$

where $a = \pm 0.4$ inches

$\alpha =$ on order of 1.0 to 1.1

$$30,000 = \alpha \Delta \sigma \sqrt{\pi(0.4)}$$

$$\Delta \sigma = 26,800 \text{ for } \alpha = 1.0$$

$$= 24,300 \text{ for } \alpha = 1.1$$

Due to experimental scatter associated with striation spacing measurements, the reported value of 2×10^{-6} inches could be in error by a factor of two. Therefore, the calculated value of $\Delta \sigma$ could be either raised or lowered by approximately $(2)^{1/4}$.

$\Delta \sigma$ could be in a range of 22,600 to 31,800 psi when $\alpha = 1.0$ and between 20,400 and 29,000 psi when $\alpha = 1.1$.

Additional striation spacing measurements were obtained at the base of the surface flaw. However, no data were available concerning the exact location on the fracture surface where the striation measurements were made.

Therefore, $\Delta \sigma$ calculations were made by assuming the measurements to have been taken both at the base of the initial flaw and at the largest

crack length just prior to the crack breaking through the thickness.

For this crack geometry let

$$K^2 = \left[1 + .12 \left(1 - \frac{a}{b} \right) \right]^2 \sigma^2 \frac{\pi a}{Q} \left[\frac{2t}{\pi a} \tan \frac{\pi a}{2t} \right] \quad (39)$$

which accounts for an elliptical crack near the free surface and extending over a large fraction of the cross section. (Reference [1]),

$$\text{when } a = .020$$

$$Q = 1.35$$

$$\frac{2t}{\pi a} \tan \frac{\pi a}{2t} = 1.2$$

$$\Delta K = .253 \Delta \sigma$$

Using $da/dn = C \Delta K^4$ with a striation spacing measurement of 9×10^{-7} inches

$$9 \times 10^{-7} = 2.4 \times 10^{-24} \Delta K^4$$

$$\Delta K = 2.48 \times 10^4$$

since $\Delta K = .253 \Delta \sigma$

$$\Delta \sigma = 98,000 \text{ psi}$$

This calculated stress level is grossly out of line with other computed stress levels. It would appear that the striation spacing measurement was in error assuming the measurement was made at "a" = .020 inches.

If the striation measurements were made at the largest crack length where any reasonable Y calculation could be made

$$a = .040$$

$$Q = 1.55$$

$$\frac{2t}{\pi a} \tan \frac{\pi a}{2t} = 4.08$$

$$\Delta K^4 = (1.03)^4 \Delta \sigma^4 Y^2 a^2 (6.95)$$

$$\frac{da}{dn} = C \Delta K^4$$

$$9 \times 10^{-7} = 2.4 \times 10^{-24} (1.1) \Delta \sigma^4 (9.86) (.0016) (6.95)$$

$$\Delta \sigma = 42,000 \text{ psi}$$

This value is also too high with respect to other calculated values of $\Delta \sigma$ so the striation measurement of 9×10^{-7} inches appears to be invalid.

In summary, a mean value of $\Delta \sigma = 25,000$ psi appears to be reasonable value to use in further calculations.

II. Calculation of Fatigue Life

A. Determine cyclic life to develop a through-thickness crack.

From macroscopic examination, the elliptical flaw was found to grow from 0.020 inch deep by 0.10 inch wide to 0.040 inch deep by 0.150 inch wide just prior to crack breakthrough.

Computations of the numbers of loading cycles needed to extend the crack across the component were broken down into incremental steps. In each step an average value of Q and $\tan \frac{\tau a}{2t}$ was used.

Using the relationship (equation 39):

$$K^2 = \left[1 + .12 \left(1 - \frac{a}{b} \right) \right]^2 \sigma^2 \frac{\tau a}{Q} \left[\frac{2t}{\tau a} \tan \frac{\tau a}{2t} \right]$$

with the first correction factor = 1.07

a	Q	Q ²	$\frac{2t}{\tau a}$	$\tan \frac{\tau a}{2t}$	$\frac{2t}{\tau a} \tan \frac{\tau a}{2t}$	$\left[\frac{2t}{\tau a} \tan \frac{\tau a}{2t} \right]^2$
.020	1.35	1.82	1.43	0.84	1.2	0.79
.025	1.40	1.96	1.15	1.19	1.37	0.95
.030	1.45	2.10	0.95	1.74	1.65	1.29
.035	1.50	2.25	0.82	2.75	2.26	2.26
.040	1.55	2.39	0.72	5.66	4.08	6.95

$$\frac{da}{dn} = C_2 K^4 = 2.4 \times 10^{-24} (1.07)^4 \sigma^4 \frac{\tau a}{Q} \left[\frac{2t}{\tau a} \tan \frac{\tau a}{2t} \right]^2$$

$$\frac{da}{dn} = 30.8 \times 10^{-24} \sigma^4 \frac{\tau a}{Q} \left[\frac{2t}{\tau a} \tan \frac{\tau a}{2t} \right]^2$$

$$\int \frac{da}{a^2}$$

$$N_f = \frac{1}{30.8 \times 10^{-24} \Delta \sigma^4 \left[\frac{2t}{ra} \tan \frac{ra}{2t} \right]^2}$$

between "a" = 0.020 and 0.025 inches:

$$\Delta \sigma = 25,000 \text{ psi and } \left[\frac{2t}{ra} \tan \frac{ra}{2t} \right]^2 = 0.87$$

$$N_f = \frac{50-40}{30.8 \times 10^{-24} (39 \times 10^{16}) (0.87)} = 960,000 \text{ cycles}$$

between "a" = 0.025 and 0.030 inches:

$$N_f = \frac{40-33.3}{30.8(39)(1.12) \times 10^{-8}} = 500,000 \text{ cycles}$$

between "a" = 0.030 and 0.035 inches:

$$N_f = \frac{33.3-28.6}{30.8(39)(1.78) \times 10^{-8}} = 220,000 \text{ cycles}$$

between "a" = 0.035 and 0.040 inches:

$$N_f = \frac{28.6-25}{30.8(39)(4.60) \times 10^{-8}} = 65,000 \text{ cycles}$$

Neglecting the number of cycles associated with crack extension from 0.040 to 0.045 inches, the total number of cycles to propagate the surface flaw through the skin thickness is calculated to be:

960,000
 500,000
 220,000
 65,000
 1,745,000 cycles.

B. Determine cyclic life from through thickness crack to failure.

For through thickness crack extension let

$$\Delta K = \alpha \Delta \sigma \sqrt{\pi a} \text{ where } \alpha = 1.0 \text{ to } 1.2$$

Using a_0 = half length of elliptical crack at the pop-through position

$$a_0 = 0.075 \text{ inches.}$$

$$\frac{da}{dn} = C \Delta K^4 \text{ with } C = 2.4 \times 10^{-24}$$

$$\Delta \sigma = 25,000 \text{ psi}$$

$$\frac{da}{dn} = 2.4 \times 10^{-24} \alpha^4 \Delta \sigma^4 \pi^2 a^2 = 9.2 \times 10^{-6} a^2$$

when $\alpha = 1$:

$$N_f = \frac{1}{9.2 \times 10^{-6}} \int_{.075}^{a_f} \frac{da}{a^2} = \frac{13.35}{9.2 \times 10^{-6}}$$

$$N_f = 1.45 \times 10^6 \text{ cycles}$$

when $\alpha = 1.2$:

$$N_f = 705,000 \text{ cycles.}$$

The total number of cycles of through thickness crack extension will, therefore, probably be in excess of 10^6 cycles.

The total calculated fatigue life is then about 2.8×10^6 cycles.

The actual number of incurred cycles, assuming one load excursion per cycle, is calculated to be $56.7 \text{ hours} \times 230 \text{ rpm} = 780,000$ cycles.

The computed life is, therefore, found to be about 3.5 times greater than the actual life.

III. Final Comments

The computations give reasonable agreement with the actual case history. To account for the factor of three in error for total life, several factors could be taken into consideration:

a. For these calculations, σ_{mean} was taken as $\Delta\sigma/2$. From data supplied by the manufacturer, it is suggested that $\sigma_{\text{mean}} = 35,000$ psi rather than $= 12,500$ psi used in the calculations. From the literature, it is found that if the mean stress is tripled, the growth rate will be approximately tripled, thus, leading to a reduction in cyclic life by a factor of three. This consideration of σ_{mean} could well account for the observed discrepancy.

The calculated value of $\Delta\sigma = 25,000$ psi falls within the manufacturer's estimate of the stress range (i.e., 12,000 to 28,000 psi).

b. If it is assumed that the component environment was more severe than the laboratory tests of Carman and Katlin[43] (from which "C" was

calculated), then the calculated number of cycles would be expected to be lower since "C" should be higher for more aggressive environments. However, Mei, et. al., have pointed out that as K_{Ic} increases, the material becomes less sensitive to environment with respect to fatigue crack propagation. With 4340 steel at a $\sigma_{ys} = 140,000$ psi, it is expected that K_{Ic} would be fairly high so "C" might not be very dependent on environment.

c. It is significant that the analysis as well as giving a reasonable estimate of fatigue life, also critically evaluates the data and rejects incorrect information (e.g., the striation spacing measurements of 9×10^{-7} inches taken at the base of the elliptical flaw).

EXAMPLE 2

ANALYSIS OF AILERON POWER CONTROL CYLINDER SERVICE FAILURES

1. Introduction

The aileron power cylinder contains four parallel bores, pressurized by two separate pumps. Many failures of this component have occurred either by failure through the component outer wall to the cylinder bore or between two cylinder bores. In either case, loss of pressure has resulted in aircraft malfunction.

Test results indicate that the normal mean pressure in these cylinder bores is about 1500 psi and varies between 750 and 2250 psi due to aerodynamic loading fluctuations. During an in-flight aileron maneuver, the pressure should rise to 3000 psi with transient pulses as high as 4500 psi due to hydraulic surge conditions associated with rapid command for aileron repositioning. Fatigue cracks have been nucleated mainly at metallurgical defects and grown to a critical length. To rectify this problem, the component was redesigned with the external wall-to-cylinder bore thickness being increased by 0.10 inch while the bore-to-bore wall thickness was not changed. After this design change, failures were confined to the area between the cylinder bores. Subsequent redesign has involved new material selection.

Information concerning failure of this component was obtained from conversations with engineering personnel and from three failure data sources:

Case I - An actual fractured component was available for study with no additional information except that it was of the older design.

Case II - A report was furnished concerning the failure of the component with the new design.

Case III - A report of the component failure with the old design.

All the available data for these cases has been entered into Table XV in Section D.1 according to the "Suggested List of Raw Data Necessary for Complete Failure Analysis of Component".

2. Component Analysis

The component material was 2014-T6. The tensile and yield strengths, and fracture toughness values for this material are reported to be:

<u>Longitudinal</u>	<u>Long Transverse</u>
$\sigma_{TS} = 73.5 \text{ KSI}$	$\sigma_{TS} = 72.1 \text{ KSI}$
$\sigma_{ys} = 68.3 \text{ KSI}$	$\sigma_{ys} = 56.4 \text{ KSI}$
$K_{IC} = 26.8 \text{ KSI}\sqrt{\text{IN}}$	$K_{IC} = 21.5 - 24.5 \text{ KSI}\sqrt{\text{IN}}$

In this component the longitudinal direction appears to be parallel to the bore axis. The hoop stress in the cylinder is most likely acting in the short transverse direction.

Extensive plane strain conditions are to be expected in a component when the thickness and crack length are greater than:

$$\left[\frac{K_{IC}}{\sigma_{ys}} \right]^2$$

Using the transverse values for yield strength of 56 KSI and the minimum K_{IC} value of 21.5 KSI \sqrt{IN} , (consideration being given to short transverse crack orientation), extensive plain strain conditions would be expected if the thickness and final failure crack length were greater than 0.15 inch. In all failures examined, this was the case.

a. Analysis for Case I:

As described in the data sheets, an elliptical surface flaw, 0.25 inch deep and 9/16 inch long, was observed to grow from the inner bore of one cylinder towards the bore of the adjacent cylinder as shown in Figure 38. A series of concentric markings suggested the mode of failure in this stage of the failure to be fatigue. After this stage, the crack appeared to propagate by a different mechanism through the thickness and parallel to the bore axis for a total length of 1-1/16 inches at which time unstable fracture occurred.

The key geometrical data are:

thickness (t) = 0.33 inch

elliptical crack depth (a) = 0.25 inch

elliptical crack length (2c) = 0.56 inch

a/2c = 0.445

elliptical flaw correction factor (Q) = 2.2

bore diameter (D) = 2-3/16 inches

through thickness crack length (2a₁) = 1-1/16 inches

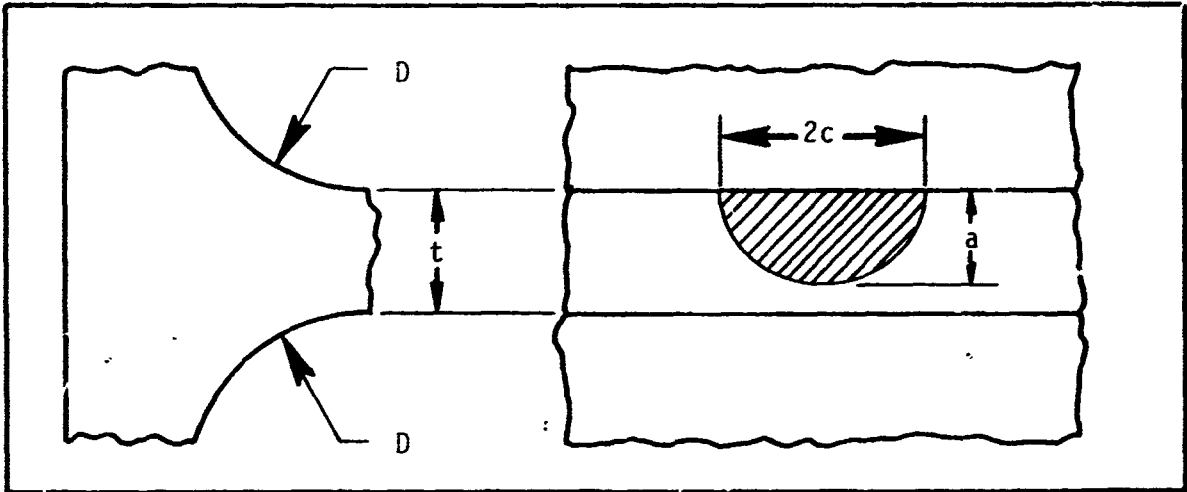


Figure 38. Actuator Cylinder Geometry and Fracture Description for Case I

It was assumed that unstable fracture occurred in the short transverse direction with a through thickness crack length of 1-1/16 inches. The lower value of the K_{IC} data was used in the calculations as the critical value since the fracture was in the short transverse direction rather than in the long transverse direction.

$$K_{IC} = \sigma \sqrt{\pi a_1} \quad (40)$$

$$21,500 = \sigma \sqrt{\frac{8.5}{16}}$$

$$\sigma = 16,600 \text{ psi}$$

This calculated value represents an estimate of the stress level at fracture

Since the cylinders have a large diameter to thickness ratio, pressurization could be analyzed in terms of a thin walled cylinder formulation. Since both cylinders are pressurized, the hoop stress between cylinder bores is estimated to be

$$\sigma_{\text{hoop}} = \frac{2PD}{2t} \quad (41)$$

Using the component dimensions and the calculated stress level at fracture (i.e., 16,600 psi) the pressure level at fracture is calculated to be

$$16,600 = \frac{2P\left(\frac{35}{16}\right)}{2(.33)}$$

$$P = 2500 \text{ psi}$$

Since the normal mean pressure in the cylinder bores is about 1500 psi and reaches a maximum of about 2250 psi, it is reasonable to conclude that unstable fracture was precipitated during pressure buildups associated with an aileron repositioning maneuver.

The change in fracture mechanism when the elliptical crack reached a depth and length of 0.25 and 0.56 inches, respectively, could have been due to the onset of static stress corrosion cracking at a stress intensity level equivalent to K_{ISCC} . For such an elliptical flaw

$$K^2 = \left[1 + .12\left(1 - \frac{a}{c}\right)\right]^2 \sigma^2 \frac{\pi a}{Q} \left[\frac{2t}{-a} \tan \frac{-a}{2t}\right] \quad (42)$$

For the given flaw geometry

$$K^2 = \left[1 + .12 \left(1 - \frac{.25}{.28} \right) \right]^2 \frac{\sigma^2 (.66)}{2.2} \tan \tau \left[\frac{.25}{.66} \right]$$

$$K = .88c$$

It is assumed that the major stress associated with static stress corrosion cracking is the stress associated with the mean pressure level of 1500 psi. The associated hoop stress is, therefore

$$\sigma_{\text{hoop}} = \frac{2(1500)\left(\frac{35}{16}\right)}{2(.33)} = 9900 \text{ psi}$$

Using this stress level, the stress intensity level for the onset of static stress corrosion cracking is calculated to be

$$K_{\text{ISCC}} = .88(9900)$$

$$K_{\text{ISCC}} = 8700 \text{ psi}\sqrt{\text{in}}$$

For cracking in the short transverse direction, the computed K value is a reasonable estimate of the K_{ISCC} level.

b. Analysis for Case II:

The pertinent data concerning the failure of the component with the new design are included in Table XV.

There is some concern about the accuracy of reported magnifications for key photographs. It is generally not the best practice to rely exclusively upon photographic evidence when performing a failure analysis. The reporter shall make careful measurements to be included in the text or suitable tables and then also provide photographs of the areas of

interest. In this case history, certain information was only available from photographs which contained no dimensional reference.

Comparing typical component dimensions in Case I with dimensions on Figure 4 of the Case II report revealed, the magnification (not stated in the Case II report) to be 1.4x. On this basis, the thickness between the cylinder walls is calculated to be 0.38 inch. Since the redesign on this component called for no change in wall thickness between the cylinder bores, it is not clear why the thickness was different in these two cases. In addition, the profile of the wall thickness shown in Figure 12 of the Case II report for the reported magnification is found to be 0.45 inch which represents a further discrepancy from the measured thickness in Case I.

From the Case II report, with particular reference to Figure 4, an elliptical flaw was shown to propagate across the ligament connecting the two cylinder bores. The fatigue crack (delineated by a series of concentric rings) was seen to propagate through the wall thickness to produce a through thickness crack 15/16 inch on the side of the origin and 3/16 inch on the surface of the other cylinder bore as shown in Figure 39. In the report, it was felt that this crack shape represented the final configuration prior to fracture. However, closer examination revealed evidence of further stable crack extension by some additional mechanism. It is again suggested that this stable crack extension is probably associated with stress corrosion cracking, occurring at relatively low stress intensity factor levels as reflected by the relatively smooth

nature of the fracture surface. The total length of the through thickness flaw was observed to be approximately 1.2 inches (Figure 39).

The pertinent data for this analysis are:

thickness (t) = 0.38 inch

elliptical flaw depth (a) = through thickness

elliptical flaw length (2c) = 15/16 and 3/16 inches

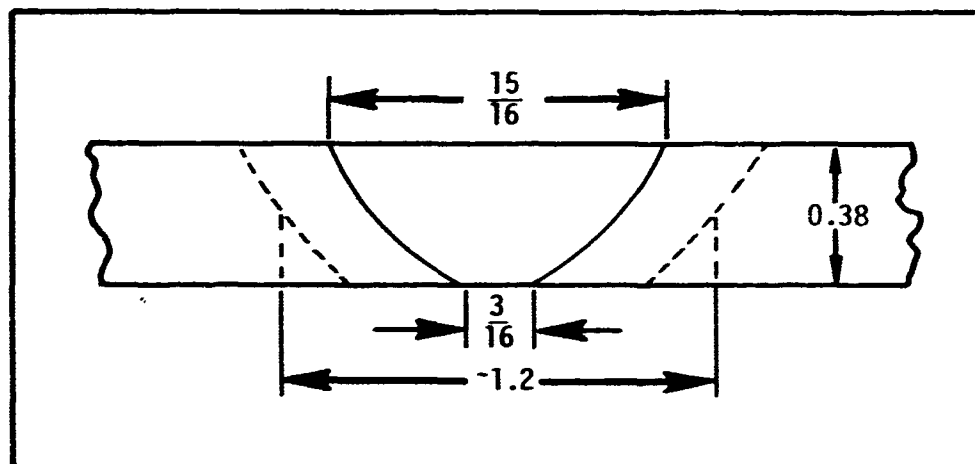


Figure 39. Component Geometry and Fracture Description for Case II

bore diameter (D) = 2-3/16 inches

through thickness crack length ($2a_1$) = 1.2 inches

Since failure occurred in the short transverse direction, the lower value of the K_{IC} range was used in the computation.

$$K_{IC} = \sigma \sqrt{\pi a_1}$$

$$21,500 = \sigma \sqrt{\pi(0.6)}$$

$$21,500 = 1.38\sigma$$

$$\sigma = 15,600 \text{ psi}$$

Using the thin walled cylinder formulation, the bore pressure at the time of fracture could be calculated

$$\sigma_{\text{hoop}} = \frac{2PD}{2t}$$

$$15,600 = \frac{2P\left(\frac{35}{16}\right)}{2(.38)}$$

$$P = 2700 \text{ psi (or 2350 psi if the thickness were 0.33 inch).}$$

It again appears that fracture occurred during pressurization to the 3000 psi level.

The magnitude of K_{ISCC} could be checked again by estimating the K_{I} level associated with the partial through thickness crack where the static stress corrosion cracking mechanism was initiated. Whereas the through thickness crack had lengths of 15/16 and 3/16 inches on each surface respectively, an estimate of the stress intensity condition could be made using the maximum and average values of the crack length "2a".

Therefore, let "2a" = range between 9/16 and 15/16 inches.

Using a stress level of 8700 psi associated with a cylinder bore

pressure of 1500 psi, the range of K levels is calculated to be

$$K = \sigma\sqrt{\pi a}$$

$$K = 8700 \sqrt{\pi \frac{4.5}{16}} = 8200 \text{ psi}\sqrt{\text{in}}$$

and

$$K = 8700 \sqrt{\pi \frac{7.5}{16}} = 10,600 \text{ psi}\sqrt{\text{in}}$$

which is in good agreement with the calculated value in Case I.

Thus far, from the calculated results in Case I and Case II, it may be concluded that cylinder bore pressure was greater than 2500 psi at the time of failure indicating that fracture occurred during a pressurization event. In addition, computed values of K_{ISCC} are found to be in the range of 40 - 50% of K_{IC} . These conclusions are reasonable and appear to validate the fracture mechanics approach to the analysis of the problem.

c. Analysis for Case III:

In the Case III report there is further concern with respect to the accuracy of the stated magnifications of the photographs. From the text of the report a preexistent surface flaw (with "2c" = 11/16 inch) was observed to propagate most of the way through the thickness before unstable fracture. From Figure 5 of the Case III report, the value of "2c" on the surface was 2 inches (it was 2-3/16 inches just below the surface). The photograph is reported to be 2.5x magnification but this would give $2c = 2/2.5 = 0.8$ inch which is not in agreement with the report text value of 11/16 inch. To correct this, it appears that the

correct magnification should have been 3x. On this basis, the observed "2c" values of $2\frac{3}{16}$ " would actually be $\frac{2 - 2\frac{3}{16}}{3} = 0.67$ to 0.73 inches, which agrees with the 11/16 inch (or 0.69 inch) value mentioned in the Case III report. In addition, on the basis of 2.5x the thickness between the cylinder bores was determined to be 0.4 inch. However, the actual component was 0.33 inch. If the true magnification was actually 3x, then the computed value of thickness would be 0.33 inch and in agreement with the true value. It is, therefore, assumed that the proper magnification is 3x in Figure 5 of the Case III report.

In this case an elliptical crack is again initiated on the surface of the cylinder wall and propagates towards the adjacent bore. The flaw, which was observed to open normal to the bore hoop stress, did not propagate completely through the thickness, and consisted of a series of concentric rings again suggesting the role of fatigue damage during crack extension. It was not possible to ascertain whether further growth occurred beyond the elliptical flaw due to the lack of sufficient photographic information.

The pertinent data for this analysis are:

thickness (t) = 0.33 inch

elliptical flaw depth (a) = 0.29 inch

elliptical flaw length (2c) = 0.69 inch

a/2c = 0.42 so that Q = 2.15

As in Case I the hoop stress for an average bore pressure of 1500 psi was found to be 9900 psi.

For a deep elliptical flaw, K may be estimated by

$$K^2 = \left[1 + .12 \left(1 - \frac{a}{c} \right) \right]^2 \sigma^2 \frac{\pi a}{Q} \left[\frac{2t}{\pi a} \tan \frac{\pi a}{2t} \right] \quad (43)$$

$$K_{ISCC} = 12,600 \text{ psi}\sqrt{\text{in}}$$

Since the crack depth to section thickness ratio in this case history is approximately 88%, the computation of K may be subject to substantial errors due to less precise determination of the individual correction factors (e.g., inaccuracy of the tangent formula correction at large a/t values) and the possibility of substantial plasticity corrections necessary when the unfractured ligament becomes very small. Nevertheless, the agreement between the results in Case I, II and III is reasonable.

3. Analysis Conclusions

a. The cylinder bore pressure at the time of failure was calculated to be greater than 2500 psi indicating that fracture occurred during pressure buildups associated with an aileron repositioning maneuver. In addition, a probable K_{ISCC} value of approximately 9000 $\text{psi}\sqrt{\text{in}}$ was computed. These values, which are considered to be reasonable estimates, were computed from both fracture mechanics and simple strength of materials relationships and demonstrate the usefulness of fracture mechanics concepts in the analysis of this failure.

b. Failure in all three cases was associated with crack extension in the short transverse direction normal to the direction of the hoop stresses.

c. An elliptical crack grew initially by a fatigue process and then presumably by a stress corrosion mechanism during the latter stages of extension.

d. The accuracy and proper implementation of the analysis method was compromised considerably by the lack of dimensional references in photographs of the fractured surface. It is critically important that greater care be taken when reporting the photographic magnification of macrofractographs in magnifications up to about 20x. The use of fracture mechanics concepts requires the accurate knowledge of specimen dimensions and flaw geometry. It is necessary to educate the failure report writer that a macrophotograph serves an important function in a quantitative analysis in addition to giving the reader a "general and overall" (and apparently dimensionally inexact) view of the fracture surface.

EXAMPLE 3

ANALYSIS OF CRACK DEVELOPMENT DURING A CENTER WING SECTION

STRUCTURAL FATIGUE TEST

This analysis reviews the failure of a wing center section lower plate in a structural fatigue test. The lower plate was a steel alloy with a verified yield strength of 218 ksi. The test structural section was subjected to a known program of loads which led to a computed stress level of 120 ksi at the instant of final failure. Other stress levels associated with subcritical flaw growth, i.e., bands of fatigue crack growth, computed in a like manner will be introduced into the analysis later.

The crack emanated on two sides of a hole on the same side of the plate and spread during fatiguing into a semicircular flaw with portions on each side of the hole as indicated on the photographs to follow. The circumstances surrounding final failure will be independently analyzed by three separate methods:

1. Direct crack tip stress intensity analysis of the instant of final failure,
2. Analysis of shear lips accompanying final failure, and
3. Analysis of fatigue crack growth rates just preceding final failure.

These independent analyses illustrate quantitative cross-checking of circumstances of final failure using fracture mechanics analysis.

1. Direct Analysis of the Final Failure

The flaw geometry at final failure is shown in Figure 40. The objective of this analysis is to bracket the critical stress intensity, K_c , associated with the final failure by calculation of upper and lower limits (or bounds) on the applied stress intensity.

The lower limit can be calculated by ignoring the influence of the hole and thinking of the crack as a semi-circular surface flaw of radius, $a = 0.34$ inch and ignoring the hole underestimates in the actual applied stress intensity. With a free surface correction of 1.12 conservatively

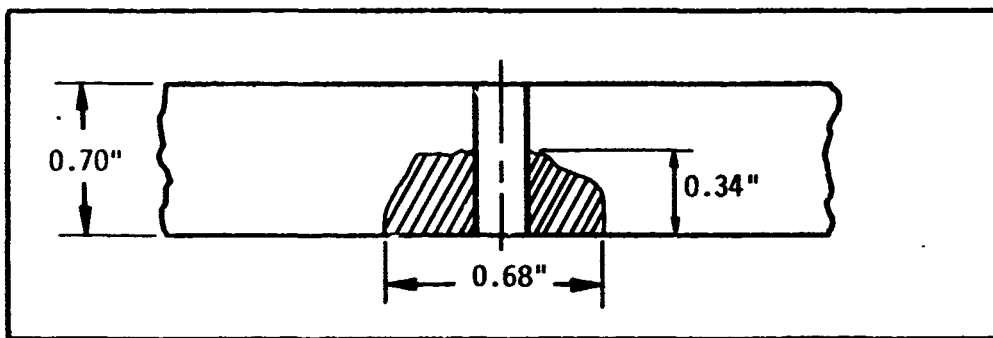


Figure 40. Plate Flaw Geometry at Final Failure

reduced to 1.05, the proper formula is:

$$K_L = \frac{1.05 \sigma \sqrt{\pi a}}{(\pi/2)} \quad (44)$$

$$K_L = \frac{1.05(120)\sqrt{\pi(0.34)}}{(\pi/2)}$$

$$K_L = 83 \text{ ksi}\sqrt{\text{in}}$$

This is a slight underestimate of the actual applied stress intensity, K, but is believed to be within about 10% of the correct value. No K_{IC} data is specifically available for this component failure analysis, therefore, an actual value or probable "measured" value cannot be stated.

An upper limit may be calculated by taking a through the thickness (of the plate) crack length, $2a = 0.68$ inch. Noting earlier discussion of cracks near holes, the hole has little influence on K here, thus the proper formula is:

$$K_U = \sigma\sqrt{\pi a} = 120\sqrt{\pi(0.34)}$$

or

$$K_U = 124 \text{ ksi}\sqrt{\text{in}}$$

This result is a considerable overestimation of the actual applied K by about 30 to 40%. (Moreover, it could absolutely not be an underestimate since in growing catastrophically the crack must have passed this configuration and if it did so without arrest, the value of applied K here must be higher than that for commencement of rapid propagation, the case under discussion.)

Therefore, the critical applied K for the crack at the instant of final failure is bracketed in the following way:

$$83 = K_L \quad < \quad K_C \quad \ll \quad K_U = 124 \text{ ksi}\sqrt{\text{in}}$$

(10%) (30 to 40%)

From these considerations, the estimated K_c value for the failure of this material is:

$$K_c = 85 \text{ to } 100 \text{ ksi}\sqrt{\text{in}}$$

or a best single value of

$$K_c = 90 \text{ ksi}\sqrt{\text{in}}$$

2. Estimation From Shear Lip Size

From the photographs of the fracture in Figure 41, the shear lips accompanying final failure are easily observed. From measurements adjusted for magnification of the photos, the width of the lip along each surface is slightly less than 1/32 inch.

The material obviously exhibits clear distinct shear lips and in such a case the shear lip width is fairly well approximated by the calculated plastic zone radius, r_y , (for plane stress) where:

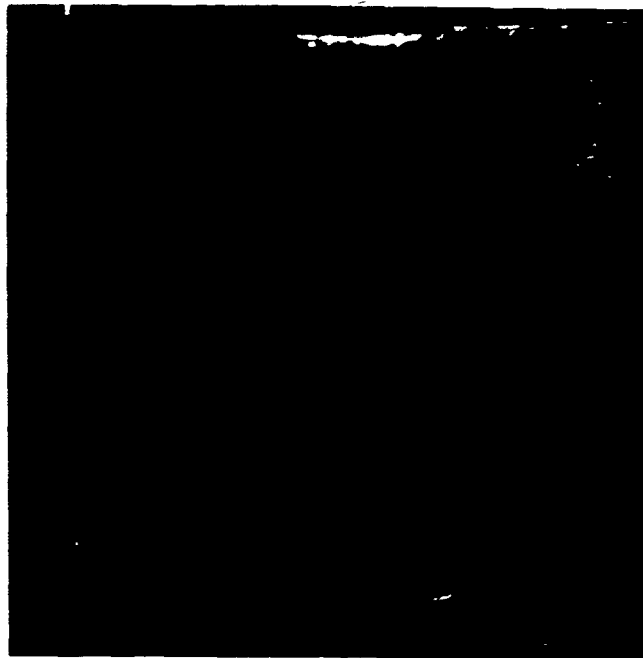
$$r_y = \frac{K^2}{2\sigma_{yp}^2} \quad (45)$$

Substituting the yield point stress of the material, $\sigma_{yp} = 218 \text{ ksi}$:

$$1/32" > r_y = \frac{K^2}{2-(218)^2}$$

or

$$K_c < 103 \text{ ksi}\sqrt{\text{in}}$$



8741

FM-1

5X



8740

10X



8739

FMD

10X

Figure 41. Photographs of Fracture Surface After Final Failure

Thus, a best estimated K_C value is approximately

$$K_C = 90 \text{ ksi}\sqrt{\text{in}}$$

It should be noted that this number is calculated from entirely different and independent data than the previous identical estimate based on direct analysis of final failure conditions. Thus, further confidence is developed in the quantitative validity of the analysis.

3. Fatigue Cracking Rates Preceding Final Failure

The fracture surfaces shown in the photos show bands (of different texture or color) due to programmed fatigue cracking. Each band represents cycling to a particular load level for a certain number of cycles.

Just before final failure, the load program is known and the bands of fatigue cracking can be readily identified with particular known loadings.

For the last large band before failure, the number of cycles applied was $\Delta N = 15$ and the computed stress level was $\sigma = 20$ to 130 ksi (in proportion to load). From the photo of the fracture surface, the width of the band is $\Delta a = 1/80$ inch. Thus, the rate of crack growth was

$$\frac{da}{dn} = \frac{\Delta a}{\Delta n} = \frac{1}{80} \cdot \frac{1}{15} = 8.3 \times 10^{-4} \text{ in/cyc}$$

Figure 42 shows data on high strength steel alloys from Reference[43] for the rate of crack growth da/dn compared to the range of the stress

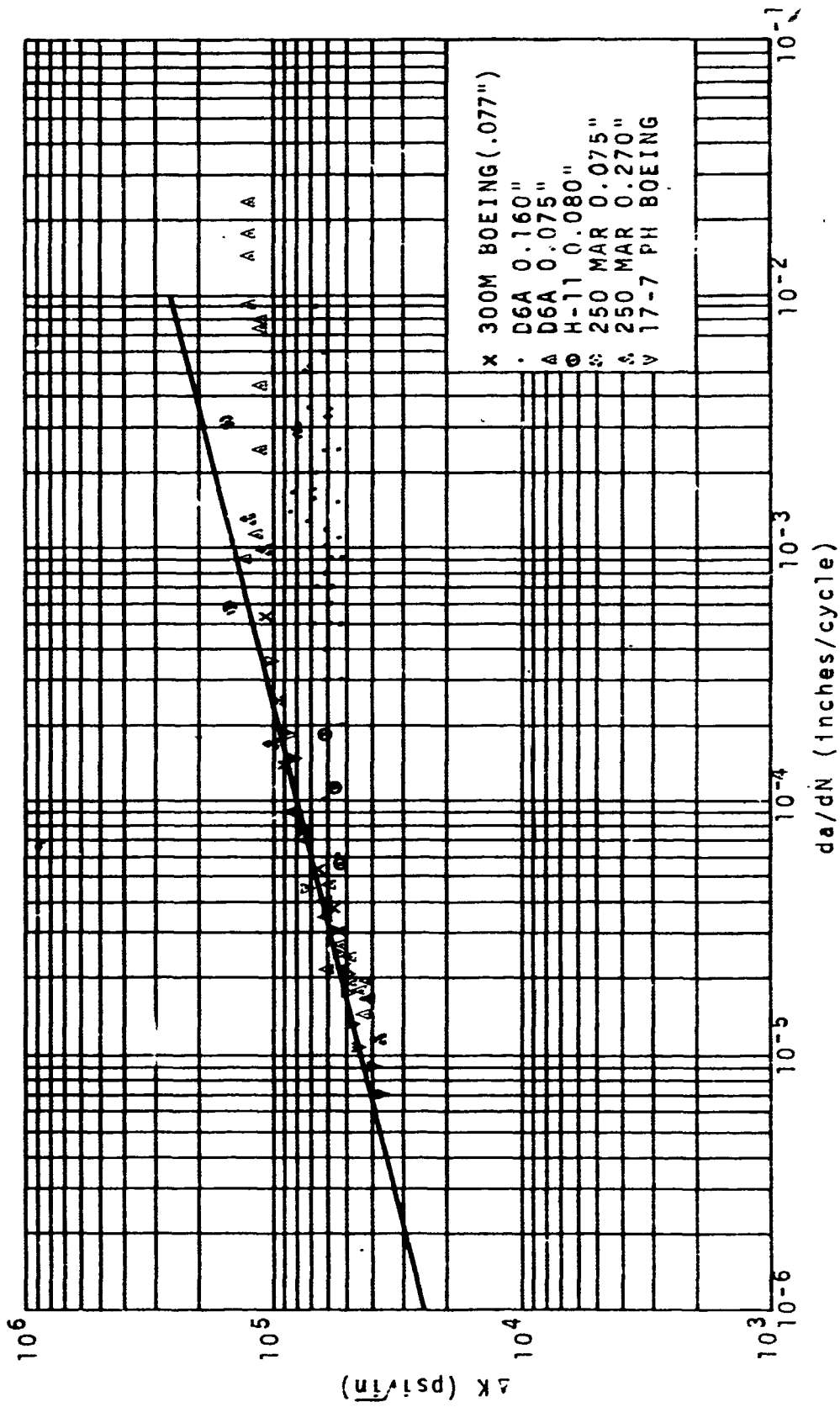


Figure 42. Data on High Strength Steels Showing Deviation from the Usual Curve
 ($K = K_{max}; \beta = \infty$) [43]

intensity factor, ΔK . Using the above value for crack growth rate in Figure 42, a best estimate of the applied ΔK is:

$$\Delta K = 70 \text{ ksi}\sqrt{\text{in}} \text{ (best estimate)}$$

To find the maximum value of applied K during this cycling, ΔK should be multiplied by the ratio of maximum load (σ_{max}), to the load range ($\Delta\sigma = \sigma_{\text{max}} - \sigma_{\text{min}}$) or

$$K_{\text{max}} = 70 \cdot \frac{130}{110} = 88 \text{ ksi}\sqrt{\text{in}}$$

during cycling just before failure.

This calculation can be repeated for the next to the last band where:

$$\Delta n = 2 \text{ cycles}$$

$$\sigma = 20 \text{ to } 144 \text{ ksi}$$

$$\Delta a = \frac{1}{160} \text{ inch}$$

or

$$\frac{da}{dn} = \frac{1}{160} \cdot \frac{1}{2} = 3 \times 10^{-3} \text{ inch/cycle.}$$

In Figure 42 this implies:

$$\Delta K = 75 \text{ ksi}\sqrt{\text{in}} \text{ (best estimate).}$$

Again, using this data to compute the maximum K applied prior to failure

$$K_{\max} = \Delta K \frac{\sigma_{\max}}{\Delta \sigma} = \frac{75(144)}{124} = 90 \text{ ksi}\sqrt{\text{in}}$$

These two calculations leading to K_{\max} values of $90 \text{ ksi}\sqrt{\text{in}}$ just before failure represent minimums, but minimums very close to the values for K_c for final failure. Thus again $K_c = 90 \text{ ksi}\sqrt{\text{in}}$ has been verified by three independent methods of calculation. Consequently, these final failure conditions are fully documented beyond reasonable doubts.

Viewing the structural component in a different manner, one can also see that the fatigue crack growth rates just before failure could be predicted by backwards calculation. The backwards calculation, if based on methods in Reference [43], required only the knowledge of stress levels and the crack shape and size.

4. Component Analysis Conclusions

The failure occurred due to growth of fatigue cracks whose rates of growth can be fully anticipated. Fatigue may then be listed as the "cause" of the failure and the problem may be avoided by several means:

- a. Reducing stress levels will reduce fatigue crack growth rates by approximately the 4th power of the ratio of stress level reduction.
- b. Eliminating the hole would reduce local stress concentration effects in initiating cracking and thereby would greatly prolong obtaining a sizeable crack.
- c. Crack inspection intervals could be set to assure no failures between inspections.

This example has thus served its purpose here by providing a good illustration of the improvement of failure analysis methods employing fracture mechanics.

EXAMPLE 4

FAILURE ANALYSIS OF LOWER FRONT WING SPAR CAP

The failure reports contained rather complete spar cap geometry and fracture surface description, including a fractured component. From the photographs and the part specifications, it was possible to estimate the size of the flaw leading to failure.

The crack nucleated at a 0.193 inch fastener hole and spread throughout the flange of the spar cap. It progressed (somewhat like a corner crack) into the heavy section of the spar cap where instability occurred. The cross section dimensions of the spar cap and geometry of the actual fractured surface are shown in Figure 43.

In the heavy section of the spar cap (.500 in thick section), it is probable that considerable plane strain conditions would be encountered since the necessary thickness for plane strain should be

$$t \geq 2.5 \left[\frac{K_{Ic}}{\sigma_{ys}} \right]^2 \geq \frac{2.5}{9} \text{ inch}$$

which is less than the section size in question.

The component was subjected to a series of random loads during its 6012 hour life and failed after a positive 5g, 20 degree dive and pull out maneuver.

An estimate of stress level in the critical area is possible based upon strain gage readings from uncracked components subjected to a range

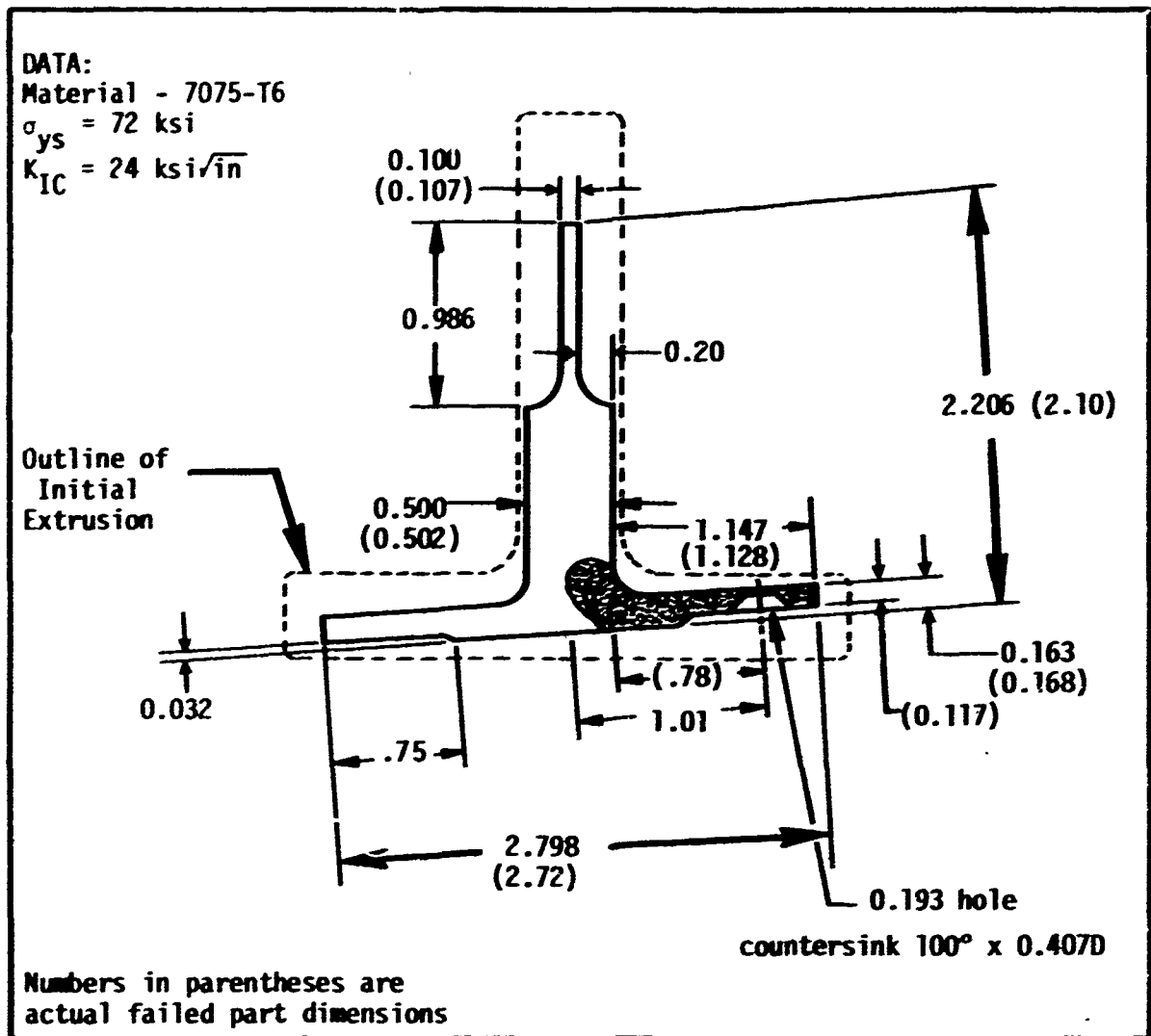


Figure 43. Spar Cap Cross Section Geometry and Fracture Description

of g loads.

Using a load factor of 5.25g in the vicinity of the final crack length, the associated stress was found to be = 20,000 psi.

1. Component Analysis

Since no direct method is available to estimate the stress intensity level, a reasonable solution can only be obtained by a series of simple approximations.

a. Approximation for 1.4 inch edge crack:

First, assume that the K level at instability is approximated by the stress intensity conditions at the tip of an edge crack 1.40 inch long (1.15 inch flange length + 0.25 corner crack depth). Since the major section containing the corner crack is much thicker than the cracked flange and the other flange is not broken, there should not be much bending superimposed on the tensile opening of the cracked flange.

$$K = \alpha \sigma \sqrt{\pi C} \quad (46)$$

$$\text{where } \alpha = 1.1$$

$$\sigma = 20,000 \text{ psi}$$

$$a = 1.4 \text{ inches}$$

$$\alpha = 1.1 (20,000) \sqrt{\pi(1.4)}$$

$$K = 1.1 (20,000) (2.1) = 46,000 \text{ psi}\sqrt{\text{in}}$$

This value should serve as an upper limit of the K level at fracture since the importance of the contribution of the cracked flange to cause the failure

should decrease with decreasing flange thickness. The contribution of the cracked flange (0.168 inch thick) should not be as great as the crack embedded in the 0.500 inch thick main spar section. In the limit, if the flange thickness were to decrease to zero, then there would be no contribution of the cracked flange to the necessary conditions for failure.

b. Approximation for no flange crack influence:

Under the conditions described above where the flange thickness is reduced to zero, the K level at fracture could be approximated by the corner crack in the 0.50 x 1.0 inch section. This estimate should place a lower limit of the K level at fracture.

The corner crack shape is not circular but rather extends to its greatest depth at roughly 45 degrees to the corner. However, for ease of computation, the corner crack will be treated as a circular flaw extending 0.25 inch into the thicker section. This simplification should place a moderate overestimation of the lower limit of K being computed.

$$K \geq (1.12)^2 \frac{2}{\pi} \sigma \sqrt{\pi r}$$

$$K \geq (1.25)(0.64)(20,000) \sqrt{\pi(0.25)}$$

$$K \geq 14,000 \text{ psi}\sqrt{\text{in}}$$

2. Analysis Conclusions

On the basis of these two simplified computations, the stress intensity level necessary for fracture (the K_{Ic} level in all likelihood) should be

between 14 - 46 ksi $\sqrt{\text{in}}$. 7075-T6 aluminum alloy does have $K_{IC} = 24$ ksi.

Since the contribution of each factor, i.e., the 1.4 inch long cracked flange and the 0.25 inch corner crack, should depend upon the relative thickness of the flange section to the main section of the spar, it should be possible to crudely estimate the critical stress intensity level at the point of fracture on the basis of a weighted average (with respect to thickness) of the two K limits.

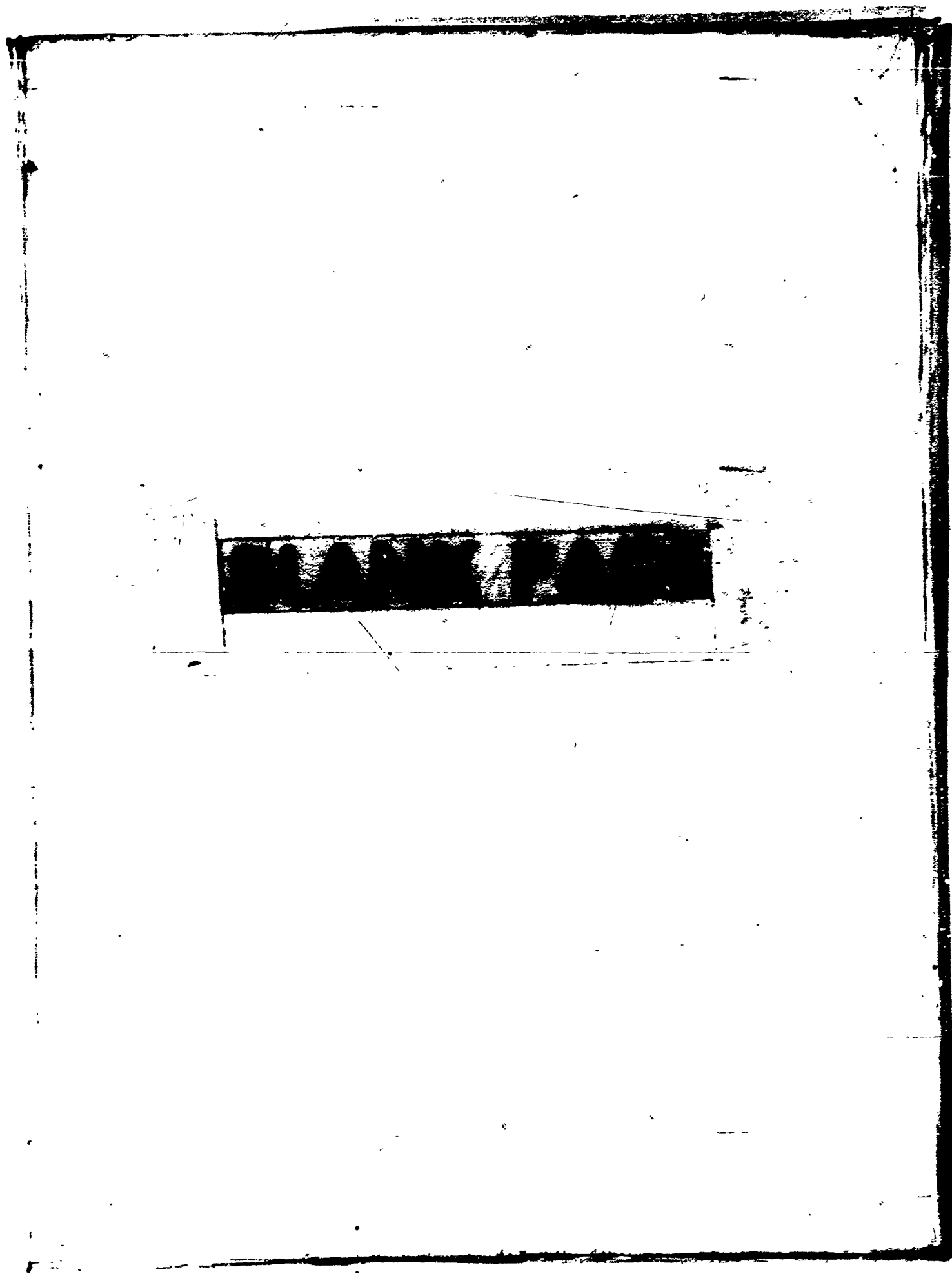
The effective K at fracture was considered to lie between the two extreme values computed above. Using an equivalent thickness of unity, the weighted average K value on the basis of the relative thickness of the two sections of the component should be closer to the lower limit since the corner crack occurred in the 0.5 inch section as compared to the 1.4 inch crack in the 0.168 inch section. This would indicate a relative influence of 75% and 25% respectively for the two thicknesses. Thus:

$$K_{\text{effective}} = \frac{3}{4} (14,000) + \frac{1}{4} (46,000)$$

$$K_{\text{effective}} = 10,500 + 11,500$$

$$K_{\text{effective}} = 22,000 \text{ psi}\sqrt{\text{in}}$$

which is in good agreement with fracture under plane strain conditions in this alloy. This computed value is plausible in view of the absence of shear lips at the instability point.



EXAMPLE 5

FAILURE ANALYSIS OF WING CARRY-THROUGH FORGING

1. Introduction

After a service life of 5269 hours, a four-inch long crack was observed in a forged 7075-T6 wing spar. The crack initiated at a longitudinal split located parallel to the major stress direction as shown in Figure 44. The split was nucleated along planes of weakness resulting from the forging process. It has been assumed that the crack initiated at the longitudinal flaw and grew normal to the major stress direction to a semicircular surface flaw shape with a radius of 0.43 inch. At this point, the crack reached a critical size in the 0.8 inch wide by 0.6 inch deep flange resulting in rapid fracture. The unstable crack then ran along the three inch long web section (about 0.3 inch thick) and was finally arrested near the region of larger cross sectional area. At this point stable crack growth by a fatigue process was resumed.

Additional data concerning detailed measurements of the flaw geometry before and after instability were obtained from the actual fractured component which was available for detailed examination. The necessary failure analysis information is tabulated in Table XV of Section III.D.1. In addition, the fracture surface was examined in the Del Research Laboratory using electron fractographic techniques. Additional data from this study are also reported and analyzed.

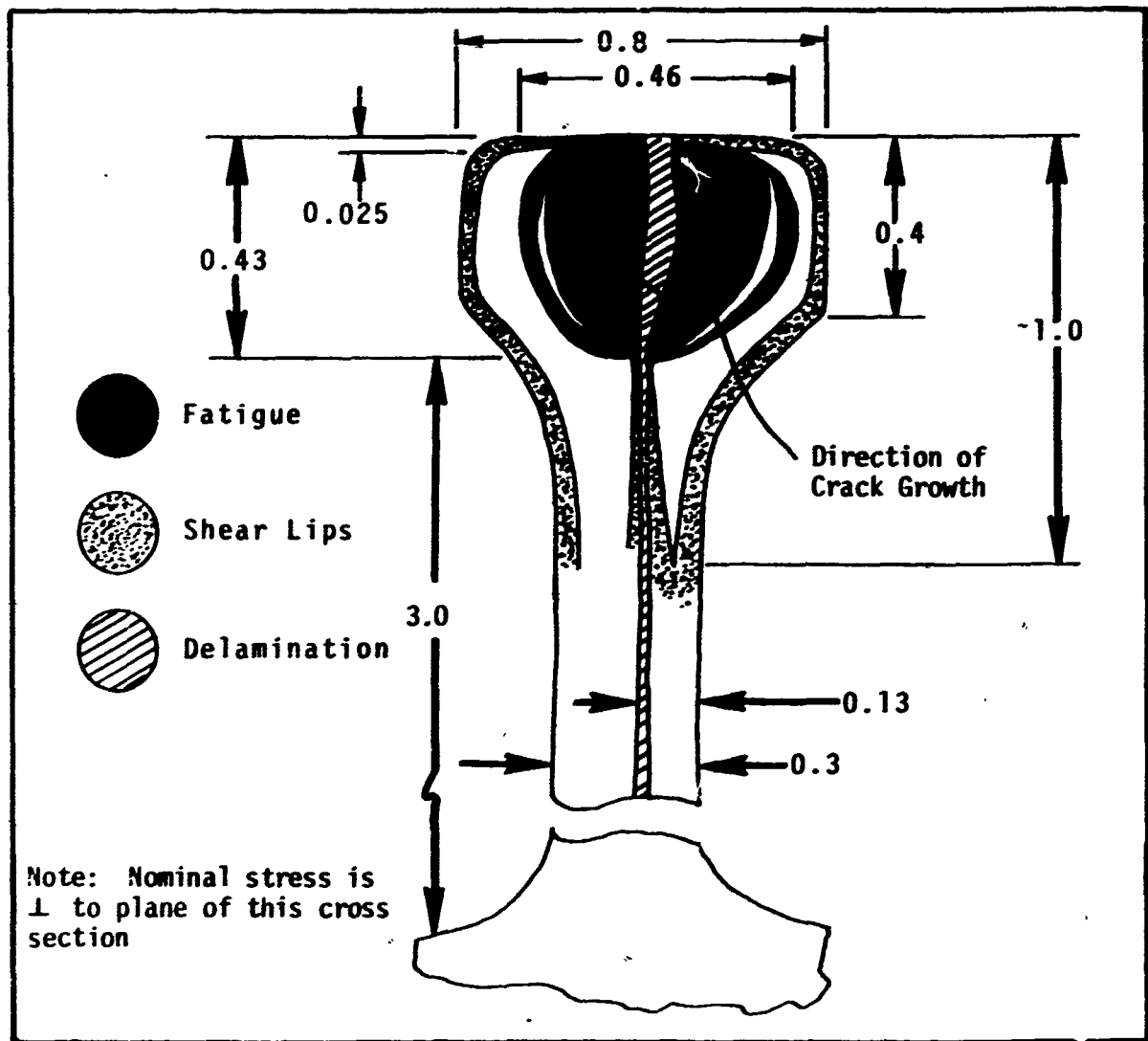


Figure 44. Fracture Surface Appearance of Wing Carry-Through Forging

2. Component Failure Analysis

From the failure report[44], the actual component, and discussions with engineering personnel, a minimum necessary amount of information was gathered to allow for an approximate fracture analysis of the component.

The spar material was 7075-T6 aluminum alloy and was reported to have the following properties:

$$K_{IC} = 24 \text{ ksi}\sqrt{\text{in}}$$

$$\sigma_{ys} = 68 \text{ ksi}$$

A measure of the severity of the stress state can be obtained by a comparison of the relative plastic zone size to the thickness of the component containing the crack. Approximate plane strain conditions are expected when the component thickness is greater than

$$\left[\frac{K_{IC}}{\sigma_{ys}} \right]^2$$

For this case,

$$\left[\frac{K_{IC}}{\sigma_{ys}} \right]^2 = \left[\frac{24}{68} \right]^2 = 0.125 \text{ inch}$$

Since the flange section was 0.8 inch x 0.5 inch, plane strain conditions were probably associated with the failure.

From the sketch of the critical flaw dimensions in the flange (Figure 44), the flaw was of a semicircular configuration at the point of instability. It is our considered judgment that the starting crack, which initiated at the forging delamination, grew laterally along a front extending approximately 0.46 inch in length. In this way, the stress intensity factor increased as the "tunnel" shaped crack moved laterally in both directions. This viewpoint is supported by the observation of a "pop-in" just prior to final failure.

The orientation of the "pop-in" markings indicates a lateral direction of crack propagation.

As the crack moved laterally, a small shear lip was developed at the flange surface which represented the extent of plane stress conditions in this component. Therefore, by equating the size of the plane stress plastic zone at instability to this shear lip (approximately 0.025 inch), it was possible to estimate the stress intensity condition at failure.

$$r_p = \frac{1}{2\pi} \left[\frac{K_{MAX}}{\sigma_{ys}} \right]^2 = 0.025 \text{ in} \quad (47)$$

$$\left[\frac{K_{MAX}}{\sigma_{ys}} \right]^2 = 0.157$$

$$K_{MAX} = 0.4\sigma_{ys}$$

$$K_{MAX} = 27,000 \text{ psi}\sqrt{\text{in}}$$

The computed value of the stress intensity factor compares favorably with the K_{IC} value of the material, indicating the existence of plane strain conditions at fracture.

Using the computed value of $K = 27,000 \text{ psi}\sqrt{\text{in}}$ and the half crack length of the tunnel crack (" a " = 0.23 inch), it was possible to compute the prevailing stress state.

$$K = \sigma\sqrt{\pi a} \quad (48)$$

$$27,000 = \sigma\sqrt{\pi(0.23)}$$

$$\sigma = \frac{27,000}{.85} = 31,800 \text{ psi}$$

The computed maximum stress associated with fracture is in good agreement with the actual stress state estimated to be in the neighborhood of 35,000 psi.

In the above computation a more precise estimate of the stress intensity level was not attempted since the two major correction factors would have been somewhat self-compensating. For example, a correction factor should have been added to account for the crack being as large as one half the section size. On the other hand, the curved crack front should have suggested the use of a smaller effective crack length than the maximum length used in the calculation.

The delamination was observed to extend into the web section, thereby, dividing that region into two sections, 0.13 and 0.17 inch thick, respectively. In the 0.13 inch section, a clearly defined transition from flat fracture to 100 percent shear failure was observed after the crack had extended to a length of about 1.0 inch. Using this observation it was possible to estimate the plane stress fracture toughness level.

$$t = \frac{1}{\beta_c} \frac{K^2}{2 \sigma_{ys}} \quad (49)$$

For the full shear case, β_c is estimated to be in the range of 4 to 2 π . Therefore, for $t = 0.13$ inch the limits are:

$$.13 = \frac{1}{4} \frac{K^2}{2 \sigma_{ys}} \quad \text{and} \quad .13 = \frac{1}{2\pi} \frac{K^2}{2 \sigma_{ys}}$$

Using the value of $\sigma_{ys} = 68,000$ psi, it is found that

$$K_c = 49,000 \text{ psi}\sqrt{\text{in}} \text{ to } 61,000 \text{ psi}\sqrt{\text{in}}$$

These values are in excellent agreement with the results of Zinkham[10].

A few selected fractographs revealing fatigue striations were included in the failure report. It was not possible to make any meaningful computations based on these photographs. First, the crack length at which these striations were observed was not known and second, it was not clear whether these striation spacings were representative values of fatigue crack growth rate in that region of the fracture. To make use of fractographic evidence in this failure analysis, the specimen was examined at the Del Research Laboratory. Replicas were made from selected regions along the crack and examined in the electron microscope. It was immediately obvious that the component had been subjected to a random loading pattern since striation spacings varied nonuniformly along the entire crack length as shown earlier in Figure 36 on page 150. At approximate crack lengths of 0.50, 0.15 and 0.23 inches the range of observed striation spacings varied from 3.1×10^{-6} - 4.5×10^{-5} , 4.1×10^{-6} - 6.9×10^{-5} , and 9.4×10^{-6} - 2×10^{-4} , respectively. Since striation spacings can be related to the stress intensity factor range[45], it is possible to estimate the stress intensity conditions from these fractographic observations. It is extremely important that this task be approached with caution since the size of the striation for a given load application is also dependent upon the previous loading history[46]. For example, prior overloads will result in a smaller striation spacing than expected for a given load application[26].

This effect should be important in random loading conditions. Nevertheless, taking many readings of striation spacing in a given region should, for a first approximation, represent the range of stress intensity range levels at the advancing crack tip. Using the data for 7075-T6 aluminum alloy presented in the paper by Johnson and Paris[11], estimates of stress intensity factor range were obtained. For the crack length of 0.05 inch, using the above mentioned range of observed striation spacings, the stress intensity factor range was estimated to be between $7500 \text{ psi}\sqrt{\text{in}}$ and $14,600 \text{ psi}\sqrt{\text{in}}$ as a result of the fluctuating loads. For a tunnel crack

$$\Delta K = \Delta\sigma\sqrt{\pi a}$$

$$\Delta\sigma = \frac{7500}{\sqrt{\pi(0.05)}} \text{ and } \frac{14,600}{\sqrt{\pi(0.05)}}$$

$$\Delta\sigma = 18,800 - 36,500 \text{ psi}$$

For the crack length of 0.15 inch, in a similar manner, the stress intensity range was found to vary between $8000 \text{ psi}\sqrt{\text{in}}$ and $16,300 \text{ psi}\sqrt{\text{in}}$. The stress range computed for these data was

$$\Delta\sigma = 11,600 - 23,700 \text{ psi.}$$

Finally, for the crack length of 0.23 inch, the stress intensity range levels varied between $9900 \text{ psi}\sqrt{\text{in}}$ and $21,200 \text{ psi}\sqrt{\text{in}}$ (estimated from large striation, or stretch zone, at the point of crack instability). The stress range computed for these data was

$$\Delta\sigma = 11,600 - 25,000 \text{ psi}$$

On the basis of these computations, the averaged maximum stress

range is estimated to be about 28,400 psi as compared to a previously calculated maximum stress level of 32,000 psi, both values being within the engineering estimate of 35,000 psi as a maximum value. The agreement in computed values indicates that the mean stress was not high and that the component was loaded in a nominally low load - maximum load manner. In further support for this conclusion is the fact that the largest striation spacing before the onset of void coalescence corresponded to a stress intensity range level of 21,200 $\text{psi}\sqrt{\text{in}}$ which compares reasonably well with the computed maximum stress intensity level of 27,000 $\text{psi}\sqrt{\text{in}}$.

3. Analysis Conclusions

a. The crack was nucleated at a forging defect which delaminated under loading parallel to the maximum stress direction.

b. The long narrow crack grew laterally to a semicircular shape prior to instability.

c. On the basis of shear lip calculations, the maximum stress intensity level was computed to be 27,000 $\text{psi}\sqrt{\text{in}}$ indicative of plane strain conditions. The associated stress level was found to be 31,800 psi in good agreement with engineering estimates of 35,000 psi as the maximum stress level.

d. On the basis of fractographic observations, it was concluded that the component had been subjected to a random loading history with a maximum stress amplitude of approximately 28,400 psi. The agreement in magnitude of the maximum stress and stress range values suggests that the component was not subjected to a high mean stress.

e. The analysis clearly demonstrates the utility of macroscopic and microscopic fractographic observations in failure analysis.

EXAMPLE 6

SUMMARY OF CENTER WING SECTION ANALYTICAL INVESTIGATION

The following summarizes the analytic investigation of the center wing section lower skin for a military aircraft. This failure analysis example is taken almost verbatim from an Air Force Flight Dynamics Laboratory report[49] since it exemplifies the use of Fracture Mechanics concepts in failure analysis.

1. Residual Strength Investigation

Perhaps the most powerful and currently accepted method for analyzing the residual strength of fatigue cracked structures is by the use of the Griffith-Irwin theory of fracture mechanics. This theory states that rapid crack growth or fast fracture will occur when the stress intensity factor K (a measure of the stress field intensity at the crack tip), calculated at the time of failure reaches the allowable value of K_c for the specified material.

The stress intensity factor K may be determined for various geometrical configurations by use of the theory of elasticity. For the case of a finite width plate containing a central crack the expression is:

$$K = \sigma \sqrt{\pi a} \sqrt{\frac{2b}{\pi a} \tan \frac{\pi a}{2b}} \quad (50)$$

where

a = half crack length

$2b$ = plate width

σ = gross area stress in plate

For the case of a crack emanating from a circular hole, as shown in Figure 45, the equation has the form

$$K = \sigma\sqrt{\pi L} \left[F\left(\frac{L}{R}\right) \right] \quad (51)$$

where

L = crack length not including the hole

R = radius of hole

$F\left(\frac{L}{R}\right)$ = factor which is a function of the ratio L/R and has different values depending on whether the crack L is present on one or both sides of the hole.

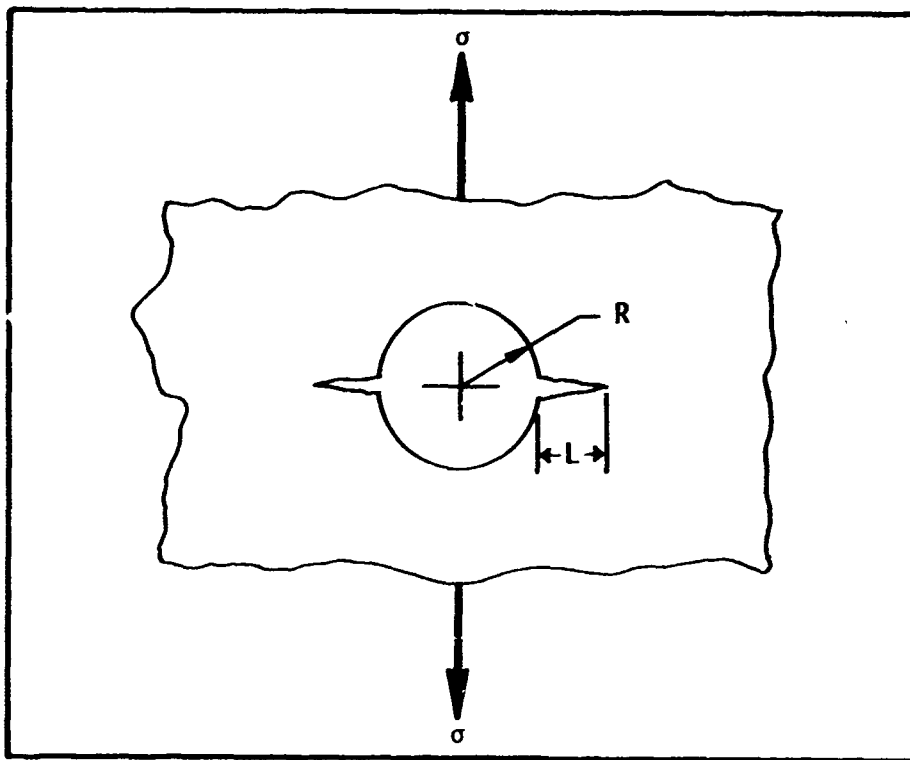


Figure 45. Geometry for a Crack Emanating from a Circular Hole in a Plate

For each of these cases the crack is assumed to extend through the thickness.

For the wing skin the hole diameters under consideration are 1/4 inch and 5/16 inch. The total effective half-crack length approaches a value equal to the hole radius plus the side-crack length (i.e., $L + R$) for relatively small values of L . For the two hole diameters, these values of L and R are as follows:

<u>Hole</u>	<u>Side Crack</u>
<u>R</u>	<u>L</u>
1/8 in.	0.030 in.
5/32 in.	0.035 in.

The value of K_c (fracture toughness) is dependent upon plate thickness, temperature, geometry and material and must be determined by test. Essentially, K_c decreases with increasing thickness and approaches a value of K_{Ic} known as plane strain fracture toughness. Typical values for 7075-T6 aluminum are listed below for various thicknesses.

<u>Thickness</u>	<u>K_c</u>	<u>K_{Ic}</u>
0.125	50 ksi	-
0.250	39 ksi	-
1.000	30.8 ksi	30.8 ksi

The critical value of the failing stress may be calculated for any value of crack length by substituting $K = K_c$ (or K_{Ic}) and solving for σ .

For this wing plate, equation (50) was used with $2b$ equal to the distance between fastener rows. A crack in one row is not affected by one in an adjacent row so long as $2b \gg 2a$. Figure 46 includes a plot of critical crack length versus gross area stress for three values of K_c . The load factor (N_z) to stress relationships were obtained from the aircraft manufacturer. Additional information relative to the length of through-crack emanating from the hole is included. The data points plotted on the lower curve are from the aircraft manufacturer and show that similar assumptions have been made in the analyses. It is important in this discussion to consider stress level rather than load factor because of the variation in the configuration for each aircraft.

One additional point that should be mentioned is that the thickness of the actual skins varies normal to the principal loading (σ). The original taper was designed to give constant σ across the width. No data has been supplied to the writer to indicate that a variation in σ for the actual aircraft exists. This analysis of course assumes constant σ and constant thickness*. Any test procedures for the full scale panels should account for the thickness variation in order to be meaningful.

2. Crack Propagation Investigation

Several attempts were made to calculate the number of cycles required to cause catastrophic failure of the wing skins for prescribed initial

*Editorial Note: Stress and thickness variations considered here would be small and gradual and would cause very little difference in analysis.

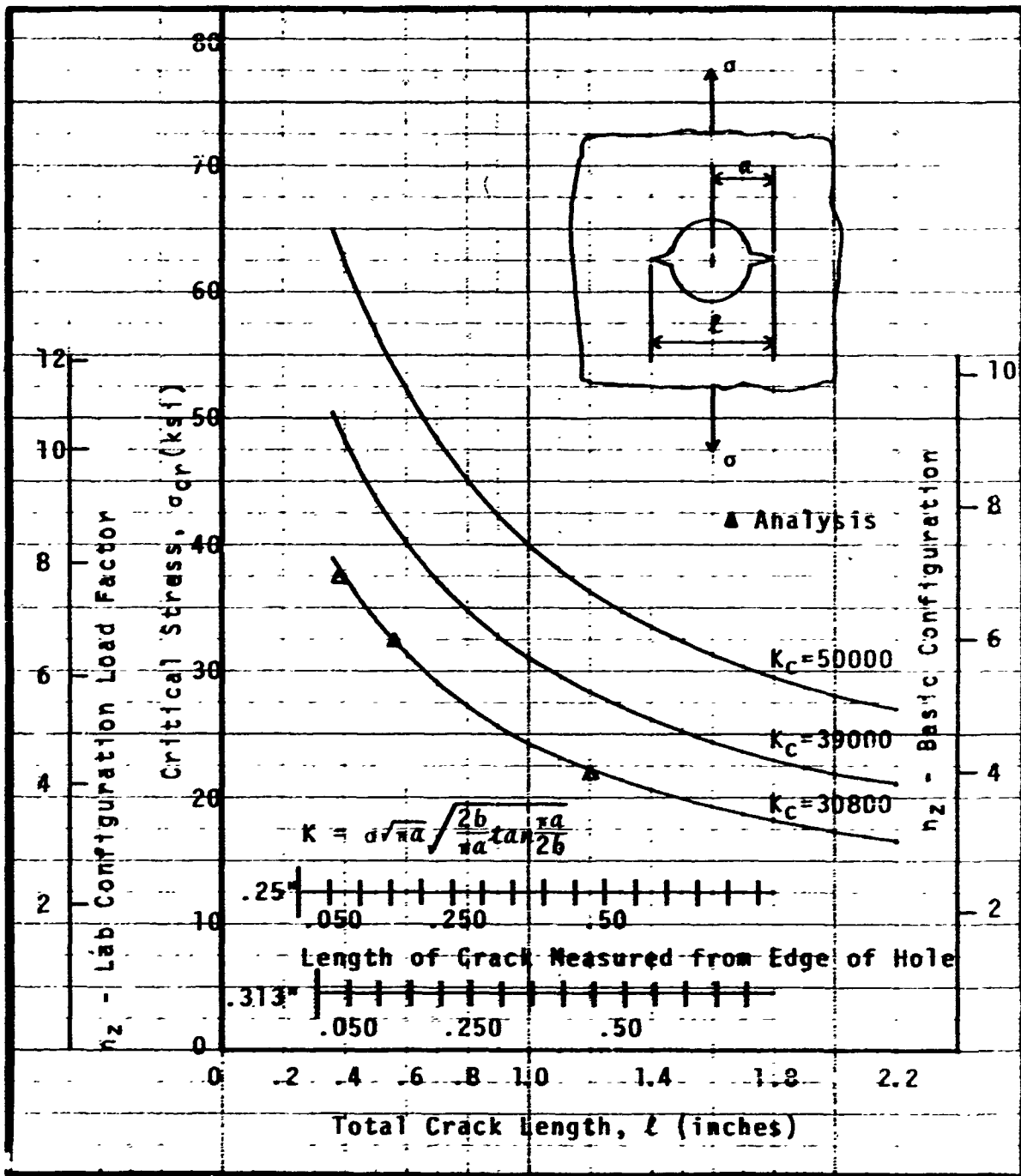


Figure 46. Plot of Critical Crack Length vs. Stress for a 7075-T6 Panel

damage. The initial assumption was 0.050 inch through cracks emanating from both sides of a 5/16 inch fastener hole. In all the following analyses, the crack growth equation formulated by Forman was used[32]. This theory states that the rate of crack growth is related to the stress intensity factor range in the following manner:

$$\frac{da}{dN} = \frac{C(\Delta K)^n}{(1-R)K_C - \Delta K} \quad (52)$$

where

ΔK = range of stress intensity factor K

R = ratio of minimum K to maximum K

K_C = critical stress intensity for fracture
(fracture toughness)

C = material constant (C = 5×10^{-13} for 7075-T6)

n = numerical exponent = 3.0

The difficulty in approaching the crack propagation phase of this study was caused by an incomplete definition of the loading spectrum. Several stress spectra were furnished by the aircraft manufacturer in terms of stress versus cumulative occurrences. Each was representative of 5500 hours of flight. In order to be most accurate, however, the order of application of the stress spectra must represent the order of the actual mission flown. Alternate methods of applying high to low, or low to high, stresses will not yield accurate results. The best alternate (when flight by flight stress profiles are not known) is to block the spectrum in relatively low hour values and randomize the order of application. Experimental evidence of this procedure is reported in Reference [42].

Attempts to run the 5500 hour spectrum with the computer program in Reference [32], resulted in only a few cycles of allowable life before catastrophic failure due to the fact that the representative high "g" stress levels occurred initially. Running all of the low stresses initially would not be valid.

It was finally decided that the best attempt to ascertain remaining life was to assume that one high (6g) excursion of stress occurred per flight. Therefore, cycling at this constant level would approximate the life of the aircraft, (assuming that the low stress levels do not cause significant growth).

The solution of equation (52) for a constant stress of 30,000 psi (approximately 6g) and $R = 0$ yields 186 cycles. Of course, the mechanics of crack growth change with varying stress amplitudes. High excursions of stress may cause temporary arrest and the damaging effect of high cycle, low stresses cannot be ignored. Therefore, the value of 186 cycles is unconservative. The results, however, serve to establish the severity of cracks remaining in service. This value is the basis for one estimate of 200-300 hours of remaining life.

Additional computer runs were made using another aircraft training mission profile. The total flight time per mission was only 47 minutes, however, three weapon delivery passes were made and at least 2 high "g" occurrences occurred per flight. The total number of stress cycles per flight was 615. The 1 "g" level of stress was approximately 5000 psi, thus allowing the use of this loading spectra for this analysis. The

results showed that the original 0.050 inch crack should go catastrophic after 53 flights. A subsequent analysis, deleting 1 high stress occurrence, yielded 73 flights before failure. These results, we believe, tend to strengthen the conclusion that a serious problem exists if cracks as large as 0.050 inch are present in the skins.

3. Additional Analyses

An additional analysis was made for the case of a small corner crack starting in a fastener hole as shown in Figure 47. No exact solution for the stress intensity factor is available, however, an approximate value may be determined by considering the crack acting in a uniform stress field equal to 3σ so as to account for the concentration due to the hole*. The stress intensity factor can be approximated by:

$$\begin{aligned}
 K &= 3\sigma\sqrt{\pi a_0} \left(\frac{2}{\pi}\right)(1.12)^2 & (53) \\
 &= 4.245\sigma\sqrt{a_0}
 \end{aligned}$$

The crack will grow in a manner indicated in Figure 47 and will eventually progress through the thickness. Once the crack penetrates the skin, the expression for the stress intensity factor becomes that of the through-crack, as represented by equation (51).

An estimate of the cycles required to grow from $a_0 = 0.005$ inch to 0.040 inch on the surface yields a value of 3600 cycles for the constant amplitude cyclic stress of 30,000 psi previously used. If this value is

*Editorial Note: See Section III.A.2 (beginning on page 105) for a more complete analysis of growth of cracks nearby holes.

compared to the 186 cycles required to grow catastrophic from 0.050 inch through-cracks, we see that there is an order of magnitude difference.

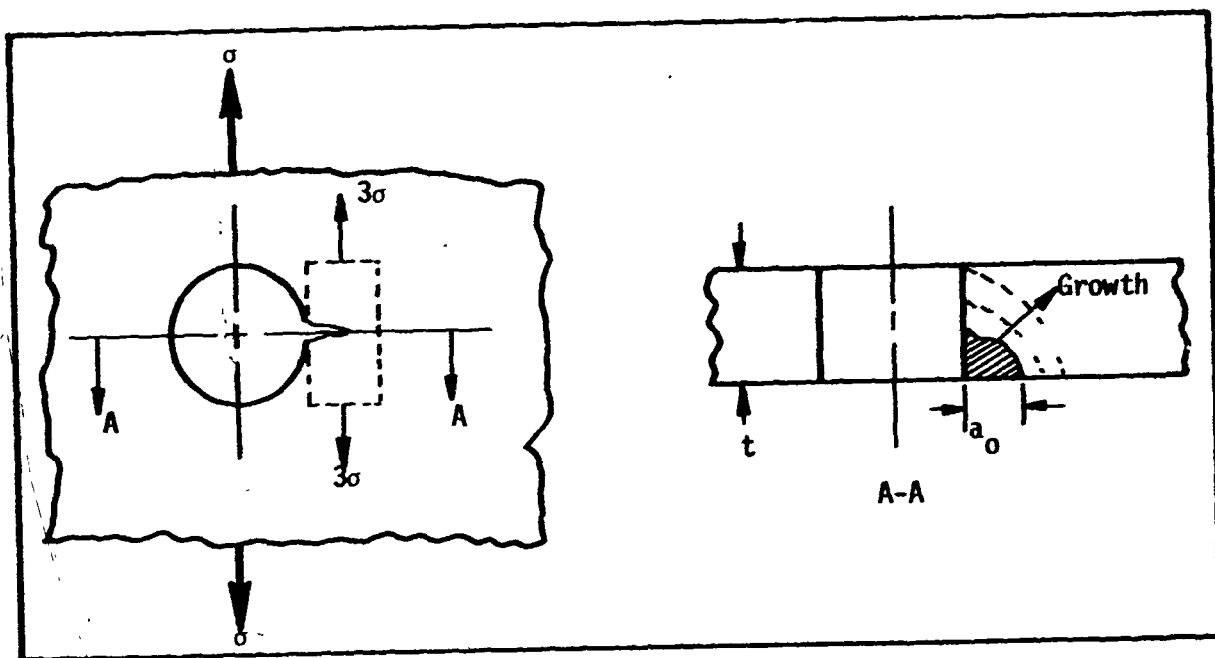


Figure 47. Geometry of a Corner Crack Emanating from a Hole in the Plate

SECTION IV
PROGRAM CONCLUSIONS

The initial investigation and analysis of aircraft structural failures provided an insight into the complexity and limitations of identifying and defining the actual life of structural components. The results of this program may not provide specific and complete answers to the failure analysis problem, but rather provide the guidance and direction for further and more definitive examination and evaluation. From this viewpoint it is believed that this program has provided a valuable contribution toward development of an analysis tool. Some of the more significant program conclusions and recommendations are summarized in the following paragraphs.

The search for definitive and comprehensive in-service failure data is a complex and difficult task, particularly for purposes of conducting data correlation and analysis. This program was intended to provide a broad survey of various Air Force and commercial aircraft failures, and required contacts with numerous information sources on a large number of failure problems. The identification, screening and correlation of specific failures from these sources was difficult to establish and quantify. Identification of discrete failures and failure circumstances were difficult, particularly on older failures and less critical problem areas. Also, component identification

and in-service history was not readily available nor of known accuracy unless it involved a current failure problem. A more thorough investigation is, therefore, required to obtain a quantitative correlation of aircraft structural failure histories.

From the failure data gathered and correlated it can be concluded that the greater percentage of metal failures occur in the wing inboard main frame, wing center or inboard skins, and the aft fuselage frame. The landing gear did not make up a significant percentage (less than 7%) of the total failures, however, it did constitute a large percentage (about 47%) of the more severe or critical failures. The materials experiencing the highest number of significant failures were the 7075-T6 aluminum alloy and the 4340 steel. This is to be expected since such alloys are used in structural components where stresses are high and design or analysis is complex. Some 75% of these failures occur in forged material in which stress corrosion or fatigue is identified as the cause of failure. Influencing factors such as corrosion, fit-up stresses, residual stresses and stress risers are identified as further contributing to the failure problem in most all cases. In about 50% of the cases the origin of failure is at a rivet or bolt hole, or at a sharp corner. If any valid analysis development effort is to be concerned with the solution of these more significant areas it must evaluate and define these parameters or variables.

Throughout the failure data gathering phase it was extremely difficult to secure documentation on failure circumstances and features which are necessary in the successful utilization of fracture mechanics analysis methods. Much data related to origin of failure, fracture surface description, structural load history and operational environment was not available or not clearly defined. Although a few recent failure investigations of critical fleet failure problems have utilized fracture mechanics, generally this analysis method has not been used because it is not adequately understood and involves rather complex metallurgical and stress field interpretations. More complete documentation on the metallurgy-fracture surface-stress history of the failed part is necessary in data gathering efforts for such analysis methods.

The utilization of fracture mechanics analysis methods as a tool for investigating failures or predicting component life is a valid and factual approach. As presented in this report, the analysis technique was adapted and modified to enable its application to actual fleet structural failure problems. However, due to the lack of detailed data from these service failures a single, comprehensive analysis formulation could not be developed which would accurately account for all analysis variables and factors. The generation of additional data through laboratory examination or experimental testing was not included as a part of this program. Emphasis, therefore,

was placed on defining analysis criteria and guidelines for the utilization of fracture mechanics for actual in-service failure investigation.

The limited scope of the program did not enable the establishment of a discrete failure analysis solution, however, it does provide a valuable baseline and direction for more specific failure investigation. It is recommended that future efforts in failure analysis examine and define selected key variables which are important in the successful utilization of fracture mechanics methods. These efforts should include the detailed review of specific in-service component failures and experimental verification.

REFERENCES

1. Paris, P. and Sih, G., "Stress Analysis of Cracks", Fracture Toughness Testing and Its Applications, ASTM, STP 381, 1965.
2. Sih, G., Paris, P. and Irwin, G., "On Cracks in Rectilinearly Anisotropic Bodies", Inter. Journal of Fracture Mechanics, Vol. 1, No. 3, 1966.
3. See for example, papers in recent years (1964-1969) on cracks in homogeneous bodies by Sih and Erdogan of Lehigh University and the references in [1] for a resume of early work.
4. Anon, "Plane Strain Fracture Toughness Testing", ASTM, STP 410, 1967.
5. Rice, J.R., "The Mechanics of Crack Tip Deformation and Extension by Fatigue", Symposium on Fatigue Crack Growth, ASTM, STP 415, 1967.
6. McClintock, F. and Irwin, G., "Plasticity Aspects of Fracture Mechanics", Fracture Toughness Testing and Its Applications, ASTM, STP 381, 1965.
7. Paris, P., "The Mechanics of Fracture Propagation and Solutions to Fracture Arrestor Problems", Document No. D2-2195, The Boeing Company, 1957.
8. Irwin, G.R., "Analysis of Stresses and Strains Near the End of a Crack Traversing a Plate", Trans. ASME Journal of Applied Mechanics, 1957.
9. Irwin, G.R., "Fracture Mode Transition for a Crack Traversing a Plate", ASME, Journal of Basic Engineering, June 1960.
10. Zinkham, R.E., "Anisotropy and Thickness Effects in Fracture of 7075-T6 and -T651 Aluminum Alloy", Journal of Engineering Fracture Mechanics, Vol. 1, No. 2, August 1968, p. 275.
11. Johnson, H. and Paris, P., "Sub-Critical Flaw Growth", Journal of Engineering Fracture Mechanics, Vol. 1, No. 1, 1968.
12. Wei, R. and Landes, J., "Correlation Between Sustained Load and Fatigue Crack Growth in High-Strength Steels", ASTM Materials Research and Standards, Vol. 9, No. 7, July 1969.
13. Feeney, J., McMillan, J., and Wei, R., "Environmental Fatigue Crack Propagation of Aluminum Alloys at Low Stress Intensity Levels", Document No. D6-60114, The Boeing Company, May 1969.
14. Clark, A.B.J. and Irwin, G.R., "Crack Propagation Behaviors", Experimental Mechanics, June 1966.
15. Irwin, G.R., Krafft, J.M., Paris, P.C. and Wells, A.A., "Basic Aspects of Crack Growth and Fracture", Naval Research Laboratory Report No. 6598, November 1967.

16. Names, J., Carr, F.L. and Larson, F.R., "Macrofractographic Techniques", Chapter 13 of Techniques of Metals Research, Vol. II, part 1, Interscience Publishers, 1966.
17. Tiffany, C.F. and Masters, J.N., "Applied Fracture Mechanics", in ASTM STP 381, pp. 249-277, 1965.
18. Wei, R.P. and Landes, J.D., "Correlation Between Sustained Load and Fatigue Crack Growth Rates in High Strength Steels", ASTM Materials Research and Standards, Vol. 9, No. 7, July 1969.
19. British Welding Inst., Frankford Arsenal. See discussion by M. Burdekin in ASTM STP 381, 1965.
20. Kehl, G.L., "Principles of Metallographic Laboratory Practice", McGraw-Hill Book Company, New York, 1949.
21. Anon, "Electron Fractography", STP 436, ASTM, July 1968.
22. Phillips, A., Kerlins, V., and Whiteson, B.V., "Electron Fractography Handbook", AFML-TR-64-416, Air Force Materials Laboratory, Wright-Patterson Air Force Base, Ohio, January 1965.
23. Beachem, C., "The Interpretation of Electron Microscope Fractographs", NRL Report 6360, U.S. Naval Research Laboratory, Washington, DC., January 21, 1966.
24. Whiteson, B.V., Phillips, A., Kerlins, V., and Rawe, R.A., "Special Fractographic Technique for Failure Analysis", Electron Fractography, STP 436, ASTM, July 1968, p. 151.
25. Brothers, A., Spitzig, W., Wiebe, W., and Wolff, U., "Conditions of Fracture Toughness with Fractographic Features", ASTM Committee E-24, Subcommittee II Report, April 1969.
26. Von Euw, E., "Effect of Single Peak Overloading on Fatigue Crack Propagation", M.S. Thesis, Lehigh University, 1968.
27. Birkle, A.J., Wei, R.P., and Pellissier, G.E., "Analysis of Plane Strain Fracture in a Series of 0.45C-Ni-Cr-Mo Steels with Different Sulfur Contents", ASM Trans. Quart. 59, 1966, p. 981.
28. Brown, W.F., Jr., and Srawley, J.E., "Plane Strain Crack Toughness Testing of High Strength Metallic Materials", ASTM STP 410, 1967.
29. Brown, B.F., and Beachem, C.D., "A Study of the Stress Factor in Corrosion Cracking by Use of the Pre-cracked Cantilever Beam Specimen", Corrosion Science, Vol. 5, 1965, p. 745.

30. Peterson, M.H., Brown, B.F., Newbegin, R.L., and Grooves, R.E., "Stress Corrosion Cracking of High Strength Steels and Titanium Alloys in Chloride Solutions at Ambient Temperature", Corrosion, Vol. 23, 1967, p. 142.
31. Paris, P.C., "The Growth of Cracks due to Variations in Load", Ph.D. Dissertation, Lehigh University, September 1962.
32. Forman, R.G., Kearney, V.E., and Engle, R.M., "Numerical Analysis of Crack Propagation in Cyclic-Loaded Structures", Journal of Basic Engineering, September 1967, p. 459.
33. Johnson, R.E., Cammett, J.T., and Coles, A., "Analysis and Application of Cyclic Crack Growth Rate Curves", Third National Symposium on Fracture Mechanics, August 1969, Lehigh University.
34. Wei, R.P., "Some Aspects of Environment-Enhanced Fatigue Crack Growth", Journal of Engineering Fracture Mechanics, Vol. 1, No. 4, 1969.
35. Barcom, J.M., "Corrosion-Fatigue Crack Propagation Below K_{ISCC} ", Third National Symposium on Fracture Mechanics, August 1969, Lehigh University.
36. Miller, G., "The Dependence of Fatigue Crack Growth Rate on the Stress Intensity Factor and the Mechanical Properties of Some High Strength Steels", ASM Trans. Quart. 61, 1968, p. 442.
37. Paris, P.C., and Schmidt, R., "Very Slow Fatigue Crack Growth Rates in a Steel Alloy", Third National Symposium on Fracture Mechanics, August 1969, Lehigh University.
38. Davis, S.O., Tupper, N.G., and Niemi, R.M., "Effect of Specimen Type and Crack Orientation on Fracture Toughness", Engineering Fracture Mechanics, Vol. 1, No. 1, June 1968, p. 213.
39. Begley, J.A., "A Study of Fracture Transition Phenomena in Aluminum Alloy 7075-T651", Ph.D. Dissertation, Lehigh University, 1969.
40. Bowie, O.L., "Analysis of an Infinite Plate Containing Radial Cracks Originating from the Boundary of an Internal Circular Hole", Journal of Mathematics and Physics, Vol. 35, 1956.
41. Paris, P.C., "The Fracture Mechanics Approach to Fatigue", Proc. 10th Sagamore Conference, p. 107, Syracuse University Press, 1965.
42. Schijve, J., Broek, D., DeRijk, P., Nederveen, A., and Sevenhuysen, P.J., "Fatigue Tests with Random and Programmed Load Sequences, with and Without Ground-to-Air Cycles. A Comparative Study on Full-Scale Wing Center Sections", AFFDL-TR-66-143.

43. Carman, C.M., and Katlin, J.M., "Low Cycle Fatigue Crack Propagation Characteristics of High Strength Steels", ASME Paper No. 66-Met-3, Journal of Basic Engineering, 1966.
44. Henderson, R. and Yoder, G., "Wing Carry Through Forging", Report Number MAA68-69, Wright-Patterson Air Force Base, November 1968.
45. Hertzberg, R.W. and Paris, P.C., "Application of Electron Fractography and Fracture Mechanics to Fatigue Crack Propagation", Proc. 1st Int. Conf. on Fracture, Vol. 1, p. 466, 1965.
46. McMillan, J.C. and Hertzberg, R.W., "Application of Electron Fractography to Fatigue Studies", Electron Fractography, ASTM STP 436, p.89.
47. Love, "The Mathematical Theory of Elasticity", Fourth Edition, 1927, Section 88.
48. Mulherin, J.H., Armiento, D.F., and Marcus, H., "The Relationship Between Fracture Toughness and Stress Concentration Factors for Several High-Strength Aluminum Alloys", ASME Paper 63-WA-306, November 1963.
49. Wood, H.A., "Center Wing Section Study-Summary of Analytic Investigation", AFFDL Memorandum, 15 January 1968.
50. Smith, H.R., Piper, D.E., and Downey, F.K., "A Study of Stress-Corrosion Cracking by Wedge-Force Loading" Journal of Engineering Fracture Mechanics, Vol. 1, Nr. 1, pp. 123-128, 1968.

APPENDIX A

COMPUTER PROGRAMS USED FOR AFM 66-1 DATA RETRIEVAL

I. PROGRAM RCCT

The RCCT computer program was written at the Building 57 Open Shop Facility, W-PAFB. A printout of this program is given in Figure A-1, and is a simple program in operation. It reads the data records on the magnetic tape and stores them on the memory disk while in the process it counts the number of records it reads. After completing the tape it prints out the total number of records it read, and then each individual record is printed out as it was originally stored on the magnetic tape. A sample of the output is shown in Figure A-2.

Previous to obtaining any output it was known that there were ten possible formats for the arrangement of the 66-1 data within each record, on the program magnetic tape. After a thorough study was made of the output from RCCT, it was determined that three of the ten formats were used for all the failure data contained on the magnetic tape. Examples of those three formats are marked on Figure A-2. During this format search the number of data records on each tape was also determined.

```

$SETUP 10      05547,2690
$SETUP 14      DISK,PRINT
$IBJOB        MAP
$IBFTC RCCT    M94,XR7
              DIMENSION CD(15),GARB(14)
              CALL READ (10,GARB,14,I)
              K=0
1             CALL READ (10,CD,15,I)
              I=I+1
              GO TO (2,3,1) ,I
2             K=K+1
              WRITE (14,5) (CD(I),I=1,14)
5             FORMAT(14A6)
              GO TO 1
3             WRITE (6,4) K
4             FORMAT(1H124H THE NR. OF RECORDS READ 19)
              STOP
              END
$IBMAP TPS
              ENTRY .UN10.
              .UN10. PZE UNIT10
UNIT10 FILE  ,,READY,LIST,INPUT,BLK=450,BCD
              ENTRY .UN14.
              .UN14. PZE UNIT14
UNIT14 FILE  ,UT1,READY,LIST,INOUT,BLK=450,BCD
              END
$FOF

```

Figure A-1. The Computer Program RCCT

KC1350	54000112	A2121AH0112EM110A23CAF8F1900100308AEY S	Q46622 F0DAJ1
KC1350	54000112	A2121AH0112EM110B23C8G81900100108AEY S	Q40402 F0DAJ1
KC1350	54000117	A2121AH0117EM1110B23AEG80700100108AEY S	Q76684 F0DAJ1
KC1350	54000117	A2121AP0117EM110B1A4P1GM1900100058AEY S	Q36698 F0DAJ1
KC1350	54000117	A2121AP0117EM110B11MAGGM1900100108AEY S	Q76698 F0DAJ1
KC1350	54000117	A2121AP0117EM110B11JAEGM1900100108AEY S	Q76690 F0DAJ1
KC1350	540001512	A2121AP112EB1140B23TOPM1900100058AEY S	Q56495 F0DAJ1
KC1350	540001512	A2121AP112EB11210B23JARM19001000308AEY S	Q56495 F0DAJ1
KC1350	54000112	A2121AP0112FB0910A13CAKCH0700100208AEY S	Q26612 F0DAJ1
KC1350	54000112	A2121AC0112FB0910A13CAKCH0700200138AEY S	Q36625 F0DAJ1
KC1350	54000112	A2121AC0112FB0910B11KARGH1900100038AEY S	Q36640 F0DAJ1
KC1350	54000117	A2121AP0117EB0810B11PKGM1900100038AEY S	Q26692 F0DAJ1
KC1350	54000117	A2121AC0117EB0910A13CAKCH0700100108AEY S	Q26696 F0DAJ1
KC1350	54000117	A2121AP0117H30910A11JARGM1900100028AEY S	Q36700 F0DAJ1
KC1350	54000117	A2121AP0117H30910A11KAGGM1900100038AEY S	Q36692 F0DAJ1
KC1350	54000117	A2121AP0117H30910A11JARGM1900100038AEY S	Q36694 F0DAJ1
KC1350	540001512	A2121AC112EB0810B11KRCGM1900100038AEY S	Q28490 F0DAJ1
KC1350	54000399	A2122AH0049EM110B23HAGG1900100208AEY S	PA0231 F0DAJ1
KC1350	54000399	A2122AH0049EM110B23AAARR1900100308AEY S	PA0234 F0DAJ1
KC1350	54000399	A2122AH0049EM110B23ECKFB19001000808AEY S	PA0235 F0DAJ1
Q015A020411900+1	70000C1127AE0D000F2709A111HFK190010010XLMU C	P23400 J3EAC1	
Q02RA0521603	000C0C3731Y8RA661FF2509A234AAWF190000100XLMU C	H50340 F0EAC1	
Q02RA0521603	000C0C3731Y8RA661FF2639B234AAWF190000030XLMU C	H50340 F0EAC1	
Q015A0204-062-212-25	00000C2335AD7919HF1809A11311GF190010010NZAS S	L50011 J3JAC1	
Q015A0204-062-2703	00000C2335AD5444HF1409A11322GF190010020NZAS S	N80009 D3JAC1	
Q015A0221-53849	00000B3234KRA6071FF2509A2350FA190010040MSFT D	N01050 F3HAC1	
Q015A021+123743	00000J2139AP0571FE2600A11932FM190010040XLMU C	O93403 J3FAC1	
Q02RA05204724P17	00000J3234KRA60767F2309H23FAECM190000020XLMU C	N51406 J0FAC1	
Q02RA05006724P17	00000J3234KRA60767F2509A23EACGM190000030XLMU C	N53406 D0FAC1	
Q02RA05204724P17	00000J22131AH7615EP1009A14740AM190010030XLMU C	P22154 J3EAC1	
Q015A0204-127-04-303	0000023231XHC390EP1009A23520AM190010010FRNV T	N11129 D3EAC1	
Q02RA05204556G11	0000023231XHC390EP1009A23520AM190010010FRNV T	N31129 D3EAC1	
Q02RA05204556G11	0000023231XHC390EP1009A23520AM190010010FRNV T	N31129 D3EAC1	
Q02RA05204556G11	0000023231XHC390EP1009A23520AM190010010FRNV T	M70037 D3EAC1	
Q02RA05204556G11	0000023231XHC390EP1009A23520AM190010010FRNV T	J11138 D3EAC1	
Q02RA05204556G11	0000023231XHC390EP1009A23520AM190010010FRNV T	J11138 D3EAC1	
Q02RA05204556G11	0000023231XHC390EP1009A23520AM190010010FRNV T	J11138 D3EAC1	
Q02RA05204556G11	0000023231XHC390EP1009A23520AM190010010FRNV T	Q03102 E3HAC1	
Q02RA05204556G11	0000023231XHC390EP1009A23520AM190010010FRNV T	PA1474 D8EAC1	
Q02RA05204556G11	0000023231XHC390EP1009A23520AM190010010FRNV T	M73495 D8EAC1	

(3)

(2)

(1)

Figure A-2. RCCT Output

II. PROGRAM SELECT

The program called SELECT was written after examination of the output from RCCT. A printout of SELECT is given in Figure A-3a and b. Although considerably more complex than RCCT, the operation of SELECT is very straightforward. First, since the data is stored in thirty-record blocks, twenty thirty-record blocks are read at one time. Each of these six-hundred records is examined by the computer. Using the Suffix Code, which indicates the aircraft system, to select the data records of interest the program determines what data is significant. Those records selected continue through the loop where the format is determined. Once this is done, the correct output is determined for that format. The data is then arranged so that each of the three different formats produces outputs which are consistent, and the data is then printed out. After each of the six-hundred records are searched, six-hundred more are read-in and the process is repeated until all data has been analyzed. Each time data is read, from the magnetic tape, a message is printed out which tells how many data records were read to that point. A sample of the output from SELECT is shown in Figure A-4.

Unlike RCCT, SELECT has selective inputs other than just the magnetic tape. A list of these inputs and their explanation is given in Table A-I. A sample of this input data is shown as the last few lines of Figure A-3b. By changing the aircraft Suffix Codes under the input variable N(K), any aircraft system or systems can be printed out as long as there are no more than sixteen Suffix Codes.

```

SSETUP 7      2690,NORING
$IPJOB      MAP
$IBMAP FILES NODECK
            ENTRY .UN07.
.UN07. PZE    UNIT07
UNIT07 FILE  .A(1),READY,INPUT,BLK=450
            END
$IBFTC SELECT M94,XR7
            DIMENSION I(20,30,20),N(22)
            DATA (N(K),K = 1,6)/1HA,3H000,1H0,1H3,1H8,6H
            READ (5,13) LL,KK,Q,R,(N(K),K = 7,LL)
13  FORMAT (I2,2XI',2X2A6/16(1XA2))
            DO 12 JJ = 1,KK
12  READ (7,11) X
11  FORMAT(A1)
            WRITE (6,10) Q,R
            II = KK - 1
            JJ = 0
19  READ (7,25) (((I(K,L,J),K = 1,20),L = 1,30),J = 1,20)
25  FORMAT(30(A3,1XA3,A5,A1,A5,A3,2XA3,A5,2A1,A4,A2,2A5,2A1,A3,2XA4,5
1XA1,12XA1,10X))
            II = II + 20
            WRITE (6,18) II
18  FORMAT(/20X53HTHE NUMBER OF 30-RECORD BLOCKS READ TO THIS POINT IS
1 15//)
            JJ = JJ + 3
            IF(JJ,GE,50) GO TO 40
            GO TO 41
40  JJ = 0
            WRITE (6,10) Q,R
41  DO 60 K = 1,20
            DO 60 L = 1,30
            IF(I(9,L,K).EQ.N(1)) GO TO 26
            GO TO 60
26  DO 27 J = 7,LL
27  IF(I(12,L,K).EQ.N(M)) GO TO 28
            GO TO 60
28  IF(I(20,L,K).EQ.N(5)) GO TO 29
            IF(I(1,L,K).EQ.N(2).AND.(I(20,L,K).EQ.N(3).OR.I(20,L,K).EQ.N(4)))
1GO TO 30
            IF(I(20,L,K).EQ.N(3).AND.I(3,L,K).EQ.N(6))GO TO 36
            GO TO 60
36  WRITE (6,31) I(5,L,K),I(6,L,K),I(14,L,K),I(12,L,K),I(17,L,K),I(13,
1L,K),I(10,L,K),I(19,L,K),I(8,L,K),I(15,L,K),I(16,L,K),I(18,L,K)
31  FORMAT (2XA5,A3,26XA5,3XA2,6XA3,4XA5,6XA1,9XA1,8XA5,6XA1,7XA1,8XA4
1)

```

Figure A-3a. The Computer Program SELECT

```

      GO TO 34
29  WRITE (6,32) I(11,L,K),I(2,L,K),I(3,L,K),I(4,L,K),I(5,L,K),I(14,L,
      1K),I(12,L,K),I(7,L,K),I(13,L,K),I(10,L,K),I(19,L,K),I(8,L,K)
32  FORMAT (6XA4,6XA3,A6,A1,A5,5XA5,3XA2,6XA3,4XA5,6XA1,9XA1,8XA5)
      GO TO 34
30  WRITE (6,33) I(11,L,K),I(3,L,K),I(4,L,K),I(5,L,K),I(6,L,K),I(14,L,
      1K),I(12,L,K),I(17,L,K),I(13,L,K),I(10,L,K),I(19,L,K),I(8,L,K),I(15
      2,L,K),I(13,L,K),I(18,L,K)
33  FORMAT (6XA4,6XA6,A1,A5,A3,5XA5,3XA2,6XA3,4XA5,6XA1,9XA1,8XA5,6XA1
      1,7XA1,5XA4)
34  JJ = JJ + 1
      IF(JJ.GE.50) GO TO 35
      GO TO 60
35  JJ = 0
      WRITE (6,10) Q,R
10  FORMAT (1H149X34HAFLC AFM 66-1 FAILURE DATA FOR THE //61X2A6///3X
      17HA/C-S/N8X11HPART NUMBER8X3HWUC3X4HSUFF3X7HHOW-MAL3X4HDATE3X7HTYP
      2-MNT3X7HCOMMAND3X8HWORK-CEN2X6HACTION2X8HWHN-DISC2X8HHOURS-.1//)
60  CONTINUE
      GO TO 19
      END
SDATA
22  3321      KC/C-135
      CA CV CX CI CS EA EB ED EE EF EH 05 09 23 24 40
SEQF

```

Figure A-3b. SELECT Continued

ALL AFM 66-1 FAILURE DATA FOR THE

KC/C-119

A/C-S/N	PART NUMBER	WUL	SUFF	HMW-MAL	DATE	TYP-INT	COMMAND	WORK-CEN	ACTION	WHN-DISC	HOURS-1
3516	5+6389+901	1177	CX	190	19019	H	S	2217	A	M	0010
3522	5C+2866+3	1176	CX	190	23019	H	S	2218	A	M	0010
3522	9+61702+1	1197	CX	190	23019	B	S	2218	A	M	0020
1409	5+8553+51	1194H	CX	190	23019	P	S	2217	I	M	0030
4037	50-245H-15	23JUG	CX	190	23019	B	S	2219	A	H	0015
3622	5+4214+62	1194U	CX	190	24019	C	S	52107	A	H	0010
0079	5-85618	23PQC	CX	190	22019	P	S	52141	I	M	0040
0079	5-85618	23PQC	CX	190	23019	P	S	52141	I	M	0140
1446	50-2672-2	1123M	CX	070	26019	P	S	53310	A	M	0035
1502	50+245H+41	23JUG	CX	190	27019	P	S	52122	A	M	0120
7986	5+85537	23PQH	CX	190	28019	P	S	52164	A	M	0120
7986	5+85618	23PQC	CX	190	29019	P	S	52144	A	M	0170
0717	5+8142+9	1443D	CX	190	21019	P	S	52146	A	M	0070
0017	5+57632	23CHA	CX	190	21019	P	S	52146	A	M	0010
0017	5+64026+39	1461A	CX	190	21019	P	S	52146	A	M	0030
0017	5+HR142+2	14270	CX	190	21019	B	S	52146	A	M	0010
0000	153245+2	13262	CX	190	12128	H	F	46610	A	M	0010
0000	153250	13262	CX	190	12128	H	F	46610	A	M	0010
0000	1481025	13331	CX	190	16128	H	F	46610	A	M	0010
0000	5+H3025	13331	CX	070	19128	H	F	46610	A	M	0010

255

THE NUMBER OF 30-RECORD BLOCKS READ TO THIS POINT IS 40

1771	5+63171+21	11666	CX	190	19128	P	S	52100	A	M	0020
4045	5+85654	23PQJ	CX	190	19128	H	S	52100	A	F	0020
4045	5+85654	23PQJ	CX	190	19128	H	S	52100	A	F	0045
0013	5+1+H265	23PQL	CX	190	19128	P	S	52100	A	M	0040
5900055		1114H	EH	190	1939H	H	S	52100	A	D	0740
59001510		14137	EH	190	0509H	C	S	52000	F	M	0005
59001510		1432A	EH	190	0509H	C	S	52000	F	M	0005
59001510		1194R	EH	190	1009H	C	S	52000	F	M	0005
59001510		24ECJ	EH	190	1109H	C	S	52000	F	M	0005
5900062		11JFN	EH	190	0509H	C	S	52000	F	M	0005
5900062		11JFN	EH	190	1109H	C	S	52000	F	M	0005
5900062		11JFN	EH	190	1209H	C	S	52000	F	M	0005
5900062		1194K	EH	190	1209H	C	S	52000	F	M	0005
61000347		11443	EH	070	2609H	F	S	52110	A	M	0010
6100001		11000	ED	190	0939H	F	S	52110	A	M	0010
61007944		11117	ED	190	1739H	C	S	42119	A	M	0030
61007993		11117	ED	190	1739H	C	S	42119	A	M	0010
61004579		23JQA	ED	190	1909H	F	S	42119	A	M	0070
61004579		23JQG	ED	190	1909H	F	S	42119	A	M	0120
61004579		23JQG	ED	190	1909H	F	S	42119	A	M	0120

THE NUMBER OF 30-RECORD BLOCKS READ TO THIS POINT IS 60

61000262		23RAU	EH	190	1910H	B	S	12120	A	F	0040
61000262		23RAH	EH	070	1910H	B	S	12120	A	F	0330
61000397		23DAE	EG	190	1910H	C	S	12120	A	F	0020
61000397		23JUG	EH	190	1709H	C	S	12120	A	F	0040

Figure A-4. SELECT Output

TABLE A-I. INPUT DATA FOR THE COMPUTER PROGRAM "SELECT"

CARD #	VARIABLE NAME	VARIABLE LIMITS	EXPLANATION OF VARIABLE	LOCATION ON CARD
1	LL	7<LL<22	The Number of Aircraft Suffix codes plus six	Cols. 1 and 2
	KK	1<KK<*	The Number of 30-Record Blocks to be Skipped before Data Search Begins	Cols. 5 thru 8
	Q & R	Any Alphameric Characters	Printed out Name of Aircraft System	Cols. 11 thru 22
2	N(K) (K=LL-6)	One to 16 Groups of 2 Alphameric Characters One for Each K	Aircraft Suffix Codes for System printed Under Q and R	Cols. 2 thru 48 One Space Between Each 2 Characters

*Total Number of 30-Record Blocks

III. PROGRAM WUCCOL

The computer program WUCCOL was written after SELECT was written and tested. Fundamentally, WUCCOL is very similar to SELECT but WUCCOL goes considerably further in its workings. The printout of WUCCOL is given in Figure A-5. In operation the program first reads the Suffix Codes and selected Work Unit Codes. Next it reads the data on the magnetic tape, one thirty-record block at a time, and starts to analyze the data. The first thing that is checked is the Suffix Code, if it is one of the codes in the input data the computer analyzes further, if not, another record is searched.

The next step is to compare Work Unit Codes. A comparison is made between the WUC in the data record and all the WUC's from the input data. If the first two, three, four or all five characters, depending on the form of the input data, of the record's WUC correspond to any of those same features in the input data, then that particular data record is printed out using the same selection method as in SELECT. Also, the WUC just printed is compared to all the other WUC's which previously caused a printout. If the particular WUC of interest is identical to any of those that have been used previously, a one is added to a counting variable which is associated with that WUC. If, on the other hand, none of the WUCs previously read are identical to the one that was just read, then the WUC is stored as a new addition to the list of WUCs stored in the computer. Along with this, a new counting variable, associated with the new WUC, is initialized at one. After all the data records are read and searched,

```

SSETUP      2690,NORING
SIBJOB      MAP
SIBMAP FILES NODECK
           ENTRY  .UN07.
. UN07. PZE  UNIT07
UNIT07 FILE ,A(1),READY,INPUT,BLK=450
           END
SIBFTC WUCCOL M94,XR7
           DIMENSION L(25,30),M(1000,5),N(22)
           DATA (N(I),I = 1,6)/1HA,3HQ00,1H0,1H3,1H8,6H
           IQ = 50
           DO 14 I = 1,5
           DO 14 J = 1,1000
14          M(J,I) = 0
           READ (5,13) I1,I2,I3,I4,I5,Q,R,(N(I),I = 7,11)
13          FORMAT (5(1X15),2X2A6/16(1XA2))
           READ (5,15) ((M(I,J),J = 1,4),I = 1,12)
15          FORMAT (13(1XA2,3A1))
           DO 12 I = 1,13
12          READ (7,11) X
11          FORMAT (A1)
           IO = 12
           II = 13 - 1
19          IF (II,GE,15) GO TO 70
           READ (7,25) ((L(I,J),I = 1,25),J = 1,30)
25          FORMAT (30(A3,A1,A2,A1,A6,A1,A5,A3,2XA3,A5,2A1,A4,A2,A5,A2,5A1,A3,
12XA4,5XA1,12XA1,10X))
           II = II + 1
           DO 60 I = 1,30
           IF (L(11,I).EQ.N(1)) GO TO 26
           GO TO 60
26          DO 27 J = 7,11
27          IF (L(14,I).EQ.N(J)) GO TO 28
           GO TO 60
28          GO TO (51,52,53,54),I4
51          DO 56 J = 1,12
           IF (L(16,I).EQ.M(J,1).AND.L(17,I).EQ.M(J,2).AND.L(18,I).EQ.M(J,3).A
1ND.L(19,I).EQ.M(J,4)) GO TO 57
           GO TO 56
57          M(J,5) = M(J,5) + 1
           CALL WRIT (L,N,IQ,Q,R,I)
56          CONTINUE
           GO TO 60
54          DO 84 J = 1,10
84          IF (L(16,I).EQ.M(J,1).AND.L(17,I).EQ.M(J,2).AND.L(18,I).EQ.M(J,3))
1GO TO 55

```

Figure A-5a. The Computer Program WUCCOL

```

      GO TO 60
53 DO 83 J = 1,10
83 IF(L(16,I).EQ.M(J,1).AND.L(17,I).EQ.M(J,2)) GO TO 55
      GO TO 60
52 DO 82 J = 1,10
82 IF(L(16,I).EQ.M(J,1)) GO TO 55
      GO TO 60
55 DO 61 J = 1,12
61 IF(L(16,I).EQ.M(J,1).AND.L(17,I).EQ.M(J,2).AND.L(18,I).EQ.M(J,3).A
      ND.L(19,I).EQ.M(J,4)) GO TO 62
      I2 = I2 + 1
      DO 64 K = 1,4
64 M(I2,K) = L(K+15,I)
      M(I2,5) = 1
      CALL WRIT (L,N,IQ,Q,R,I)
      GO TO 60
62 M(J,5) = M(J,5) + 1
      CALL WRIT (L,N,IQ,Q,R,I)
60 CONTINUE
      GO TO 19
70 I6 = I2 - 1
      DO 10 I = 1,I6
      I7 = I + 1
      DO 10 J = I7,I2
      IF(M(I,5).LT.M(J,5)) GO TO 16
      GO TO 10
16 DO 17 K = 1,5
      MM = M(J,K)
      M(J,K) = M(I,K)
17 M(I,K) = MM
10 CONTINUE
      WRITE (6,80) ((M(J,I),I = 1,5),J = 1,12)
80 FORMAT (1H1//7(6X11:HUC NO.)/50(7(5XA2,3A1,3H - I4)/))
      STOP
      END

```

Figure A-5b. WUCCOL Continued

```

$IBFTC WRITA M94,XR7
SUBROUTINE WRIT (L,N,IQ,Q,R,I)
DIMENSION L(25,30),N(22)
IF(IQ.EQ.50) GO TO 35
GO TO 20
35 IQ = 0
WRITE (5,10) Q,R
10 FORMAT (1H149X34HAFLC AFM 66-1 FAILURE DATA FOR THE //60X2A6///7X
13HA/C9X3HS/N10X11MPART NUMBER8X3HWUC5X4HSUFF2X7HHDW-MAL3X4HDATE3X7
2HTYP-MNT1X3HCOM4X5HWK-CN4X3HACT2X5H... DI2X6HHS-.1)
20 IF(L(25,I).EQ.N(5)) GO TO 29
IF(L(1,I).EQ.N(2).AND.(L(25,I).EQ.N(3).OR.L(25,I).EQ.N(4))) GO TO
130
IF(L(25,I).EQ.N(3).AND.L(5,I).EQ.N(6)) GO TO 36
RETURN
29 WRITE (6,32) L(13,I),(L(J+2,I),J = 1,5),(L(J+15,I),J = 1,4),L(14,I
1),L(9,I),L(15,I),L(12,I),L(24,I),L(10,I)
32 FORMAT (19XA4,7XA2,A1,A6,A1,A5,5XA2,3A1,5XA2,5XA3,5XA5,2(5XA1),5XA
15)
GO TO 34
30 WRITE (6,33) L(13,I),(L(J+4,I),J = 1,4),(L(J+15,I),J = 1,4),L(14,I
1),L(22,I),L(15,I),L(12,I),L(24,I),L(10,I),L(20,I),L(21,I),L(23,I)
33 FORMAT (19XA4,7XA6,A1,A5,A3,5XA2,3A1,5XA2,5XA3,2(5XA5,2(5XA1)),5XA
14)
GO TO 34
36 WRITE (6,31) (L(J,I),J = 1,4),L(7,I),L(8,I),(L(J+15,I),J = 1,4),L(
114,I),L(22,I),L(15,I),L(12,I),L(24,I),L(10,I),L(20,I),L(21,I),L(23
2,I)
31 FORMAT (5XA3,A1,A2,A1,5XA5,A3,25XA2,3A1,5XA2,5XA3,5XA5,2(5XA1),5XA
15,2(5XA1),5XA4)
34 IQ = IQ + 1
RETURN
END
$DATA
18 35 4000 4 5020 C-141A
CW CB 01 12 27 30 50 51 52 53 54 55
11BA0 11BB0 11BD0 11BE0 11BG0 11BH0 11BK0 11BL0 11CA0 11CB0 11CC0 11CD0 11CE0
11CF0 11CG0 11CH0 11DA0 11EA0 11EB0 11EC0 11ED0 11EE0 11FA0 11FB0 11FC0 11FD0
11FE0 11GA0 11GB0 11GC0 11GD0 11GE0 11HA0 11HB0 11HC0
SEOF

```

Figure A-5c. WUCCOL Continued, Subroutine Writ

the computer prints out the list of WUCs with the number of times each appeared in the data. This printout is printed in order, so that the WUC that appeared the greatest number of times comes first. A sample data record printout is shown in Figure A-6. A printout of the WUC list is shown in Figure A-7.

The input data to WUCCOL is similar in many ways to that of SELECT. A list and explanation of this data is given in Table A-II. The final point that needs explanation is the method of searching and selecting the correct WUCs. To do this the input variable I4 is used. If I4 = 1, the input is a set of specific, five-character WUCs and the data record's WUC must correspond exactly to one of the WUCs in the input data before a printout and correlation are made. If I4 = 2, the first two digits of the WUC are all that has to correspond before a printout occurs. If I4 = 3, the first two digits and the first character must correspond. And, if I4 = 4, the first two digits and the first two characters must correspond. If any of the spaces in the WUC input data are left blank or set to zero, as when I4 = 2, 3 or 4, they are filled by the information in the WUCs from the data record. In this way if information on all airframe parts are desired, simply put down one WUC (i.e., 11000) such that each time a WUC beginning with 11 comes up in the data, it is printed out. A sample set of input data can be found on the last lines of Figure A-5c. With this computer program, all the 66-1 statistical data presented in this report, was obtained.

TABLE A-II. INPUT DATA FOR THE COMPUTER PROGRAM "WUCCOL"

CARD #	VARIABLE NAME	VARIABLE LIMITS	EXPLANATION OF VARIABLE	LOCATION ON CARD
1	I1	7<I1<22	The Number of Aircraft Suffix Codes plus Six	Cols. 2 thru 6
	I2	1<I2<1000	The Number of Work Unit Codes to be Searched	Cols. 8 thru 12
	I3	1<I3<*	The Number of 30-Record Blocks to be Skipped Before Data Search Begins	Cols. 14 thru 18
	I4	1<I4<4	This Variable Determines the Search Pattern of the Work Unit Codes: 1 for Specific Work Codes 2 for First 2 Digits Only 3 for 2 Digits Plus 1 Character 4 for 2 Digits Plus 2 Characters	Cols. 20 thru 24
	I5	1<I5<*	The Number of 30-Record Blocks to be Read During the Search	Cols. 26 thru 30
2	Q & R	Any Alphameric Characters	Printed Out Name of Aircraft System	Cols. 33 thru 44
	N(K) (K=11-6)	1 to 16 Groups of 2 Alphameric characters, 1 for each K	Aircraft Suffix Codes for System Printed Under Q and R	Cols. 2 thru 43 one space between each two characters
	M(I,J) (J=12) (I=1,2,3,4)	1 to 1000 Groups of 5 Alphameric Characters, one for each I2	Aircraft Work Unit Codes for System Printed Under Q and R	Cols. 2 thru 73 on each card, one space between each 5 characters

*Total Number of 30-Record Blocks